

12-11-2015

# The Middle Stone Age on the Margins: Chronological and Archaeological Contexts for Hominin Behavioral Evolution in the Middle and Late Pleistocene of East Africa.

Nicholas T. Blegen

*University of Connecticut - Storrs*, [nicholas.blegen@uconn.edu](mailto:nicholas.blegen@uconn.edu)

Follow this and additional works at: <https://opencommons.uconn.edu/dissertations>

---

## Recommended Citation

Blegen, Nicholas T., "The Middle Stone Age on the Margins: Chronological and Archaeological Contexts for Hominin Behavioral Evolution in the Middle and Late Pleistocene of East Africa." (2015). *Doctoral Dissertations*. 937.  
<https://opencommons.uconn.edu/dissertations/937>

The Middle Stone Age on the Margins: Chronological and Archaeological Contexts for Hominin Behavioral Evolution in the Middle and Late Pleistocene of East Africa.

Nick Blegen, PhD

University of Connecticut, 2015

The later Middle through early Late Pleistocene (~100–400 ka) of East Africa is an important time and place for the evolution of our species. This period records the first appearance of *Homo sapiens* and spans significant technological changes including the decline of large handheld stone tools characteristic of the Acheulean, the development of stone tool technologies collectively known as the Middle Stone Age (MSA). These include diverse Levallois prepared core techniques and the manufacture and use of pointed weapons. It is in association with MSA technologies in sub-Saharan Africa that most of the behaviors characteristic of modern humans first appear. This doctoral dissertation provides new chronological and archaeological data relevant to hominin behavior associated with MSA technology in the Middle and Late Pleistocene of East Africa. Improved chronological resolution is achieved through tephrostratigraphy, the correlation of volcanic ashes, combined with chronometric dating in two regions: the Kapthurin Formation in the Rift Valley, Baringo, Kenya and the eastern Lake Victoria Basin of western Kenya. New data on hominin behavior is provided by archaeological excavations of two sites: 1) The 196-226

Nick Blegen, PhD – University of Connecticut, 2015

ka Sibilo School Road Site in the Kapthurin Formation. 2) The 33–49 ka site of Nyamita Main in the eastern Lake Victoria Basin. The archaeology of the Kapthurin Formation and the eastern Lake Victoria Basin are connected thematically by the presence of MSA technology. These basins are also connected stratigraphically and chronologically, as this study shows, by tephra correlations between them. Results of this work demonstrate: 1) Levallois prepared core techniques, important aspects of MSA technology, are shown to be >380 ka in the Kapthurin Formation, ~100 kyr older than previously estimated in East Africa. 2) Long distance transport (>166 km) of high quality obsidian for stone tool manufacture was a feature of hominin behavior associated with Middle Pleistocene MSA technology ~200 ka ago. 3) MSA technology persisted in East Africa later than 49 ka and perhaps later than 33 ka, after Later Stone Age technologies, often considered categorically superior, are documented in the region. By demonstrating both the early and late presence of various aspects of MSA technology and associated hominin behavior this work shows that tephrostratigraphy and the excavation of new archaeological material in East Africa are productive means of producing new and important data on the MSA and the evolution of human behavior.

The Middle Stone Age on the Margins: Chronological and Archaeological Contexts for Hominin  
Behavioral Evolution in the Middle and Late Pleistocene of East Africa.

Nick Blegen

B.A., University of Illinois Urbana-Champaign, 2006

M.A., University of Connecticut, 2009

A Dissertation

Submitted in Partial Fulfillment of the

Requirements for the Degree of

Doctor of Philosophy

at the

University of Connecticut

2015



Copyright by

Nick Blegen

2015

APPROVAL PAGE

Doctor of Philosophy Dissertation

The Middle Stone Age on the Margins: Chronological and Archaeological Contexts for Hominin Behavioral Evolution in the Middle and Late Pleistocene of East Africa.

Presented by

Nicholas T. Blegen, B.A., M.A.

Major Advisor \_\_\_\_\_  
Sally McBrearty

Associate Advisor \_\_\_\_\_  
Daniel Adler

Associate Advisor \_\_\_\_\_  
Natalie Munro

Associate Advisor \_\_\_\_\_  
Christian A. Tryon

University of Connecticut  
2015

## Acknowledgments:

I thank the members of my committee Sally McBrearty, Christian Tryon, Daniel Adler and Natalie Munro for the time and effort they put into helping me with the process of putting together this dissertation. For archaeological advice I thank Sally McBrearty, Christian Tryon, Dr. J. Tyler Faith, Dan Adler and Natalie Munro. For geological, geochemical and laboratory advice I thank Frank Brown, Christian Tryon, Daniel Peppe and Gideon Hartman. For field assistance I thank Bonface Kimeu, Julius Marti, Bernard Muende, Bernard “Kenyanze” Ngenyo, Mathew Macharwas, Daniel Dmbeke, Simeon Chelal, ‘Brown,’ and Joshua Siembo. Personally, I thank Marie Brault for all her support throughout much of the process of this work. I thank my parents Marilyn Blegen and Gregory Blegen for their love and support. I would like to extend my sincere gratitude to Frank Brown for assistance, hospitality, input and advice throughout the process of tephra and obsidian preparation, analysis and interpretation. Fieldwork in Baringo was conducted under research permit NCST/RCD/12B/012/2 issued to Blegen and was made possible by National Science Foundation funding grant (BCS 0917965) to Sally McBrearty and NSF DDIG # 1343740 to Nick Blegen as well as GSA Dissertation grant to Blegen and University of Connecticut internal funding and Department of Anthropology grants to McBrearty and Blegen. Fieldwork on Rusinga Island and Karungu was conducted under research permits NCST/RC-

D/12B/012/2 issued to Blegen, NCST/5/002/R/576 issued to Tryon, NCST/RCD/12B/012/31 issued to Faith, NCST/RCD/12B/01/07 issued to Peppe, and NCST/5/002/R/605 issued to Beverly, and an exploration and excavation license issued by the National Museums of Kenya (NMK).

Table of Contents	Page
Introduction.....	1
Paper #1: Distal tephras of the eastern Lake Victoria Basin, Equatorial East Africa: Correlations, chronology and a context for early modern humans.....	16
Paper #2: Tephrostratigraphy and archaeology of the Kapthurin Formation, Kenya: revised chronology and new ages for Acheulean and Middle Stone Age sites.....	91
Paper #3: Evidence of long-distance obsidian transport and early Middle Stone Age technology at the ~200 ka BP Sibilo School Road Site GnJh-79), Baringo, Kenya:.....	172
Paper #4: The East African Middle Stone Age at <50,000 years ago: Evidence from Nyamita Main (GrJa-3), Rusinga Island, western Kenya.....	228
Summary and Conclusion.....	269
References.....	273

## Introduction:

This doctoral dissertation provides new chronological and archaeological data relevant to hominin behavior associated with Middle Stone Age (MSA) technology in the later Middle Pleistocene (130–400 ka) and Late Pleistocene (10–130 ka) of East Africa. Chronological resolution is achieved primarily through tephrostratigraphy, the correlation of volcanic ashes, combined with chronometric dating in two regions: the Kapthurin Formation in the Rift Valley, Baringo, Kenya and the eastern Lake Victoria Basin of western Kenya. New archaeological information is provided through excavations of the 196–226 ka Middle Pleistocene Sibilo School Road Site in the Bedded Tuff Member of Kapthurin Formation and 33–49 ka Late Pleistocene site of Nyamita Main from the Wasiriya beds of Rusinga Island in the eastern Lake Victoria Basin.

Though separated by ~200 km and sampling largely different time periods, the archaeology of the Kapthurin Formation and the eastern Lake Victoria Basin are connected thematically by the presence of MSA technology, defined by the presence stone tools such as points as well as prepared-core technologies. These basins are also connected stratigraphically and chronologically, as this study shows, by tephra correlations of the Wakondo Tuff between them. The introduction will: 1) Review the palaeontological and archaeological background of Middle and Late Pleistocene Africa with an emphasis on East Africa, 2) Describe the theoretical approach to interpreting hominin and behavioral evolution through this time period, and 3) Describe specific methodological approaches—tephrostratigraphy and archaeological excavations—employed in the four jour-

nal-formatted articles constituting this dissertation.

## 1) Paleoanthropology of Middle–Late Pleistocene Africa with emphasis on East Africa:

This dissertation focuses primarily on the chronological context and characteristics of lithic technologies and associated hominin behavior in Middle–Late Pleistocene East Africa. To understand the broader context of this specific regional and topical focus the hominin palaeontological record and associated archaeological record of stone tool technology in the Middle–Late Pleistocene of Africa is briefly summarized below.

### Hominin paleontology of the African later Middle and Late Pleistocene:

The hominin fossil record of the first half of the Middle Pleistocene (780-130 ka) is characterized by cranial features constituting a mixture of primitive traits retained from *Homo erectus* or other ancestral taxa and either derived traits associated with later modern *Homo sapiens* as well as unique features not strictly associated with either the *Homo erectus* or *Homo sapiens*. Important specimens include the Bodo cranium from Ethiopia, East Africa, the Kabwe (Broken Hill) cranium from Zambia and the Saldana calvarium from Elandsfontein, South Africa (Clark, 1959; Rightmire, 2009; Rightmire, 1996; Singer, 1954; Singer and Wymer, 1968; Tappen, 1979; Wood-

ward, 1931). At least some of the specimens attributed to the later Middle Pleistocene Africa represent the earliest *Homo sapiens*. The three crania from the Upper Herto Member of the Bouri Formation, Ethiopia are early *Homo sapiens* fossils dated strictly by  $^{40}\text{Ar}/^{39}\text{Ar}$  and tephra correlation to between 154–160 ka (Clark, 1988; White et al., 2003). U-series/ESR dates on *Homo sapiens* specimens from Jebel Irhoud, Morocco suggest a similar age of 160 ka in North Africa (Smith et al., 2007). Slightly older are the two crania and partial skeleton attributed to *Homo sapiens* from the Kibish Formation, southern Ethiopia dated to ~195 ka by  $^{40}\text{Ar}/^{39}\text{Ar}$  on local tephra and  $^{18}\text{O}$  sapropel correlation with Mediterranean Sea cores (McDougall et al., 2005, 2008). The Omo I partial cranium is regarded as anatomically modern, but the isolated Omo II calvarium, though cranially large, preserves archaic features and debate exists as to whether these specimens represent a morphological variable population or separate taxa (Fleagle et al., 2008; Rightmire, 2009). Older still is the face and partial frontal bones from Florisbad, South Africa dated to ~260 ka by ESR (Grün et al., 1996). Disagreement exists on the anatomical attribution of the Florisbad partial cranium although several researches have advocated its inclusion in *Homo sapiens*, which would push the first appearance date for this species closer to the earliest appearances dates of the MSA (McBrearty and Brooks, 2000). Crania with less precise dating including the Lake Eyasi cranium, LH18 from the Ngaloba beds, Laetoli, KNM ER 3884 from Ileret, Kenya and Eliye Springs KMN-ES-11693, Kenya, all of which preserve both derived and primitive morphologies relative to extant *Homo sapiens* and could potentially date to the later Middle Pleistocene (Right-



mire, 2009). Fossil hominin remains from the Late Pleistocene of Africa are also scarce. The 79–105 ka exposures of Aduma, Middle Awash, Ethiopia have provided four partial crania with a generally modern anatomical appearance (Haile-Selassie et al., 2004; Yellen et al., 2005). Singa, Sudan has produced a pathological cranial specimen also attributed to modern *Homo sapiens* (McDermott et al., 1996; Spoor et al., 1998). Archaeological excavations at Klasies River Mouth (90–120 ka) have produced cranio–dental materials, at least some of which fall within the range of modern human variation (Bräuer and Singer, 1996; Rightmire and Deacon, 1991). Postcranial evidence is less taxonomically diagnostic but evidence from the Middle and Late Pleistocene Africa shows various traits considered by modern and archaic (Pearson, 2000).

Though notoriously patchy and relatively poorly dated the African Middle and Late Pleistocene hominin fossil record reviewed above displays a modular anatomical development of modern characteristics culminating in hominin species generally regarded as modern by the Late Pleistocene (Bräuer, 2008; Bräuer and Singer, 1996; Day, 1986; Pearson, 2000; Pearson et al., 2008; Rightmire, 1998, 2008, 2009).

Lithic technology of the African later Middle Pleistocene and earlier Late Pleistocene:

Similar to the hominin paleontological record, the technological features of the East African

Middle–Late Pleistocene are dynamic. The first half of the Middle Pleistocene is characterized by Acheulean technologies (McBrearty, 2001). Both the end of the Acheulean and the beginning of the MSA occur in the later Middle Pleistocene of Africa. Relative dating based on tephrostratigraphy has shown that technological elements of the Acheulean and MSA are interstratified in the Kapthurin Formation between 284–509 ka (Tryon and McBrearty, 2002, 2006). Reports of Acheulean tools associated with MSA material from the Upper Herto Member of the Bouri Formation, Middle Awash suggest interstratification of Acheulean and MSA tools through the later Middle Pleistocene between 154–160 ka in the northern Rift (Clark et al., 2003). However, the rarity of bifacial large cutting tools, less than 5% of all flaked implements collected from the Upper Herto member, the absence of bifacial preparation flakes (Clark et al., 2003: 750) as well as the weathered condition of these Acheulean tools suggest they may not be contemporary with better represented MSA material or the exceptionally well-preserved *H. sapiens* infant crania from the site. Similarly, at the site of Garba III near Melka Kunture, Ethiopia, Chavaillon and Berthelet (2004: 70-75) report Acheulean and MSA tools in the same layers, but provide no chronometric date. More recent studies of Garba III emphasize the MSA character of the assemblage (Mussi et al., 2014). The Sangoan and the Fauresmith have also both been attributed to the later Middle Pleistocene. The Sangoan, defined by picks and core-axe heavy-duty tools, overlies more characteristically Acheulean material at the site of Nsongezi, Uganda (Cole, 1967; Nelson and Posnansky, 1970; Posnansky, 1970) and Kalambo Falls, Zambia (Clark et al., 2001),

and underlies MSA material at Muguruk, western Kenya (McBrearty, 1986, 1988). Van Peer et al. (2003) claim evidence for interstratification of Sangoan-like tools and ESA materials at Sai Island, Sudan. However, the Sangoan as an industry lacks solid dating and is variably assigned to an activity variant of the late Acheulean (Clark, 1982), or part of the MSA (Sheppard and Klein-dienst, 1996). The Fauresmith, consisting of small bifaces, blades and Levallois points has also been attributed to the later Middle Pleistocene in South Africa. Recent dates on the Fauresmith at Rooidam 1, Wonderwerk Cave and Kathu Pan range from >174 to 542 ka based on a variety of Uranium-Thorium, ESR and OSL methods (Chazan et al., 2008; Kiberd, 2006; Porat et al., 2010; Szabo and Butzer, 1979; Wilkins et al., 2012). The wide chronological spread of dates for the Fauresmith and the persistent ambiguity in its definition have lead some to believe the handaxe component of the Fauresmith is Acheulean, with differences in form caused by different raw materials (Humphreys, 1970). The association of this industry with characteristic MSA points may be a product of palimpsest deposits and poor chronometric control (Herries, 2011).

Aspects of MSA prepared core technologies such as Levallois core preparation methods are rooted in Acheulean production of unifacial or bifacial large cutting tools (Tryon et al., 2005). Prepared core techniques for the production of Levallois flakes appear in the Acheulean of the Kapthurin Formation, Kenya before 509 ka (Deino and McBrearty, 2002; Leakey et al., 1969). By the Late Pleistocene, and most likely before, the Acheulean is replaced by MSA industries

with relatively diverse radial, Levallois and blade prepared core technologies aimed at production of smaller flakes and hafted tools including regionally diverse unifacial and bifacial hafted point technologies (Clark, 1988; McBrearty, 2007).

The early MSA as strictly defined by pointed flakes or tools designed for hafted use (Clark, 1988) is poorly documented relative to later MSA time periods. MSA material is present in the Kapthurin Formation >284 ka (Deino and McBrearty, 2002). The MSA sites of the Gademotta Formation in the middle Ethiopian Rift and dated from >183 to 279 ka show evidence of point production as well as diverse prepared cores made of locally available obsidian (Douze, 2011, 2012, 2014; Morgan and Renne, 2008; Sahle et al., 2013; Sahle et al., 2014; Wendorf and Schild, 1974). From the recently excavated >279 ka site of Gademotta GDM7 no Levallois point cores are reported though pseudo Levallois points and several unifacially trimmed pointed pieces produced on centripetally prepared flakes or bifacially trimmed pieces made on flakes are present (Sahle et al., 2013; Sahle et al., 2014). Discoid cores and Levallois recurrent methods are reported from GDM7 in addition to casual, blade and discord cores. Levallois preferential cores are tentatively reported from Gademotta GDM7 (but see Sahle et al., 2014: 13 figure 6g). Member I of the Kibish Formation in southern Ethiopian Rift provides two *in situ* archaeological occurrences, Kamoya's Hominid Site (KHS) and Awoke's Hominid Site (AHS), from the later Middle Pleistocene Member I and dated to ~195 ka (McDougall et al., 2005, 2008; Shea, 2008). At

these two sites characteristically MSA tools such as Levallois points, Levallois cores and bifacial foliate points are made on locally available raw materials such as lavas as well as small intensely flaked chert cobbles that may have been transported a substantial distance. In the Kapthurin Formation the ~200–250 ka site of Koimilot shows characteristically MSA tools such as Levallois points and diverse methods of Levallois flake production on locally available raw materials (Tryon, 2006; Tryon, 2010; Tryon, 2003; Tryon and Faith, 2013; Tryon et al., 2005).

By the Late Pleistocene MSA technology is ubiquitous and well developed throughout Africa. Triangular Levallois points are found throughout the continent and unifacially and bifacially trimmed foliate stone points occur in many parts of Africa (Shea, 2006). These include bifacial and unifacial industries in East Africa and the Horn of Africa, tanged and bifacial points of the Aterian north of the Saharan, unifacial and bifacial foliate points from the Senegal river in West Africa and Stillbay and Howiesen's Poort points from South Africa (Brown et al., 2012b; Scerri, 2013; Scerri et al., 2015; Shea, 2006, 2008; Tribolo et al., 2015; Villa et al., 2009). The many and varied forms of these points may represent stylistic variation (Clark, 1988; Mehlman, 1977; Wurz, 1999). Other aspects of modern human behavior are well documented in association with MSA stone tools. Organic materials are used in a number of diverse ways. Bone tools are reported from Central and South Africa (Backwell et al., 2008; Brooks et al., 2004; Brooks et al., 1995; Henshilwood et al., 2001; Yellen et al., 1995). Ostrich eggshell is used for canteens (Texier et al.,

2010). Several studies argued mollusk shells are were used as pieces of personal adornment (Assefa et al., 2008; d'Errico et al., 2005; Henshilwood et al., 2004). Use of ochre as pigment and symbolic expression (Henshilwood et al., 2009; Henshilwood et al., 2002; Henshilwood et al., 2011; Villa et al., 2015) as well as hafting mastic are reported from multiple sites in South Africa (Wadley et al., 2004) and long distance transport of high quality materials such as obsidians is well documented in East Africa (Ambrose, 2012; Brown et al., 2013; Merrick and Brown, 1984; Merrick et al., 1994).

In summary, MSA technology appears some ~100 ka before the earliest known appearance of *Homo sapiens* in East Africa. MSA technology is also present in association with the first appearance of several modern behaviors including symbolic expression in Africa. MSA technology also persists ~50 kyr after anatomical and behaviorally modern human are documented as the only hominin species remaining in Africa. Thus, MSA technology is present before, during and after the acquisition of modern human biology and behavior.

## 2) Theoretical perspective:

McBrearty and Brooks (2000) provide an integrated synthesis of the African Pleistocene paleontological and archaeological records and argue that the evolution of modern human biology

and behavior is characterized by a gradual process of adaptations incrementally acquired in the Middle through Late Pleistocene of Africa. The results of this process are the biologically and behaviorally modern *Homo sapiens* known from the Late Pleistocene and Holocene of Africa and throughout the world. This model rejects any single cause (see Klein, 2000, 2008) for the appearance of behaviorally modern characteristics and suggests that understanding the evolution of *Homo sapiens* and the reasons for this species' unique traits relies on understanding the timing and pattern in which behaviorally modern traits were incrementally acquired throughout the Middle and Late Pleistocene of Africa.

By decoupling the evolution of all modern traits from a single cause, place and time period this model logically predicts aspects of human behavior including lithic technologies will both first appear and disappear at different times relative to one another in the archaeological record.

Recent work in the Middle Pleistocene of Africa and Eurasia supports this model in showing that important technological innovations of the Middle Pleistocene such as diverse Levallois core preparation methods (Adler et al., 2014) and hafting (Wilkins et al., 2012) probably emerged independently, multiple times, in different regions of Eurasia and Africa and are likely older than previously realized. Thus, a detailed regional understanding of the timing and characteristics of important technological innovations of the Middle–Late Pleistocene in East Africa is essential for any improved understanding of *Homo sapiens*' biological and behavioral evolution.

### 3) Methodological Approaches:

Two related approaches to testing the model outlined above are: 1) Gain an improved temporal resolution for Middle–Late Pleistocene sediments in order to refine the dates of existing archaeological material and 2) To produce new archaeological material in well-dated contexts showing aspects of modern human behavior are of previously unrecognized antiquity or modernity. Both these approaches improve our understanding of the timing and aspects of modern behavior elucidating the order and process in which these features occur.

Method 1) The first two papers of this dissertation improve stratigraphic and chronological resolution of the eastern Lake Victoria Basin and Kapthurin Formation of the Baringo Basin. Several approaches to establishing and improving geochronological frameworks in paleoanthropology are applied or cited in the four papers of this dissertation, but all are informed by and relate to the science of tephrostratigraphy, the lithostratigraphic and geochemical correlation of volcanoclastic deposits and their use as widespread markers in the geological record (Feibel, 1999).

East Africa provides abundant potential to demonstrate the stratigraphic and chronometric relationships among paleoanthropological sites via this method. Rifting of the East African Rift



System (Hay, 1976) provides the mechanisms for volcanic eruptions and rapid sedimentation and burial of paleoanthropological materials. The tectonic extension of this system also provides a means of subsequent exposure through continued normal faulting (Chorowicz, 2005). A well-established Pliocene and early Pleistocene tephrostratigraphic framework exists for paleoanthropological sites in Kenya, Ethiopia, Tanzania and Uganda that is the outcome of nearly 50 years of research (Brown et al., 2006; Brown et al., 1992; Feibel, 1999; Hay, 1976; McHenry et al., 2008; Pickford et al., 1991; WoldeGabriel et al., 2013). Comparatively few data are available for these areas during the Middle and Late Pleistocene (Blegen et al., 2015; Brown et al., 2012a; Morgan and Renne, 2008; Sahle et al., 2014; Tryon et al., 2010; Tryon and McBrearty, 2002, 2006; Tryon et al., 2008).

Paper #1) Distal tephras of the eastern Lake Victoria basin, equatorial East Africa: correlations, chronology and a context for early modern humans

This paper provides the first detailed regional record of Late Pleistocene tephra deposits associated with artifacts or fossils from the eastern Lake Victoria basin of western Kenya. Correlations of distal tephras from the Wasiriya beds on Rusinga Island, the Waware beds on Mfangano Island and deposits near Karungu, mainland Kenya show at least eight distinct distal tephra deposits, four of which are found at multiple localities spanning >60 km of an approximately north to south transect. New optically stimulated luminescence dates help to constrain the Late Pleisto-

cene depositional ages of these deposits. Correlation of volcaniclastic deposits expand and refine the current stratigraphy of the eastern Lake Victoria basin and provides the basis for relating fossil- and artifact-bearing sediments and a framework for ongoing geological, archaeological and paleontological studies of Late Pleistocene East Africa.

Paper #2) Tephrostratigraphy and archaeology of the Kapthurin Formation, Kenya: revised chronology and new ages for Acheulean and Middle Stone Age sites.

This paper provides an updated chronology for archaeological sites of the Kapthurin Formation, Baringo Basin, Kenya based on new tephra correlations. The refined tephrostratigraphy provides new ages for twelve archaeological sites from the later Middle Pleistocene through the earlier Late Pleistocene (~100–130 ka) of the Kapthurin Formation. These include a new minimum age of  $\geq 380 \pm 7$  ka for eight archaeological sites demonstrating diverse Levallois technology, almost 100 kyr older than previously estimated in East Africa. Additionally, correlation of the tuff capping the MSA site of Keraswanin (GnJh-78) to the Wakondo Tuff in the eastern Lake Victoria Basin ~200 km west provides new minimum ages of ~100 ka and extends the chronology of the Kapthurin Formation ~135 kyr.

Method 2) The third and fourth papers of this dissertation provide new information on the ar-

chaeology of the MSA from some of the earliest and latest MSA sites in Africa.

Paper #3) Evidence of long-distance obsidian transport and early Middle Stone Age technology at the ~200 ka BP Sibilo School Road Site GnJh-79), Baringo, Kenya:

The McBrearty and Brooks (2000) model has been widely applied and generally successful at predicting previously unrealized antiquity of aspects of modern human behavior in the African Pleistocene record. These include lithic technologies, ecological adaptations and aspects of symbolic expression (d'Errico et al., 2005; Henshilwood et al., 2004; Henshilwood, 2005; Henshilwood et al., 2001; Henshilwood et al., 2009; Henshilwood et al., 2002; Henshilwood et al., 2011; Jacobs et al., 2006; Marean, 2010; Marean et al., 2007; McBrearty and Brooks, 2000; Sahle et al., 2013; Sahle et al., 2014). The third paper in this dissertation follows in this tradition and presents geological work, archaeological excavations and artifact analysis from the 196–226 ka Sibilo School Road Site. This work shows diverse MSA technology including Levallois prepared core technologies and Levallois points as well as evidence of long-distance transport (~166 km) of raw materials were both well established features of later Middle Pleistocene hominin behavior in East Africa before 196 ka. Further, obsidian raw materials at the site transported long distances are reduced more intensely producing significantly smaller flake products.

Paper #4) The East African Middle Stone Age at < 50,000 years ago: The evidence from Nyamita

Main (GrJa-3), Rusinga Island, western Kenya.

A less widely investigated implication of the McBrearty and Brooks (2000) model is the explanation for the disappearance of MSA technology. If most or all aspects of modern human behavior are found in MSA contexts in the Pleistocene of Africa, then the disappearance of the MSA technologies after > 250 kyr of success and proliferation demands an explanation. This fourth paper in this dissertation begins to address this interesting problem and reports the MSA archaeology and paleontology at Nyamita Main (SASES= GrJa-3) from the Late Pleistocene Wasiriya beds of the Nyamita Valley, Rusinga Island in the eastern Lake Victoria Basin. New excavations as well as artifact and fossil analysis provide an updated archaeological, paleontological and taphonomic context for this site and provide data from an excavated context in the eastern Lake Victoria Basin. This work provides a modest but important data point attesting to the late survival of typologically and technological features of classic MSA in East Africa after the appearance of Later Stone Age technology in the region.

The common theme underlying the theory, methods and four papers of this dissertation is that the acquisition of modern human behavior is a process and like any process it is a function of time. Thus, understanding the timing of behavioral innovations will improve our understanding of the process.

Paper #1:

Distal tephras of the eastern Lake Victoria Basin, Equatorial East Africa: Correlations, chronology and a context for early modern humans.

Nick Blegen\*

Department of Anthropology

University of Connecticut

Storrs, CT 06269, USA

E-mail: [nicholas.blegen@uconn.edu](mailto:nicholas.blegen@uconn.edu), [nick.blegen@gmail.com](mailto:nick.blegen@gmail.com)

\*Corresponding author= Nick Blegen +1 (847) 436-3854

Christian A. Tryon

Department of Anthropology

Harvard University

Peabody Museum

11 Divinity Ave

Cambridge, MA 02138, USA

E-mail: [christiantryon@fas.harvard.edu](mailto:christiantryon@fas.harvard.edu)

J. Tyler Faith

School of Social Science

University of Queensland

Brisbane, QLD 4072, Australia

E-mail: [j.faith@uq.edu.au](mailto:j.faith@uq.edu.au)

Daniel J. Peppe

Terrestrial Paleoclimatology Research Group

Department of Geology

Baylor University

Waco, TX 76798, USA

E-mail: [daniel\\_peppe@baylor.edu](mailto:daniel_peppe@baylor.edu)

Emily J. Beverly

Terrestrial Paleoclimatology Research Group

Department of Geology

Baylor University

Waco, TX 76798, USA

E-mail: [Emily\\_Beverly@baylor.edu](mailto:Emily_Beverly@baylor.edu)

Bo Li

Centre for Archaeological Science

School of Earth & Environmental Sciences

University of Wollongong

Wollongong NSW 2522 Australia  
bli@uow.edu.au

Zenobia Jacobs  
Centre for Archaeological Science  
School of Earth & Environmental Sciences  
University of Wollongong  
Wollongong NSW 2522 Australia  
zenobia@uow.edu.au

(PUBLISHED in the journal Quaternary Science Reviews)

## Abstract

The tephrostratigraphic framework for Pliocene and Early Pleistocene paleoanthropological sites in East Africa has been well established through nearly 50 years of research, but a similarly comprehensive framework is lacking for the Middle and particularly the Late Pleistocene. We provide the first detailed regional record of Late Pleistocene tephra deposits associated with artifacts or fossils from the Lake Victoria basin of western Kenya. Correlations of Late Pleistocene distal tephra deposits from the Wasiriya beds on Rusinga Island, the Waware beds on Mfangano Island and deposits near Karungu, mainland Kenya, are based on field stratigraphy coupled with 916 electron microprobe analyses of eleven major and minor element oxides from 50 samples. At least eight distinct distal tephra deposits are distinguished, four of which are found at multiple localities spanning >60 km over an approximately north to south transect. Our correlation and characterization of volcanoclastic deposits expand and refine the current stratigraphy of the eastern Lake Victoria basin. This provides the basis for relating fossil- and artifact-bearing sediments and a framework for ongoing geological, archaeological and paleontological studies of Late Pleistocene East Africa, a crucial time period for human evolution and dispersal within and out of Africa.

Keywords: tephrostratigraphy; East Africa; Middle Stone Age; human evolution

## 1. Introduction

Fossil evidence suggests the earliest members of our species, *Homo sapiens*, first appeared in equatorial East Africa by 195 ka (Brown et al., 2012a; McDougall et al., 2005). This area likely served as one point of departure for subsequent Late Pleistocene hominin dispersals across and out of Africa (Rito et al., 2013; Rose et al., 2011). The archaeological record and environmental context of these early *H. sapiens* populations are essential data for understanding the evolutionary success of our species (e.g., Tryon and Faith, 2013). Continental and regional syntheses of the Pleistocene African archaeological and environmental records are often characterized by mismatches in temporal and spatial scales (reviewed in Blome et al., 2012; Tryon and Faith, 2013). Deep cave sequences in northern and particularly southern Africa have provided finely resolved, rich archaeological and environmental records (e.g., Avery et al., 1997; Clark-Balzan et al., 2012; Deacon, 1979; Garcea and Barton, 2010; Henshilwood et al., 2002; Jacobs et al., 2006; Marean et al., 2007; Marean et al., 2000; Singer and Wymer, 1982; Wadley and Jacobs, 2006). However, deeply stratified cave sequences are largely lacking in East Africa, where the archaeological



record consists of generally low-density open-air sites (Tryon and Faith, 2013). Demonstrating stratigraphic equivalence among these open-air sites via the correlation of tephra provides the means to assess landscape-scale spatial variation in past environments and human behaviors.

East Africa has the potential to demonstrate the equivalence among sites via tephrostratigraphy, the geochemical and lithostratigraphic correlation of tephra as widespread markers in the geological record (Brown, 2014; Lowe, 2011a, b). Rifting along the East African Rift System (EARS; Chorowicz, 2005) provides the mechanisms for volcanic eruptions, rapid sedimentation and burial of archaeological and paleontological sites, as well as their subsequent exposure through continued faulting. Although there is a well-established Pliocene and Early Pleistocene tephrostratigraphic framework for paleoanthropological sites in Kenya, Ethiopia, Tanzania and Uganda that is the outcome of nearly 50 years of research (e.g., Brown et al., 2006; Brown et al., 1992; Feibel, 1999; Hay, 1976; McHenry et al., 2008; Pickford et al., 1991; WoldeGabriel et al., 2013; WoldeGabriel et al., 2005) comparatively few data are available for these areas during the portions of the Middle and Late Pleistocene that saw the origin and dispersal of *H. sapiens* (for published exceptions, see Brown et al., 2012a; Morgan and Renne, 2008; Sahle et al., 2014; Tryon et al., 2010; Tryon and McBrearty, 2002; Tryon and McBrearty, 2006; Tryon et al., 2008).

We address this problem by focusing on archaeological and paleontological sites associated with tephra deposits in and around the eastern Lake Victoria basin, and develop a Late Pleistocene tephrostratigraphic and chronometric framework for the region. At 66,400 km<sup>2</sup>, Lake Victoria is the largest lake in Africa by surface area (Adams, 1996). The habitats surrounding this lake have undergone substantial climate-driven changes throughout the Quaternary (Bootsma and Hecky, 2003; Nicholson, 1998), likely with profound impacts on human and other animal communities (e.g., Faith et al., 2011; Faith et al., 2015; Tryon et al., 2010; Tryon et al., 2012). However, until recently, an understanding of environmental variation prior to the Last Glacial Maximum has been poorly constrained, and the nature of spatial variation in environments and human behavior obscured.

We present the results of 916 electron microprobe analyses to geochemically characterize and correlate 50 distal tephra deposits from 32 measured sections across Rusinga Island, Mfangano Island, and Karungu on the Kenyan mainland (Fig. 1 a, b), spanning a roughly north-south oriented transect over 60 km in the eastern Lake Victoria basin (eLVB). Four tuffs: the Wakondo Tuff, the Nyamita Tuff, the Nyamsingula Tuff, and the Bimodal Trachyphonolitic Tuff are suffi-

ciently distinct and widespread lithostratigraphic markers for correlation within and between discontinuous outcrops at distantly located paleontological and archaeological localities. Optically stimulated luminescence (OSL), Uranium-Thorium disequilibrium (U-Th) and AMS  $^{14}\text{C}$  dates constrain the depositional history and ages of these tuffs to >33 to ~100 ka. This stratigraphic sequence of tuffs, radiometric dates, and intercalated fossil- and artifact-bearing sediments provides the fundamental framework to assess paleoecological and archaeological variation across time and space in the eastern portion of the Lake Victoria basin.

## 2. Pleistocene distal tephra deposits, fossils, and artifacts in the eastern Lake Victoria basin

The Lake Victoria basin formed in the depression between the eastern and western branches of the EARS, probably within the last few million years (reviewed in Danley et al., 2012). The northeastern part of the Lake Victoria Basin (Fig. 1c) is unlikely to have been volcanically active since the cessation of rifting and volcanism associated with the failed Nyanza Rift in the Early Miocene (e.g., Peppe et al., 2009; Van Couvering, 1972). During the Pleistocene, the eLVB formed a repository for sediments, including volcanoclastic deposits from eruptions originating from sources outside of the basin. Tephra input appears to be from multiple sources of the central

and southern Kenyan Rift in the eastern branch of the EARS (Fig. 1b), demonstrated by tephra deposits from Kenyan and Tanzanian volcanoes mapped in areas as far west as  $\sim 35^{\circ}10'E$  (see Fig. 1b; Dawson, 2008; Peters et al., 2008; Tryon et al., 2010; Williams, 1991). Pleistocene tephra in the eLVB west of  $35^{\circ}10'E$  have been previously reported from Rusinga Island (Garrett et al., 2015; Tryon et al., 2010; Van Plantinga, 2011; Williams, 1991) and from sediment cores near Buvuma Island (Kendall, 1969: 139) within Lake Victoria, but are poorly documented due to a focus on economic geology or igneous and metamorphic suites in the region (e.g., Le Bas, 1977; Le Bas et al., 1986).

Localities with Pleistocene tephra, fossils and artifacts attributed to the Early Stone Age (ESA), Middle Stone Age (MSA), and Later Stone Age (LSA) archaeological technocomplexes are known from the eLVB in Kenya as discussed below (Faith et al., 2015; Tryon et al., 2010), as well as from Loiyangalani (HcJd-1) in the ash-rich Serengeti Plain of the eLVB in Tanzania (Fig. 1b, Anderson and Talbot, 1965; Bower and Gogan-Porter, 1981; Bower et al., 1985; Pickering, 1959; Thompson, 2005). A number of these western Kenyan sites occur  $\sim 80$ - $100$  km east of Lake Victoria's Winam Gulf, and are associated with at least two widespread marker tuffs considered useful for local field correlation. Pickford (1984) termed these the "Nyando Ash" or "Nyando



Ashes” (Fig. 1). From the area of mapped exposures of the “Nyando Ashes,” McBrearty (1981) excavated lithic artifacts and fossils from within reworked Pleistocene tephra at Songhor near the head of the Nyando River (Fig. 1b,c). McBrearty (1991, 1992) also described a sequence of twelve tuffaceous deposits at the site of Simbi in an area mapped as Nyando Ashes (Fig. 1b,c) and reported a preliminary  $^{40}\text{Ar}/^{39}\text{Ar}$  age range of ~50-200 ka (McBrearty, 1992). These preliminary dates appear to confirm the Pleistocene age of the Nyando Ashes, but the number of tuffaceous deposits documented at Songhor, Simbi and Rusinga (Garrett et al., 2015; McBrearty, 1991, 1992; Tryon et al., 2010; Van Plantinga, 2011) indicates that there are more than the two tephra deposits originally suggested by Pickford (1982; 1984).

Here we couple the first geochemical investigation of the “Nyando Ashes” with geological, archeological, and paleontological data developed during our field program investigating Pleistocene tephra, fossils, and artifacts along the margins of Lake Victoria on Rusinga Island, Mfangano Island and Karungu on the Kenyan mainland (Beverly et al., 2015b; Garrett et al., 2015; Tryon et al., 2010; Tryon et al., 2014; Van Plantinga, 2011).

3. The Wasiriya beds of Rusinga Island, the Waware beds of Mfangano Island and the Pleisto-

cene exposures of Karungu

### 3.1 The Wasiriya beds

The Wasiriya beds are exposed over an area of approximately 10 km<sup>2</sup> on the hill slopes around Rusinga Island (Fig. 2, Tryon et al., 2010). These sediments were informally named by Pickford (1984, 1986) based on previous mapping and descriptions (Kent, 1942; Van Couvering, 1972).

The first measured sections, sedimentary lithological descriptions and geochemical characterizations and correlation of tephras from the Wakondo and Nyamita localities on Rusinga Island were reported by Tryon et al. (2010). These are shown in Fig. 2, supplemented by new data from the Nyamsingula locality.

The Wasiriya beds are exposed in sections that are >10 m at their thickest points, and are comprised of three primary recognized lithologies: 1) poorly sorted coarse sand and gravel channels cemented by carbonate representing episodic channel erosion and deposition, 2) fine grained mudstone, siltstone, and silty sandstones preserving evidence of incipient soil development indicating a slightly more stable landscape, and 3) tephra that has undergone varying amounts

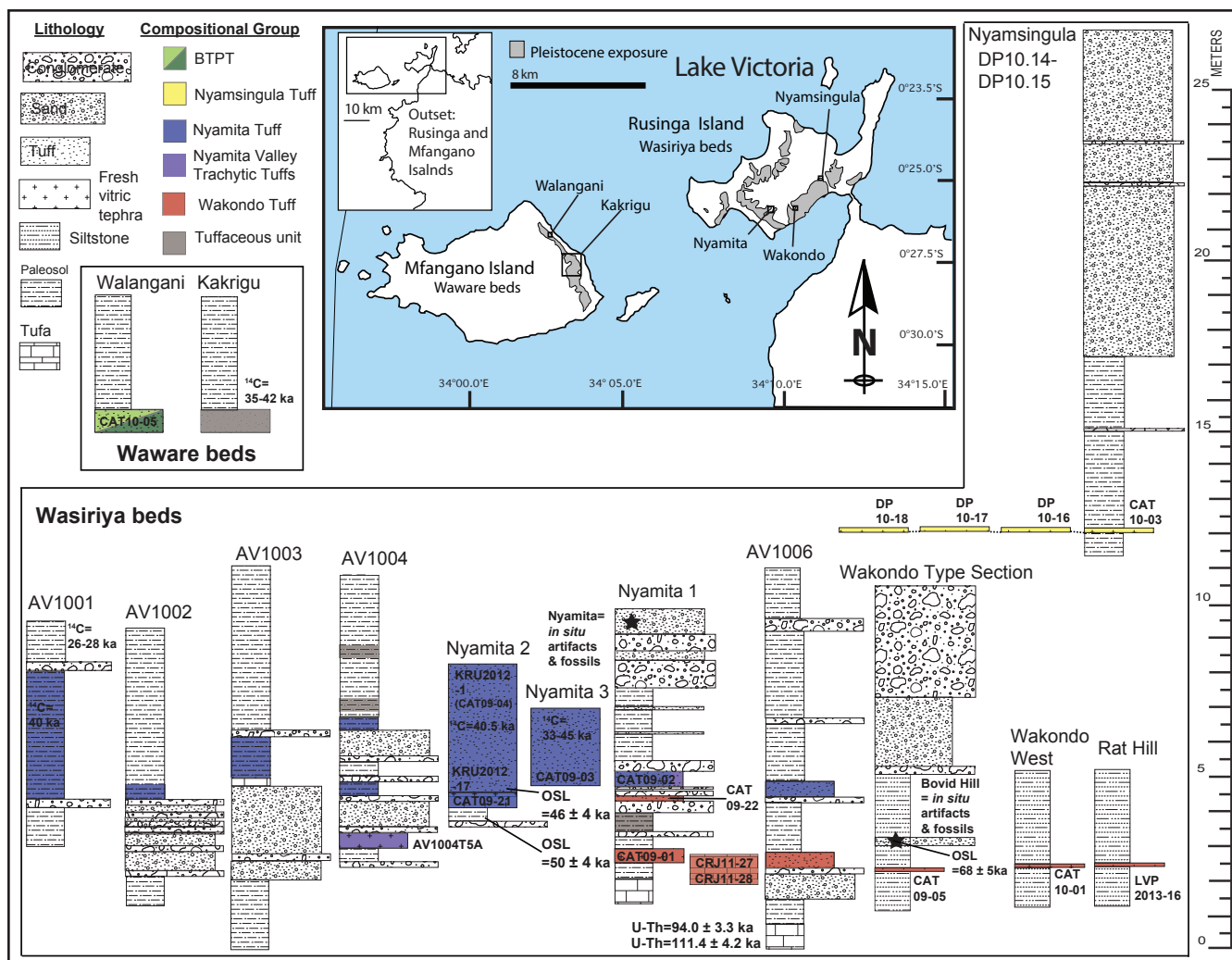


**Figure 2:** Top Center: Map of Rusinga Island and Mfangano Island showing the extent of Pleistocene outcrops of the Wasiriya beds, the Waware beds as well as archaeological and paleontological localities discussed in the text (after Tryon et al., 2010, 2012). Below: Stratigraphic columns of measured and sampled sections, arranged west (on left) to east (right). Lithologies are indicated for all units. Tuffs with electron microprobe determined chemical composition are color-coded to compositional group and labeled with sample number (ex: CAT09-21). Tuffaceous units not chemically characterized and assigned are shown in grey. Dotted lines represent tuff units that can be traced laterally in the field between two or more measured sections.



of reworking and incipient pedogenesis , (Tryon et al., 2010, 2012). AMS  $^{14}\text{C}$  dates of gastropod shells primarily from tuffaceous sediments at the Nyamita 2 and Nyamita 3 localities (Tryon et al., 2010) indicate a minimum age of 33 ka for these and underlying deposits (Tryon et al., 2010, 2012). These dated snails (*Limicolaria* cf. *martensiana*) only occur in sediments close to or at the modern surface, and are found in different types of sediments at the same elevation and position relative to the modern soil surface. These specimens also primarily occur in life position suggesting they apparently died during aestivation. Based on these observations, we interpret that the snails burrowed into the Wasiriya beds following deposition of the sediment, but prior to lithification, and thus they provide a minimum age for the deposits. U-series dates of  $94.0 \pm 3.3$  ka and  $111.4 \pm 4.2$  ka on tufa at the base of the Wasiriya beds sequence exposed at Nyamita (Fig. 2) provide a maximum age for the overlying sediments (Beverly et al., 2015). Stone artifacts from the Wasiriya beds include MSA Levallois cores and Levallois points as well as bifacial and unifacial trimmed points (Tryon et al., 2010). Fauna are abundant and include both extinct and extant taxa (Faith et al., 2011; Pickford, 1984; Pickford and Thomas, 1984; Tryon et al., 2010). Water-dependent taxa are present (e.g., Hippopotamus), but the majority of specimens indicate open, semi-arid grasslands distinct from the evergreen bushlands, woodlands, and forests historically found in the region (Garrett et al., 2015; Tryon et al., 2010, 2014).

### 3.2 The Waware beds

The Waware beds of Mfangano Island, Lake Victoria, Kenya are relatively poorly exposed over an area of  $\sim 7 \text{ km}^2$  on the northeastern periphery of the island (Fig. 2; Tryon et al., 2012). Pickford (1984, 1986) informally named the Waware beds revising previous work (Whitworth, 1961). These deposits, which are all  $< 5 \text{ m}$  thick, preserve fluvial sediments with incipient soil development and reworked tuffaceous deposits that unconformably overlie Miocene sediments (Tryon et al., 2012). The fossil and artifact bearing portions of the Waware beds deposits are comprised of fine-grained sandy mudstone and siltstone beds with evidence for varying degrees of pedogenesis interbedded with occasional coarser grained sandstone and conglomerate channel deposits (Tryon et al., 2012).

Based on perceived similarity of Lake Victoria's base level at the times these various beds were deposited, Pickford (1984: 105) inferred that the Waware beds on Mfangano, the Wasiriya beds on Rusinga, and the Apoko Formation of the Homa Peninsula were deposited during the same time period in the Late Pleistocene. The only radiometric ages for the Pleistocene Waware beds

on Mfangano Island are AMS  $^{14}\text{C}$  dates of 35-42 ka on gastropod shells from the Kakrigu locality (Fig. 2; Tryon et al., 2012). As is the case in the Wasiriya beds on Rusinga Island, the snails (*Limicolaria* cf. *martensiana*) postdate deposition of the Waware beds, and therefore provide minimum age constraints. Based on the similar radiocarbon ages from the snails and that the lithofacies of the Waware and Wasiriya beds are identical, we have also suggested that the Waware and Wasiriya beds are most likely contemporaneous (e.g. Garrett et al., 2015; Tryon et al., 2012). The archaeology of Mfangano Island as described from surface collected stone artifacts also consists of Levallois technology and bifacial points (Tryon et al., 2012). The fauna are similar to those from Rusinga Island and also indicate an open and arid environment relative to the present (Garrett et al., 2015; Tryon et al., 2012).

### 3.3 Karungu

The Pleistocene beds of Karungu, Kenya, crop out around the town of Sori on the Kenyan mainland (Fig. 3). These beds are discontinuously exposed over an area of  $\sim 40 \text{ km}^2$  and are up to 10.5 m in thickness, overlying eroded topography of Miocene bedrock (Pickford, 1984). The Pleistocene deposits are best exposed at the localities of Kisaaka, Aringo, Aoch Nyasaya and Obware

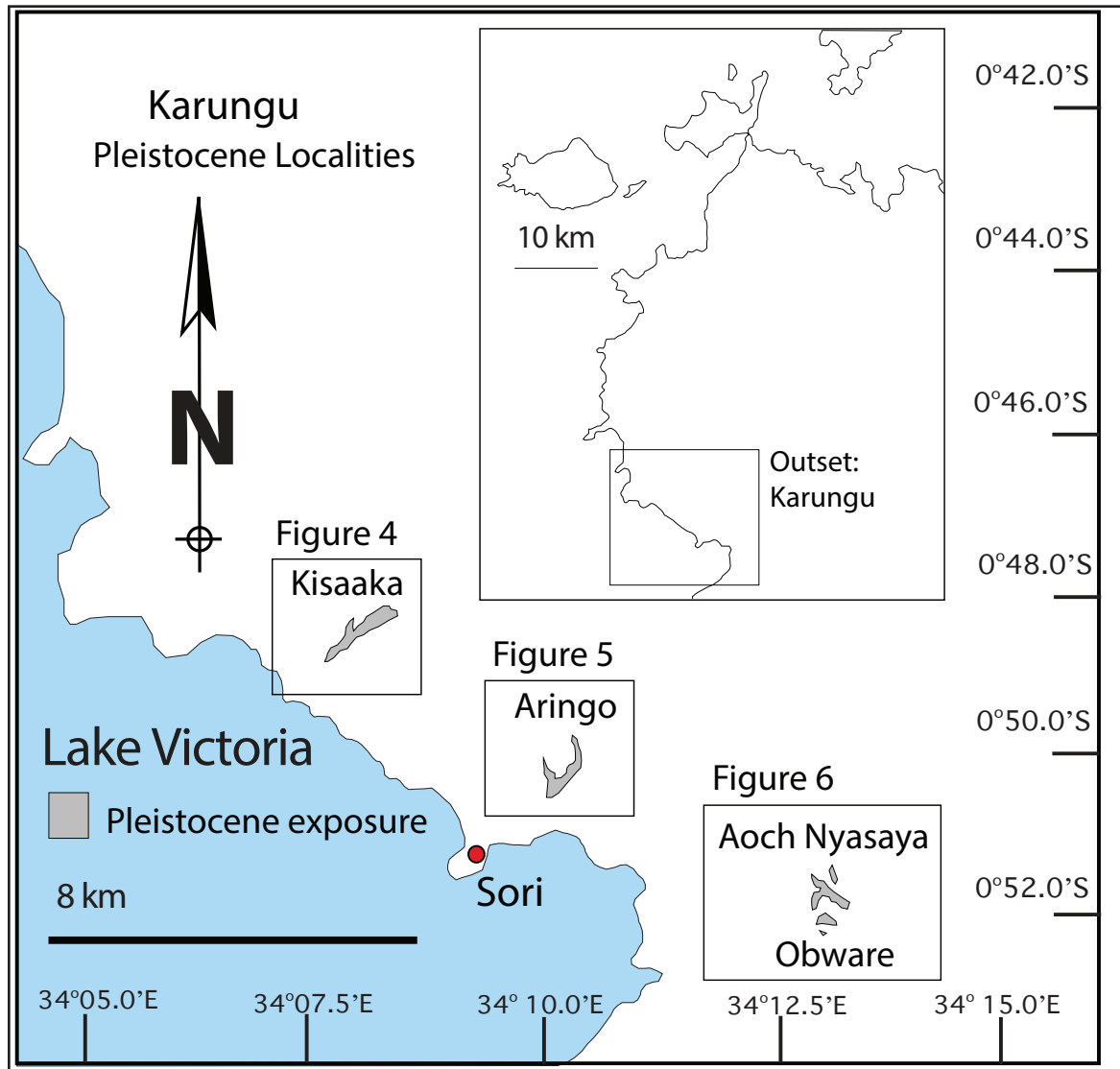


Figure 3: Map of Karungu area around the town of Sori showing localities of Pleistocene exposure: Aringo, Aoch Nyasaya, Kisaaka and Obware.

(Figs. 4, 5, 6; Faith, 2014; Faith et al., 2014), with the most extensive and thickest exposures at Kisaaka (Figs. 3, 4; Beverly et al., 2015b; Faith et al., 2015). The deposits are Karungu are comprised of fine grained siltstone and mudstone beds that have been pedogenically modified into paleo-Vertisols and paleo-Inceptisols, conglomeratic beds that represent fluvial channels, variably reworked tephra, and tufas deposited by local springs (Beverly et al., 2015b; Faith et al.,

2015). On the basis of field characteristics of two widespread tuffs at Karungu, Pickford (1984) proposed correlations among exposures at Karungu, and between Karungu and other western Kenyan Pleistocene localities where the “Nyando Ashes” were also present.

Like the Wasiriya beds and Waware beds described above, all *in situ* and most surface collected stone artifacts documented during fieldwork at Karungu from 2010-2013 are characteristically MSA, including Levallois cores and bifacially worked MSA points. The fauna from Karungu resembles that of the Wasiriya and Waware beds in displaying both extinct and extant taxa, the majority of which indicate an open and semi-arid grassland environment (Faith, 2014; Faith et al., 2015).

#### 4. Tephra Correlation Materials and Methods

##### 4.1 Materials

All 50 tuff samples analyzed for this study were collected from or can be stratigraphically linked to a series of 32 sections <0.50 m to >10 m thick measured from Pleistocene outcrops on Rusinga Island, Mfangano Island and Karungu between 2009 and 2013. Geographic locations, lithologies, and the location of archaeological and paleontological sites are shown in figures 2-6 and 8 with geographic coordinates for each stratigraphic section provided in Table 2. Whenever



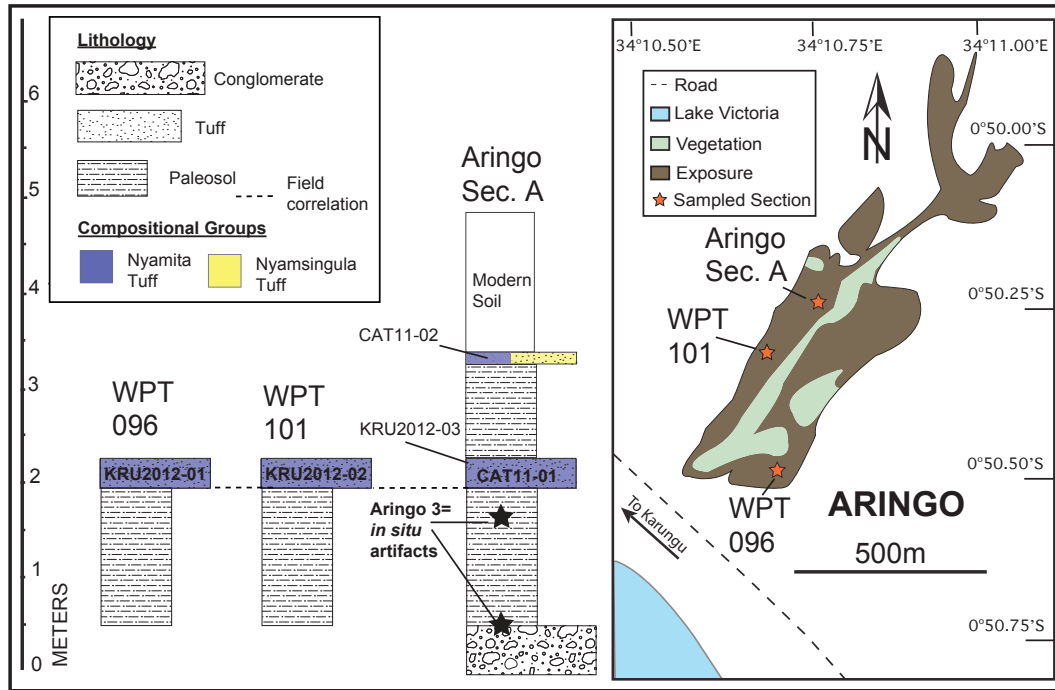


Figure 5: Right: Map of Aringo locality showing extent of Pleistocene exposure (after Beverly et al., 2015) and locations of measured and sampled sections. Left: Stratigraphic columns of measured sections at Aringo, arranged south (on left) to north (right). Lithologies indicated for all units. Tuffs with electron microprobe determined chemical composition are color-coded to compositional group and labeled with sample number.

possible, tuffs were sampled from sections with multiple tephra deposits exposed in stratigraphic succession. Field correlations were made by walking exposures and by using a Jacob's staff and Abney level to establish the stratigraphic equivalence between exposed tuffs. Both field and laboratory methods of correlation are necessary as exposures are discontinuous and tephra deposits in the eLVB vary widely in their thickness, amount of subsequent soil development, and amount and/or size of natural glass.

## 4.2 Methods

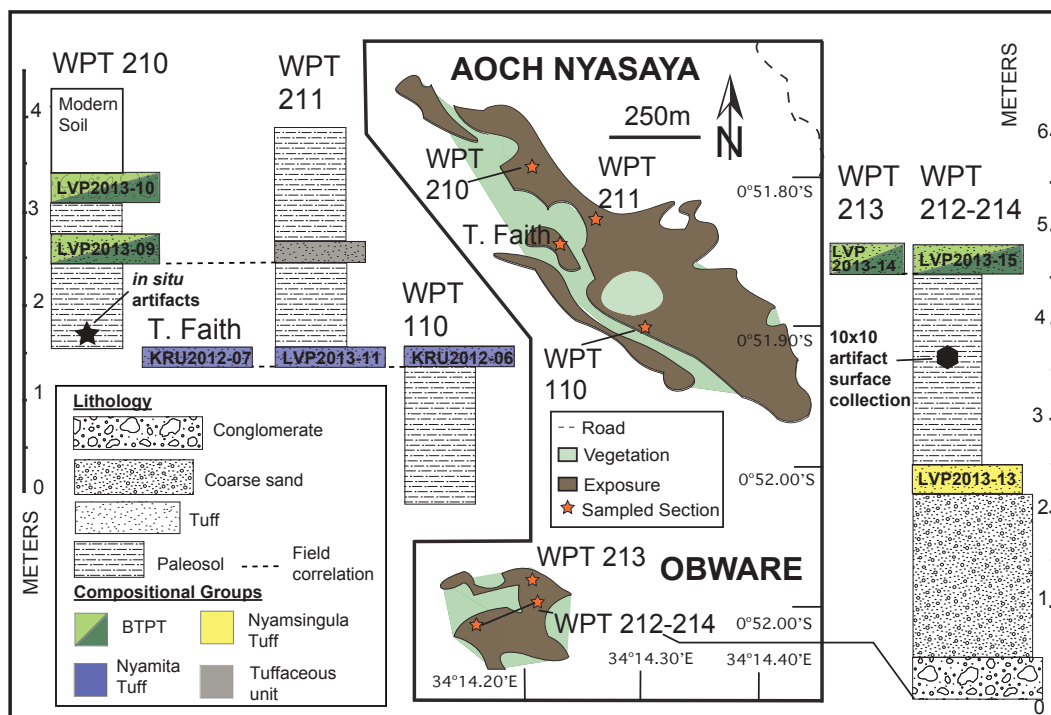


Figure 6: Center: Map of Aoch Nyasaya and Obware showing extent of Pleistocene exposure and locations of measured sections (after Beverly et al., in press). Left: Stratigraphic columns of measured sections at Aoch Nyasaya, arranged northwest (left) to southeast (right). Right: Measured section at Obware. Lithologies are indicated for all units. Tuffs with electron microprobe determined chemical composition are color-coded to compositional group and labeled with sample number. Dotted lines represent tuff units that can be traced laterally in the field between two or more measured sections. Sections were not measured for samples KRU2012-7 at Aoch Nyasaya or LVP2013-14 at Obware.

All samples were examined in hand specimen, with low power (10x) magnification in the field, and in thin section from selected specimens using a petrographic microscope at 40-100x magnifications. However, like the vast majority of tephra deposits in East Africa (Brown and McDougall, 2011), the lithological characteristics of the tuffs in outcrop and under magnification are generic and insufficient for correlation due to aeolian fractionation (density-driven separation of the vitric, crystal and lithic phases with increased distance from the source) and varied syn- and



Table 1: Mean major and minor element oxides by weight percent. One standard deviation from the mean listed below each element oxide mean.

<b>Wakondo Tuff</b>	No	M,N	SiO <sub>2</sub>	TiO <sub>2</sub>	ZrO <sub>2</sub>	Al <sub>2</sub> O <sub>3</sub>	FeO	MnO	MgO	CaO	Na <sub>2</sub> O	K <sub>2</sub> O	F	Cl	Sum	less O	Sum less O	H <sub>2</sub> O	Total
CAT09-05	17	1,1	61.67	0.54	0.07	15.51	7.97	0.36	0.32	1.02	9.01	4.75	0.46	0.31	102	0.26	101.73	0.03	100.87
			1.39	0.09	0.04	0.28	0.19	0.02	0.02	0.03	0.54	0.51	0.19	0.01	2.36	0.08	2.41	0.88	1.88
CAT09-01	20	1,1	60.56	0.51	0.08	15.65	8.11	0.36	0.33	1.04	9.18	4.79	0.38	0.31	101.32	0.23	101.09	0.62	100.81
			1.03	0.09	0.05	0.15	0.14	0.03	0.02	0.04	0.24	0.26	0.06	0.02	1.15	0.03	1.14	0.88	0.47
CAT09-22	11	1,1	58.73	0.56	0.07	15.28	7.41	0.31	0.33	1.02	9.12	4.61	0.25	0.28	97.97	0.17	97.8	2.27	99.24
			0.81	0.09	0.07	0.28	0.42	0.04	0.02	0.03	1.08	0.5	0.11	0.02	1.14	0.05	1.11	0.8	0.79
CAT10-01	18	1,1	61.53	0.56	0.09	15.34	7.94	0.36	0.32	1.02	8.73	4.5	0.27	0.31	100.97	0.18	100.78	-0.3	99.6
			2.26	0.06	0.04	0.34	0.22	0.03	0.02	0.06	0.76	0.72	0.04	0.02	3.71	0.02	3.72	1.31	2.81
KRU2012-15	18	1,1	57.23	0.52	0.08	15.41	7.78	0.35	0.33	0.98	8.34	4.3	0.44	0.31	96.07	0.25	95.81	5.63	100.58
			2.15	0.06	0.04	0.38	0.22	0.02	0.02	0.04	0.88	0.84	0.11	0.01	4.13	0.05	4.14	1.6	2.72
CRJ11-27	8	1,1	59.5	0.59	0.12	16.04	8.05	0.35	0.33	1.09	5.96	1.76	0.39	0.32	94.51	0.23	94.27	3.87	97.25
			1.3	0.08	0.02	0.21	0.19	0.03	0.02	0.05	0.59	1.02	0.17	0.01	2.15	0.07	2.14	1.71	0.88
CRJ11-28	8	1,1	59.39	0.62	0.11	15.77	8.03	0.33	0.34	1.05	5.53	1.88	0.4	0.29	93.73	0.23	93.49	3.78	96.39
			0.73	0.09	0.03	0.21	0.17	0.03	0.02	0.04	1	1.22	0.23	0.03	2.83	0.1	2.83	1.57	1.55
LVP2013-16	10	1,1	62.07	0.55	0.1	15.61	8.34	0.36	0.35	1.1	8.67	4.93	0.52	0.28	102.89	0.28	102.61	0.24	101.91
			1.51	0.06	0.05	0.56	0.5	0.02	0.03	0.1	1.08	0.31	0.25	0.02	3.47	0.1	3.55	1.5	2.1
<b>Nyamita Tuff</b>	No	M,N	SiO <sub>2</sub>	TiO <sub>2</sub>	ZrO <sub>2</sub>	Al <sub>2</sub> O <sub>3</sub>	FeO	MnO	MgO	CaO	Na <sub>2</sub> O	K <sub>2</sub> O	F	Cl	Sum	less O	Sum less O	H <sub>2</sub> O	Total
CAT09-21	21	1,1	64.38	0.59	0.05	15.62	6.76	0.29	0.36	1.13	7.73	5.02	0.26	0.17	102.36	0.15	102.21	-0.66	100.8
			1.16	0.08	0.04	0.14	0.13	0.03	0.02	0.04	0.28	0.42	0.15	0.01	1.51	0.06	1.49	1.09	0.53
CAT09-02b	12	1,2	62.03	0.58	0.04	15.55	6.78	0.29	0.36	1.13	7.58	4.83	0.13	0.18	99.47	0.09	99.38	1.46	100.08
			1.54	0.08	0.05	0.16	0.17	0.03	0.01	0.03	0.39	0.39	0.05	0.02	2.13	0.02	2.14	0.86	1.55
CAT09-03	27	1,1	60.47	0.58	0.07	15.87	6.86	0.29	0.36	1.2	7.14	4.54	0.27	0.17	97.81	0.15	97.66	1.41	98.31
			1.31	0.09	0.04	0.49	0.1	0.03	0.02	0.05	0.69	1.24	0.1	0.02	2.71	0.04	2.71	1.16	2.15
CAT 11-01	17	1,1	59.99	0.6	0.06	15.32	6.62	0.27	0.36	1.1	7.72	4.79	0.09	0.18	97.09	0.08	97.01	3.13	99.4
			1.88	0.1	0.04	0.37	0.16	0.03	0.01	0.05	0.56	0.37	0.04	0.02	2.91	0.02	2.91	1.5	1.7
CAT11-02a	19	1,2	60.04	0.55	0.06	15.47	6.58	0.28	0.35	1.11	7.69	5.06	0.27	0.16	97.62	0.15	97.47	3.31	100.05
			1.42	0.08	0.04	0.36	0.55	0.05	0.04	0.07	0.33	0.58	0.13	0.02	2.13	0.06	2.12	1.38	1.13

CAT11-05	16	1,1	59.37	0.58	0.08	16.03	6.93	0.37	0.37	1.18	5.32	1.72	0.24	0.18	92.38	0.14	92.23	3.42	94.88
			1.82	0.08	0.05	0.48	0.27	0.11	0.02	0.06	1.13	0.92	0.2	0.01	3.55	0.08	3.52	1.43	2.38
KRU2012-01	19	1,1	61.28	0.57	0.05	15.5	6.48	0.28	0.34	1.11	7.68	4.99	0.08	0.16	98.51	0.07	98.44	2.44	100.16
			1.25	0.1	0.05	0.28	0.57	0.03	0.04	0.08	0.39	0.26	0.06	0.02	1.53	0.03	1.53	1.07	1.07
KRU2012-02	20	1,1	60.68	0.6	0.08	15.29	6.55	0.26	0.33	1.06	7.41	4.8	0.08	0.16	97.3	0.07	97.23	2.81	99.31
			0.98	0.11	0.04	0.4	0.54	0.06	0.07	0.23	1.28	1.41	0.05	0.04	2.27	0.03	2.26	1.55	1.07
KRU2012-03	19	1,1	54.76	0.63	0.05	15.84	6.79	0.28	0.37	1.1	7.67	4.57	0.3	0.16	92.54	0.16	92.38	9.13	100.75
			2.15	0.08	0.04	0.13	0.15	0.03	0.02	0.04	0.33	0.56	0.13	0.01	2.64	0.06	2.65	1.33	1.47
KRU2012-06	20	1,1	56.31	0.61	0.04	15.47	6.68	0.27	0.37	1.05	7.4	4.36	0.27	0.18	93	0.15	92.84	7.83	99.93
			2.42	0.07	0.04	0.64	0.2	0.03	0.03	0.09	0.81	0.75	0.1	0.03	4.38	0.04	4.39	1.33	3.42
KRU2012-07	14	1,1	60.14	0.61	0.04	15.42	6.95	0.27	0.36	1.12	7.83	4.98	0.12	0.17	98.01	0.09	97.92	1.97	99.12
			1.29	0.06	0.04	0.38	0.17	0.03	0.03	0.04	0.5	0.33	0.05	0.01	2.03	0.02	2.02	1.2	1.97
KRU2012-10	16	1,1	59.08	0.56	0.02	15.89	6.84	0.28	0.36	1.12	7.63	4.76	0.27	0.16	96.97	0.15	96.82	5.83	101.48
			1.2	0.06	0.05	0.3	0.12	0.03	0.01	0.04	0.47	0.64	0.05	0.01	2.18	0.02	2.19	1.1	1.58
KRU2012-11	18	1,1	58.79	0.6	0.05	15.72	6.77	0.27	0.36	1.08	7.59	4.16	0.29	0.17	95.53	0.16	95.37	7.15	102.12
			1.18	0.06	0.05	0.19	0.12	0.03	0.01	0.06	0.53	0.63	0.07	0.02	2.07	0.03	2.06	0.94	1.68
KRU2012-13	18	1,1	57.9	0.56	0.05	15.61	6.75	0.3	0.36	1.09	7.36	4.23	0.35	0.17	94.72	0.18	94.54	7	100.79
			1.78	0.08	0.04	0.39	0.15	0.03	0.03	0.05	0.53	0.65	0.21	0.02	2.96	0.09	2.96	1.14	2.34
KRU2012-16	18	1,1	59.56	0.57	0.04	15.82	6.67	0.28	0.35	1.09	7.9	4.86	0.31	0.18	97.63	0.17	97.46	4.73	101.45
			1.02	0.08	0.08	0.19	0.22	0.03	0.04	0.04	0.42	0.41	0.11	0.06	1.5	0.06	1.48	1.22	0.65
KRU2012-17	17	1,1	59.14	0.58	0.04	15.75	6.63	0.28	0.36	1.08	7.62	4.11	0.37	0.17	96.13	0.19	95.94	4.82	100.02
			1.49	0.07	0.05	0.16	0.13	0.03	0.02	0.03	0.37	0.48	0.17	0.01	2.05	0.07	2.07	1.38	1.04
KRU2012-18	10	1,1	61.47	0.56	0.08	15.4	6.55	0.28	0.38	1.08	7.37	4.77	0.47	0.17	98.59	0.24	98.35	2.76	100.37
			1.92	0.09	0.04	0.51	0.42	0.03	0.11	0.07	0.72	0.27	0.17	0.02	3.53	0.07	3.53	1.68	2.19
LVP2013-01	20	1,1	62.18	0.59	0.08	15.92	6.67	0.3	0.35	1.13	6.98	5.11	0.44	0.17	99.93	0.22	99.71	2.28	101.24
			0.95	0.04	0.04	0.27	0.22	0.02	0.01	0.05	0.36	0.22	0.17	0.01	1.67	0.07	1.73	1.04	1.63
LVP2013-02	19	1,1	62.13	0.58	0.1	15.89	6.71	0.28	0.33	1.1	7.09	5.01	0.44	0.17	99.82	0.22	99.6	2.7	101.55
			0.75	0.05	0.04	0.14	0.08	0.03	0.04	0.09	0.5	0.21	0.08	0.02	1.35	0.04	1.35	1.32	0.58
LVP2013-03a	3	1,2	62.48	0.59	0.06	15.97	6.73	0.27	0.34	1.12	6.99	5.24	0.42	0.16	100.38	0.21	100.17	2.11	101.53
			0.36	0.03	0.03	0.1	0.1	0.01	0.01	0.04	0.23	0.14	0.02	0	0.68	0.01	0.69	0.92	0.24

LVP2013-04	20	1,1	61.41	0.6	0.08	15.56	6.57	0.29	0.36	1.11	6.9	5.06	0.46	0.16	98.56	0.23	98.33	2.65	100.25
			0.8	0.04	0.04	0.25	0.1	0.03	0.02	0.05	0.35	0.22	0.06	0.01	1.38	0.02	1.38	1.15	1.02
LVP2013-06	20	1,1	61.75	0.59	0.09	15.82	6.61	0.29	0.36	1.1	6.92	5.15	0.44	0.16	99.28	0.22	99.06	2.34	100.67
			1.01	0.03	0.06	0.24	0.14	0.03	0.02	0.04	0.26	0.2	0.05	0.01	1.62	0.02	1.63	1.32	1.05
LVP2013-07a	14	1,2	62.25	0.6	0.1	15.98	6.55	0.28	0.36	1.08	6.83	5.12	0.49	0.16	99.8	0.24	99.56	1.77	100.6
			1.32	0.05	0.04	0.33	0.14	0.02	0.01	0.06	0.38	0.23	0.17	0.02	2.14	0.07	2.19	1.5	1.14
LVP2013-11	16	1,1	63.25	0.59	0.1	16.28	6.56	0.31	0.36	1.15	7.12	5.19	0.45	0.16	101.52	0.23	101.29	1.23	101.79
			0.74	0.05	0.05	0.21	0.39	0.04	0.02	0.06	0.37	0.24	0.1	0.01	1.37	0.04	1.39	1.69	0.9
12KIS26	16	1,1	62.96	0.58	0.09	16.27	6.44	0.29	0.36	1.15	6.87	5.08	0.46	0.17	100.73	0.23	100.49	2.35	102.12
			1.08	0.03	0.04	0.22	0.1	0.06	0.02	0.07	0.35	0.23	0.06	0.02	1.62	0.03	1.62	1.48	0.64
12KIS28	13	1,1	62.82	0.61	0.08	16.13	6.56	0.3	0.37	1.11	7.04	5.01	0.53	0.17	100.72	0.26	100.45	0.02	99.75
			1.72	0.04	0.04	0.36	0.15	0.03	0.02	0.05	0.45	0.26	0.12	0.01	2.78	0.05	2.8	0.01	2.79
<b>Nyamsingula Tuff</b>	No	M,N	<b>SiO<sub>2</sub></b>	<b>TiO<sub>2</sub></b>	<b>ZrO<sub>2</sub></b>	<b>Al<sub>2</sub>O<sub>3</sub></b>	<b>FeO</b>	<b>MnO</b>	<b>MgO</b>	<b>CaO</b>	<b>Na<sub>2</sub>O</b>	<b>K<sub>2</sub>O</b>	<b>F</b>	<b>Cl</b>	<b>Sum</b>	<b>less O</b>	<b>Sum less O</b>	<b>H<sub>2</sub>O</b>	<b>Total</b>
CAT10-03	15	1,1	58.16	0.45	0.18	16.22	6.73	0.3	0.27	0.99	9.24	5	0.61	0.4	98.57	0.35	98.22	3.54	101.01
			1.16	0.06	0.04	0.29	0.34	0.03	0.04	0.06	0.44	0.4	0.12	0.06	1.49	0.06	1.48	0.87	0.79
CAT11-02b	6	2,2	59.88	0.41	0.18	15.83	7.18	0.33	0.19	1.03	8.97	4.73	0.44	0.38	99.55	0.27	99.28	1.35	99.83
			0.62	0.06	0.03	0.2	0.27	0.05	0.02	0.06	0.44	0.2	0.07	0.05	1.23	0.04	1.23	1.06	0.5
DP10-16	20	1,1	58.84	0.44	0.19	16.31	6.6	0.3	0.3	1.02	8.99	5.05	0.58	0.39	99.02	0.33	98.69	2.56	100.51
			1.11	0.04	0.06	0.31	0.4	0.03	0.04	0.08	0.46	0.47	0.09	0.07	1.42	0.05	1.4	0.92	0.73
DP10-17	15	1,1	59.14	0.43	0.18	16.3	6.45	0.29	0.28	1.02	9.29	4.82	0.59	0.4	99.19	0.34	98.85	2.73	100.87
			0.81	0.08	0.05	0.27	0.18	0.04	0.02	0.04	0.44	0.32	0.1	0.04	1.49	0.05	1.47	0.62	1.19
DP10-18	17	1,1	59.41	0.45	0.19	16.31	6.34	0.28	0.29	1.03	9.04	4.98	0.58	0.38	99.27	0.33	98.94	2.58	100.82
			0.84	0.08	0.04	0.17	0.12	0.03	0.04	0.03	0.63	0.25	0.17	0.04	1.47	0.08	1.44	1.02	0.89
LVP2013-3b	31	2,2	60.94	0.44	0.22	16.17	7.16	0.33	0.19	1.01	8.06	4.89	0.81	0.38	100.59	0.43	100.16	1.96	101.32
			0.98	0.04	0.06	0.23	0.23	0.03	0.02	0.08	0.45	0.28	0.13	0.05	1.51	0.06	1.53	1.18	1.06
LVP2013-7b	6	2,2	61.17	0.44	0.21	16.32	7.14	0.32	0.19	1	7.93	4.88	0.78	0.4	100.78	0.42	100.36	1.98	101.54
			0.4	0.05	0.04	0.14	0.11	0.02	0.02	0.07	0.54	0.13	0.09	0.05	1.07	0.05	1.09	0.95	0.49
LVP2013-8	13	1,1	60.99	0.45	0.21	16.16	7.04	0.32	0.2	1.02	7.62	4.82	0.75	0.36	99.93	0.4	99.53	1.8	100.55
			2	0.05	0.04	0.61	0.27	0.03	0.03	0.08	0.7	0.28	0.07	0.04	3.56	0.03	3.58	1.31	2.68
LVP2013-13	12	1,1	61.39	0.46	0.24	16.99	6.41	0.3	0.31	1.03	7.57	5.14	0.78	0.36	100.98	0.41	100.57	2.17	102.02

			1.56	0.05	0.06	0.42	0.31	0.02	0.04	0.07	0.8	0.29	0.1	0.07	2.35	0.06	2.38	1.35	1.48
12KIS34	19	1,1	60.32	0.43	0.22	16.15	7.01	0.31	0.21	1.03	7.89	4.79	0.89	0.39	99.65	0.46	99.19	2.78	101.18
			1.65	0.1	0.07	0.33	0.3	0.03	0.08	0.15	0.7	0.32	0.27	0.11	2.44	0.13	2.49	1.47	1.69
<b>BTPT</b>	No	M,N	<b>SiO<sub>2</sub></b>	<b>TiO<sub>2</sub></b>	<b>ZrO<sub>2</sub></b>	<b>Al<sub>2</sub>O<sub>3</sub></b>	<b>FeO</b>	<b>MnO</b>	<b>MgO</b>	<b>CaO</b>	<b>Na<sub>2</sub>O</b>	<b>K<sub>2</sub>O</b>	<b>F</b>	<b>Cl</b>	<b>sum</b>	<b>less O</b>	<b>Sum less O</b>	<b>H<sub>2</sub>O</b>	<b>Total</b>
CAT11-07a	7	1,2	62.25	0.66	0.1	12.72	9.14	0.44	0.2	0.99	8.2	4.76	0.38	0.26	100.11	0.22	99.89	0.72	99.6
			0.52	0.11	0.07	0.14	0.18	0.04	0.01	0.05	0.25	0.17	0.12	0.02	0.82	0.05	0.83	0.58	0.35
CAT11-07b	13	2,2	61.92	0.81	0.02	15.22	7.07	0.33	0.43	1.4	7.25	5.46	0.2	0.11	100.21	0.11	100.1	1.14	100.46
			0.86	0.11	0.04	0.3	0.39	0.04	0.08	0.11	0.46	0.17	0.2	0.02	1.28	0.09	1.22	0.71	0.79
CAT10-05a	9	1,2	62.24	0.69	0.12	12.64	9.01	0.44	0.21	0.97	7.08	4.44	0.51	0.26	98.61	0.27	98.34	0.53	97.86
			0.43	0.03	0.03	0.14	0.19	0.03	0.02	0.04	0.51	0.16	0.06	0.02	1.05	0.03	1.04	0.67	0.77
CAT10-05b	3	2,2	61.28	0.79	0.04	15.23	6.94	0.36	0.43	1.37	6.21	5.43	0.32	0.11	98.51	0.16	98.35	0.1	97.68
			1.73	0.07	0.02	0.5	0.24	0.03	0.02	0.07	0.27	0.23	0.02	0.03	3.06	0.01	3.07	1.14	1.93
LVP2013-09a	15	1,2	64.03	0.68	0.13	13.33	8.97	0.44	0.21	1.05	7.45	4.64	0.62	0.24	101.79	0.32	101.47	0.25	100.73
			0.85	0.06	0.04	0.47	0.49	0.04	0.03	0.11	0.4	0.15	0.12	0.02	1.28	0.05	1.26	0.79	1.23
LVP2013-09b	12	2,2	62.97	0.78	0.06	15.74	7	0.35	0.42	1.4	6.5	5.36	0.43	0.1	101.1	0.2	100.9	1.12	101.24
			0.86	0.06	0.05	0.35	0.41	0.04	0.06	0.08	0.34	0.13	0.06	0.02	1.15	0.03	1.14	1.44	1.35
LVP2014-10a	14	1,2	62.66	0.66	0.12	12.78	8.86	0.43	0.2	0.97	7.37	4.63	0.54	0.26	99.49	0.29	99.2	-0.21	98
			1.49	0.07	0.04	0.4	0.5	0.05	0.04	0.09	0.68	0.16	0.06	0.02	2.23	0.03	2.22	1.22	2.15
LVP2014-10b	6	2,2	62.05	0.78	0.02	15.5	6.84	0.34	0.41	1.38	6.52	5.37	0.33	0.1	99.64	0.16	99.48	0.2	98.92
			0.47	0.07	0.03	0.37	0.24	0.04	0.07	0.08	0.43	0.18	0.04	0.02	0.9	0.02	0.89	1.1	0.62
LVP2014-14a	7	1,2	63.81	0.65	0.13	12.57	8.24	0.34	0.13	0.98	6.39	4.61	0.47	0.25	98.57	0.25	98.32	1.22	98.62
			1.04	0.04	0.06	0.47	0.37	0.03	0.02	0.08	0.26	0.22	0.06	0.04	1.54	0.03	1.53	1.16	0.83
LVP2014-14b	13	2,2	62.1	0.77	0.05	14.73	6.78	0.31	0.37	1.45	5.79	5.3	0.32	0.11	98.07	0.16	97.91	1.2	98.35
			1.77	0.1	0.05	0.55	0.44	0.04	0.13	0.13	0.48	0.35	0.07	0.03	2.46	0.03	2.47	1.78	1.24
LVP2013-15a	5	1,2	65.25	0.63	0.12	13.25	8.73	0.4	0.18	1.09	6.81	4.66	0.54	0.24	101.89	0.28	101.61	0.38	101.01
			1.72	0.03	0.08	0.62	0.54	0.04	0.13	0.17	1.01	0.23	0.08	0.03	1.7	0.03	1.68	1.65	0.39
LVP2013-15b	21	2,2	63.2	0.77	0.05	15.33	6.82	0.31	0.41	1.52	6.2	5.42	0.37	0.1	100.5	0.18	100.32	2.49	102.05
			1.27	0.04	0.04	0.47	0.36	0.04	0.1	0.09	0.26	0.16	0.05	0.02	1.42	0.02	1.41	1.48	0.54

Unique Tuffs	No	M,N	SiO <sub>2</sub>	TiO <sub>2</sub>	ZrO <sub>2</sub>	Al <sub>2</sub> O <sub>3</sub>	FeO	MnO	MgO	CaO	Na <sub>2</sub> O	K <sub>2</sub> O	F	Cl	Sum	less O	Sum less O	H <sub>2</sub> O	Total
AV1004T5A	15	1,1	63.83	0.52	0.2	10.8	8.05	0.35	0.14	0.66	7.16	3.74	0.65	0.31	96.41	0.34	96.06	1.57	96.73
			2.08	0.07	0.04	0.16	0.14	0.03	0.03	0.02	0.83	0.52	0.17	0.02	2.9	0.07	2.9	1.46	1.88
CAT09-02a	5	1,2	64.8	0.62	0.17	10.51	9.39	0.37	0.13	0.68	7.54	3.31	0.56	0.35	98.44	0.32	98.12	1.23	98.3
			1	0.08	0.07	0.12	0.22	0.02	0.01	0.03	0.72	0.79	0.04	0.01	2.43	0.02	2.42	1.3	1.25
X-5A-3	14	1,1	57.9	0.63	0.15	13.75	9.2	0.43	0.37	1.22	8.39	4.81	0.53	0.21	97.62	0.27	97.34	0.48	96.8
			1.46	0.07	0.06	0.14	0.19	0.03	0.01	0.04	0.38	0.17	0.09	0.02	1.49	0.04	1.49	0.77	0.81
LVP2013-05	14	1,1	71.21	0.13	0.41	10.3	3.96	0.06	0.02	0.1	4.75	4.14	1.18	0.44	96.7	0.6	96.11	4.62	100.29
			0.95	0.03	0.07	0.43	0.19	0.02	0.01	0.04	0.22	0.13	0.11	0.04	1.15	0.05	1.17	0.61	1.05

post-depositional environments. Although crystal composition can be useful in some settings where glass is not preserved (e.g., McHenry, 2012; McHenry et al., 2008; Smith et al., 2011), we base our correlations on chemical analysis of volcanic glass shards, characterized by electron probe microanalysis of eleven major element oxide proportions (Brown and Nash, 2014). Glass composition provides the most diagnostic ‘fingerprint’ for correlation purposes (Lowe, 2011a). Correlation identifies deposits that derive from the same eruption, but because tephra can be reworked during and following initial sedimentation (see Orton, 1996 for an extensive review), the presence of the same tephra in multiple outcrops does not necessarily define an isochron or time-plane. Following the terminology of Feibel et al. (1989), all deposits of correlated tephra will share the same eruptive age, but the depositional age will vary according to local conditions. Ideally, dates from multiple outcrops would be used to assess local variance in depositional age, but this is not always feasible. We thus assume only general age equivalence for correlated deposits. However, in some cases at Karungu, Rusinga, and Mfangano additional geological evidence, such as pristine glass shards and evidence that the tephra are airfall deposits (e.g., tephra blanketing and uniformly filling paleotopography) indicates that there has been little to no reworking of some the tuffs, suggesting that depositional ages likely approximate eruptive ages. Importantly, at Karungu, Rusinga, and Mfangano, we document a stratigraphic sequence com-

prised of chemically distinct and correlated tuffs is repeated at several localities. This sequence of correlative tephra thus serves as a relative dating tool for interpreting the age relationships of interbedded sediments and fossil- and artifact-bearing sites in the eLVB.

#### 4.3 Preparation

All preparation protocols were adapted from the University of Utah Electron Microprobe lab recommendations (see Brown and Fuller, 2008; Nash, 1992). Bulk samples of tuff (10-30 g) were prepared by disaggregation with pestle and mortar and sieved through 250 and 125  $\mu\text{m}$  mesh screens, retaining the fraction between. Samples were then washed repeatedly with deionized water and the suspended clay fraction was decanted until the effluent was clear. Cleaned tephra was then treated with 10% nitric acid in sonic bath for five minutes to remove carbonates. Tephra samples were subsequently treated for five minutes with 5% hydrofluoric acid in a sonic bath to remove metal salts and clays potentially adhering to the surface of the glass shards. Samples were then rewashed in deionized water until the effluent was clear, and dried in an oven at 90°C for at least six hours or until all visible moisture was removed. Dried samples were magnetically separated on a Franz isodynamic magnetic separator in two successive runs, the first at low (0.1-0.3) amperage to separate the strongly magnetic mineral components such as olivine, augite and

opaque minerals, and the second run at higher amperage (~0.9-1.0) in order to separate weakly magnetic natural glass from nonmagnetic feldspars and quartz. Glass separates were mounted in twelve-well epoxy grain mounts at the University of Utah. Standard mount sizes are 1" (25 mm) round mounts with maximum height of 1". The University of Utah electron microprobe lab provided carbon coating of samples with a Denton Benchtop Turbo IV high vacuum evaporator. Each mount contained an MM3 standard obsidian (Brown and Fuller, 2008) so that the samples and standard have the identical thickness of carbon coating. Samples described in Tryon et al. (2010) and Van Plantinga (2011) were previously analyzed in the microprobe as resin-impregnated polished thin sections prepared by Spectrum Petrographics, Inc. To reduce inter-analysis variation resulting from the use of different instrumentation and analytical protocols (cf. Kuehn et al., 2011) that may confound correlation efforts, the current dataset includes new preparation and analysis of all samples from Rusinga Island previously analyzed by Tryon et al. (2010), and sample AV1006T5A from Van Plantinga's (2011) study of the Nyamita Valley (Rusinga Island). New and published results show good correspondence particularly for elements other than those known to be highly mobile (e.g.,  $\text{SiO}_2$ ,  $\text{Na}_2\text{O}$ ,  $\text{K}_2\text{O}$ ) and poorly suited for correlation.

#### 4.4 Analysis



The relations among the vitric, crystal, and lithic phases of the tephra deposits were examined in thin section using plane and polarized light, backscattered electron imagery, and energy dispersive electron probe microanalyses (EPMA). Geochemical characterization of the vitric (glass) phase for thin sections and grain mounts via EPMA used a Cameca SX-50 in the Department of Geology and Geophysics at the University of Utah, USA. Analyses were conducted using PC1, TAP, PET and LiF crystals on four wavelength-dispersive spectrometers, with an accelerating voltage of 15 keV, a beam current of 25 nA, and a spot size of 10 mm. The analytical routine for glass included Si, Ti, Zr, Al, Fe, Mn, Mg, Ca, Na, K, O, F, and Cl. A natural obsidian standard (MM3) was used for calibration of O-Ka, Si-Ka, Al-Ka, K-Ka. Mineral standards include fluorite (F-Ka), tugtupite (Cl-Ka) albite (Na-Ka), diopside (Ca-Ka, Mg-Ka), hematite (Fe-Ka), rutile (Ti-Ka), rhodonite (Mn-Ka), and cubic zirconia (Zr- La). Rounds of three standard analyses bracketed rounds of four sample unknowns where 15-20 shots were taken per sample (Nash, 1992). Accidental mineral analyses of feldspars or quartz or analyses with aberrantly low totals (< 90%) were excluded from this study. Oxygen was measured directly allowing for an estimate of the water contents of the shards. This provides a measure of the quality of the analysis (Nash, 1992). Na was measured first on the TAP crystal with an analysis time of four seconds on the analytical peak and two seconds on background on either side of the peak, in order to minimize

Na loss under the electron beam. On-peak and background measurement times are as follows (Pk/Bg sec): Si (15/15), Ti (25/25), Zr (37/22), Al (15/15), Fe (25/25), Mn (25/25), Mg (40/40), Ca (20/16), Na (4/4), K (20/16), O (20/20), F (20/20), Cl (20/20). Concentrations are calculated using the PAP matrix correction procedure (Pouchou and Pichoir, 1991). Correction for “excess” F by interference of the Fe La peak with F Ka peak was accomplished by measuring a F-free Fe-bearing standard (hematite) to yield a correction factor of 0.031. Background intensities are measured on both sides of the analytical peak for all elements but F on the PC1 crystal, where off-peak background is measured to one side, and on-peak background intensity is interpolated using the estimated slope of the continuum (Pouchou and Pichoir, 1991).

By choosing analytical conditions identical to those widely used by the Department of Geology and Geophysics at the University of Utah, we are able to directly integrate our data from the eLVB to a large body of published data on extra-basinal tephra that may be potential correlates (e.g., Brown and Fuller, 2008; Brown et al., 2012a). The selected beam size and current can cause underestimates of volatile element abundance (especially Na) and over-representation of Si, leading to higher than expected totals (Hayward, 2011; Hunt and Hill, 2001; Morgan), and it is for these reasons that we use the restricted element list defined below for our correlations.

Table 2: Representative or type samples of the named tuffs and discrete chemical modes discussed in this study GPS coordinates for each type or representative sample or mode provided. Results of randomization of type sample or mode means and standard deviations to determine mean similarity coefficient values and lower 95% similarity coefficient confidence limits.

Tuff	Type Sample		SC 7 element oxides used in this study	
			Mean	Lower 95% Confidence Limit
		S 00° 25.565' E		
		034° 10.347'		
			0.95	0.93
		S 00° 25.246'		
		E 034° 09.599'	0.95	0.93
		S 00° 24.706' E		
		034° 11.126'	0.93	0.89
		S 00° 48.342' E		
		034° 08.216'	0.95	0.92
		S 00° 48.342'		
		E 034° 08.216'	0.9	0.85
		S 00° 25.584' E		
		034° 09.554'	0.95	0.92
		S 00° 25.369'		
		E 034° 09.615'	0.96	0.93
		S 00° 03.324'		
		E 035° 13.084'	0.96	0.94
		S 00° 48.278'		
		E 034° 08.274'	0.85	0.76

However, inter-laboratory comparisons confirm that the equipment and

protocols used by the Utah labora-

tory (lab 5 in Kuehn et al., 2011)

work exceptionally well for tephra

of a wide range of compositions.

#### 4.5 Interpretation

Correlation of two or more tephra

deposits is best viewed as a hy-

pothesis with different methods of

distinguishing tephra providing

independent tests of any hypothe-

sized correlation (Feibel, 1999). Failure to distinguish tephra from different samples by means

of stratigraphy, lithology, petrography and element oxide compositions measured with an elec-

tron microprobe constitutes robust evidence for correlation (Tryon et al., 2008, 2010). Reported

major element oxides are not normalized because element oxide totals including estimated water content were high and exploratory data analysis using normalization did not alter interpretation. However, samples plotted on the total alkali-silica (TAS) diagram (Fig. 7) necessarily have totals normalized to 100% for comparison with whole-rock samples (Le Bas et al., 1986).

Our samples include both fresh vitric tephra deposits, as well as those subsequently reworked by fluvial processes or overprinted by pedogenesis. We define fresh vitric tephra as poorly consol-

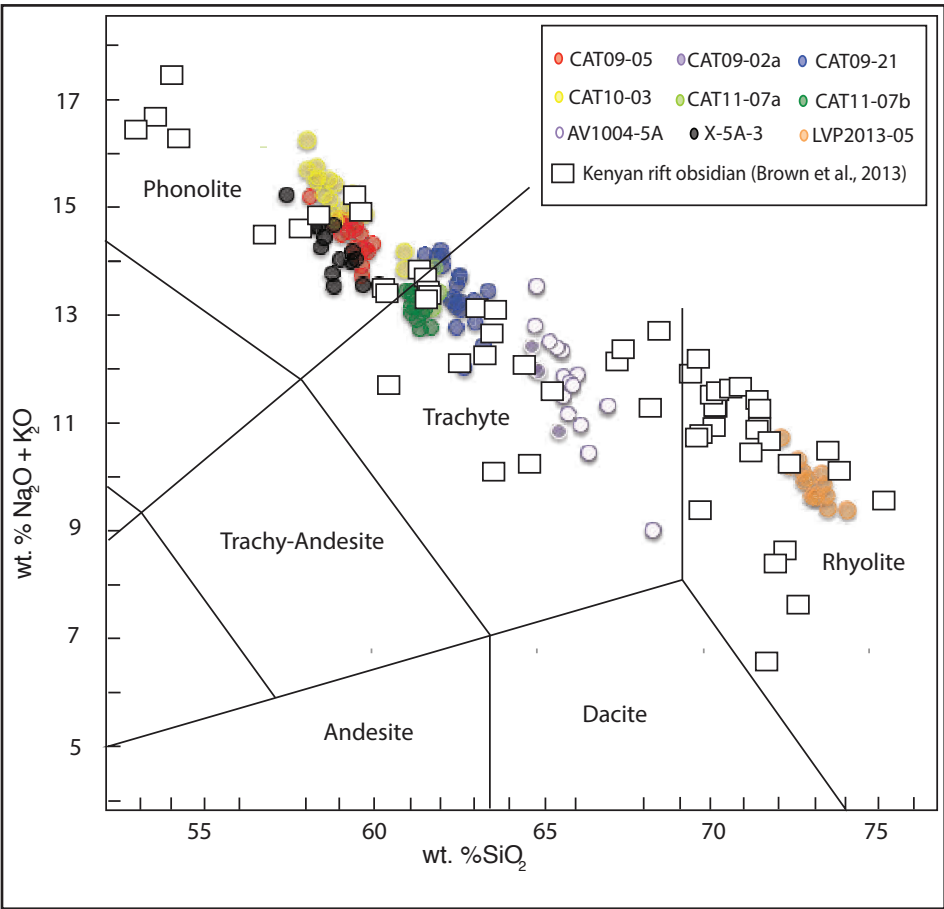


Figure 7: Total-alkali Silica graph (after Le Bas et al., 1986) of type samples of all eight distinct tuffs discussed in this study along with obsidian samples from the Kenya Rift. All obsidian data are from Brown et al. (2013).

idated, well-sorted  
ash-sized ( $\leq 2$  mm)  
vitric ashes following  
the terminology of  
Schmid (1981: 42).  
We indicate where  
tephras of this lithol-  
ogy were sampled  
in Figs. 2 and 4. The

tuffs are more lithified and show incipient pedogenesis or other evidence for bioturbation. The glass shards in these samples are set in a predominantly silt to fine-sand groundmass, and grain boundaries on the glass shards are sharp, indicating little mechanical abrasion through grain to grain collisions through reworking (Tryon et al., 2010). Lithic and crystal phases from the eruption cannot always be reliably distinguished from those found in detrital sediments, and thus our correlations rely on chemical composition of the glass component for all samples.

In the majority of samples, all analyzed glass shards clustered around a discrete mean and represent a unimodal glass composition (Table 1; Figs. 8, 9), further indicating minimal reworking even in those ash beds visibly altered by fluvial or pedogenic processes during or after initial deposition. However, some samples displayed bimodal compositions. Bimodal compositions within a single sample were separated into ‘a’ and ‘b’ compositions and treated as potentially different tephras for analysis (Fig. 9). Identifying the consistent presence of a bimodal composition is an important step in distinguishing tephra deposits that contain two modes of glass as a product of magmatic processes during eruptions (e.g., due to a differentiated magma chamber or sampling host rock during magma ascent), and therefore represent the same eruptive event, from those that contain two modes as a product of post-depositional mixing. Bivariate plots of Cl

versus  $\text{TiO}_2$  visually display the discrete modes of the tuffs discussed in this study (Fig. 9). We chose this combination because it most clearly displays similarities and differences within and between all correlative groups of tuffs on a single plot (Fig. 9). Both  $\text{TiO}_2$  and Cl are immobile elements that are unaffected by hydration and analytical variations between samples.

Postdepositional hydration, ion exchange and migration of the alkalis in analysis are known to affect silica (Si), sodium (Na), potassium (K) and possibly fluorine (F) content (Cerling et al., 1985; Hunt and Hill, 2001). These diagenetic and analytical conditions that selectively affect measurement and calculation of  $\text{SiO}_2$ ,  $\text{Na}_2\text{O}$ , and  $\text{K}_2\text{O}$  have prompted us to follow Brown et al., (2012a) in excluding these element oxides for correlation purposes. We use a restricted list of seven element oxides,  $\text{TiO}_2$ ,  $\text{Al}_2\text{O}_3$ , FeO, MnO, MgO, CaO, and Cl in computation of similarity coefficients and other statistical analyses. We depart slightly from Brown et al., (2012a) by including  $\text{Al}_2\text{O}_3$ . This element oxide is important in distinguishing discrete chemical modes within samples attributed to a widespread bimodal deposit (the BTPT, described below).

All correlations are supported by similarity coefficients (SCs) to quantify similarity between means of glass analyses from samples after which a tephra is named, the ‘type sample’, and the

mean value of all other modes in our dataset (Table 2; Brown et al., 2012a; Tryon et al., 2008).

For any two-tephra comparisons, SCs are the mean of the ratios obtained by dividing pairs of sample means (with the larger value of the two samples always the denominator such that the ratio is always  $\leq 1$ ) element by element as defined in Borchardt et al., (1972: 302). In this study we have restricted SC analysis to the seven element oxides noted above (see Brown et al., 2012a). Resulting SCs range from 0 (complete dissimilarity) to 1 (perfect similarity).

Previous studies have proposed arbitrary cutoffs for interpreting SCs in terms of potential correlation. For example, Kuehn and Foit (2006) propose a value of  $\geq 0.95$  for definitive correlation, whereas Froggatt (1992) recognizes that values  $\geq 0.92$  are typically accepted for correlations. In this study, we implement randomization procedures to develop empirically informed SC cutoffs for accepting or rejecting potential correlations. For each of the tephra type or representative samples, we use the mean and standard deviation of each element oxide to generate 5,000 random normally-distributed samples using the R statistical package (R Development Core Team, 2014); this effectively represents 5,000 replicates of the type tephra. We then calculate SCs between each of the 5,000 replicates and the type sample, which is used to generate a frequency distribution of expected SC values when comparing two samples of the same tuff. From this dis-

tribution, we determine the lower SC limit that encompasses the upper 95% of observations. We use this value as the cutoff for rejecting potential correlations. For example, an SC value between an unknown tuff and a type sample that falls below this cutoff is excluded for consideration as a potential correlate. To increase the stringency of our protocol, we also require that the seven element oxides of the unknown tuff considered in our analysis overlap within two standard deviations of the mean of the type sample. This is because an unknown sample that is very similar in composition for most element oxides (e.g., 6 of 7) to a type sample will record a relatively high SC value, even if one oxide is distinct and outside the range of expected values. The SCs included in this analysis were used as a data exploration and confirmation technique. All correlations were investigated in more detail utilizing the known stratigraphy of a site and visual inspection of the tephra datasets.

## 5. Radiometric Dating

There are a number of available methods that focus on the vitric or crystal phases of a tephra to determine its eruption age (Feibel et al., 1989) including fission track, thermoluminescence, and  $^{40}\text{Ar}/^{39}\text{Ar}$  methods; other approaches such as U-Pb dating of zircons more accurately dates crystal formation rather than eruption (e.g., Simon et al., 2008). We have not been able to apply any of



these methods to directly estimate the eruption ages of any of the eLVB tephra deposits because of iron-oxide mineral inclusions in the glass shards and because datable minerals are either too fine-grained or sparse to be dated.

The alternative approach used here is to determine the depositional age of the tephra (Feibel et al., 1989). Differences in the time between eruption and initial deposition (sedimentation) of fallout deposits can range from minutes to hours for areas proximal to the source volcano, to several years for finer particles that enter the stratosphere. Once deposited, tephra can be remobilized and reworked through normal sedimentary processes, and thus the timing of re-deposition may differ substantially from the initial depositional age.

We use two methods to estimate the depositional age of the eLVB tuffs. The first, already mentioned, is the direct AMS  $^{14}\text{C}$  dating of gastropod shells found in life position within tuffs from Rusinga Island and Mfangano Island. As the snails burrowed into the previous deposited sediments, they post-date deposition, but apparently pre-date lithification, providing a minimum age for the deposits. The second method was to utilize optically stimulated luminescence dating to determine sediment burial ages.

## 5.1 Optical dating

We used optical dating of sediments to constrain the age of tephra deposition. All dates derive from localities on Rusinga Island. We collected two sediment samples (RUP-1 and RUP-2) respectively above and below the type sample of the Nyamita Tuff at section Nyamita 2 (Figs 2, 10; Li et al., 2015). As discussed in detail below, textural, microscopic, and geochemical data strongly suggest that this deposit underwent little to no reworking following deposition, and thus depositional age likely approximates eruptive age. At Wakondo we collected three samples (RUP-3, RUP-4 and RUP-5) from the same sedimentary unit in a channel complex ~1 m above the Wakondo Tuff. The age of the channel complex provides a minimum age for the deposition of the Wakondo Tuff. For all samples, we extracted 180-212  $\mu\text{m}$  in diameter potassium-rich (K) feldspar grains, using standard procedures, for dating; no quartz grains were present in the sediment samples. We measured individual grains of K-feldspar from each of the samples for equivalent dose ( $D_e$ ) determination, using a two-step post-IR IRSL measurement procedure (Thomsen et al., 2008), in which a prior-IR IRSL stimulation at 200 °C (Li and Li, 2012) and a post-IR IRSL stimulation at 275 °C were adopted, to overcome possible age underestimation caused by anomalous fading (Huntley and Lamothe, 2001; Wintle, 1973). The dose rates were estimated

using a combination of laboratory-based beta counting, field-based gamma spectrometry measurements, together with calculations of the cosmic ray and internal beta dose rates. The applicability of the pIRIR method for the samples in this study and the reliability of the measurements were determined using a suite of different tests. A description of the method and De and dose rate measurement procedures and the test results are presented in detail in Supplementary Information and in Li et al. (2015).

## 6. Results

### 6.1 Tephra Correlation

Element oxide wt. % abundances, and comparisons using SCs indicate the presence of eight distinct distal tephra deposits of nine chemical compositions (Fig. 9, Table 1, 3, 4). Seven of these tephra deposits occur across Rusinga Island, Mfangano Island, and Karungu, four of which are sufficiently widespread to merit names and type or representative localities. These four units in stratigraphic order from the base upwards are the Wakondo Tuff, the Nyamita Tuff, the Nyamsingula Tuff, and the Bimodal Trachyphonolitic Tuff (BTPT). The first three of these deposits

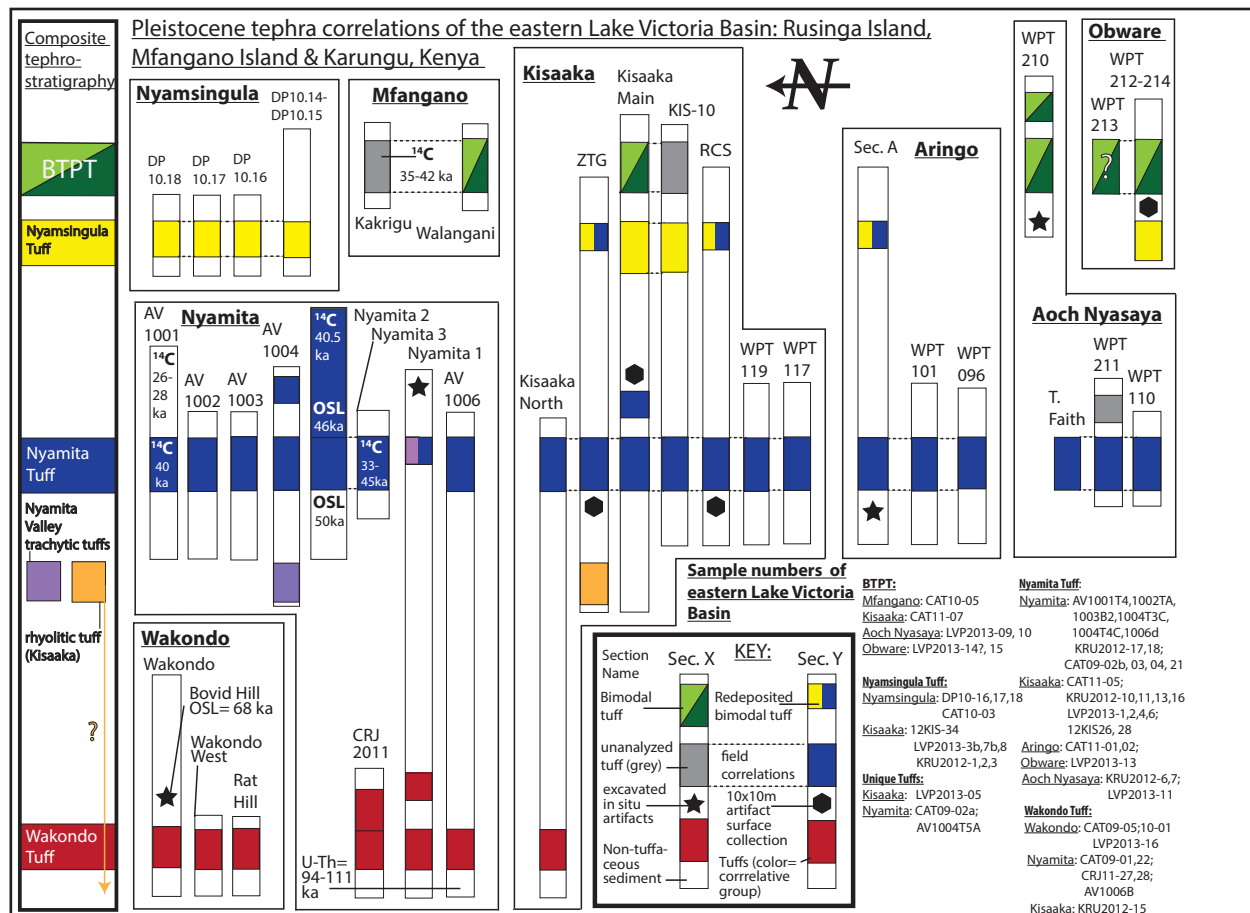


Figure 8: Schematic stratigraphic sections for all analyzed samples from the eastern Lake Victoria Basin. Composite section of Pleistocene tephra with unique colors corresponding to unique tephra named on the left of the figure. Individual tuff samples shown as rectangles with sample numbers for each sample at each Pleistocene locality listed on bottom right. Discrete chemical modes of glass found in a single sample shown as unique colors within a single rectangle. Tuffs with glass shards of multiple compositions due to mechanical mixing have colors separated with a vertical line. Tuffs with distinct modes of glass as a product of magmatic processes during eruption have colors representing modes separated by a diagonal line. Grey rectangles are tuff samples lacking good chemical analysis. Dotted lines represent tuff units that can be traced laterally in the field between two measured sections. White area represents non-volcanoclastic sediments not used for correlation.

include fresh vitric tephra and are named on the basis of a geographic type locality following the

North American Stratigraphic code (Nomenclature, 2005). No such deposits of the BTPT have

been found in the eLVB, and we thus provide a provisional name based on its characteristic bi-

modal chemical composition. Figure 8 shows these deposits in stratigraphic order along with the

three unique tuffs from the eLVB: two compositionally similar trachytes from Rusinga Island's

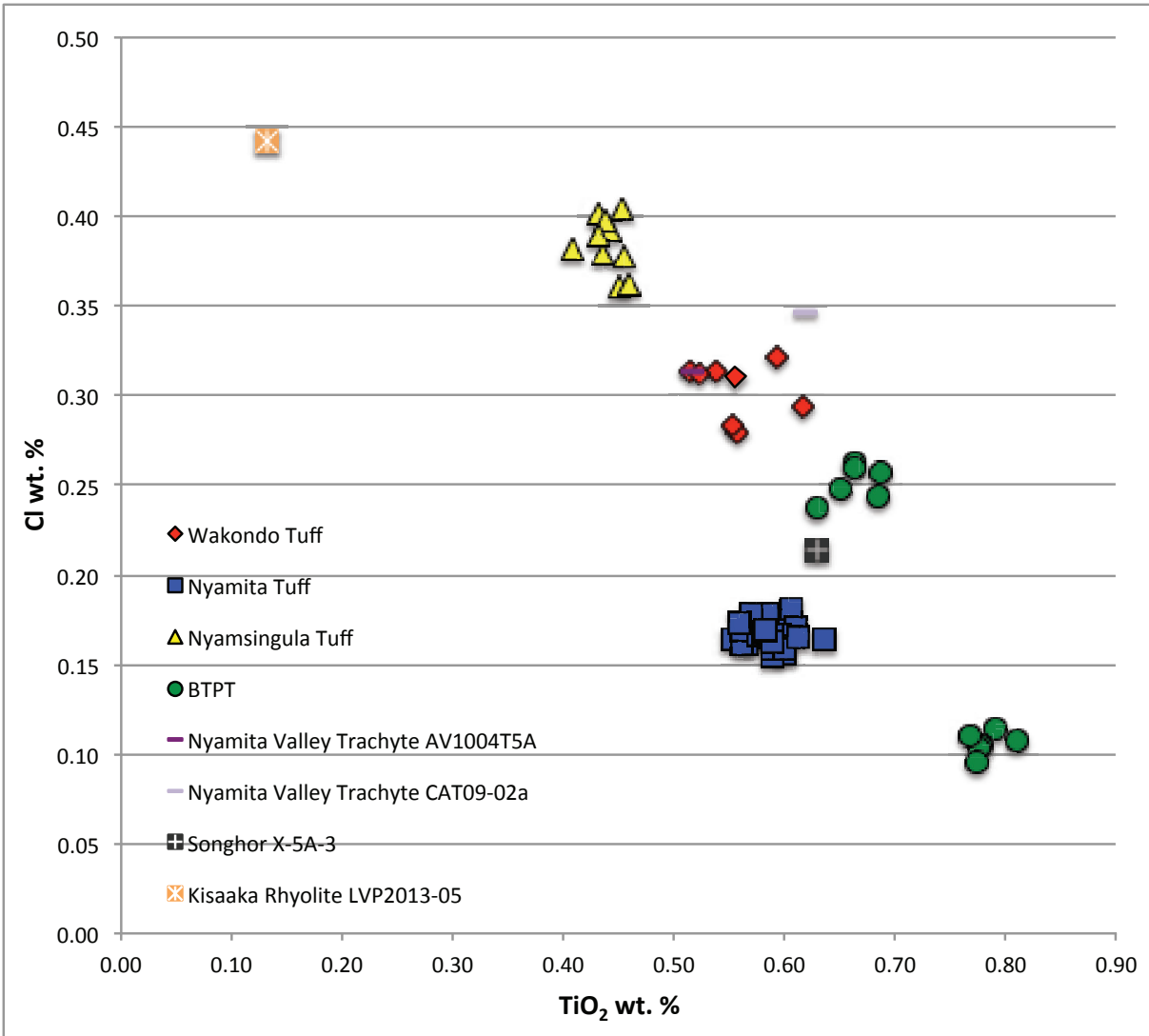


Figure 9: Bivariate plot of Cl against TiO<sub>2</sub> for means of all samples discussed in this study.

Nyamita Valley, and a single rhyolite from the Kisaaka locality at Karungu. The eighth distinct tuff, from Songhor (Figs 1b, 1c), is outside the area of the eLVB that is the primary focus of this study. Thus this tuff is not shown in Figure 8, but is important in that it suggests a still untapped potential for tephra correlation in and around the eLVB.

### 6.1.1 The Wakondo Tuff

The Wakondo Tuff is named after the Wakondo locality on Rusinga Island where it was first recognized by Tryon et al. (2010). Because of its fresh lithology, abundant glass and documented stratigraphic position at Wakondo (Fig. 2; Tryon et al., 2010: 5), sample CAT09-05 serves as the type sample of this tephra (Fig. 10a, b).

#### 6.1.1.1 Composition of the Wakondo Tuff

The type sample (CAT09-05) is a ~20-cm-thick, massively bedded, weakly consolidated, grey-green fresh, vitric ash composed of microscopic pumices and pumice fragments (50-200  $\mu\text{m}$ ) and sinuous glass shards generally  $< 5\mu\text{m}$  to  $\sim 100\mu\text{m}$  with oval and linearly stretched vesicles.

At the type section, the Wakondo Tuff is interbedded within ~4 m of siltstone (Fig. 2; Tryon et al., 2010). The Wakondo Tuff is a phonolite (Fig. 7; Tryon et al., 2010; Van Plantinga, 2011). All samples attributed to it are unimodal (Fig. 9; Table 1). There is minimal evidence for reworking of the Wakondo Tuff at its type locality.





Figure 10: (A) Photograph of the Wakondo Tuff at Wakondo, Rusinga Island. (B) Note the fresh grey vitric character of the tuff in close-up view of the outcrop. (C) Photograph of the type section Nyamita 2 from the Nyamita Valley, Rusinga Island. The type sample of the Nyamita Tuff, CAT09-21, taken from the fresh, vitric tephra deposit at the base of the tuff in this section is indicated. OSL samples RUS-1 and RUS-2 bracketing CAT09-21 also indicated. (D) Photograph of sample CAT10-03, type sample of the Nyamsingula Tuff, from section DP10.14-DP10.15 at the locality of Nyamsingula, Rusinga Island. Note the fresh grey, ashy fine texture of the fresh, vitric tephra deposit and the discrete contrast with the overlying soil. (E) Panoramic photograph of the section Kisaaka Main and the surrounding exposure showing (from bottom to top) the Nyamita Tuff (LVP2013-01, 02), the Nyamsingula Tuff (LVP2013-08) and the representative sample (CAT11-07) of the BTPT in stratigraphic sequence. Also note the lateral extent of the Nyamita Tuff at Kisaaka.

#### 6.1.1.2 Similarity coefficients of the Wakondo Tuff

SC values calculated between CAT09-05 and the randomized replicates of this sample produced an average SC value of 0.95 and a lower 95% confidence limit of 0.93 (Table 2). The seven samples correlated to the Wakondo Tuff have a SC of 0.95 or higher when compared to the type sample CAT09-05 (Table 3). All other tephra samples have SCs of 0.89 or lower when compared with samples of the Wakondo Tuff (Table 3).

#### 6.1.1.3 Additional exposures of the Wakondo Tuff

In the Wasiriya beds of Rusinga Island, samples attributed to the Wakondo Tuff occur at the Wakondo locality (type sample CAT09-05 and two other minimally reworked deposits, CAT10-01 and LVP2013-16 (Fig. 2). At the Nyamita locality, the Wakondo Tuff is present as sample CAT09-01, a fresh, vitric tephra deposit at the base of the section at Nyamita 1 and a reworked and redeposited bed up-section sampled as CAT09-22 (Fig. 2). The Wakondo Tuff has not been found on Mfangano Island. At Karungu, the Wakondo Tuff is found at the northernmost section (Kisaaka North) sampled as KRU2012-15 (Fig. 4).



Table 3: Similarity coefficients for all distinct modes of samples analyzed in this study based on the restricted seven-element list. Samples listed vertically (left) and compared with the type samples of every chemically unique tuff or mode listed horizontally (top). Lower 95% confidence limit for each type sample or mode listed in parentheses. Colored squares are samples or modes with similarity coefficient  $\geq$  the 95% lower confidence limit determined by randomization when compared to the type sample and overlap at two standard deviations for the seven element oxides used for correlation when compared to the type sample. Black squares are the type sample or mode compared to itself.

Sample	Wakondo Tuff CAT09-05 (.93)	Nyamita Tuff CAT09-21 (.93)	Nyamsingula Tuff CAT10-03 (.89)	BTPT 'a' CAT11-07a (.92)	BTPT 'b' CAT11-07b (.85)	AV1004 T5A (.92)	CAT09-02a (.93)	Song- hor Tuff X-5A-3 (.93)	Rhyo- litic Tuff LVP2013-05 (.76)
CAT09-05		0.85	0.87	0.82	0.75	0.81	0.76	0.83	0.35
CAT09-01	0.98	0.85	0.86	0.81	0.75	0.81	0.75	0.83	0.35
CAT09-22	0.95	0.89	0.87	0.82	0.78	0.77	0.73	0.83	0.35
CAT10-01	0.99	0.85	0.86	0.83	0.76	0.81	0.77	0.84	0.35
KRU2012-15	0.98	0.85	0.87	0.82	0.76	0.82	0.75	0.82	0.35
CRJ11-27	0.96	0.87	0.85	0.82	0.77	0.79	0.77	0.85	0.35
CRJ11-28	0.95	0.88	0.85	0.83	0.78	0.78	0.76	0.85	0.34
LVP2013-16	0.95	0.87	0.83	0.83	0.77	0.78	0.75	0.87	0.33
CAT09-21	0.85		0.83	0.75	0.83	0.68	0.66	0.85	0.32
CAT09-02a	0.85	0.99	0.83	0.74	0.82	0.68	0.65	0.84	0.32
CAT09-03	0.83	0.97	0.81	0.73	0.84	0.67	0.64	0.85	0.31
CAT 11-01	0.83	0.97	0.82	0.73	0.82	0.67	0.64	0.84	0.32
CAT 11-01	0.84	0.97	0.81	0.74	0.82	0.67	0.65	0.84	0.32
CAT11-02	0.85	0.96	0.83	0.73	0.81	0.68	0.64	0.82	0.32
CAT11-05	0.86	0.94	0.79	0.76	0.83	0.69	0.68	0.89	0.31
KRU2012-01	0.85	0.96	0.82	0.73	0.81	0.68	0.64	0.82	0.32
KRU2012-02	0.84	0.94	0.81	0.74	0.81	0.67	0.65	0.81	0.32
KRU2012-03	0.83	0.97	0.81	0.75	0.84	0.67	0.65	0.84	0.31
KRU2012-06	0.85	0.96	0.82	0.75	0.81	0.68	0.66	0.84	0.32
KRU2012-07	0.83	0.97	0.80	0.74	0.83	0.67	0.66	0.85	0.32
KRU2012-10	0.84	0.97	0.83	0.73	0.82	0.68	0.64	0.83	0.31
KRU2012-11	0.84	0.97	0.82	0.74	0.82	0.67	0.65	0.83	0.32
KRU2012-13	0.86	0.98	0.84	0.74	0.83	0.69	0.65	0.84	0.32
KRU2012-16	0.86	0.97	0.84	0.74	0.81	0.69	0.65	0.83	0.32
KRU2012-17	0.84	0.97	0.83	0.74	0.82	0.68	0.65	0.83	0.32
KRU2012-18	0.84	0.96	0.82	0.73	0.82	0.68	0.64	0.83	0.32
LVP2013-01	0.85	0.98	0.83	0.74	0.83	0.68	0.65	0.84	0.31
LVP2013-02	0.85	0.97	0.84	0.74	0.81	0.68	0.65	0.82	0.32
LVP2013-03a	0.83	0.97	0.82	0.73	0.82	0.67	0.64	0.82	0.31
LVP2013-04	0.84	0.98	0.82	0.74	0.83	0.67	0.65	0.83	0.32
LVP2013-06	0.84	0.98	0.82	0.73	0.83	0.67	0.65	0.83	0.31
LVP2013-07a	0.83	0.97	0.82	0.73	0.82	0.67	0.65	0.82	0.32
LVP2013-11	0.84	0.97	0.82	0.74	0.84	0.68	0.65	0.84	0.31
12KIS26	0.83	0.98	0.82	0.73	0.82	0.67	0.64	0.84	0.32
12KIS28	0.83	0.97	0.82	0.74	0.83	0.67	0.65	0.84	0.31
CAT10-03	0.86	0.82		0.75	0.70	0.74	0.70	0.71	0.40
DP10-16	0.88	0.83	0.97	0.74	0.71	0.73	0.69	0.73	0.40
DP10-17	0.86	0.82	0.98	0.74	0.70	0.72	0.69	0.72	0.41

DP10-18	0.87	0.82	0.96	0.74	0.70	0.73	0.69	0.72	0.40
LVP2013-3b	0.85	0.77	0.92	0.79	0.70	0.79	0.75	0.71	0.39
LVP2013-7b	0.84	0.78	0.93	0.79	0.69	0.78	0.74	0.70	0.40
LVP2013-8	0.87	0.79	0.92	0.81	0.71	0.79	0.75	0.72	0.39
LVP2013-13	0.89	0.84	0.95	0.74	0.72	0.73	0.70	0.74	0.39
12KIS34	0.85	0.79	0.94	0.79	0.70	0.77	0.73	0.71	0.40
KRU2012-4	0.85	0.77	0.91	0.79	0.70	0.78	0.74	0.71	0.40
CAT11-07a	0.82	0.75	0.75		0.68	0.78	0.81	0.86	0.34
CAT11-07b	0.75	0.83	0.71	0.68		0.62	0.60	0.78	0.28
CAT10-05a	0.82	0.75	0.75	0.98	0.69	0.78	0.80	0.86	0.34
CAT10-05b	0.77	0.83	0.71	0.70	0.97	0.62	0.62	0.80	0.28
LVP2013-09a	0.82	0.77	0.75	0.96	0.71	0.76	0.78	0.88	0.33
LVP2013-09b	0.77	0.83	0.71	0.69	0.97	0.62	0.61	0.79	0.28
LVP2014-10a	0.82	0.75	0.75	0.98	0.68	0.79	0.81	0.85	0.34
LVP2014-10b	0.76	0.84	0.72	0.69	0.97	0.62	0.60	0.79	0.28
LVP2014-14a	0.82	0.76	0.75	0.89	0.70	0.86	0.85	0.80	0.36
LVP2014-14b	0.76	0.86	0.74	0.69	0.94	0.62	0.60	0.79	0.29
LVP2013-15a	0.82	0.78	0.74	0.92	0.70	0.79	0.81	0.87	0.33
LVP2013-15b	0.74	0.84	0.72	0.66	0.94	0.60	0.58	0.76	0.28
AV1004-5A	0.81	0.68	0.74	0.78	0.62		0.91	0.70	0.41
CAT09-02a	0.76	0.66	0.70	0.81	0.60	0.91		0.73	0.41
X-5A-3	0.83	0.85	0.72	0.86	0.78	0.70	0.73		0.31
LVP2013-05	0.35	0.32	0.40	0.34	0.28	0.41	0.41	0.31	

### 6.1.2 The Nyamita Tuff

The Nyamita Tuff is named after locally extensive but discontinuous ~ 1 km exposures of this deposit along the Nyamita Valley of Rusinga Island (Garrett et al., 2015; Tryon et al., 2010; Van Plantinga, 2011). We follow Tryon et al. (2010) in using sample CAT09-21 from section Nyamita 2 in the Nyamita Valley as the type sample for this tuff (Figs. 2, 10c; Tryon et al., 2010).

#### 6.1.2.1 Composition of the Nyamita Tuff

The type sample CAT09-21 is a 0.33-m-thick fresh, vitric deposit of unconsolidated grey ash, found at the base of a ~3.5-m-thick massive deposit of the Nyamita Tuff (Fig. 10c; Tryon et al., 2010). The type sample contains abundant grey glass shards generally 5 -100  $\mu\text{m}$ . The Nyamita Tuff is a trachyphonolite (Fig. 7), with samples distinguished by their consistent and low average Cl content of  $0.16 \pm 0.02$  weight percent (Table 1, Fig. 9). There is no evidence for reworking of the type deposit of the Nyamita Tuff.

#### 6.1.2.2 Similarity coefficients of the Nyamita Tuff

SC values calculated between CAT09-21 and the randomized replicates of this sample produced an average of 0.95 and a lower 95% confidence limit of 0.93 (Table 2). Samples attributed to the Nyamita Tuff have SCs between 0.94 and 0.99 compared with the type sample CAT09-21 (Table 3). Other samples compared with CAT09-21 have SCs of  $\leq 0.89$ .

#### 6.1.2.3 Additional exposures of the Nyamita Tuff

Field observations suggested that the Nyamita Tuff is the most common and widespread tuff in the eLVB, a hypothesis subsequently confirmed by chemical correlation. CAT09-21 samples the freshest vitric tephra deposit from Rusinga Island's Nyamita Valley, but this tuff can be physically traced laterally to section Nyamita 3, visually correlated using a Jacobs staff and Abney level between all localities in Nyamita Valley, and chemically correlated throughout the Nyamita Valley over a north-south transect for ~1 km (Garrett et al., 2015; Tryon et al., 2010; Van Plantinga, 2011: 20). The present study demonstrates near ubiquity of the Nyamita Tuff at 21 of 32 measured sections in the eLVB, including 13 of 15 measured sections of Pleistocene exposures at Karungu (Figs. 4, 5, 6, 8). Although locally widespread on Rusinga Island, the Nyamita Tuff is absent from our studied exposures on Mfangano Island. At Karungu, the Nyamita Tuff occurs as a fresh, vitric tephra deposit in three samples (12KIS28, LVP2013-01 and LVP2013-04) in three measured sections at Kisaaka (KIS-10, Kisaaka Main and Kisaaka North respectively; Fig. 4). The bottom ~10-15 cm of the ~75-cm-thick tuffs from which these three samples were taken contain similar grey ash-sized grains, are powdery to the touch in hand samples, display abundant ~50-100  $\mu\text{m}$  angular glass shards visible at 40-100x magnification using a petrographic microscope, and are most commonly found in micro-lows on the landscape indicating that the basal portions of the tuffs were deposited by airfall and at most minimally reworked. The upper

~60 cm of these tuffs at sections KIS-10, Kisaaka Main and Kisaaka North are slightly more re-worked deposits grey-brown to tan color, with a more silty texture in hand sample with small ~1 cm Mn-stained root casts and more detrital grains visible in thin section. Field observations show the Nyamita Tuff is laterally continuous for ~1 km at the locality of Kisaaka (Figs. 4, 10e) and at this specific locality chemical correlation confirms this lithostratigraphic correlation. Chemical correlations presented here show all samples from the laterally continuous units (KRU2012-10, KRU2012-11, KRU2012-13, 12KIS26, 12KIS28, LVP2013-01, LVP2013-02, CAT11-05, LVP2013-06, LVP2013-04, KRU2012-06) are chemically homogenous, unimodal and indistinguishable therefore constituting robust evidence for correlation. This laterally continuous exposure of the Nyamita Tuff at Kisaaka also drapes the gilgai topography of the paleosols on which it sits (Fig. 11). This demonstrates laterally extensive evidence for airfall deposition, burial and preservation of the Nyamita Tuff at Kisaaka.

The presence of fresh, vitric tephra deposits of the Nyamita Tuff in the Nyamita Valley and at Kisaaka ~50 km to the south, the consistent chemical homogeneity of Nyamita Tuff samples and their stratigraphic position in relation to other marker beds make the Nyamita Tuff a locally useful lithostratigraphic marker (Fig. 8).

In addition to being widespread, Nyamita Tuff outcrops are the thickest of any tephra deposit in our sample, with a maximum observed thickness of ~4 m at Nyamita and >2m in and around the Kisaaka North section of Karungu (Figs. 2, 4, 10c). The extent to which these thicknesses represent post-depositional sedimentary admixture is as yet undetermined. The Nyamita Tuff may represent either deposits of the largest eruption preserved in the eLVB, and/ or a period of major changes in the local erosional and depositional regime.

### 6.1.3 The Nyamsingula Tuff

The Nyamsingula Tuff was first recognized at the Pleistocene exposures of the western Nyamsingula locality on Rusinga Island (Figs. 2, 7). Nyamsingula contains four laterally traceable outcrops of fresh, grey, vitric ash (CAT10-03, DP10-16, DP10-17, DP10-18) with indistinguishable compositions all attributed to the Nyamsingula Tuff (Fig. 2). We use a particularly fresh, vitric tephra deposit, sampled as CAT10-03 from near the base of the 15-m-thick section DP10.14-DP10.15, as the type sample for the Nyamsingula Tuff (Figs. 2, 10d).

#### 6.1.3.1 Composition of the Nyamsingula Tuff

In outcrop CAT10-03 is a 20 cm-thick grey, vitric ash (Fig. 10d) of abundant grey glass with microscopic pumices, pumices fragments, some 50-200  $\mu\text{m}$ , round to subround and slightly oval often overlapping vesicles. The Nyamsingula Tuff is a phonolite (Fig. 7) and distinguished by its high average aluminum ( $\text{Al}_2\text{O}_3 > 16.0 \text{ wt. \%}$ ), low average titanium ( $\text{TiO}_2 \sim 0.45 \text{ wt. \%}$ ) and high average chlorine content ( $\text{Cl} \sim 0.40 \text{ wt. \%}$ ) (Fig. 9, Table 1).

#### 6.1.3.2 Similarity coefficients of the Nyamsingula Tuff

SC values calculated between CAT10-03 and the randomized replicates of this sample produced an average SC value of 0.93 and a lower 95% confidence limit of 0.89 (Table 2). All samples attributed to the Nyamsingula Tuff have a SC of 0.91 or greater compared to the type sample CAT10-03, and no other sample has a SC of over 0.87 compared to CAT10-03 (Table 3). Additionally, samples of Nyamsingula Tuff are consistently found stratigraphically above the Nyamita Tuff and below the Bimodal Trachyphonolitic Tuff.

#### 6.1.3.3 Additional exposures of the Nyamsingula Tuff

On Rusinga Island the Nyamsingula Tuff is known only from the type locality, and it is not present on Mfangano Island. At the Karungu exposures this tuff is found at Kisaaka, Aringo and Obware. At the Kisaaka Main and KIS-10 sections, the Nyamsingula Tuff overlies the Nyamita Tuff (Fig. 4). At the RCS and ZTG sections at Kisaaka, modes 'b' of samples LVP2013-03 and LVP2013-07 are attributed to the Nyamsingula Tuff, admixed with glass from underlying deposits of the Nyamita Tuff, indicating local syn- or post-depositional reworking. Similar admixture of the glass of the Nyamsingula Tuff and Nyamita Tuff is seen at Aringo Section A (CAT11-02; Fig. 5). The Nyamsingula Tuff is also present at Obware at the WPT 212-214 section (Fig. 6). At Kisaaka Main and at Obware, the Nyamsingula Tuff is overlain by the Bimodal Trachyphonolitic Tuff (Figs. 4, 6, 8).

#### 6.1.4 The Bimodal Trachyphonolitic Tuff (BTPT)

The BTPT is named for its distinctive composition. The representative sample chosen for this tuff is CAT11-07 from section Kisaaka Main at the locality of Kisaaka, Karungu because it



contains abundant glass and the sample occurs in stratigraphic sequence with other named tuffs (Figs. 4, 8, 10e). Unlike the other three named tuffs discussed in this study, no example of fresh, vitric tephra for the BTPT have yet been found, and thus we do not designate a formal name and type locality. Samples attributed to the BTPT are always found as a ~10-50-cm-thick bed with varying degrees of pedogenic development, near the modern surface and often incorporated into paleosols. Bed thickness ranges from 10-55-cm, commonly with small (<5 mm) Mn-stained root casts.

#### 6.1.4.1 Composition of the BTPT

Despite their weathered appearance in outcrop and hand sample, all samples of the BTPT preserve fresh glass of a distinctive grey-brown, green-brown or light brown color under plane-polarized light. Glass occurring as microscopic pumices and pumice shards sometimes over 200  $\mu\text{m}$  with round to stretched vesicles is common in most samples of this tuff, but smaller shards 5-25  $\mu\text{m}$  occur. As the name suggests, this tuff is a trachyphonolite (Fig. 7), with glass compositions divided into two chemically distinct modes (Fig. 9, Table 1). One mode (CAT11-07a) is distinguished by low aluminum content ( $\text{Al}_2\text{O}_3$  ~12.5 wt. %) and high iron content ( $\text{FeO}$  ~8-9 wt

%), and the second mode (CAT11-07b) is distinguished by its higher aluminum content ( $\text{Al}_2\text{O}_3 \sim 15.25 \text{ wt } \%$ ) and lower iron content ( $\text{FeO} \sim 6.5\text{-}6.75 \text{ wt } \%$ ). The bimodal nature of the BTPT is illustrated in Figure 9. For clarity we label the low aluminum mode ‘a’ and the higher aluminum mode ‘b’ in all samples attributed to the BTPT (Fig. 9, Table 1). Each of these two compositional modes is distinct from each other and from all other tephra samples found in the eLVB (Fig. 9). The two compositional modes found in all samples of the BTPT are petrographically distinct from all other glass shards in this study, but indistinguishable from one another. These two modes exhibit glass chemistry indicative of density dependent zonation of a magma chamber (Macdonald et al., 1994) and are always found together whereas neither of the two modes is found in samples attributed to other tuffs from the eLVB. For these reasons we interpret the bimodal composition of these samples as the result of magmatic processes during eruption (cf. Shane et al., 2008) rather than post-depositional mixing.

#### 6.1.4.2 Similarity coefficients of the BTPT

SC values calculated between CAT11-07a and the 5000 randomized replicates of this sample produced an average SC value of 0.95 and a lower 95% confidence limit of 0.92. The same

procedure calculated for CAT11-07b produced an average SC value of 0.90 and a lower 95% confidence limit of 0.85 (Table 2). The lower SC values generated here reflect the relatively high variability (standard deviations) of Al, Fe, and Ca oxides measured in glasses from mode CAT11-07b. Previous studies note the difficulty in using similarity coefficients with heterogeneous tephra deposits (Riehle et al., 2008). However, all samples attributed to the BTPT share a mode 'a' similarity coefficient of 0.92 or higher with the type sample CAT11-07a. No other sample has a SC of over 0.86 compared to CAT11-07a. All samples attributed to the BTPT also share a SC of  $\geq 0.94$  with the 'b' mode of the type sample CAT11-07b (Table 3). No other sample has a SC of over 0.84 compared to CAT11-07b. The agreement of the SCs from both modes of the BTPT (Table 3), the distinctive brown color of BTPT glass and consistent stratigraphic observations in the field (Figs. 4, 6) make a strong case for correlation of these five tuffs attributed to the BTPT.

#### 6.1.4.3 Additional exposures of the BTPT

The BTPT is not currently known from Rusinga Island. It is present on Mfangano Island, at the Walangani locality sampled as CAT10-05. It is also present at Karungu at Aoch Nyasaya and Obware, in addition to the representative locality at Kisaaka (Figs. 5, 6). A single sample from

Obware, LVP2013-14, was found at the same stratigraphic level as LVP2013-15 (Fig. 6), and based on our field lithostratigraphic correlation this tephra deposit likely also correlates with the BTPT. While LVP2013-14b shares a SC of 0.94 with CAT11-07b, LVP2013-14a shares a SC of 0.89 with CAT11-07a, below the 95% lower confidence limit (Table 3). For this reason we refrain from confidently designating LVP2013-14 to the BTPT here, but note that the similarities of the glass color, stratigraphic position and the bimodal nature of the tuff suggest that it is a diagenetically altered unit of the BTPT.

#### 6.1.5 Unnamed trachytic tuffs of the Nyamita Valley

Two unnamed trachytic tuffs occur in the Nyamita Valley. The first was originally identified as a distinct mode of glass (CAT09-02a) from the upper-most tuff at section Nyamita 1 (Fig. 2, Tryon et al., 2010). Glass shards attributed to CAT09-02a are distinct based on major element oxide composition but are morphologically indistinguishable from shards attributed to CAT09-02b from the same tuff (Tryon et al., 2010). The CAT09-02a trachytic mode has lower magnesium and calcium contents than seen in any of the other trachytic tuffs in the eLVB (Table 1). We refrain from naming a tuff based on this mode, but we present SCs to show that it is distinct from

all other tephras in this study. Randomization of mean element oxides from CAT09-02a produced an average SC value of 0.95 and a lower 95% confidence limit of 0.93 (Table 2).

A similar trachytic tuff was also identified in isolation (AV1004T5A) at another section, AV1004, further north in the Nyamita Valley (Fig. 2; Van Plantinga, 2011). At section AV1004 this tuff is stratigraphically below samples of the Nyamita Tuff (Figs. 2, 7; Van Plantinga, 2011). Backscattered electron imagery of glass from this tuff sample is provided in Figure (11c). The relative similarity of glass from AV1004T5A to that from CAT09-05 at similar magnification demonstrates the need for chemical compositional data to differentiate these samples. SC values calculated between AV1004T5A and the 5000 randomized replicates of this sample produced an average SC value of 0.95 and a lower 95% confidence limit of 0.92 (Table 2).

The SC between sample AV1004T5A and CAT09-02a is just outside of the 95% confidence limit at 0.91 while SCs between either of these samples and every other tuff reported here is less than 0.86. CAT09-02a has a mean FeO of 9.39 wt. %, which is greater than 2 standard deviations above the mean FeO content of AV1004T5A ( $8.05 \pm 0.14$ ). Because of these differences, we refrain from diagnosing correlation here, but we note the overall chemical similarity of these tuffs

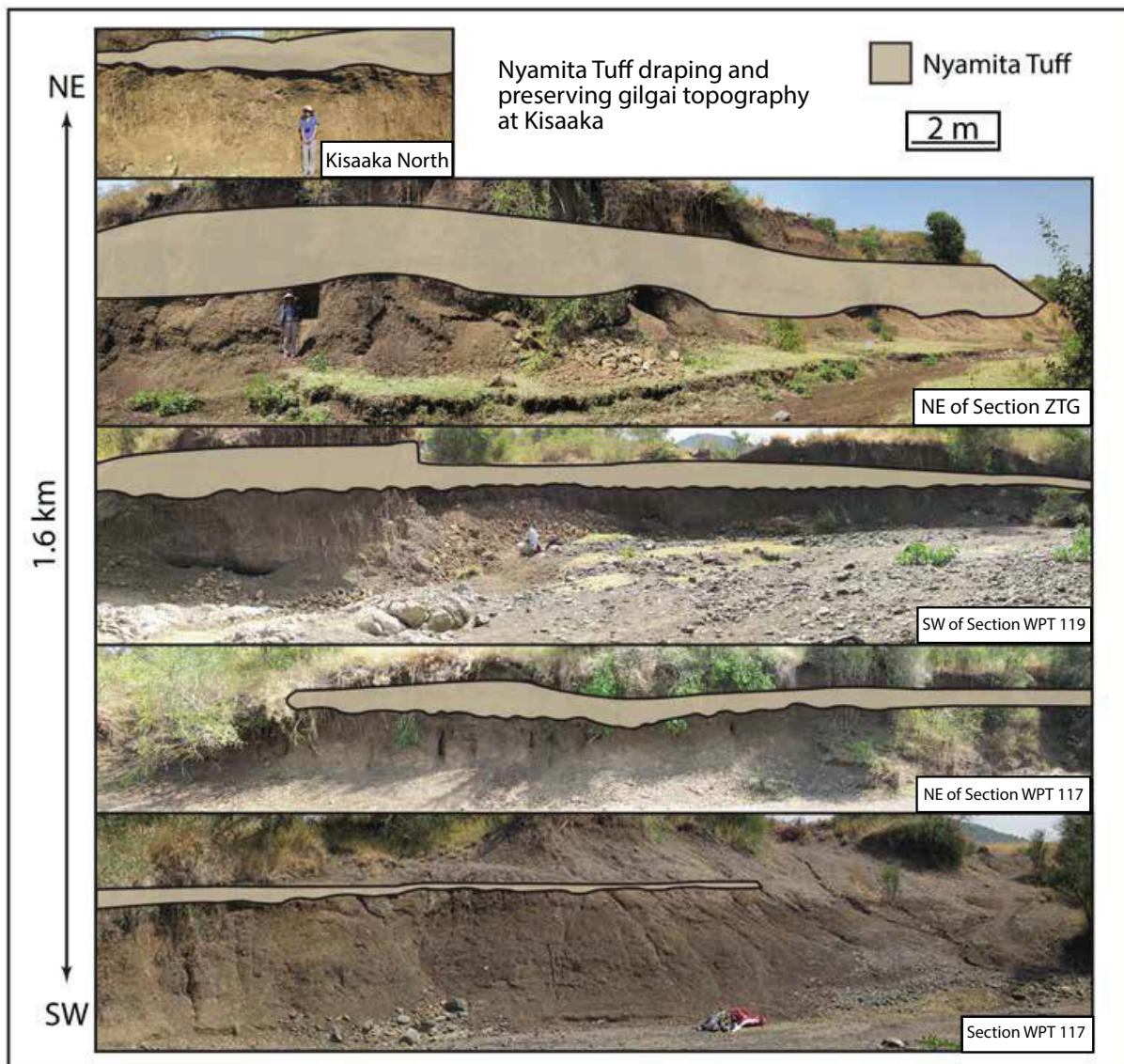


Figure 11: Photographs of the Nyamita Tuff exposed throughout the locality of Kisaaka (modified from Beverly et al., in review). The Nyamita Tuff drapes gilgai topography of the paleo-Vertisol. This topography is formed when the smectitic clays of Vertisols shrink and swell with the wet and dry seasons. The rapid airfall deposition of the tuff preserved these micro-highs and lows on the landscape from fluvial truncation.

and suggest they may represent tephras from a similar source, or perhaps one or more phases of the eruption leading to the Nyamita Tuff not found elsewhere. If more samples of similar trachytic glass are found, these samples may also prove to be end-members of a tuff with variable iron content, as is the case with the Nyamsingula Tuff.

#### 6.1.6 Unnamed rhyolitic tuff

A rhyolitic tuff is known from a single sample, LVP2013-05, from near the base of section ZTG at Kisaaka, Karungu (Fig. 4). At this section LVP2013-05 forms a ~4.5-m-long, 0.17-m-thick lens of fresh, light-grey, vitric ash ~1 meter above the base of section and ~1.75m below the Nyamita Tuff. Sample LVP2013-05 is a fresh, vitric tephra deposit consisting of fine silt to clay-sized sediment dominated by abundant gray glass shards of  $<5\ \mu\text{m} - 20\ \mu\text{m}$ . This is the only rhyolitic tephra deposit in our sample, categorically distinct from all other trachytic and phonolitic samples in this study (Fig. 7). SC values calculated between LVP2013-05 and the 5000 randomized replicates of this sample produced an average SC value of 0.85 and a lower 95% confidence limit of 0.76 (Table 2).

Rhyolitic sample LVP2013-05 from Kisaaka is compositionally similar to a sample of an obsidian source, MER 10, from Ololbutot 2 Oserion Farm, south of Lake Naivasha (SC = 0.83 with LVP2013-05; see Table 3; Fig. 1; Brown et al., 2013). The observed SC, although low because of high variation in rhyolites, is within the range of expected values for replicates of LVP2013-05

(Table 3) and all means of all major element oxides overlap at  $\pm 1$  standard deviation providing confident correlation (Brown and Nash, 2014). Analysis of the MER 10 obsidian sample, like all tuff samples analyzed for this study including LVP2013-05, were done on the same microprobe at the University of Utah using the same standards and protocols (Brown et al., 2013). As obsidians are effusive volcanics found close to their vent source, this correlation suggests that at least some of the tephras found at or near the base of the eLVB section originated from sources near Lake Naivasha in the central Kenyan rift.

#### 6.1.7 A “Nyando Ash” from Songhor

We analyzed a single sample of the “Nyando Ashes”

(Pickford, 1984) from the Pleistocene sediments of Songhor (X-5A-3) originally collected by McBrearty (1981) during her excavations there (Table 1, Fig. 1b-c). In thin section, X-5A-3 is gray silt-sized sediment dominated by abundant  $<5\ \mu\text{m} - 100\ \mu\text{m}$  glass shards with acutely angled margins and round to slightly oval vesicles. This tuff is a phonolite (Fig. 9), similar to the Wakondo and Nyamsingula Tuffs, but distinguishable from these other phonolites by lower  $\text{Al}_2\text{O}_3$  ( $\sim 13.75$  wt %) and higher FeO (9.2 wt %). This sample does not correlate with any other



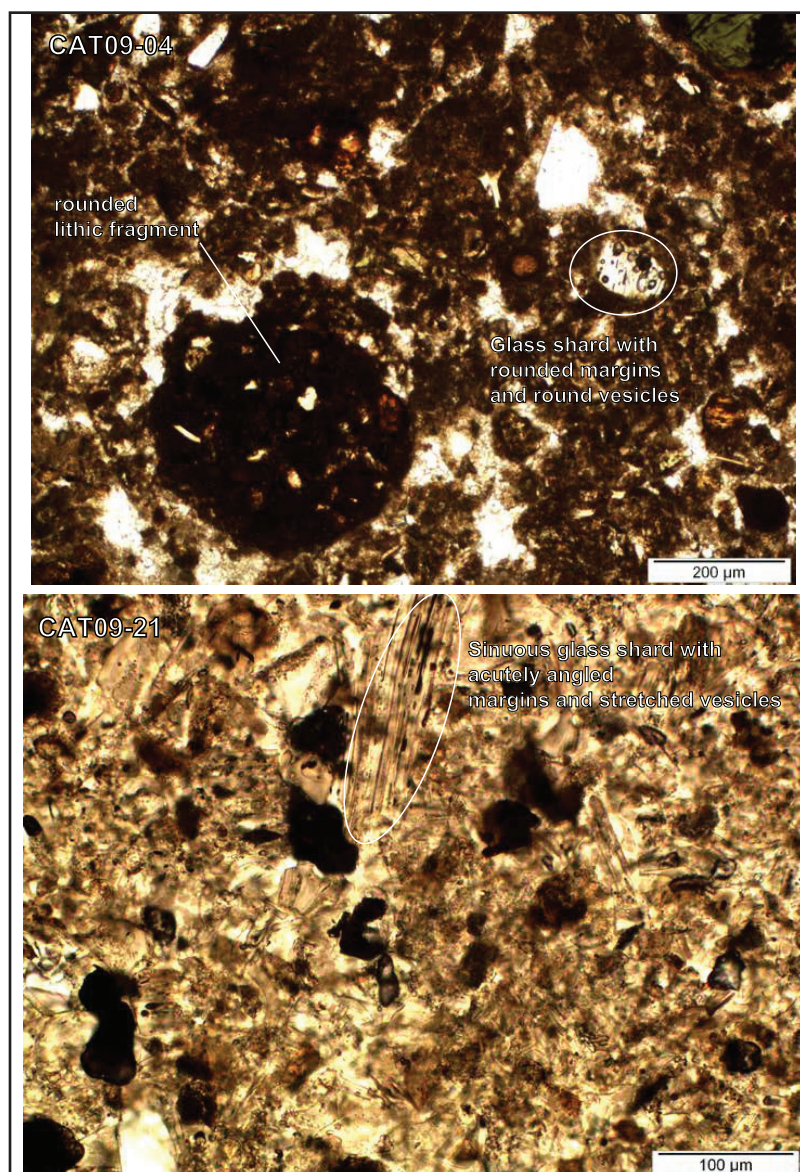


Figure 12: Photomicrographs of resin-impregnated thin sections from samples CAT09-21 (bottom) and CAT09-04 (top) collected from the Nyamita 2 stratigraphic section in the Nyamita Valley, Rusinga Island, shown in stratigraphic order. Stratigraphic positions of samples are shown in Figures 2, 10c. Basal sample CAT09-21 is fresh vitric tephra composed almost entirely of volcanic glass shards (dark spots on photomicrograph are voids or bubbles formed during sample preparation) and some secondary calcite is present. The OSL samples RUS 1 is from directly above CAT09-21 and dated  $46 \pm 4$  ka and RUS 2 from directly below CAT09-21 and is dated  $50 \pm 4$  ka. This sample is interpreted as a primary fallout tephra that has been, at most, minimally reworked. Overlying sample CAT09-04 is a reworked and bioturbated portion of the same deposit, with sparse glass shards set in a silt-clay matrix with epiclastic minerals and lithic fragments. All glass shards in these samples are attributed to the Nyamita Tuff on the basis of geochemical composition (CAT09-04 was analysed on the microprobe as 'KRU2012-18').

tuff known from the eLVB.

SC values calculated between X-5A-3 and the 5000 randomized replicates of this sample produced average SC value of 0.96 and a lower 95% confidence SC limit of 0.93 (Table 2). No other sample analyzed here produced a SC value greater than 0.89 when compared to X-5A-3 (Table 3).

## 6.2 Optical dating results

The optical dating results

for all five samples are presented in Table 4 and the De distributions are presented in

Table 4: Dose rate data, De values and pIRIR ages for the 2 samples from Nyamita and 3 samples from Wakondo.

Sample name	Moisture content		Dose rates (Gy/ka)			Total dose rate (Gy/ka)	De (Gy)	pIRIR age (ka)
	(%)	Beta	Gamma	Cosmic	Internal			
Nyamita RUP-1	11.5	$1.73 \pm 0.09$	$0.83 \pm 0.04$	$0.18 \pm 0.03$	$0.84 \pm 0.07$			$46.4 \pm 3.6$
RUP-2	4.5	$1.71 \pm 0.08$	$1.01 \pm 0.04$	$0.16 \pm 0.02$	$0.84 \pm 0.07$			$49.7 \pm 3.5$
Wakondo RUP-3	4	$2.17 \pm 0.10$	$1.37 \pm 0.06$	$0.21 \pm 0.03$	$0.84 \pm 0.07$			$73.8 \pm 6.3$
RUP-4	5.7	$2.18 \pm 0.11$	$1.29 \pm 0.06$	$0.21 \pm 0.03$	$0.84 \pm 0.07$			$67.5 \pm 6.3$
RUP-5	7.5	$2.28 \pm 0.12$	$1.41 \pm 0.07$	$0.21 \pm 0.03$	$0.84 \pm 0.07$			$63.6 \pm 6.0$

Fig. S3 as radial plots. Ages of  $46 \pm 4$  (RUP-1) and  $50 \pm 4$  ka (RUP-2) were calculated for the samples collected above and below sample CAT09-21 (Fig. 2), providing age constraints for the deposition of the type sample of the Nyamita Tuff (Table 4). Both ages are statistically consistent with each other at  $1\sigma$ , and represent our best constraints on the depositional age of the Nyamita Tuff. The type sample, CAT09-21, around which the optical dating samples were collected, is a fresh vitric deposit indicating airfall deposition (Fig. 12) Thus, the depositional age likely closely approximates the eruptive age of the Nyamita Tuff.

For the samples from Wakondo, Bovid Hill locality, the ages range from  $64 \pm 6$  (RUP-5) to  $74 \pm 6$  ka (RUP-3) for samples from a channel complex that occurs  $\sim 1$  m stratigraphically above the type sample of the Wakondo Tuff (CAT09-05) (Fig. 2; Jenkins et al, 2012). All three optical dating ages are statistically consistent with each other at  $1\sigma$  and there is no stratigraphic evidence

to suggest that the sediments from which the samples were collected were deposited at different times. It is, therefore, our best estimate to obtain a weighted mean age of  $68 \pm 5$  ka for the depositional age of the Bovid Hill locality channel complex from Wakondo (Table 4). These age constraints provide a minimum age of  $68 \pm 5$  ka for the deposition of the underlying Wakondo Tuff.

## 7. Discussion: Succession, age, and transport of the eLVB tephras

We recognize a single sequence of tephras among Pleistocene outcrops from Rusinga Island, Mfangano Island, and Karungu, exposed along a north-south transect of >60 km. From bottom to top, the sequence includes the Wakondo Tuff, the Nyamita Tuff, the Nyamsingula Tuff, and the Bimodal Trachyphonolitic Tuff (BTPT), with an additional three compositionally unique tephras. Multiple radiometric dates bound the deposition of these tephras and intercalated sediments to between ~100 ka and ~33 ka. Although tuffs may be locally correlated in the field where exposure is good, geochemical compositional data are required for accurate correlation between discontinuous outcrops and over longer distances between localities. No sample from Rusinga Island, Mfangano Island, or Karungu correlates with the “Nyando Ashes” from Songhor.

Tryon et al. (2010) hypothesized an origin in the Kenyan Rift (particularly Longonot and Suswa

volcanoes, Fig. 1) for eLVB tephras based on the absence of known Pleistocene-age volcanoes in Lake Victoria basin, the fine grain size of the ashes, and the restricted distribution of trachyte- and particularly phonolite-producing eruptions in East Africa during the Pleistocene. This hypothesis is empirically supported by our correlation of the distal rhyolitic ash sample LVP2013-05 to obsidian vent sources at Oserian Farm south of Lake Naivasha in the Kenyan Rift (Fig. 1), 250 km east. These distant sources have important implications for understanding the depositional mode of the eLVB tephra and interpreting both their stratigraphic position and age.

The topography of the Mau escarpment on the western edge of the Kenyan Rift prevents rivers from running east-west between the eLVB and the Rift Valley volcanoes, eliminating the possibility for long-distance fluvial transport of the tephras, as is the case in the Lake Turkana Basin (Feibel, 2011). As suggested elsewhere (Faith et al., 2015; Tryon et al., 2010, 2012, 2014), the Pleistocene sediments on Rusinga Island, Mfangano Island, and Karungu formed when Lake Victoria was absent or substantially diminished, excluding deposition or reworking by large scale lacustrine processes. Airfall deposition is thus the most likely method of transit for these tephras from the Kenyan Rift (or elsewhere) into the eLVB. Direct evidence for airfall deposition can be seen at Kisaaka, where the Nyamita Tuff drapes and preserves gilgai topography over ~1 km of

lateral exposure (Fig. 11). In the rock record, gilgai topography is rarely preserved because the granular peds of the A horizon in vertisols are easily transported and are often eroded during the next depositional event, truncating the characteristic undulations (Caudill et al., 1996; Driese et al., 2003; Driese et al., 2000; Mora and Driese, 1999). The preservation of the gilgai topography at Kisaaka demonstrates that airfall deposition of this tephra is preserved for at least some of the exposures of the Nyamita Tuff in the eLVB (Fig. 11).

Although there is evidence to indicate that at least some of the tephra are airfall deposits, the eLVB tephra were deposited on a landscape that included small, probably seasonally active channels (Tryon et al., 2010, 2012, 2014) and springs (Beverly et al., 2015b). Some deposits show clear evidence for reworking, including at least three deposits of the Nyamita Tuff in the Nyamita Valley (Fig. 2), three deposits of Nyamita Tuff at Kisaaka (Fig. 4) and a single deposit at Aringo Section A (Fig. 5). Such deposits are recognized on the basis of chemically distinct, multimodal populations of glass shards, a mixture of detrital clasts and volcanic glass, and/or evidence of pedogenesis, as is likely the case for the upper portions of the Nyamita 2 section (Fig. 2). These processes indicate that the age of the deposition of some tuffs may differ from the age of the

eruption that produced it. Where reworking occurs, it is most commonly between a chemically unimodal and lithologically coherent unit of the Nyamita Tuff and some smaller, stratigraphically superjacent tuff deposit. These redeposited units are easily recognized in the field based on their lithology and evidence for pedogenesis. Chemically, the reworked tephra are multimodal with one mode belonging to shards of the reworked Nyamita Tuff and the other modes from the superjacent tuff deposit, usually the Nyamsingula Tuff (see Figs, 4, 5), or the BTPT redeposited ~20 cm up-section in clumped clasts (Fig. 6).

While some syn- and post-depositional reworking of the ash occurred, such events are distinguishable from primary deposition of the tuffs under consideration. For most tuffs in this study, glass is chemically homogenous and fresh indicating rapid burial in an environment where paleosol formation is a recurrent feature (e.g. Beverly et al., 2015b; Van Plantinga, 2011). The documented airfall deposition of tuff units such as those at Kisaaka, as well as the fairly rapid burial of such tuff units, facilitates lithostratigraphic correlation between identified stratigraphic units at temporal scales (~10 to 10<sup>4</sup> years), the time scales widely employed in paleoecological and archaeological studies of ancient landscapes (e.g. Behrensmeyer et al., 2000; Potts et al., 1999).

OSL dates bracketing the fresh vitric ash of the type sample of the Nyamita Tuff in Rusinga Island's Nyamita Valley indicate an age of ~49 ka for its deposition there (see Table 5 and supplementary information). Sedimentary features (e.g., the sample consists almost entirely of glass shards) suggest that the dated deposit (CAT09-21) underwent minimal reworking following deposition, and thus its depositional age likely approximates eruption age (Fig. 12). We propose that this 49 ka date provides the earliest age of deposition of the Nyamita Tuff in the Nyamita Valley of Rusinga Island. It also likely reflects an approximate age for the continuous lateral deposits of the Nyamita Tuff at Kisaaka, which drape the gilgai topography indicating they are airfall deposits (Figs 4, 11). Additionally, the 49 ka data for the Nyamita Tuff in the Nyamita Valley also provides a maximum age for the other deposits of the Nyamita Tuff that were not unequivocally deposited via airfall.

Glass shards from the ~2 m of overlying tuffaceous sediment (sampled in thin section as CAT09-04 and analyzed as KRU2012-18) overlying the dated type sample (CAT09-21) at Nyamita 2 are also chemically attributable to the Nyamita Tuff. However, glass from the upper 2m at Nyamita 2 occurs in a deposit that has undergone substantial post-depositional turbation (Fig. 12) indicating a considerably different depositional history than the underlying deposit from which CAT09-



21 was taken and which is dated to 49 ka. Gastropods occur in the upper ~ 2m of the deposit, and one gastropod from the deposited was dated using AMS radiocarbon to ~40.5 ka. Based on our field observations, the gastropods at Nyamita 2 most likely burrowed into the tuff after deposition, but before lithification. Thus, the minimum age for re-deposition of the reworked Nyamita Tuff at Nyamita 2 is ~40.5 ka, or <9 ka after deposition of the vitric, airfall deposit at the base of Nyamita 2. Radiocarbon dates on intrusive snail shells at adjacent Nyamita Tuff outcrops from the Nyamita Valley (Fig. 2) range from 33-45 ka (Table 5). These radiocarbon dates indicate that the Nyamita Tuff was reworked and redeposited throughout the Nyamita Valley >33 ka.

We interpret the widespread Nyamita Tuff as the most useful marker bed in the eLVB. Its position near the middle of the tephrosequence, its distinctive and relatively homogenous chemical composition and its OSL age estimate of ~49 ka for its initial deposition make it well suited as an informal boundary between upper and lower portions of the eLVB sedimentary sequence (Fig. 8). However, the age of the sediments above the Nyamita Tuff, including the Nyamsingula Tuff and BTPT, are poorly constrained. They postdate the  $\leq 49$  ka deposition of the Nyamita Tuff, and may fall into the 33-45 ka range of dates suggested by the gastropod shells, when snails were actively burrowing into the Nyamita Tuff, which formed the land surface (or near subsurface) at the



time. Archaeological evidence provides further support for this inferred age, as all of the tuffaceous eLVB sediments contain only Middle Stone Age (MSA) artifacts, and no Later Stone Age (LSA) material has been found (Faith et al., 2015; Tryon et al., 2010, 2012, 2014). Elsewhere in

Table 5: Age estimates for tuffs discussed in this study.

<b>Tuff</b>	<b>Minimum Age (ka)</b>	<b>Method</b>	<b>Maximum Age (ka)</b>	<b>Method</b>
BTPT	35-42	$^{14}\text{C}$	49	Nyamita Tuff below +tephra correlations.
Nyamsingula	35-42	BTPT +tephra correlation	49	Nyamita Tuff+tephra correlations.
Nyamita	49	OSL	49	OSL
Nyamita Valley Trachytes	49		94-111	U-Th
Rhyolitic tuff	49	OSL of Nyamita Tuff + tephra correlation	94-111?	
Wakondo	68	OSL	94-111	U-Th on tufa from Nyamita Valley.
Wakondo			100	Compositional similarity to Suswa phonolites.

East Africa, MSA technologies are replaced by LSA ones during the same 35-45 ka interval (Tryon and Faith, 2013), and if the sediments were much younger than this we would expect to have recovered an LSA archaeological component above the Nyamita Tuff in sediment interbedded with the Nyamsingula Tuff and BTPT.

Below the Nyamita Tuff, OSL dates of ~68 ka from the Wakondo locality, collected from sediments above the Wakondo Tuff, provide a minimum age for the deposition of the Wakondo Tuff (Tables 4, 5). U-series dates of  $94.0 \pm 3.3$  ka and  $111.4 \pm 4.2$  ka from tufa deposits at the base of the sequence at Nyamita (Fig. 2, Table 5; Beverly et al., 2015b ) provide a maximum age for the deposition of the Wakondo Tuff, as well as for the entire sedimentary sequence. Compared to sediments above the Nyamita Tuff, which were likely deposited over  $\leq 16$  kyr (i.e. 33 – 49 ka), the lower portion of the tephr sequence appears to span a considerably longer interval, from ~49 ka - 100 ka.

The tephr stratigraphy presented here coupled with accompanying chronometric dates provides a robust and testable hypothesis for the depositional age of and correlation between late Pleistocene fossil- and artifact-bearing deposits on Rusinga and Mfangano Islands and near Karungu.

The tephrostratigraphic framework supports our lithostratigraphic correlations between stratigraphic sections on Rusinga and at Karungu. Additionally, the tephrostratigraphy presented here allows the correlation of distant exposures over ~60 km. The tephrostratigraphic and chronometric framework presented here represents our hypothesis that dated and non-dated localities that have been correlated lithostratigraphically and/or using tephrostratigraphy are approximately contemporaneous. The hypothesis that the sedimentary deposits are contemporaneous can be further tested by constraining the eruptive age of tephras through a combination of correlation to more proximal, pumiceous facies and through methods that allow direct dating of the tephra (i.e.,  $^{40}\text{Ar}/^{39}\text{Ar}$ , U/Pb).

The tephrostratigraphic sequence presented here thus provides the initial basis for sampling spatial and temporal variation in paleoenvironments and hominin behaviors across ancient landscapes in the eLVB. Such an approach, with tephrostratigraphic correlation as one of many integrative tools, has proven highly successful through decades of research at Early and Middle Pleistocene deposits in the Turkana Basin, at Olorgesailie in Kenya, and at Olduvai Gorge, Tanzania (Ashley et al., 2009; Behrensmeyer et al., 2000; Blumenshine et al., 2012; Hay, 1976; Potts et al., 1999; Rogers et al., 1994; Stern, 1994). Our efforts in this direction are just beginning (Faith

et al., 2012; Faith et al., 2015; Garrett et al., 2015; Tryon et al., 2014; Van Plantinga, 2011), and the tephrostratigraphy of the region presented here makes an important contribution towards the goal of developing a detailed chronostratigraphic framework of contemporaneous Late Pleistocene sites around the Lake Victoria Basin.

## 8. Conclusions:

Analyses of distal tephras from the eLVB demonstrate the presence of eight distinct tephras of at least nine chemical compositions. Chemical characterization combined with field stratigraphy show that four of these tephras correlate over a distance >60 km: the Wakondo Tuff, the Nyamita Tuff, the Nyamsingula Tuff, and the Bimodal Trachyphonolitic Tuff (BTPT). Radiometric dates bound the tephrostratigraphic sequence. The base of the sequence is ~100 ka, based on U-series dates from tufa deposits that underlie the entire sedimentary sequence (Beverly et al., 2015b). These dates also provide a maximum age for the deposition of the Wakondo Tuff, and OSL dates of ~68 ka from sediments above the Wakondo Tuff provide a minimum age for its deposition. The Nyamita Tuff, which is bounded by OSL age estimates of  $46 \pm 4$  (RUP-1) and  $50 \pm 4$  ka (RUP-2) was likely deposited ~49 ka, a depositional age that may closely approximate its eruptive age. The Nyamsingula Tuff and the BTPT, which caps the sequence, were then de-

posited in sequence between  $\sim 49$  and  $\geq 35$  ka, based on dates on gastropod shells that post-depositionally burrowed into the underlying Nyamita Tuff. The upper boundary of these sediments is poorly dated, but consistent with the available archaeological data. No Later Stone Age (LSA) artifacts have yet been recovered, and elsewhere in eastern Africa LSA assemblages appear  $\sim 45$ -30 ka (Tryon and Faith, 2013).

Our correlations among the tephras and the age constraints provided by a variety of geochronological and other methods, demonstrate shared depositional sequences among disparate Pleistocene exposures from two islands in Lake Victoria and multiple exposures on the Kenyan mainland spanning  $\sim 35$ -100 ka. This study broadly confirms the initial hypothesis of Pickford (1984) of widespread Pleistocene tephra deposits in the eLVB and a shared depositional history for Rusinga Island, Mfangano Island, and Karungu, but differs substantially in the details, particularly in the number of tephras present and the need for geochemical compositional data for reliable correlation.

This study further provides the stratigraphic control necessary for ongoing paleoenvironmental and human behavioral reconstructions based on fossils, soils, and artifacts from Pleistocene dates on gastropod shells that post-depositionally burrowed into the underlying Nyamita Tuff.

The upper boundary of these sediments is poorly dated, but consistent the available archaeological data. No Later Stone Age (LSA) artifacts have yet been recovered, and elsewhere in eastern Africa LSA assemblages appear ~45-30 ka (Tryon and Faith, 2013).

Our correlations among the tephras and the age constraints provided by a variety of geochronological and other methods, demonstrate shared depositional sequences among disparate Pleistocene exposures from two islands in Lake Victoria and multiple exposures on the Kenyan mainland spanning ~35-100 ka. This study broadly confirms the initial hypothesis of Pickford (1984) of widespread Pleistocene tephra deposits in the eLVB and a shared depositional history for Rusinga Island, Mfangano Island, and Karungu, but differs substantially in the details, particularly in the number of tephras present and the need for geochemical compositional data for reliable correlation.

This study further provides the stratigraphic control necessary for ongoing paleoenvironmental and human behavioral reconstructions based on fossils, soils, and artifacts from Pleistocene exposures in the eastern Lake Victoria Basin. Furthermore, we predict that the Wakondo Tuff, Nyamita Tuff, Nyamsingula Tuff, the BTPT, and other eLVB distal tephra deposits will be found

in Pleistocene sediments in other depositional basins in East Africa, substantially expanding the scale of the work presented here.

Paper #2

Tephrostratigraphy and archaeology of the Kapthurin Formation, Kenya: revised chronology and new ages for Acheulean and Middle Stone Age sites.

Nick Blegen\*

Department of Anthropology

University of Connecticut

Storrs, CT 06269, USA

E-mails: [nicholas.blegen@uconn.edu](mailto:nicholas.blegen@uconn.edu), [nick.blegen@gmail.com](mailto:nick.blegen@gmail.com)

\*Corresponding author= Nick Blegen +1 (847) 436-3854

Sally McBrearty

Department of Anthropology

University of Connecticut

Storrs, CT 06269, USA

[mcbrearty@uconn.edu](mailto:mcbrearty@uconn.edu)

(TO BE SUBMITTED TO The Journal of Human Evolution)



## Abstract:

We present an updated chronology for archaeological sites of the Kapthurin Formation, Baringo Basin, Kenya based on new tephra correlations. This refined tephrostratigraphy provides new ages for twelve archaeological sites from the later Middle Pleistocene (130–400 ka) through the early Late Pleistocene (100–130 ka) of the Kapthurin Formation. The Middle through Late Pleistocene of East Africa is an important time period for both the behavioral and biological evolution of *Homo sapiens*. This period records significant technological changes including the end of the Acheulean, development of diverse Levallois prepared core techniques and the beginning of the Middle Stone Age. This period also records the first appearance of *Homo sapiens* in Africa. The Kapthurin Formation, Baringo, Kenya is well suited to research questions related to these issues as this formation spans a significant portion of the Middle Pleistocene and has a long history of paleoanthropological research. Results presented here provide a new minimum age of  $\geq 380 \pm 7$  ka for eight archaeological sites demonstrating diverse Levallois technology in East Africa  $\geq 380$  ka. New tephra correlations of the tuffs capping the Middle Stone Age sites of Keraswanin (GnJh-78) and tephra correlation as well as preliminary  $^{40}\text{Ar}/^{39}\text{Ar}$  dates for the Sibilo School Road Site (GnJh-79) provide new minimum ages of 100 ka and 200 ka for these sites respectively. The updated chronological and archaeological record of the Kapthurin Formation shows

Levallois approaches to core preparation are more diverse and ~100, 000 years older than previously estimated in East Africa. The correlation of the tuff capping the site of Keraswanin in the Baringo Basin to the Wakondo Tuff >200 km west in the eastern Lake Victoria Basin of western Kenya also demonstrates a new, long-distance inter-basinal tephra correlations for the late Pleistocene of East Africa.

#### Introduction:

The Middle Pleistocene of Africa (130 – 780 ka) is an important time period for the study of human evolution. In this time period the Acheulean, a technocomplex characterized by large, hand-held stone tools such handaxes and cleavers and lasting over ~1.5 myr through much of Africa and western Eurasia, is replaced by stone tools of the Middle Stone Age (MSA) in Africa and the Middle Paleolithic (MP) in western Asia and Europe. MSA and MP technocomplexes are characterized by a wider range of tool forms, including hafted tools, and greater technological diversity in stone tool production methods, particularly Levallois approaches to core preparation and reduction (Adler et al., 2014; Clark, 1988; Porat et al., 2010; Tryon et al., 2005; Wilkins et al., 2012). Additionally, the later Middle Pleistocene of East Africa also records the first appearance of our species, *Homo sapiens* (McDougall et al., 2005). Thus, the timing of this technologi-

cal shift and its relationship to the origin of our species in East Africa is an important problem for understanding the behavioral and biological evolution of our species.

McBrearty and Brooks (2000) argue that the evolution of modern behavior is characterized by a gradual process of behavioral adaptations incrementally acquired alongside biological adaptations throughout the Middle and Late Pleistocene of Africa, resulting in the biologically and behaviorally modern *Homo sapiens* known from the Late Pleistocene. This model posits that understanding behavioral evolution relies on understanding the pattern and timing in which behaviorally modern traits such as new technologies, subsistence strategies and ecological adaptations were acquired throughout the Middle and Late Pleistocene. Recent work in the Middle Pleistocene of Africa and Eurasia also shows that important technological innovations of the Middle Pleistocene such as diverse Levallois core preparation methods (Adler et al., 2014) and hafting (Wilkins et al., 2012) emerged independently, multiple times, in different regions of Eurasia and Africa and are likely older than previously realized. Thus, a detailed regional understanding of the timing and characteristics of important technological innovations of the Middle Pleistocene in East Africa is important for understanding the circumstances of this event and for relating these behavioral developments to changes in environment and biological evolution relevant to

the evolution of *Homo sapiens*.

The age and pattern of technological and other behavioral innovations in the MSA is relatively well understood due to the robust body of work on the Late Pleistocene of southern Africa (Deacon, 1979; Henshilwood et al., 2002; Jacobs et al., 2006; Marean et al., 2007; Marean et al., 2000; Singer and Wymer, 1982; Wadley and Jacobs, 2006). A comparable framework of behavioral and technological change is also being established for the Late Pleistocene in East Africa (Brooks et al., 2006; Diez-Martín et al., 2009; Mehlman, 1977). However, a comparably complete archaeological record is still being compiled for the East African early MSA (eMSA), the MSA of the Middle Pleistocene > 130 ka (McBrearty and Tryon, 2006; Tryon, 2006; Tryon et al., 2005). This relative lack of knowledge regarding the character and chronology of East African eMSA limits our understanding of hominin behavior at this crucial time period for human evolution leading to the perception that the Middle Pleistocene MSA is technologically static and that modern behavior lags behind modern anatomy in the evolution of *Homo sapiens* (Klein, 2000). This study seeks to add to the increasing body of knowledge on the East African eMSA (Douze, 2014; Morgan and Renne, 2008; Sahle et al., 2014; Shea, 2008; Wendorf and Schild, 1974) by demonstrating technological change in the lithic assemblages of the Middle and early Late Pleis-

tocene of the Kapthurin Formation, Baringo, Kenya. Archaeological excavation of new material can partially address this problem, but to understand the process of technological change this archaeological material must be chronologically dated as precisely as possible.

East Africa provides abundant potential to demonstrate the stratigraphic and chronometric equivalence among paleoanthropological sites via the science of tephrostratigraphy, the geochemical and lithostratigraphic correlation of volcanoclastic deposits and their use as widespread markers in the geological record (Feibel, 1999). Rifting of the East African Rift System (Hay, 1976) provides the mechanisms for volcanic eruptions and rapid sedimentation and burial of paleoanthropological materials. The tectonic extension of this system also provides a means of subsequent exposure through continued normal faulting (Chorowicz, 2005). A well-established Pliocene and Early Pleistocene tephrostratigraphic framework has been established for paleoanthropological sites in Kenya, Ethiopia, Tanzania and Uganda (Brown et al., 2006; Brown et al., 1992; Feibel, 1999; Hay, 1976; McHenry et al., 2008; Pickford et al., 1991; WoldeGabriel et al., 2013). Comparatively few data are available for these areas during the Middle and Late Pleistocene (Blegen et al., 2015; Brown et al., 2012; Morgan and Renne, 2008; Sahle et al., 2014; Tryon et al., 2010; Tryon and McBrearty, 2002; Tryon and McBrearty, 2006; Tryon et al., 2008). The Kapthurin For-

mation, and the Bedded Tuff Member of this formation in particular, have played an important role in incorporating tephra science to refine the dating of archaeological material relevant to the archaeology of modern human origins (Deino and McBrearty, 2002; Tallon, 1976, 1978; Tryon, 2003; Tryon and McBrearty, 2006).

This study presents results of systematic programs of archaeological survey and geological sampling of the northern exposures (north of the Kasurein River) of the Kapthurin Formation (Fig. 1a). By laterally expanding the tephrostratigraphic framework and linking more distal tephtras in the Bedded Tuff Member to proximal outcrops at the source volcano, Korosi, dated to  $380 \pm 7$  ka (Dunkley et al., 1993) the work presented here refines the stratigraphy and chronology relevant to the archaeology of the later Middle Pleistocene and early Late Pleistocene.

In particular, the updated tephrostratigraphy presented here demonstrates sites situated at or beneath the base of the Bedded Tuff Member, containing Levallois prepared core technology, date to  $\geq 380$  ka,  $\sim 100$  kyr earlier than allowed by previous estimates between  $>284$  ka (Deino and McBrearty, 2002; McBrearty and Tryon, 2006; Tryon and McBrearty, 2002; Tryon and McBrearty, 2006). The updated tephrostratigraphy and chronology presented here also provides new

ages for two new recently excavated MSA sites. Analysis of the coarse pumiceous tuff capping the Sibilo School Road Site (GnJh-79) in the north of the Kapthurin Formation provides a new minimum age >200 ka for the MSA material at the Sibilo School Road Site. Correlation of the tuff capping the MSA site of Keraswanin in Baringo Basin to the Wakondo Tuff ~200 km west in the eastern Lake Victoria Basin provide a ~100 ka age estimate for MSA archaeological material at Keraswanin based on age constraints for the Wakondo Tuff (Beverly et al., 2015; Blegen et al., 2015). This correlation also demonstrates one of only a few inter-basinal tephra correlations for the Late Pleistocene of East Africa and provides an important first step in expanding and refining the tephro and chronostratigraphic framework of the Late Pleistocene in East Africa (Blegen et al., 2015; Brown et al., 2012).

The Kapthurin Formation background and previous research:

Geographic extent of the Kapthurin Formation:

The Kapthurin Formation is a series of sedimentary and volcanic deposits exposed to the west of Lake Baringo in the Central Rift Valley of Kenya (Fig 1a). These sediments are generally flat-ly-

ing and unconformably overlie tilted and faulted sediments of the Chemeron Formation, forming the upper portion of a sedimentary sequence spanning ~16 million years from the middle Miocene to the Late Pleistocene and Holocene (Hill et al., 1986; Martyn, 1969; Tallon, 1976, 1978). Sediments attributed to the Kapthurin Formation are exposed over an area of ~150 km<sup>2</sup> to the west of Lake Baringo with a maximum thickness reaching 125–150 m near the central axis of the basin around the east to west trending Ndau and Kapthurin rivers immediately west of the modern Nakuru road (Fig. 1a; Tallon, 1976, 1978). The vast majority of Kapthurin Formation exposures occur between the towns of Marigat and Kampi-ya-Samaki within 10 –15 km west of the main road, but sediments of the Kapthurin Formation crop out discontinuously as far south as the Perikerra River (Fig. 1a) and correlations presented here confirm that Kapthurin Formation exposures are encountered as far as ~10 km north of the town of Loruk (McCall et al., 1967; McCall, 1967; Spooner, n.d.; Tallon, 1976, 1978). Deposits generally become thinner in the north of the Kapthurin Formation (north of the Kasurein River, see Fig 1a) and are covered by modern sediments and the waters of modern Lake Baringo to the east of the main road.

Stratigraphy of the Kapthurin Formation:





Gravels Member (K1) is nonconformably overlain by the volcaniclastic Pumice Tuff Member (K2). This member is comprised of a voluminous pumiceous eruption, the Pumice Tuff, secondarily thickened to > 20m of variably bedded pumices near the central axis of the Kapthurin Basin between the Barsemoi and Kasurein rivers. This pumice eruption was coincident with a large effusive lava flow, the Lake Baringo Trachyte which comprises the other part of the Pumice Tuff Member (Tallon, 1976). The Middle Silts and Gravels Member (K3) overlies the Pumice Tuff Member and contains several thin (<1m) layers of fine-grained tuffs (Tallon, 1976, 1978). The most significant of these is the “Grey Tuff.” The Grey Tuff was formally named for a unit exposed in the Lebus river in the south of the Kapthurin Formation (Tallon, 1976). The fine-grained, fresh, vitric dark grey to grey primary fall-out lithology of this tuff has been used as a stratigraphic marker bed in the central axis of the Kapthurin Basin north of the Kapthurin River to the Barsemoi River in order to laterally correlate several paleontological sites including two hominin fossil sites (Leakey et al., 1969; McBrearty et al., 1996; Tallon, 1976, 1978; Wood and Van Noten, 1986). The Bedded Tuff Member (K4), situated above K3 and below K5, is composed of a series of over a dozen alternating sedimentary and volcaniclastic units measuring a maximum thickness of 30– 35 m near the central axis of the Kapthurin Basin centered between the Kapthurin and Ndau Rivers (Tryon, 2003). The Bedded Tuff Member is also widely exposed

laterally and is the only member of the Kapthurin Formation observed north of the Kasurein River (Tallon, 1976, 1978) where it overlies the Lake Baringo Trachyte. In places the Kapthurin Formation is unconformably overlain by deposits of the Holocene age Loboil Silts (Bishop et al., 1971; Renaut and Owen, 1980).

#### Chronometric Dating of the Kapthurin Formation:

The Kapthurin Formation temporally spans much of the Middle Pleistocene from > 610 ka to < 235 ka (Deino and McBrearty, 2002; Martyn, 1969; Tallon, 1976, 1978; Tryon and McBrearty, 2002; Tryon and McBrearty, 2006). A maximum age of 1.57 Ma is provided by a K / Ar date on the Ndau Trachymugearite, a lava flow of the upper Chemeron Formation exposed in the Ndau and Kapthurin Rivers (Hill et al., 1986). Dates of  $545 \pm 3$  ka and  $543 \pm 4$  ka by the  $^{40}\text{Ar}/^{39}\text{Ar}$  method on the contemporaneous Lake Baringo Trachyte and Pumice Tuff respectively provide the oldest direct chronometric dates in the Kapthurin Formation (Deino and McBrearty, 2002).

However, all Kapthurin Formation sediments are normally magnetized (Dagley et al., 1978; McBrearty, 1999), and thus postdate the Matuyama– Brunhes boundary, currently estimated at  $778.0 \pm 1.7$  (Love and Mazaud, 1997). A single tuff unit, The Grey Tuff, within the Middle Silts and

Gravels Member, is directly dated to  $509 \pm 9$  ka by the  $^{40}\text{Ar}/^{39}\text{Ar}$  method (Deino and McBrearty, 2002).

The Bedded Tuff Member has produced two  $^{40}\text{Ar}/^{39}\text{Ar}$  dates on trachytic pumiceous tuffs from the upper half of this member (Fig. 1b). The older of these is a date of  $284 \pm 12$  ka on a pumiceous trachytic tuff from the Ndau River Section (NRS) north of the Ndau River (Deino and McBrearty, 2002). The younger is a date of  $235 \pm 2$  ka from a coarse pumiceous tuff from the locality Johnny Leakey's Compound (JLC) from the Kampi-ya-Samaki peninsula near the town of Kampi-ya-Samaki (Deino and McBrearty, 2002).

The  $235 \pm 2$  and  $284 \pm 12$  ka  $^{40}\text{Ar}/^{39}\text{Ar}$  dates produced by Deino and McBrearty (2002) agree with previous K / Ar dates of  $250 \pm 12$  and  $240 \pm 8$  ka sampled in the same region (Hill et al., 1986; Tallon, 1978: 372). Large scale faulting followed the deposition of the Bedded Tuff Member of the Kapthurin Formation (Tallon, 1976, 1978). Age estimates achieved by the Uranium-series (U-series) method on hydrothermal silica in-filling cracks from faulted exposures of the Lake Baringo Trachyte produced dates ranging from 198 to 345 ka on at least four major episodes of faulting (Le Gall et al., 2000; Tallon, 1978). Field observations also show the localities of JLC where tuff samples dated to  $235 \pm 2$  ka were collected and nearby correlative exposures of this

tuff on the Kampi-ya-Samaki peninsula are generally dipping five degrees northeast. The structural movement of these beds thus postdates deposition and this supports the U-series dates on fault cracks in suggesting a Middle Pleistocene age of >200 ka for deposition of all sediments of the Bedded Tuff Member of the Kapthurin Formation.

#### Archaeology of the Kapthurin Formation:

Sediments in the Kapthurin Formation contain dozens of archaeological and paleontological localities, including several hominid sites (Cornelissen et al., 1990; Deino and McBrearty, 2002; Johnson and McBrearty, 2010; Leakey et al., 1969; McBrearty et al., 1996; Tryon, 2003; Tryon and McBrearty, 2002; Tryon and McBrearty, 2006; Wood and Van Noten, 1986). Paleontological material collected to date derives primarily from sites in the Middle Silts and Gravels Member (K3), and below the Grey Tuff dated to  $509 \pm 9$ ka (Cornelissen et al., 1990; Deino and McBrearty, 2002; McBrearty et al., 1996). Archaeological sites are more evenly distributed throughout the section. Leakey et al. (1969) report the excavation of *in situ* archaeological material from the Hominid Site, Edward Kandini's Gulley (EKG= GnJh- 10) in the Middle Silts and Gravels Member from below a tuff unit later classified as the Grey Tuff (Cornelissen et al., 1990; Tallon,

1978) and dated to  $509 \pm 9$  ka by the  $^{40}\text{Ar}/^{39}\text{Ar}$  method (Deino and McBrearty, 2002). Johnson and McBrearty (2010) describe two additional archaeological sites with evidence of blade technology >500 ka from the Middle Silts and Gravels Member of the Kapthurin Formation.

The Bedded Tuff Member contains sites displaying aspects of both Acheulean and MSA technology (McBrearty, 1999, 2001; McBrearty et al., 1996; Tryon, 2006; Tryon and McBrearty, 2002; Tryon and McBrearty, 2006; Tryon et al., 2005). Seven archaeological sites are located in Middle Silts and Gravels Member (K3) immediately below the disconformity separating the Middle Silts and Gravels Member (K3) from base of the Bedded Tuff Member (K4). These include the “Factory Site”, Paul Abell Trench (PAT= GnJh-13), GnJh-15, GnJh-17 and the four separate collections of the Leakey’s “Living Site” (Cornelissen, 1992; Cornelissen et al., 1990; Leakey et al., 1969). These four separate assemblages of the “Living Site” include the surface collected and piece plotted material of the Leakey Handaxe Area (LHA= GnJh-02), the surface collected and excavated material of the Leakey Handaxe Rectangle (LHR =GnJh-03) excavated in the center of the “Living Site” area, the excavated material of the Peter Nzube Gulley (PZG= GnJh-11) a step-trench located ~300 meters east of the LHR excavation on the eastern margin of the “Living Site” area and the Leakey Handaxe Site excavation (LHS=GnJh-12) located on the western

margin of the “Living Site” area ~200 m west of the LHR excavation (Cornelissen, 1992; Leakey et al., 1969). It is important to distinguish these four individual assemblages within the Leakey’s “Living Site” area because, though they are from the same stratigraphic interval, they are not part of a single contiguous site or archaeological layer and all four assemblages appear different typologically, technologically and metrically. Archaeological sites found in or between tuffs at the base of the Bedded Tuff Member include Rorop Lingop (GnJi-28) and GnJh-63 (Tryon, 2003; Tryon and McBrearty, 2006). All the above sites found in or immediately below the base of the Bedded Tuff Member contain aspects of Acheulean and Levallois prepared core technologies (Cornelissen et al., 1990; Leakey et al., 1969; Tryon, 2003; Tryon and McBrearty, 2002; Tryon and McBrearty, 2006). The MSA archaeological site of Koimilot from stratigraphically higher up in the Bedded Tuff Member is reviewed in Tryon (2006; 2010; 2003), Tryon et al., (2005) and Tryon and McBrearty (2006). Two recently excavated archaeological sites from the Kapthurin Formation provide new archaeological material and are discussed here. These are the Sibilo School Road Site (GnJh-79) and Keraswanin (GnJh-78) shown in figures 3 and 4 respectively. The general attributes of these sites are summarized here in Table 1 (after Tryon and McBrearty, 2006) and the technological characteristics of the lithic assemblages are summarized in Table 2 (after Tryon and Faith, 2013).

Table 1: Summary of all Kapthurin Formation archaeological sites named or classified by SASES code in this study.

Name	SASES	Archaeological attribution	Member	Tuff above	Tuff below	Age	Archaeology and Depositional Environment	References
Leakey Hominid Site Edward Kandini Gulley (EKG)	GnJh-10	Non diagnostic, Acheulian?	K3	Grey Tuff		>509 ± 7ka	Artifacts (n=21) excavated from fluvial sand-silt deposits in K3 ~8m below the Grey Tuff. Artifacts are non diagnostic.	Leakey et al., 1969
	GnJh-42	Non diagnostic, Acheulian?	K3			>509 ± 7ka	Artifacts (n= 524) excavated from in lacustrine clay paleosol K3. Artifacts include platform cores (n=10) and blade and blade fragment debitage (n= 13)	(Johnson and McBrearty, 2010)
	GnJh-50	Non diagnostic, Acheulian?	K3			>509 ± 7ka	Artifacts (n= 338) excavated from in lacustrine clay paleosol K3. Artifacts include platform cores (n=7) and blade and blade fragment debitage (n= 6)	(Johnson and McBrearty, 2010)
Kapthurin “A” site	GnJh-15	Acheulean	K3	Lower Basaltic Tuff		> 380 ± 7ka	Artifacts (n= 5929) from >500m <sup>2</sup> excavation including ~120 single/ multiplatform cores, 2 picks and ~40 shaped tools and tools fragments, ~15 of which are small bifaces, some made on cobbles, from well-developed aleosol beneath base of K4	(McBrearty, 1999; Tryon and McBrearty, 2002, Van Noten et al., 1987)
	GnJh-17	Acheulean, Sangoan?	K3	Lower Basaltic Tuff		> 380 ± 7ka	Artifacts (n=9712) from eight excavated strata (144m <sup>2</sup> ). Shaped tools (n=28) include 3 handaxes, 2 points, and 3 pick/ core-axes from paleosols and alluvial sediments beneath local base of K4.	(Cornelissen, 1992, Van Noten et al., 1987)
Rorop Lingop	GnJi-28	Acheulean/ MSA	K4	Upper Basaltic Tuff	Lower Basaltic Tuffs	> 380 ± 7ka	Systematically collected surface artifact sample (n 846), including <15 each of handaxes, points, and Levallois cores from 0.2 km <sup>2</sup> lacustrine/near-shore sediments within and immediately overlying K4 tephra	(McBrearty, 1999; McBrearty et al., 1996; Tryon and McBrearty, 2002)



Leakey Handaxe Area (LHA)	GnJh-02	prepared core Acheulean	K3 or lower K4			> 380 ± 7ka	Artifacts (n=416) from surface (0.3km <sup>2</sup> area) of K4. Shaped tools (n > 50) include 15 handaxes and 6 cleavers. Assemblage also contains at least 4 large preferential Levallois cores and 18 large Levallois flakes.	(Cornelissen, 1992; Leakey et al., 1969; McBrearty, 1999; Tryon et al., 2005)
Leakey Handaxe Rectangle (LHR)	GnJh-03	prepared core Acheulean	K3 or lower K4	Upper Basaltic Tuff		> 380 ± 7ka	Site includes surface collected and ~56m <sup>2</sup> excavations (n=775) in fluviolacustrine sediments ~3m below local base of K4. Lithic assemblage contains ~44 blades including at least 6 refitting sets of blades as well as 19 preferential Levallois flakes.	(Cornelissen, 1992; Leakey et al., 1969)
Peter Nzube Guley (PZG)	GnJh-11	prepared core Acheulean	K3 or lower K4	Upper Basaltic Tuff		> 380 ± 7ka	Site includes abundant small flake material mostly derived from a step trench located ~300m east of LHR at east edge of Leakey Handaxe Area in fluviolacustrine sediments ~3m below local base of K4. Artifacts (n=675) pieces including 15 small Levallois flakes and 3 discoid cores.	(Cornelissen, 1992; Leakey et al., 1969)
Leakey Handaxe Site (LHS)	GnJh-12	prepared core Acheulean	K3 or lower K4	Upper Basaltic Tuff		> 380 ± 7ka	Site includes abundant lithic material derived from 31' x 5' trench with a 12' x 11' in fluviolacustrine sediments ~3m below local base of K4. Trench is located at west end of Leakey Handaxe Area. Artifacts are mostly undiagnostic but include platform cores and at least 1 discoid and 1 Levallois preferential flake.	(Cornelissen, 1992; Leakey et al., 1969)
Leakey "Factory Site" Paul Abell Trench (PAT)	GnJh-13	prepared core Acheulean	K3	Bedded Tuff		> 380 ± 7ka	Artifacts (n=862) for a ~200m long area on slope of small hill. Artifacts come from ~14 meter below base of Bedded Tuff Member. A 10' x 4' trench recovered dense artifact concentrations of artifacts interspersed with pebble to cobble conglomerate including prepared core and flake technology as well as bifacial and unifacial Acheulean large cutting tools.	Leakey et al., 1969; Cornelissen, 1992
	GnJh-63	Acheulean	K4	Upper Basaltic Tuff	Lower Basaltic Tuffs	> 380 ± 7ka	Artifacts (n=88) from a 24m <sup>2</sup> excavation. Tools include 1 handaxes from immature paleosol within K4, and possible point from within overlying tuff.	(Tryon and McBrearty, 2002)

Sibilo School Road Site	GnJh-79	MSA	K4	NRS tuff	SSRS Unit #1 trachyte	> 284 ± 12ka	Artifacts (n= 2506) from 80 m <sup>2</sup> excavations in two trenches in a tuffaceous silt soil ~1m below a coarse pumiceous tuff correlated to NRS tuff. Artifacts include Levallois points (12), Levallois cores (6) of preferential, point and recurrent types.	Blegen (in prep), this study.
Koimilot	GnJh-74	MSA	K4	Evolved basaltic tuff	Koimo-lit	> 235 ± 2ka	Two excavated Loci (64m <sup>2</sup> ) at different stratigraphic intervals from distal alluvial fan sediments within K4. Artifacts (n=4376) include preferential and recurrent Levallois cores (n=7) and flakes (n=10), and 1 pointed uniface on a cobble.	Tryon, 2003, 2006, 2010; Tryon et al., 2005
Keraswanin	GnJh-78	MSA	K4? Or K5?	Wakondo Tuff ~100 ka		> 100 ka	Artifacts (n=8996) from ~12m <sup>2</sup> in silty paleosol ~0.30m beneath vitric tuff unit correlated to the Wakondo Tuff in western Kenya. Artifacts from surface and excavation include Levallois flakes (n=42) and cores (n=9) preferential, point and recurrent. Obsidian bifacial foliate points (n=2) and obsidian (n=2 ) and chert unifacial points (n=3) from surface.	(Blegen et al., 2010, 2011, 2012; Johnson et al., 2012)

#### History of tephra research in the Kapthurin Formation:

Because it is not possible or practical to date every outcrop of tuff by the <sup>40</sup>Ar/<sup>39</sup>Ar method

(Feibel, 1999) tephrostratigraphy in many forms has been used to assess stratigraphic position

and relative age of archaeological and paleontological sites capped by individual tuffs in the

Kapthurin Formation and particularly in the Bedded Tuff Member (Cornelissen et al., 1990; Tal-

lon, 1976, 1978; Tryon, 2003; Tryon and McBrearty, 2002; Tryon and McBrearty, 2006). Some

of the earliest formal geological and paleoanthropological research conducted in the Kapthurin

Formation notes the presents of stratigraphically and lithologically distinct tuff units used pri-

marily to distinguish strata at the member level with the Kapthurin Formation (Leakey et al., 1969; Martyn, 1969; McCall, 1967). Later researchers such as Tallon (1976) named tuff units such as the Lebus Tuff and Grey Tuff in the Middle Silts and Gravels Member and the bedded tuffs of the Bedded Tuff Member. Some of these units, particularly the Grey Tuff, were used as stratigraphic marker beds to lithologically correlate between archaeological and paleontological sites (Cornelissen, 1992; Cornelissen et al., 1990; Tallon, 1978). The first extensive programs of chemical correlation of individual tephra beds between sites focused on the numerous individual beds within the Bedded Tuff Member of the Kapthurin Formation (Tryon, 2003; Tryon and McBrearty, 2002; Tryon and McBrearty, 2006).

#### Tephrostratigraphy in the Bedded Tuff Member, Kapthurin Formation:

The geochemical compositions of the Bedded Tuff Member tuffs show a clear compositional trend from tuff units containing less compositionally evolved basaltic glass found in tuffs located stratigraphically lower in the Bedded Tuff Member section through tuffs containing progressively more evolved basaltic glass and trachytic glass stratigraphically higher (Tryon and McBrearty, 2002). The compositional change occurs along a single trendline, observable in a

Table 2: Artifact categories for archaeological assemblages from sites in the Kapthurin Formation, Baringo, Kenya. Note ‘1’ = present and ‘0’ = absent (after Tryon and Faith, 2013).

Site	Age (ka)	Platform Core	Discoid Core	Levallois preferential	Levallois recurrent	Levallois point/core	Blades/ Blade core	re-touched point	Large biface	Pick, elongated cobble, Heavy Duty tool	exotic raw material	Total Tech categories	total number pieces
Leakey Hominid Site (EKG= GnJh-10)	>509	1	0	0	0	0	0	0	0	0	0	1	21
GnJh-50	>509	1	0	0	0	0	1	0	0	0	0	2	524
GnJh-42	>509	1	0	0	0	0	1	0	0	0	0	2	338
Factory Site (PAT= GnJh-13)	>380	1	0	1	0	0	0	0	1	0	0	3	862
GnJh-15	>380	1	0	0	0	0	1	0	1	0	1	3	5929
GnJh-17	>380	1	0	0	0	0	0	0	1	1	0	3	9712
Rorop Lingop	>380	1	1	1	0	0	0	0	1	0	1	4	846
LHA (GnJh-02)	>380	1	1	1	0	0	0	0	1	1	0	5	416
LHR (GnJh-03)	>380	0	1	1	1	0	1	0	1	0	0	5	775
LHS (GnJh-12)	>380	1	1	1	0	0	0	0	1	0	0	4	395
PZG (GnJh-11)	>380	1	1	1	0	0	0	0	1	0	0	4	675
GnJh-63	>380	1	0	0	0	0	0	0	1	1	1	3	88
SSRS (GnJh-79)	196-226	1	1	1	1	1	1	0	1	0	1	7	2506

Koimilot Locus 1 (GnJh-74)	200- 250	1	1	1	1	0	0	0	0	1	0	5	3782
Koimilot Locus 2 (GnJh-74)	200- 250	1	1	1	1	1	1	0	0	0	0	6	310
Keraswanin (GnJh-78)	~100	1	1	1	1	1	1	1	0	1	1	8	8996

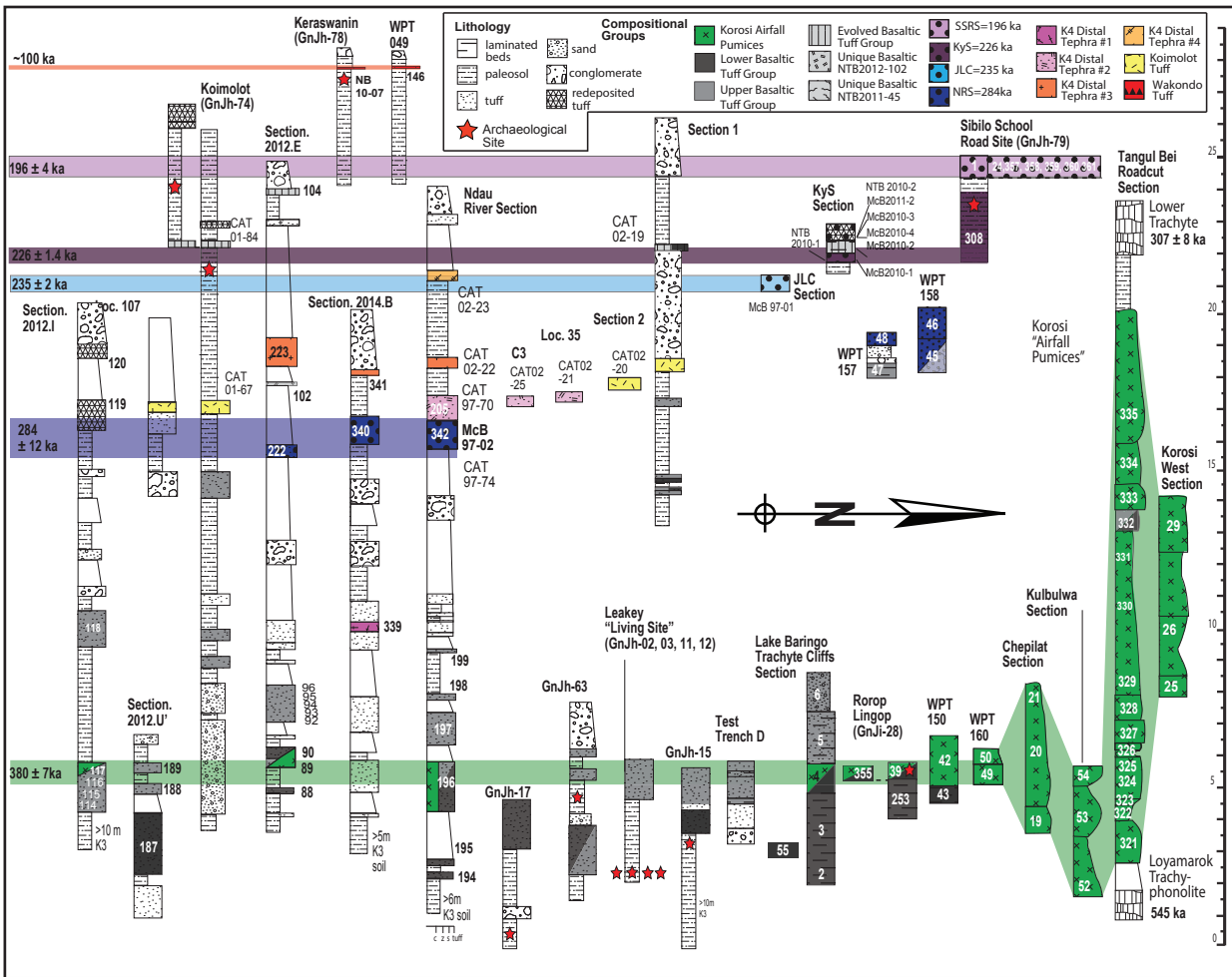


Figure 2: Schematic stratigraphic sections for all analyzed tephra samples from the Kapthurin Formation. Composite sections of tuffs of unique colors corresponding to compositionally unique tephras named in the figure key and discussed in the text. Individual tuff samples analyzed for this study (or reanalyzed from previous studies of Tryon and McBrearty, 2002, 2006) are shown with sample numbers. Chemical modes of glass found in a single sample shown as unique patterns within a single rectangle. Dotted lines represent tuff units that can be traced laterally in the field between two measured sections. White area represents non-volcaniclastic sediments not used for correlation.

number of element oxide bivariate plots (Tryon, 2003). This trend reflects the chemical evolution of a single cooling magma source by fractional crystallization as denser minerals crystallize out of solution leaving a compositionally altered residual magma chamber to produce glass of a more compositionally evolved chemistry in successive eruptions (Tryon, 2003). Thus, the chemical composition of a Bedded Tuff Member tuff falling along the compositionally evolving trendline



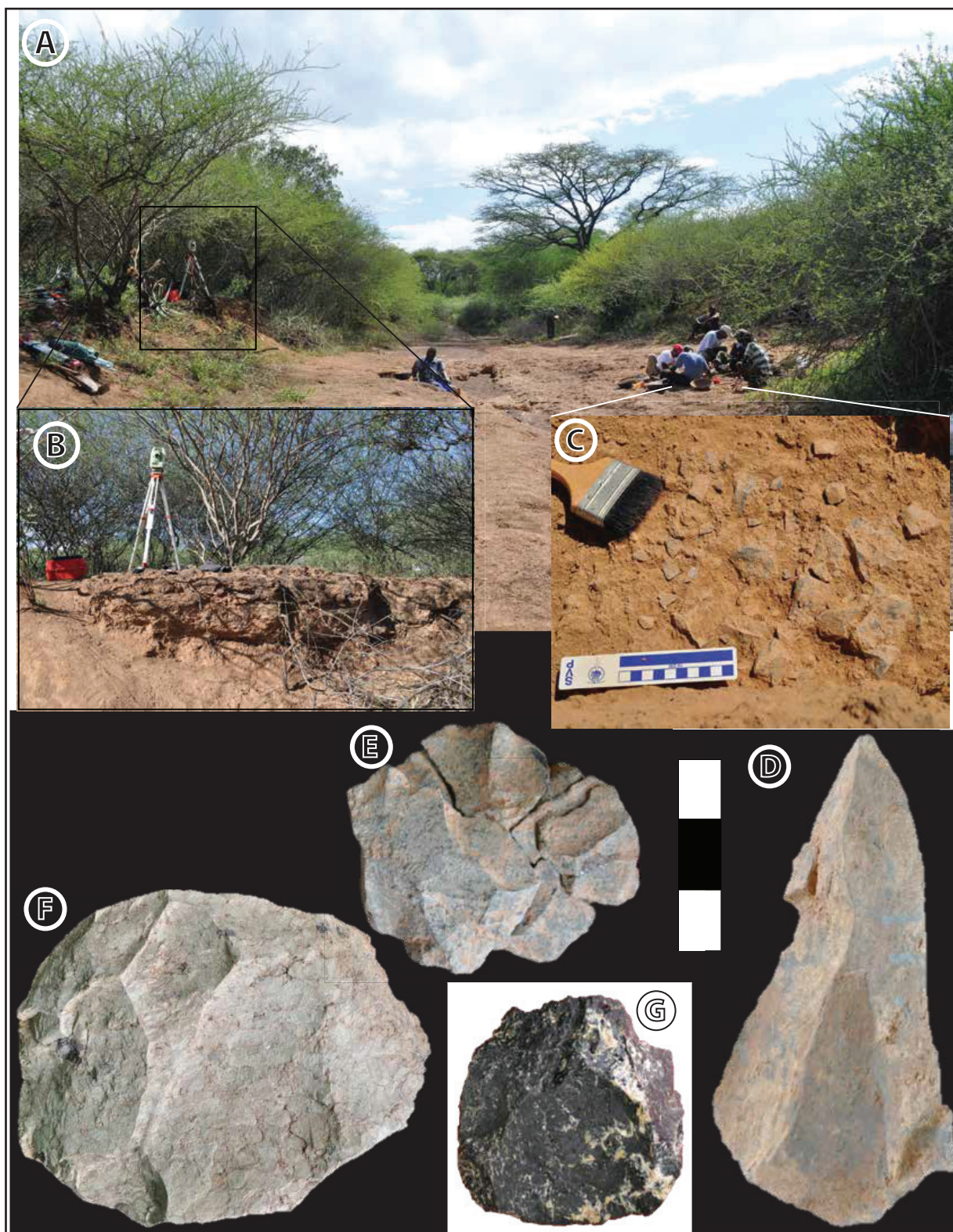


Figure. 3: A: Photographs of the Sibilo School Road Site (GnJh-79) under excavation. B: Coarse pumiceous tuff capping *in situ* archaeology at the SSRS by ~1m and correlated to the NRS Tuff dated to  $284 \pm 12$  ka by the  $^{40}\text{Ar}/^{39}\text{Ar}$  method. C: *In situ* flaked stone artifacts at the site. D. Levallois point. E. Recurrent centripetal Levallois core (phonolite) with five refits on debitage surface. F. Preferential Levallois core (yellow welded tuff). G. Preferential Levallois core (obsidian).





Figure. 4: A. Photograph of the archaeological site of Keraswanin (GnJh-78) under excavation. B: Close-up of the tuff (lighter brown) in the wall of the excavation trench and its position above *in situ* flaked-stone artifacts. C: Concentration of flaked stone artifacts including pointed pieces shown *in situ* during excavation. D: Levallois points found *in situ* shown with outlines of prepared platforms set below. E: Additional pointed pieces found at the site. F: Levallois preferential and recurrent centripetal cores from Keraswanin. G: Levallois recurrent unidirectional cores from Keraswanin. H: Obsidian points from Keraswanin (bifacially flaked set left and right) and Levallois point (set center).



indicates the relative stratigraphic position of the tuff unit within this member. This methodology is extremely useful in establishing a relative chronology used to demonstrate interstratification between Acheulean and MSA industries from archaeological sites found at or below the base of the Bedded Tuff Member (Tryon, 2003).

#### Tephra Correlation Materials and Methods:

The programs of chronometric dating for the Kapthurin Formation (Deino and McBrearty, 2002) as well as the relative tephrostratigraphy for archeological sites of the Bedded Tuff Member established by Tryon and McBrearty (2002; 2006) leave two issues to be resolved:

1) The minimum age of the base of the Bedded Tuff Member and the nine sites found at or below the base of this member are poorly constrained to an age of  $>284$  ka within a  $>200,000$  year window between 284 –509 ka (Deino and McBrearty, 2002). Increased precision of this age is of interest because archaeological sites stratigraphically situated at the base of the Bedded Tuff Member, particularly the four sites of the Leakey's "Living Site" area preserve early evidence of diverse Levallois technology in East Africa (Deino and McBrearty, 2002; Leakey et al., 1969;

McBrearty, 1999, 2001; McBrearty et al., 1996; Tryon and McBrearty, 2002; Tryon and McBrearty, 2006; Tryon et al., 2005).

2) The majority of archaeology in the Bedded Tuff Member to date concerns sites > 284 ka and containing lithic technology of Acheulean and MSA character (Cornelissen et al., 1990; Leakey et al., 1969; McBrearty, 1999; McBrearty et al., 1996; Tryon and McBrearty, 2002; Tryon and McBrearty, 2006). The single exception to date is the site of Koimilot (GnJh-74), dated to ~200–250 ka and containing evidence of diverse Levallois and other core reduction technologies as well as pointed pieces attributed to the MSA (Tryon, 2006; Tryon, 2003; Tryon and McBrearty, 2006; Tryon et al., 2005). More archaeological material from well –dated contexts is needed from the upper portion of the Bedded Tuff Member and the Upper Silts and Gravels Member to compliment the sample of archaeological material from at or beneath the base of the Bedded Tuff Member.

The tephra sampling strategy in this study complements McBrearty’s current program of archaeological survey and excavation by laterally expanding the survey area in the Kapthurin Formation to the north and west of previously surveyed and excavated localities (Figs 1a, 2). Lateral

expansion of archaeological and tephrostratigraphic programs allows for sampling of different time periods with sequences of tephra deposits augmenting the previously defined archaeological, tephrostratigraphic and chronostratigraphic framework of the formation (Deino and McBrearty, 2002; Tryon and McBrearty, 2002; Tryon and McBrearty, 2006).

#### Materials:

Tuff samples analyzed and reported in this study include 1696 individual electron microprobe analyses from 90 new samples collected from a series of 32 sections measured on outcrops of Pleistocene sediments in the Kapthurin Formation of the Baringo Basin between the summers of 2010 and 2014, as well as reanalysis of ten samples from ten previously measured sections provided by Dr. Christian Tryon (Tryon, 2003; Tryon and McBrearty, 2002; Tryon and McBrearty, 2006). Measured sections ranged widely from  $< 0.50$  to  $> 30$  m in thickness. Whenever possible, tuffs were sampled from sections with multiple tuff deposits exposed in stratigraphic succession. Field correlations were made by walking exposures and by using a Jacob's staff and abney level to establish lateral stratigraphic equivalence of tuff deposits. Both field and laboratory methods of correlation are necessary as exposure is discontinuous and tephra deposits in the Kapthurin Formation can vary widely in their thickness, amount of soil development, and amount or size of

natural volcanic glass shards.

#### Methods:

Geochemical analysis of tephra focused on electron microprobe characterization of eleven major element oxide proportions of volcanic glass shards recovered from tephra deposits and tuffaceous sediments from the Kapthurin Formation.

#### Preparation:

All preparation protocols were adapted from the University of Utah Electron Microprobe lab recommendations (Brown and Fuller, 2008). Bulk samples of tuff (10-30 g) were prepared by disaggregation with pestle and mortar and sieved through size #60 and #120 mesh screens, retaining the fraction between 60-120  $\mu\text{m}$ . Samples were then washed repeatedly with deionized water and the suspended clay fraction was decanted until effluent was clear. Cleaned tephra was then treated with 10% nitric acid in sonic bath for 5 minutes to remove carbonates. Tephra samples were subsequently treated for 5 minutes with 5% hydrofluoric acid in a sonic bath to remove metal salts and clays potentially adhering to the surface of the glass shards. Samples were then rewashed in deionized water until the effluent was clear, and then dried in an oven at

190°C. Dried samples were magnetically separated on a Franz isodynamic magnetic separator in two successive runs, the first at low (0.1-0.3) amperage to separate the strongly magnetic mineral components such as olivine, augite and opaque minerals, and the second run at higher amperage (~0.9-1.0) in order to separate weakly magnetic natural glass from nonmagnetic feldspars and quartz. Glass separates were then mounted in 12-well epoxy grain mounts at the University of Utah. Standard mount sizes are 1" (25 mm) round mounts with maximum height of 1". The University of Utah electron microprobe lab provided carbon coating of samples with a Denton Benchtop Turbo IV high vacuum evaporator. Each mount contained an MM3 standard obsidian (Brown and Fuller, 2008) so that the samples and standard have the identical thickness of carbon coating. Samples that were not prepared in the above fashion (i.e., described in Tryon, 2003; Tryon and McBrearty, 2002; Tryon and McBrearty, 2006) were previously analyzed in the microprobe as resin-impregnated polished thin sections prepared by Spectrum Petrographics, Inc. To reduce inter-analyst variation resulting from the use of different instrumentation and analytical protocols (Kuehn et al., 2011) that may confound correlation efforts, the current dataset includes new analysis of these previously analyzed samples from the Bedded Tuff Member.

Analysis:

Where possible, the relations among the vitric, crystal, and lithic phases of the tephra deposits were determined from petrographic thin sections using plane and polarized light, backscattered electron imagery, and energy dispersive electron probe microanalyses (EPMA). Geochemical characterization of the vitric (glass) phase via EPMA used a Cameca SX-50 in the Department of Geology and Geophysics at the University of Utah, USA. Analyses were conducted using PC1, TAP, PET and LiF crystals on four wavelength-dispersive spectrometers, with an accelerating voltage of 15 keV, a beam current of 25 nA, and a spot size of 10  $\mu\text{m}$ . The analytical routine for glass included Si, Ti, Zr, Al, Fe, Mn, Mg, Ca, Na, K, O, F, and Cl. A natural obsidian standard (MM3) was used for calibration of O-K $\alpha$ , Si-K $\alpha$ , Al-K $\alpha$ , K-K $\alpha$ . Mineral standards include fluorite (F-K $\alpha$ ), tugtupite (Cl-K $\alpha$ ), albite (Na-K $\alpha$ ), diopside (Ca-K $\alpha$ , Mg-K $\alpha$ ), hematite (Fe-K $\alpha$ ), rutile (Ti-K $\alpha$ ), rhodonite (Mn-K $\alpha$ ), and cubic zirconia (Zr- La). Rounds of 3 standard analyses bracketed rounds of 4 sample unknowns where 22-24 spots were taken per sample (Nash, 1992). Inter-laboratory comparisons confirm that the equipment and protocols used by the Utah laboratory (lab 5 in Kuehn et al., 2011) work exceptionally well for tephtras of a wide range of compositions. Oxygen was measured directly allowing for an estimate of the water contents of the shards. This provides a measure of the quality of the analysis (Nash, 1992). Na was measured first on the TAP

crystal with an analysis time of 4 seconds on the analytical peak and 2 seconds on background on either side of the peak, in order to minimize sodium loss under the electron beam. On-peak and background measurement times are as follows (Pk/Bg sec): Si (15/15), Ti (25/25), Zr (37/22), Al (15/15), Fe (25/25), Mn (25/25), Mg (40/40), Ca (20/16), Na (4/4), K (20/16), O (20/20), F (20/20), Cl (20/20). Concentrations are calculated using the PAP matrix correction procedure of Pouchou and Pichoir (1991). Correction for “excess” F by interference of the Fe La peak with F Ka peak was accomplished by measuring a F-free Fe-bearing standard (hematite) to yield a correction factor of 0.031. Background intensities are measured on both sides of the analytical peak for all elements but F on the PC1 crystal, where off-peak background is measured to one side, and on-peak background intensity is interpolated using the estimated slope of the continuum (Pouchou and Pichoir, 1991).

#### Interpretation:

Correlation of tephras from separate samples is best viewed as a hypothesis with different methods of distinguishing tephras providing independent tests of any hypothesized correlation (Feibel, 1999). Failure to distinguish tephras from different samples by means of stratigraphy,

lithology, petrology and element oxide compositions measured with an electron microprobe constitutes robust evidence for correlation, indicating stratigraphic and, most often, chronological equivalence (Tryon et al., 2008) Reported major element oxides are not normalized in this study because element oxide totals including estimated water content were reasonably high and exploratory data analysis using normalization did not alter interpretation. However, samples plotted on the total alkali-silica (TAS) diagram (Fig. 5) necessarily have totals normalized to 100% for potential comparison with whole-rock samples (Le Bas et al., 1986).

Our samples include both primary fall-out deposits, as well as those subsequently reworked by fluvial or pedogenic processes. Lithic and crystal phases from the eruption cannot always be reliably distinguished from those found in detrital sediments, and thus our correlations rely on chemical composition of the glass component following Brown and Nash (2014). In many of the samples, all analyzed glass shards clustered around a discrete mean and therefore represented a single dominant unimodal glass composition. However, several samples displayed variable or multi-modal compositions. Samples with two or more modes were separated by composition and treated as potentially different tephras for analysis. Identifying the consistent presence of multiple modes of composition is an important step in distinguishing tephra deposits that contain



two or more modes of glass as a product of magmatic processes during eruptions, and therefore represent the same, unique isochronous event, versus those that contain two or more modes as a product of post-depositional fluvial mixing or diagenesis.

#### Data Reduction of Bedded Tuff Member tephra:

Analyses from the Bedded Tuff Member provide an appreciable diversity of glass compositions ranging from very low  $\text{SiO}_2$  basaltic through high  $\text{SiO}_2$  trachytes and phonolites as well as a wide array of chemical compositions ranging within single tephra samples. Both of the chemical composition and linear array of glass data are addressed during data reduction in a manner following Brown and Nash (2014). The basic categorical chemical composition, mafic or felsic, of microprobe generated probe numbers can be established and subdivided into more specific compositional groups such as basalts and trachytes in a total alkali – silica graph based on relative proportions of  $\text{SiO}_2$  and  $\text{Na}_2\text{O} + \text{K}_2\text{O}$  (Fig. 5; Le Bas et al., 1986). This coarse level of chemical characterization separates the two basic compositional groups of tephra, within the Bedded Tuff Member and allows these categories of tephra to be dealt with individually.

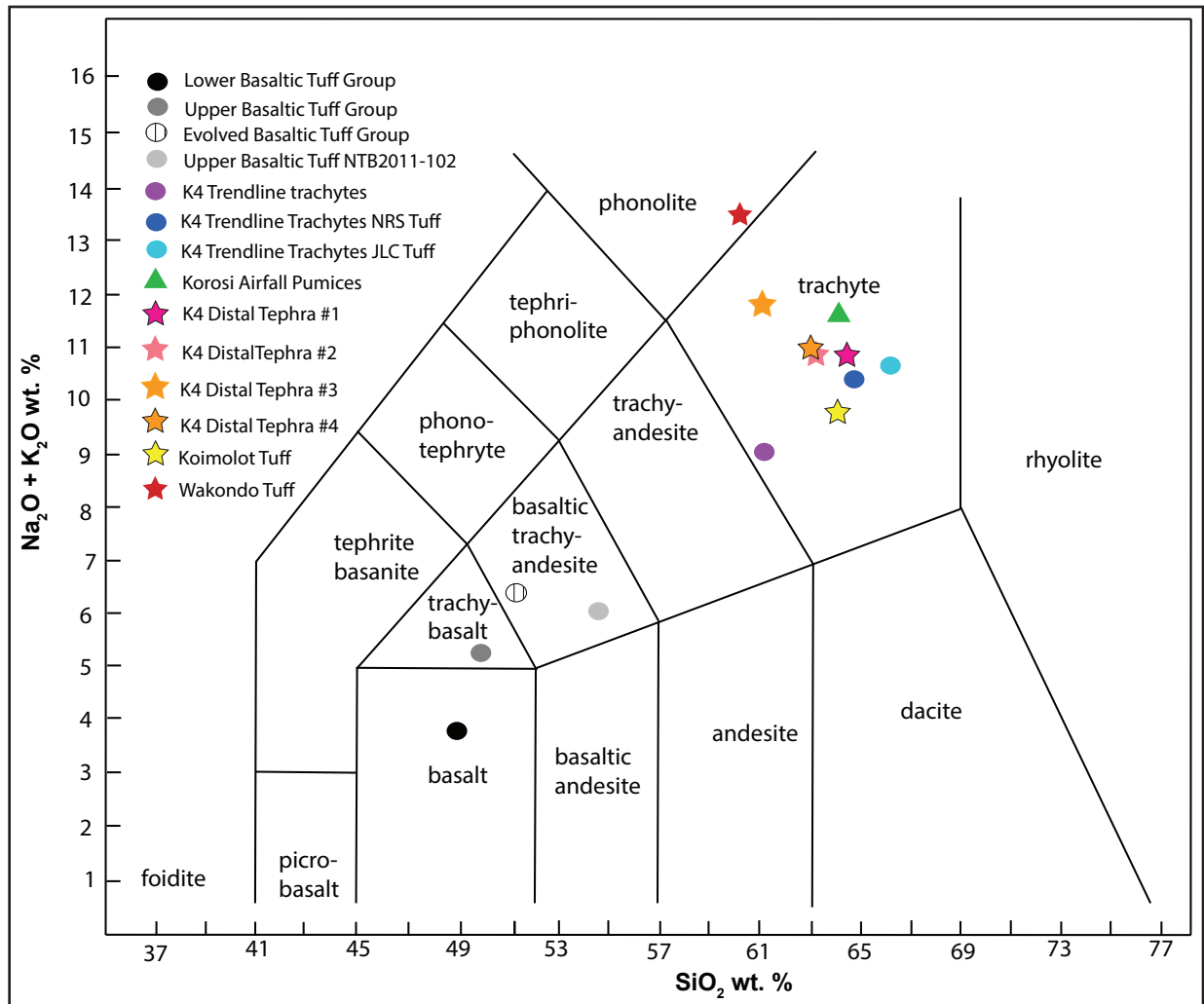


Figure. 5: Total-alkali Silica graph (after Le Bas et al., 1986) of a representative sample of all chemically distinct tuffs or tuff groups discussed in this study.

Basaltic tuffs in the Bedded Tuff Member represent a compositional continuum of a single monogenic magma chamber evolving (losing denser element oxides like  $\text{CaO}$ ,  $\text{MgO}$ ) through fractional crystallization of minerals and thereby proportionally gaining oxides and elements like  $\text{FeO}$ ,  $\text{TiO}_2$  and  $\text{Cl}$  less compatible to mineralization in the magma chamber (see Tryon and McBrearty, 2002 and refs therein). This process encompasses >200 kyr period in the Bedded Tuff Member. These basaltic tuffs cannot be identified and correlated to individual eruption but rather represent

points along a linear continuum which can be visualized in several combinations of oxide bivariate plots (Fig. 6; Tryon and McBrearty, 2002; Tryon and McBrearty, 2006). The position of any Bedded Tuff Member basaltic tephra thus indicates its position relative to other basaltic tuffs as well as to trachytic tuffs directly dated by the  $^{40}\text{Ar}/^{39}\text{Ar}$  method (Tryon, 2003; Tryon and McBrearty, 2002; Tryon and McBrearty, 2006).

Felsic tephtras in the Bedded Tuff Member can be sorted into two basic types: those conforming to the trend on of magmatic evolution described for the basaltic tephtras (Fig. 6a, f) and felsic tephtras not conforming to the trendline (Fig 7, 8). The first category, the felsic tuffs conforming the to evolving trendline of magmatic evolution are trachytes (Fig. 6) genetically related to the basaltic tuffs and represent the compositional end product of magmatic evolution of the magma chamber (Fig 6a). Like the basaltic tuffs the felsic trendline tuffs occur along a linear continuum visualized in oxide bivariate plots (Fig. 6f,) The position of any Bedded Tuff Member felsic trachyte tephra thus indicates its position relative to other basaltic tuffs conforming to the trendline of magmatic evolution (Tryon and McBrearty, 2002; Tryon and McBrearty, 2006). The felsic tuffs not conforming to the trendline of magmatic evolution are either 1) Korosi Airfall Pumices of distinct trachytic composition produced during the explosive eruption of initial formation of

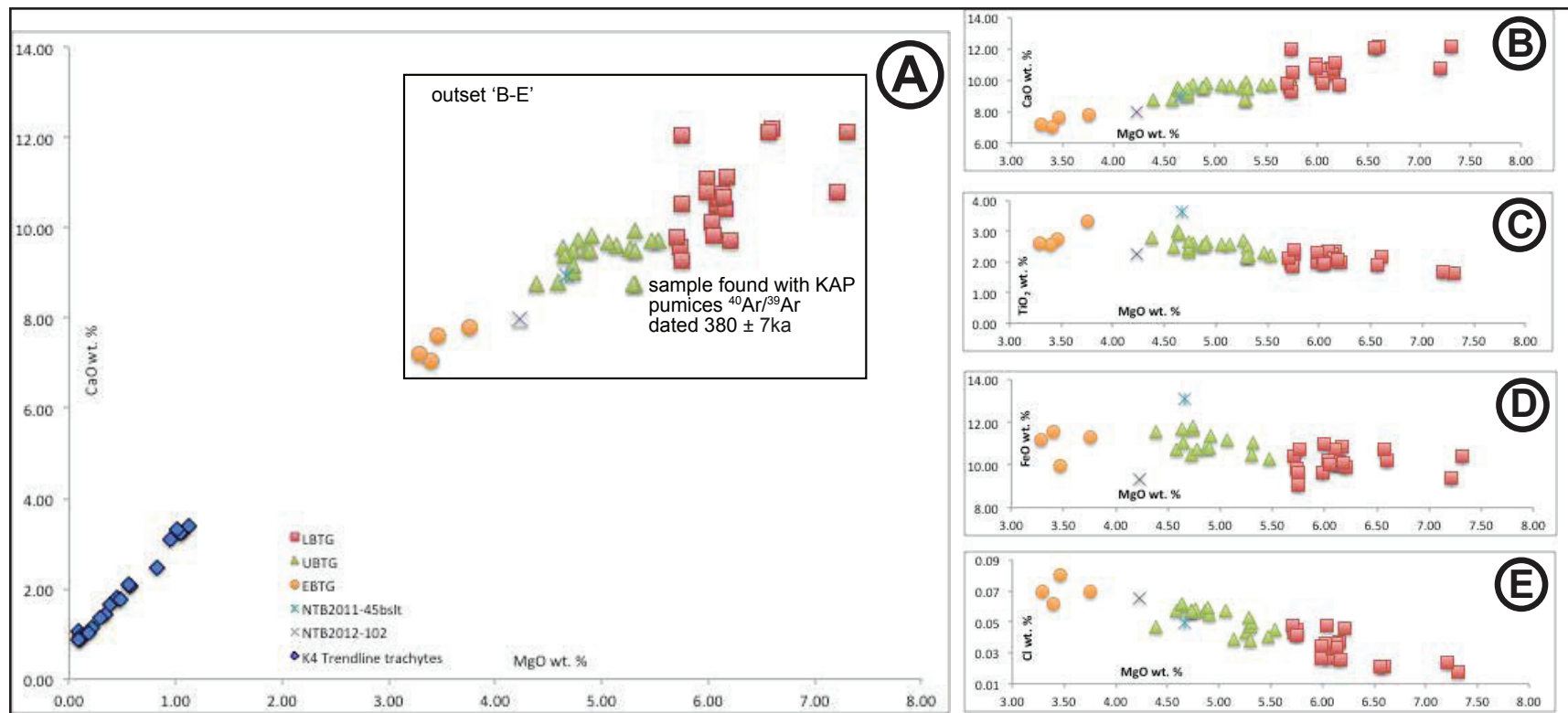


Figure. 6: A Bivariate CaO versus MgO plot for means of all samples discussed in this study with inset (top left corner of 'A') zoomed in on the felsic samples. B-E: Bivariate plots for the basaltic tuffs of the Bedded Tuff Member discussed in this study. These four plots show the compositional evolution of the magma chamber demonstrated in Tryon and McBrearty (2002, 2006) as well as the subdivisions of basaltic groups F: Bivariate CaO versus MgO plot of the means of all felsic samples in this study showing continuum of the K4 Trachytic Trendline tuffs.

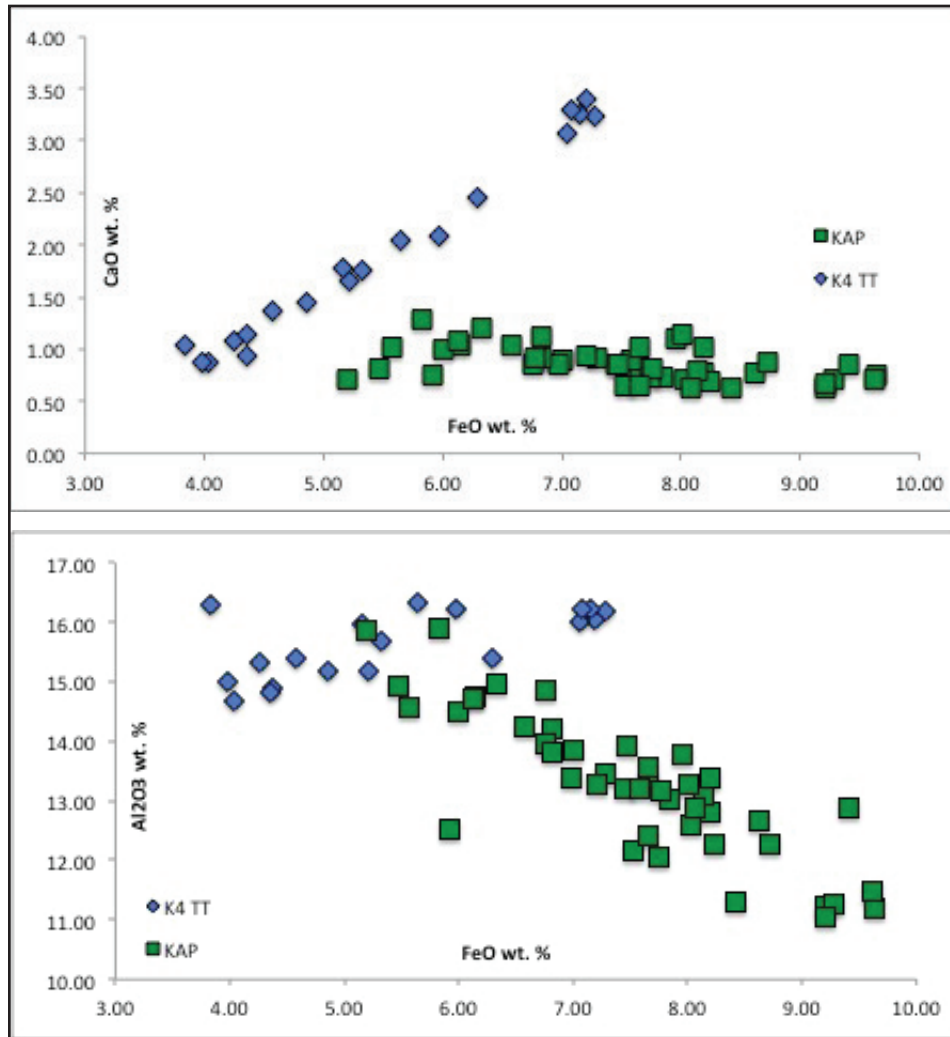


Figure. 7: Bivariate plots CaO versus FeO (top) and Al<sub>2</sub>O<sub>3</sub> versus FeO (bottom) for means of all KAP samples (green squares) and K4 TT (blue diamonds) discussed in this study.

the shield volcano Korosi (Dunkley et al., 1993), or 2) Distal tephras of unique unimodal chemical composition and likely deriving from sources other than Korosi. The Korosi Airfall Pumices are chemically characterized by compositional variation throughout a single large eruptive event. The composition of these Korosi Airfall Pumices is variable along a single linear array (see Brown and Nash, 2014: 71; Fig. 7) that can be visualized in multiple oxide bivariate plots (Fig. 7). The Korosi Airfall Pumices are chemically distinct and stratigraphically separated from

the trachytes conforming the trendline of basaltic to trachytic magmatic evolution and are thus easily distinguished (Fig. 7). The distal tephras of the Bedded Tuff Member, the second category of felsic tephras not conforming to the trendline of magmatic evolution, have unimodal chemical compositions defined by unique major element oxide chemical compositions. The six of these currently identified are easily distinguished from other tephra groups as well as from one another by their consistent unimodal chemical compositions clustering around a discrete mean and individually defined by unique chemical signatures based on the 10 element oxides  $\text{SiO}_2$ ,  $\text{TiO}_2$ ,  $\text{Al}_2\text{O}_3$ ,  $\text{FeO}$ ,  $\text{MnO}$ ,  $\text{MgO}$ ,  $\text{CaO}$ ,  $\text{Na}_2\text{O}$ ,  $\text{K}_2\text{O}$  and  $\text{Cl}$  (Brown and Nash, 2014; Fig. 8).

#### Results:

##### Tephra Correlation:

Field stratigraphic observations and microscopic petrography combined with EMPA determined element oxide wt. % abundances of 1696 individual glass analysis from 100 tuff samples taken from 32 measured sections from west and north of Lake Baringo indicate the presence of 15 distinct tephra deposits or tuff groups (Tables 3, 4; Figs. 1b, 2). These deposits fall into two general chemical categories of basaltic (Table 3) and felsic (Table 4) compositions based on the relative

abundances of silica (SiO<sub>2</sub>) (see Fig. 5; Le Bas et al., 1986). Tuffs of basaltic composition are attributed to one of three groups based on their chemical composition and stratigraphic position following Tryon (2003) and Tryon and McBrearty (2002; 2006). From stratigraphically lowest to highest these are 1) the Lower Basaltic Tuff Group, 2) the Upper Basaltic Tuff Group and 3) the Evolved Basaltic Tuff Group (Tryon and McBrearty, 2006). Tuffs of felsic composition are also attributed to one of three groups based on their chemical composition and stratigraphic position modified from Tryon and McBrearty (2002; 2006) as well as Dunkley (1993). These are, from stratigraphically lowest to highest: 1) the Korosi Airfall Pumices, a unique and voluminous eruption coincident with the initial formation of Korosi and the eruption of the lower and upper basaltic tephras. 2) The K4 trendline trachytes produced by magmatic evolution of the Korosi magma chamber. These occur after the eruption of the Korosi Airfall Pumices and most of the basaltic tephra eruptions. 3) There are at least six individually defined unique K4 distal tephras which derive from a distant source or sources and occur through the Bedded Tuff Member sequence, but mostly near the top of the Bedded Tuff Member < 284 ka. These are all discussed in lithological, compositional, stratigraphic and chronological detail below.

Basaltic tephras:

Table 3: Mean major and minor element oxides by weight percent for all samples of the basaltic category discussed in this study. One standard deviation from the mean listed below each element oxide mean.

LBTG	No.	M,N	SiO <sub>2</sub>	TiO <sub>2</sub>	ZrO <sub>2</sub>	Al <sub>2</sub> O <sub>3</sub>	FeO	MnO	MgO	CaO	Na <sub>2</sub> O	K <sub>2</sub> O	F	Cl	Sum	less O	Sum	H2O	Total
CAT02-19			46.98	1.62	0.02	15.36	10.42	0.18	7.31	12.13	2.85	0.45	0.01	0.02	97.36	0.01	97.35	1.10	98.45
	4	2,2	0.82	0.10	0.04	1.36	0.52	0.01	0.36	0.27	0.06	0.06	0.02	0.01	1.24	0.01	1.25	1.02	1.36
NTB2011-2			48.25	2.17	0.03	15.94	10.23	0.19	6.60	12.21	2.85	0.61	0.35	0.02	99.45	0.15	99.29	0.51	99.80
	9	1,1	0.76	0.06	0.03	0.25	0.92	0.02	0.40	0.97	0.38	0.22	0.05	0.01	0.83	0.02	0.85	0.39	0.91
NTB2011-3			47.32	2.03	0.02	15.80	10.08	0.17	6.07	10.49	3.06	0.75	-0.02	0.03	95.80	-0.00	95.80	0.07	95.88
	17	1,1	1.15	0.22	0.05	1.38	1.16	0.05	1.04	0.84	0.44	0.17	0.04	0.01	1.73	0.02	1.73	1.11	0.92
NTB2011-4			46.96	2.34	0.01	15.18	10.86	0.22	6.16	10.44	3.52	1.02	0.37	0.04	97.11	0.17	96.94	2.24	99.18
	4	1,3	0.11	0.32	0.03	0.20	0.41	0.03	0.59	0.54	0.28	0.27	0.03	0.02	0.21	0.01	0.20	0.26	0.43
NTB2011-39			49.29	1.97	0.01	16.33	9.86	0.19	5.73	9.56	3.68	1.07	0.37	0.04	98.10	0.16	97.94	1.08	99.02
	22	4,4	0.67	0.21	0.03	1.19	0.76	0.03	0.77	0.50	0.29	0.14	0.06	0.02	1.27	0.03	1.29	0.72	0.87
NTB2011-43			48.63	1.87	0.00	16.44	9.66	0.18	5.75	9.29	3.85	1.09	0.34	0.04	97.14	0.15	96.99	1.36	98.35
	19	1,1	0.49	0.17	0.01	1.18	0.88	0.03	0.64	0.38	0.20	0.10	0.09	0.01	0.65	0.04	0.64	0.42	0.54
NTB2011-47			47.82	2.59	0.01	15.19	10.72	0.20	5.14	9.60	3.73	1.31	0.40	0.04	96.76	0.18	96.58	1.57	98.14
	15	1,1	0.63	0.31	0.02	0.59	0.55	0.02	0.61	1.20	0.36	0.29	0.04	0.01	0.97	0.02	0.97	0.37	1.10
NTB2011-55			47.89	1.98	0.00	16.51	9.65	0.17	5.99	11.08	3.12	0.73	0.33	0.03	97.48	0.15	97.34	2.40	99.73
	20	1,1	1.40	0.45	0.00	3.20	2.12	0.05	1.73	1.37	0.47	0.24	0.09	0.02	1.38	0.04	1.40	0.65	1.28
NTB2012-64			47.45	2.27	0.04	15.02	10.16	0.20	6.13	10.75	3.19	0.85	-0.11	0.04	95.99	-0.04	96.03	2.65	98.68
	18	1,1	0.68	0.29	0.05	1.10	0.76	0.03	0.80	0.57	0.24	0.26	0.04	0.01	0.47	0.02	0.47	0.35	0.51
NTB2012-68			47.75	2.34	0.03	15.20	10.73	0.18	6.09	10.64	3.16	0.78	-0.08	0.03	96.85	-0.03	96.87	1.92	98.79
	14	1,1	0.52	0.20	0.04	0.60	0.37	0.02	0.47	0.30	0.22	0.09	0.08	0.01	0.58	0.03	0.57	0.33	0.52
NTB2012-88			47.84	2.14	0.03	16.09	10.00	0.18	6.14	10.67	3.42	0.94	-0.12	0.03	97.35	-0.04	97.40	1.48	98.88
	14	1,1	0.62	0.33	0.05	1.63	1.03	0.03	0.86	0.47	0.27	0.17	0.05	0.01	0.82	0.02	0.83	0.69	0.59
NTB2012-90			48.15	2.01	0.05	15.79	10.23	0.20	6.04	10.12	3.52	0.98	0.08	0.04	97.20	0.04	97.16	2.39	99.55
	14	1,1	0.57	0.19	0.03	1.02	0.79	0.02	0.69	0.45	0.27	0.11	0.08	0.01	1.28	0.04	1.29	0.50	1.29
NTB2012-119			48.24	2.33	0.02	15.58	11.00	0.19	5.99	10.80	3.26	0.82	-0.14	0.03	98.14	-0.05	98.19	1.98	100.16
	10	1,1	0.79	0.21	0.02	1.28	0.99	0.03	0.82	0.22	0.13	0.05	0.06	0.01	0.48	0.03	0.47	0.40	0.53
NTB2012-120			49.28	2.27	0.08	15.59	9.04	0.17	5.75	12.03	3.11	1.27	-0.10	0.04	98.53	-0.03	98.57	2.01	100.58



	9	1,1	0.44	0.39	0.05	1.33	1.40	0.03	0.89	1.44	0.57	0.39	0.07	0.01	0.80	0.03	0.80	0.64	1.07
NTB2012-187			49.07	1.98	0.13	16.07	9.89	0.18	6.21	9.73	3.63	1.13	0.06	0.05	98.11	0.04	98.07	2.23	100.30
	11	1,1	0.98	0.14	0.05	0.35	0.49	0.02	0.41	0.12	0.25	0.04	0.17	0.01	0.97	0.07	1.01	1.01	1.29
NTB2012-194			48.25	1.89	0.02	15.17	10.72	0.20	6.56	12.12	3.12	0.63	-0.14	0.02	98.57	-0.05	98.62	1.59	100.20
	8	1,1	0.83	0.10	0.04	0.37	0.50	0.02	0.28	0.23	0.23	0.04	0.03	0.01	0.65	0.01	0.65	0.64	0.30
NTB2012-195			48.12	2.09	0.05	16.68	10.09	0.18	6.18	11.11	3.24	0.84	-0.14	0.03	98.47	-0.05	98.52	2.01	100.53
0.00	11	1,1	0.26	0.22	0.04	1.40	0.99	0.03	0.73	0.60	0.34	0.11	0.06	0.01	0.62	0.02	0.61	0.35	0.51
NTB2012-196	0	0	48.44	2.11	0.04	15.83	10.40	0.19	5.71	9.81	3.78	1.09	-0.09	0.05	97.37	-0.03	97.39	1.98	99.38
0.00	12	1,2	0.81	0.23	0.06	0.71	0.64	0.02	0.56	0.42	0.14	0.17	0.05	0.01	0.80	0.02	0.80	0.55	0.89
NTB2014-332	0	0	48.99	1.66	0.01	17.04	9.36	0.18	7.21	10.78	3.27	0.74	0.33	0.02	99.62	0.14	99.47	0.62	100.09
0.00	6	2,2	0.53	0.28	0.05	1.36	0.66	0.04	0.75	0.86	0.46	0.23	0.03	0.01	0.63	0.01	0.63	0.38	0.65
NTB2014-355	0	0	49.72	1.95	0.03	15.72	10.01	0.20	6.05	9.82	3.41	1.05	0.36	0.05	98.36	0.16	98.20	1.25	99.45
0.00	6	1,2	1.08	0.24	0.03	0.45	0.52	0.02	0.88	1.09	0.43	0.32	0.03	0.01	1.26	0.01	1.26	0.58	1.44
UBTG	No.	M,N	SiO <sub>2</sub>	TiO <sub>2</sub>	ZrO <sub>2</sub>	Al <sub>2</sub> O <sub>3</sub>	FeO	MnO	MgO	CaO	Na <sub>2</sub> O	K <sub>2</sub> O	F	Cl	Sum	less O	Sum	H <sub>2</sub> O	Total
NTB2011-5	0	0	47.33	2.71	0.00	15.35	11.17	0.20	5.26	9.55	3.83	1.29	0.42	0.04	97.16	0.19	96.97	2.52	99.49
0.00	11	1,1	0.71	0.12	0.01	0.34	0.43	0.02	0.46	0.34	0.40	0.07	0.02	0.01	0.81	0.01	0.81	0.41	0.48
NTB2011-6	0	0	48.03	2.48	0.01	15.57	10.79	0.18	5.30	8.77	3.15	1.24	0.01	0.04	95.58	0.01	95.56	1.41	96.97
0.00	13	1,1	1.01	0.46	0.05	1.50	1.27	0.05	1.29	1.49	0.43	0.39	0.07	0.02	1.77	0.03	1.76	1.40	1.49
NTB2012-89	0	0	48.29	2.21	0.14	15.11	10.30	0.21	5.54	9.71	3.74	1.19	0.30	0.04	96.79	0.14	96.66	3.20	99.86
0	7	4,4	0.47	0.30	0.04	0.70	0.30	0.02	0.32	0.63	0.34	0.32	0.09	0.01	1.12	0.04	1.10	1.44	0.64
NTB2012-92	0	0	50.05	2.47	0.07	14.70	10.70	0.20	4.58	8.78	3.97	1.48	-0.05	0.06	97.00	-0.01	97.01	2.58	99.59
0.00	17	1,1	0.45	0.19	0.04	0.40	0.38	0.02	0.31	0.41	0.28	0.10	0.06	0.01	0.55	0.02	0.56	0.33	0.55
NTB2012-93	0	0	50.36	2.37	0.09	14.82	10.47	0.19	4.73	9.01	3.76	1.46	0.11	0.06	97.44	0.06	97.38	2.35	99.74
0.00	13	1,1	0.58	0.16	0.06	0.24	0.39	0.02	0.18	0.31	0.16	0.07	0.10	0.01	0.60	0.04	0.58	0.25	0.47
NTB2012-94	0	0	50.28	2.63	0.09	14.84	10.75	0.22	4.78	9.72	3.38	1.52	0.00	0.06	98.26	0.01	98.25	0.45	98.70
0.00	14	1,1	0.64	0.32	0.05	1.20	0.90	0.03	0.58	0.42	0.36	0.14	0.07	0.01	0.64	0.03	0.65	0.42	0.45
NTB2012-95	0	0	48.98	2.53	0.11	14.62	10.87	0.21	4.87	9.55	3.45	1.59	-0.08	0.06	96.76	-0.02	96.78	2.07	98.85
0.00	9	1,1	0.54	0.18	0.04	0.13	0.16	0.02	0.22	0.12	0.31	0.08	0.05	0.01	0.55	0.02	0.55	0.43	0.64
NTB2012-96	0	0	50.03	3.02	0.11	14.24	11.70	0.24	4.63	9.57	3.36	1.74	0.04	0.06	98.74	0.03	98.71	0.05	98.76
0.00	15	1,1	0.62	0.17	0.05	0.32	0.31	0.02	0.20	0.26	0.29	0.11	0.06	0.01	0.57	0.03	0.58	0.56	0.66
NTB2012-114	0	0	49.30	2.30	0.08	15.48	10.28	0.21	5.47	9.72	3.79	1.24	0.16	0.04	98.06	0.07	97.98	1.10	99.09

0.00	15	1,1	1.12	0.27	0.05	1.01	0.76	0.02	0.54	0.32	0.25	0.11	0.07	0.01	1.12	0.03	1.13	0.63	0.64
NTB2012-115	0	0	49.09	2.19	0.04	15.36	10.48	0.19	5.31	9.93	3.58	1.20	-0.09	0.05	97.32	-0.03	97.35	0.99	98.34
0.00	17	1,1	1.02	0.21	0.04	0.80	0.45	0.02	0.45	0.20	0.30	0.05	0.06	0.01	1.10	0.03	1.11	0.59	0.84
NTB2012-116	0	0	49.86	2.44	0.08	15.02	11.71	0.22	4.73	9.17	3.26	1.43	-0.07	0.06	97.90	-0.02	97.92	2.10	100.02
0.00	9	1,1	0.33	0.20	0.05	0.59	0.57	0.02	0.27	0.25	0.40	0.12	0.03	0.01	0.53	0.01	0.54	0.49	0.45
NTB2012-117	0	0	48.97	2.22	0.06	15.60	11.03	0.21	5.32	9.50	3.55	1.26	-0.14	0.05	97.63	-0.05	97.68	2.13	99.81
0.00	11	1,2	0.71	0.18	0.05	0.71	0.47	0.02	0.37	0.17	0.26	0.08	0.13	0.01	0.98	0.05	0.95	0.39	0.93
NTB2012-118	0	0	48.83	2.67	0.08	14.73	11.80	0.23	4.73	9.49	3.70	1.61	-0.03	0.06	97.89	-0.00	97.89	2.27	100.16
0.00	13	1,2	0.65	0.31	0.04	0.41	0.54	0.02	0.38	0.33	0.27	0.18	0.05	0.01	0.46	0.02	0.46	0.44	0.42
NTB2012-188	0	0	48.69	2.65	0.12	14.72	11.36	0.21	4.91	9.81	3.47	1.54	0.08	0.05	97.62	0.04	97.58	2.33	99.91
0.00	15	1,1	0.71	0.20	0.04	0.49	0.37	0.03	0.30	0.57	0.24	0.22	0.17	0.01	0.79	0.07	0.77	0.64	0.60
NTB2012-189	0	0	49.05	2.55	0.15	14.78	11.17	0.21	5.06	9.68	3.47	1.59	0.18	0.06	97.95	0.09	97.86	2.27	100.12
0.00	17	1,1	0.74	0.15	0.04	0.25	0.23	0.03	0.25	0.15	0.30	0.06	0.24	0.01	0.65	0.10	0.70	0.74	0.67
NTB2012-198	0	0	48.08	2.95	0.05	14.32	11.08	0.21	4.64	9.40	3.47	1.60	0.02	0.06	95.88	0.02	95.86	2.99	98.85
0.00	15	1,1	0.61	0.17	0.05	0.32	0.55	0.03	0.28	0.90	0.27	0.15	0.09	0.01	1.02	0.04	1.04	0.51	1.03
NTB2012-197	0	0	48.84	2.57	0.07	14.62	10.81	0.20	4.89	9.51	3.47	1.55	-0.08	0.06	96.50	-0.02	96.52	3.80	100.33
0.00	16	1,1	0.81	0.24	0.04	0.17	0.28	0.02	0.21	0.39	0.32	0.07	0.08	0.01	0.68	0.03	0.66	0.53	0.55
NTB2012-199	0	0	49.02	2.78	0.04	14.59	11.58	0.21	4.38	8.76	2.92	1.52	0.01	0.05	95.86	0.01	95.84	2.62	98.46
0.00	9	1,1	0.85	0.36	0.03	0.28	0.72	0.04	0.40	0.74	0.62	0.22	0.13	0.01	2.02	0.05	2.01	1.63	0.55
NTB2014-332	0	0	50.30	2.18	0.02	16.01	10.56	0.21	5.29	8.77	3.77	1.27	0.38	0.05	98.81	0.17	98.64	1.27	99.90
0.00	9	1,2	0.49	0.32	0.05	0.75	0.69	0.03	0.44	0.37	0.18	0.14	0.03	0.01	0.47	0.01	0.48	0.35	0.58
<b>Unique Basalts</b>	<b>No.</b>	<b>M,N</b>	<b>SiO<sub>2</sub></b>	<b>TiO<sub>2</sub></b>	<b>ZrO<sub>2</sub></b>	<b>Al<sub>2</sub>O<sub>3</sub></b>	<b>FeO</b>	<b>MnO</b>	<b>MgO</b>	<b>CaO</b>	<b>Na<sub>2</sub>O</b>	<b>K<sub>2</sub>O</b>	<b>F</b>	<b>Cl</b>	<b>Sum</b>	<b>less O</b>	<b>Sum</b>	<b>H<sub>2</sub>O</b>	<b>Total</b>
NTB2012-102	0	0	54.70	2.24	0.08	14.95	9.29	0.18	4.23	7.98	3.67	2.15	0.11	0.07	99.65	0.06	99.59	-0.16	99.43
0.00	16	1,1	0.90	0.19	0.04	0.15	0.26	0.02	0.33	0.53	0.14	0.19	0.06	0.01	0.67	0.02	0.66	0.28	0.61
NTB2011-45	0	0	47.58	3.65	0.01	13.96	13.09	0.25	4.66	8.93	3.53	1.40	0.44	0.05	97.54	0.20	97.34	2.30	99.64
0.00	5	3,3	0.64	0.34	0.01	0.72	0.76	0.01	0.50	0.42	0.33	0.24	0.05	0.01	0.43	0.02	0.43	0.17	0.29
<b>EBT</b>	<b>No.</b>	<b>M,N</b>	<b>SiO<sub>2</sub></b>	<b>TiO<sub>2</sub></b>	<b>ZrO<sub>2</sub></b>	<b>Al<sub>2</sub>O<sub>3</sub></b>	<b>FeO</b>	<b>MnO</b>	<b>MgO</b>	<b>CaO</b>	<b>Na<sub>2</sub>O</b>	<b>K<sub>2</sub>O</b>	<b>F</b>	<b>Cl</b>	<b>Sum</b>	<b>less O</b>	<b>Sum</b>	<b>H<sub>2</sub>O</b>	<b>Total</b>
CAT02-19	0	0	50.22	2.75	0.05	15.91	9.95	0.19	3.47	7.59	3.70	1.82	0.09	0.08	95.82	0.06	95.76	2.87	98.63
0.00	12	1,2	1.63	0.51	0.05	1.95	1.67	0.04	1.03	1.29	0.68	0.43	0.06	0.03	2.30	0.03	2.31	1.64	1.58
CAT02-28	0	0	49.31	3.34	0.02	15.15	11.32	0.22	3.76	7.78	3.72	1.91	0.14	0.07	96.74	0.08	96.66	1.33	98.00

0.00	18	1,1	1.16	0.55	0.05	1.20	1.32	0.04	0.76	0.58	0.40	0.28	0.06	0.01	0.51	0.03	0.51	0.56	0.49
McB2010-2	0	0	49.74	2.59	0.00	15.29	11.58	0.27	3.40	7.04	4.02	1.82	0.09	0.06	95.90	0.05	95.85	2.62	98.47
0.00	18	1,1	0.49	0.16	0.00	0.80	0.73	0.02	0.31	0.23	0.37	0.11	0.09	0.01	0.55	0.04	0.55	0.50	0.51
NTB2012-104	0	0	50.868	2.596	0.372	15.235	11.172	0.236	3.285	7.196	4.168	0.652	0.301	0.07	97.143	0.366	96.777	3.433	100.210
0	3	1,1	1.082	0.565	0.048	1.731	1.459	0.014	0.461	0.323	0.160	0.978	0.114	N/A	1.046	0.153	0.926	0.750	0.272

### Lithological Composition of the Basaltic Tuff groups:

Tuffs attributed to all three of the basaltic tuff groups can range from 0.10 m to > 2 m in thickness when viewed in an outcrop, generally have a tan, light brown or brown color and often display soil development, a silty tuffaceous well-consolidated texture with massive bedding. Tuffs of the basaltic category most often preserve abundant glass that is petrographically distinct from glass of the felsic category. Basaltic glass is brown to brown-yellow, with shards, often 100-200  $\mu\text{m}$ , with thick shard walls and large flat areas interrupted by large round vesicles (Heiken and Heiken, 1974; Lowe, 2011). Shards display rectangular margins that often intersect at almost right angles unless the shard is broken around a vesicle. Glass shards from the basaltic groups also occasionally include lathe-shaped plagioclase crystals incorporated into the body of the glass shard. The minerals aegerine and olivine crystals are also common (Tryon and McBrearty, 2002; Tryon and McBrearty, 2006). These lithological and petrographic characteristics, combined with the stratigraphic position of a sample, are valuable in the field and in laboratory sample preparation for distinguishing basaltic from felsic tuffs of the Bedded Tuff Member. However, lithological and petrographic materials are insufficient to distinguish between the specific basaltic tuff groups necessary for refined stratigraphic understanding and dating of the Bedded Tuff Member.

These specific grouping of basaltic tuffs are defined on EPMA determined chemical composition discussed below.

#### Chemical Composition of the Basaltic Tuff groups:

The basaltic tuffs encountered in this study range widely in composition (Figs. 5, 6a-e), but analyses presented here agree with Tryon & McBrearty's (2002; 2006) previous assessment that the basaltic tephra follow a continually evolving composition trend and can be reliably subdivided into compositional groups ranging from the least chemically evolved 'lower basaltic' tuffs stratigraphically lower in section to more chemically evolved 'upper basaltic' and most chemically evolved, 'evolved basaltic' tuffs successively higher. We thus follow the general conventions of nomenclature as well as the boundaries between lower, upper and evolved basaltic tuff groups established by Tryon (2003) and Tryon and McBrearty (2002; 2006). Field stratigraphy and bivariate plots of various element oxides support these groupings. From stratigraphically lowest and least chemically evolved to stratigraphically higher and most evolved these three basaltic tuff groups are: 1) The Lower Basaltic Tuff Group, 2) The Upper Basaltic Tuff Group and 3) The Evolved Basaltic Tuff Group (Tryon, 2003; Tryon and McBrearty, 2002; Tryon and McBrearty, 2006).

## The Lower Basaltic Tuff Group

The Lower Basaltic Tuff Group (LBTG) is the least evolved basalt found in this and previous studies of the Bedded Tuff Member tuffs (Table 3; Fig. 6a-e; Tryon, 2003). The Lower Basaltic Tuff Group and is characterized by distinct abundance in CaO (9.29 - 12.21 wt. %), MgO (5.75 – 7.21 wt. %) and Cl (0.02 - 0.04 wt. %) (Table 3). Seven sections measured in this study preserve exposure attributed to the Lower Basaltic Tuff Group. These are the Tangul Bei Roadcut Section, WPT 150, Rorop Lingop, Lake Baringo Trachyte Cliffs Section, a sample from the Kampi-ya-Samaki beds near the town of Kampi-ya-Samaki, NRS and Section.2012.E (Fig. 2).

## Upper Basaltic Tuff Group:

The Upper Basaltic Tuff Group (UBTG) is also characterized by distinct abundances in CaO (8.76- 9.81 wt. %), MgO (4.38- 5.71) wt. %), Cl (0.03 - 0.06 wt. %), and TiO<sub>2</sub> (2.11- 2.95 wt. %) (Table 3). Thirteen samples from seven sections preserve exposures of the UBGT presented in this study. These are the Tangul Bei Roadcut Section, section WPT 157, the Lake Baringo Trachyte Cliffs Section, three samples from the Ndau River Section, five samples sequentially taken from a single tuff unit at Section.2012.E, four samples sequentially taken from a single tuff at Section.2012.I, an additional sample at Section I and two samples from Section.2012.U' (Fig. 2).

#### Evolved Basaltic Tuff Group:

The Evolved Basaltic Tuff Group (EBTG) samples in this study are characterized by low CaO (7.04 – 7.20 wt. %) and MgO (3.29 - 3.40 wt. %); some of the lowest values of any basaltic tuff in the Bedded Tuff Member, as well as and high Cl (0.06-0.07 wt. %) and moderately high TiO<sub>2</sub> (2.59 – 2.60 wt. %) (Table 3; Figs 6a-e). Four samples from four sections in this study are attributed to the EBTG. These are sample McB2010-2 from the KyS section, CAT02-28 from KYS-5 section (Tryon and McBrearty, 2006), CAT02-19 from Section 1 (Tryon and McBrearty, 2006) and NTB2012-104 from Section.2012.E (Fig. 2).

#### Additional Unique Basaltic Tuffs NTB2011-45 and NTB2012-102:

##### NTB2011-45

A distinct basaltic mode of sample NTB2011-45 from section WPT 158 is basaltic but does not conform to either UBTG primarily because of its very high TiO<sub>2</sub> (3.65 wt. %) and high FeO (13.09 wt. %) (Table 3; Figs 6 d, c). While we refrain from defining a distinct tuff unit based on the five analyses from the multimodal tuff sample NTB2011-45 we note this basaltic mode as

potentially evidence of an additional basaltic tuff unit. The second mode of NTB2011-45 is a low-silica trachyte attributed to the K4 Trendline Trachytes (discussed below).

#### NTB2012-102

An additional tuff sample, NTB2012-102, from ~2.0 m above the NRS Tuff at Section.2012.E (Table 3; Figs. 2, 6a-e) falls within the ‘Upper Basaltic’ category and along the evolving magma chamber trendline defined by Tryon and McBrearty, (2006). However both the stratigraphic position above the NRS Tuff at Section.2012.E (Fig. 2) and compositional uniqueness of this basaltic tuff, characterized by CaO (7.98 wt. %), MgO (4.62 wt. %), TiO<sub>2</sub> (2.24 wt. %) and relatively high SiO<sub>2</sub> for a basalt (54.70 wt. %) distinguish NTB2012-102 as unique and stratigraphically informative unit.

#### Felsic tephra:

This study focuses heavily on the felsic tephra of the Bedded Tuff Member in order to augment the previous studies of Tryon (2003) and Tryon and McBrearty (2002, 2006).

All felsic tephra of the Bedded Tuff Member are trachytes-trachyandesites with the single exception of a distal phonolitic tephra at the site of Keraswanin (Fig. 5).



### The Korosi Airfall Pumices:

The units here referred to as the Korosi Airfall Pumices (KAP) exposed to the north and north-east of the town of Loruk (Figs. 1a, 2) have variably been referred to as a coarse pumiceous unit of the 'Kampi-ya-Samaki Beds' (Martyn, 1969; Spooner, n.d.; Tallon, 1978) and the 'Airfall Pumices' (Dunkley et al., 1993). We provide the first published geochemical characterization of the KAP where they have been mapped to the north and northeast of the town of Loruk (Figs. 1a, 2; Dunkley et al., 1993). We further demonstrate correlation of these KAP units to the known tephrostratigraphic framework of the Bedded Tuff Member of the Kapthurin Formation west of Lake Baringo (Figs. 1a, 2).

### Lithology of the Korosi Airfall Pumices:

Field and petrographic observations under 40-100x magnification show all exposures of the Korosi Airfall Pumices (KAP) north of the town of Loruk and east to the slopes of the volcano Korosi are coarse grained, angular 1-10 cm (commonly 1-5 cm) pumices with intact round to elongated vesicles. These deposits were produced by the magmatic eruption associated with the onset of volcanic activity at the birth of the shield volcano Korosi (Dunkley et al., 1993). When

Table 4: Mean major and minor element oxides by weight percent for all samples of the felsic category discussed in this study. One standard deviation from the mean listed below each element oxide mean.

KAP	No.	M,N	SiO <sub>2</sub>	TiO <sub>2</sub>	ZrO <sub>2</sub>	Al <sub>2</sub> O <sub>3</sub>	FeO	MnO	MgO	CaO	Na <sub>2</sub> O	K <sub>2</sub> O	F	Cl	Sum	less O	Sum	H <sub>2</sub> O	Total
NTB2011-4	0	0	61.14	0.48	0.24	11.23	9.21	0.34	0.03	0.64	6.97	4.40	0.93	0.44	96.05	0.49	95.56	5.69	101.25
0	2	2,3	0.31	0.02	0.06	0.22	0.03	0.01	0.01	0.00	2.85	0.00	0.04	0.03	3.32	0.02	3.35	3.32	0.02
NTB2011-4	0	0	62.33	0.50	0.09	13.93	7.47	0.14	0.20	0.86	6.79	4.63	0.32	0.06	97.33	0.15	97.18	3.05	100.23
0	6	3,3	1.04	0.05	0.07	1.35	1.56	0.03	0.10	0.18	0.88	0.40	0.12	0.07	1.79	0.06	1.84	1.14	1.07
NTB2011-19	0	0	60.12	0.37	0.05	14.76	6.15	0.22	0.10	1.03	6.14	4.75	0.34	0.18	94.21	0.18	94.03	5.23	99.26
0	17	1,1	0.98	0.05	0.05	0.32	0.52	0.03	0.03	0.30	1.52	0.22	0.11	0.04	2.27	0.05	2.29	1.80	1.10
NTB2011-20	0	0	60.00	0.39	0.11	13.96	6.76	0.25	0.02	0.86	4.54	4.87	0.51	0.22	92.49	0.26	92.23	6.79	99.02
0	22	1,1	1.00	0.05	0.06	0.48	0.81	0.04	0.01	0.17	2.06	0.71	0.12	0.06	2.00	0.06	2.01	1.50	1.26
NTB2011-21	0	0	60.39	0.39	0.09	13.82	6.82	0.26	0.03	0.91	4.56	5.13	0.54	0.21	93.15	0.28	92.88	6.35	99.23
0	23	1,1	1.61	0.10	0.05	0.90	1.42	0.08	0.01	0.14	1.92	0.35	0.19	0.05	2.10	0.09	2.13	1.90	1.25
NTB2011-22	0	0	61.47	0.50	0.08	13.55	7.66	0.29	0.03	1.03	6.87	4.65	0.35	0.15	96.63	0.18	96.45	3.13	99.58
0	13	1,1	1.09	0.04	0.06	0.46	0.22	0.03	0.02	0.12	0.77	0.15	0.07	0.04	1.91	0.04	1.92	1.46	0.79
NTB2011-25	0	0	60.28	0.50	0.19	11.20	9.63	0.36	0.02	0.76	3.74	4.84	0.98	0.46	92.97	0.52	92.46	6.72	99.18
0	16	1,1	0.48	0.05	0.04	0.39	0.54	0.04	0.01	0.06	1.35	0.32	0.11	0.04	1.59	0.05	1.59	1.44	0.42
NTB2011-26	0	0	60.57	0.49	0.09	13.21	7.58	0.30	0.05	0.89	6.42	4.66	0.28	0.23	94.77	0.17	94.60	4.59	99.19
0	19	1,1	1.36	0.05	0.04	0.39	0.54	0.04	0.01	0.07	1.61	0.17	0.12	0.02	3.36	0.05	3.34	1.82	2.01
NTB2011-28	0	0	60.44	0.47	0.10	12.60	8.03	0.33	0.04	0.72	3.84	4.88	0.53	0.33	92.30	0.29	92.00	7.59	99.59
0	4	1,1	0.25	0.01	0.05	0.37	0.38	0.04	0.01	0.04	2.14	0.25	0.11	0.04	2.15	0.05	2.11	1.40	0.84
NTB2011-29	0	0	62.41	0.41	0.16	12.17	7.53	0.26	0.03	0.65	5.56	4.69	0.61	0.34	94.82	0.33	94.48	4.15	98.64
0	22	1,1	1.21	0.13	0.08	1.32	1.52	0.08	0.03	0.14	1.13	0.34	0.20	0.11	1.62	0.11	1.67	1.42	1.21
NTB2011-39	0	0	64.09	0.65	0.06	12.41	7.66	0.28	0.32	0.64	6.67	3.97	0.30	0.03	97.10	0.13	96.97	2.43	99.40
0	2	2,4	3.25	0.23	0.06	0.67	1.67	0.08	0.37	0.41	1.20	1.51	0.11	0.01	1.52	0.05	1.47	1.64	0.35
NTB2011-39	0	0	62.17	0.47	0.16	13.08	8.14	0.31	0.06	0.80	6.07	4.52	0.62	0.32	96.71	0.33	96.37	4.37	100.74
0	7	3,4	1.19	0.04	0.06	0.44	0.27	0.02	0.03	0.11	1.68	0.14	0.09	0.03	2.30	0.03	2.29	2.20	0.77
NTB2011-39	0	0	62.65	0.52	0.18	11.49	9.62	0.36	0.04	0.71	5.05	4.13	0.75	0.41	95.90	0.41	95.49	3.56	99.06
0	2	4,4	0.40	0.03	0.06	0.20	0.29	0.04	0.02	0.07	4.82	0.36	0.14	0.05	4.97	0.07	4.90	4.72	0.18
NTB2011-42	0	0	63.13	0.40	0.09	14.56	5.57	0.15	0.09	1.02	6.95	4.78	0.24	0.06	97.04	0.11	96.93	2.95	99.88

0	14	1,2	1.68	0.10	0.05	0.76	1.20	0.06	0.05	0.36	0.52	0.44	0.11	0.05	1.77	0.06	1.80	1.29	1.84
NTB2011-45	0	0	61.69	0.57	0.03	14.85	6.77	0.12	0.23	0.91	6.87	4.59	0.26	0.08	96.97	0.13	96.84	2.65	99.49
0	6	2,3	2.03	0.30	0.03	1.57	1.74	0.05	0.14	0.35	0.98	1.12	0.02	0.07	1.66	0.02	1.66	0.95	2.12
NTB2011-49	0	0	61.27	0.50	0.18	13.39	8.19	0.15	0.28	1.02	6.37	4.18	0.35	0.03	95.91	0.15	95.75	3.50	99.25
0	7	1,3	1.28	0.11	0.09	1.29	2.19	0.08	0.17	0.16	0.98	0.63	0.09	0.02	2.26	0.04	2.27	1.31	1.12
NTB2011-49	0	0	60.05	0.45	0.21	11.25	9.28	0.36	0.05	0.72	6.13	4.28	0.73	0.37	93.89	0.39	93.50	4.53	98.03
0	2	2,3	2.62	0.02	0.04	0.74	0.39	0.04	0.01	0.10	1.33	0.39	0.08	0.03	5.49	0.04	5.53	2.70	2.84
NTB2011-49	0	0	61.33	0.59	0.15	13.27	8.00	0.23	0.13	1.14	6.06	4.51	0.40	0.15	95.95	0.20	95.75	4.00	99.75
0	11	3,3	0.69	0.14	0.06	0.66	1.22	0.08	0.10	0.19	0.51	0.45	0.12	0.03	0.90	0.06	0.90	0.66	0.52
NTB2011-50	0	0	60.85	0.60	0.19	12.87	9.41	0.10	0.31	0.86	6.05	4.16	0.29	0.01	95.69	0.12	95.57	3.67	99.24
0	12	1,3	1.11	0.17	0.08	0.72	1.55	0.08	0.15	0.25	0.60	0.46	0.05	0.01	1.14	0.02	1.14	0.86	0.54
NTB2011-50	0	0	60.60	0.44	0.15	11.06	9.20	0.35	0.04	0.66	5.33	4.03	0.85	0.44	93.17	0.46	92.71	5.87	98.58
0	2	2,3	2.26	0.03	0.06	0.50	0.55	0.01	0.02	0.11	4.51	0.67	0.06	0.02	8.48	0.03	8.51	5.74	2.77
NTB2011-50	0	0	61.59	0.53	0.20	12.28	8.72	0.24	0.13	0.88	5.73	4.35	0.52	0.21	95.39	0.27	95.12	3.68	98.80
0	5	3,3	1.88	0.25	0.10	1.81	2.56	0.14	0.09	0.43	1.14	0.91	0.19	0.09	2.58	0.10	2.63	1.17	1.57
NTB2011-52	0	0	61.55	0.40	0.05	14.94	5.47	0.15	0.08	0.82	6.98	5.11	0.26	0.06	95.87	0.12	95.74	1.56	97.30
0	17	1,1	1.43	0.19	0.07	0.84	1.39	0.08	0.11	0.46	0.37	0.48	0.16	0.05	1.52	0.08	1.50	0.40	1.67
NTB2011-53	0	0	59.63	0.41	0.07	14.49	6.00	0.22	0.10	1.00	5.97	4.95	0.47	0.18	93.49	0.24	93.25	5.50	98.75
0	22	1,1	1.71	0.08	0.05	1.06	0.67	0.05	0.04	0.21	1.57	0.44	0.08	0.06	4.63	0.04	4.64	2.21	3.58
NTB2011-54	0	0	64.40	0.20	0.04	16.11	3.23	0.05	0.05	0.63	6.80	4.78	0.12	0.03	96.44	0.06	96.38	2.01	98.39
0	3	1,2	0.33	0.06	0.01	1.01	0.63	0.04	0.02	0.17	0.77	0.28	0.05	0.01	1.38	0.02	1.40	0.47	0.95
NTB2011-54	0	0	60.25	0.38	0.07	14.25	6.57	0.25	0.05	1.03	6.87	4.78	0.62	0.22	95.35	0.31	95.04	5.10	100.14
0	16	2,2	1.05	0.04	0.05	0.46	0.25	0.03	0.01	0.08	0.58	0.20	0.10	0.02	1.40	0.04	1.41	1.23	0.45
NTB2012-89	0	0	63.53	0.49	0.07	14.21	6.82	0.23	0.20	1.12	6.40	4.68	0.28	0.13	98.15	0.14	98.00	2.04	100.05
0	6	1,4	1.26	0.11	0.03	0.75	1.13	0.07	0.17	0.34	0.41	0.27	0.12	0.04	1.28	0.06	1.29	1.02	1.14
NTB2012-89	0	0	63.16	0.45	0.16	13.03	7.84	0.31	0.06	0.73	5.33	4.43	0.62	0.29	96.41	0.33	96.09	4.68	100.76
0	3	2,4	1.14	0.05	0.17	1.15	1.10	0.06	0.02	0.13	1.75	0.42	0.23	0.12	1.82	0.12	1.94	2.41	1.03
NTB2012-89	0	0	65.74	0.42	0.09	12.51	5.92	0.20	0.06	0.76	5.27	4.21	0.36	0.15	95.69	0.19	95.50	3.99	99.50
0	10	3,4	2.55	0.10	0.06	2.13	0.85	0.05	0.04	0.60	1.52	0.63	0.22	0.06	2.25	0.10	2.28	1.78	1.88
NTB2012-117	0	0	62.17	0.45	0.11	12.87	8.07	0.26	0.06	0.64	6.48	3.24	0.39	0.34	95.07	0.24	94.83	5.12	99.95
0	2	2,2	1.41	0.23	0.04	0.71	1.12	0.06	0.02	0.18	1.69	0.91	0.05	0.07	0.43	0.04	0.40	0.32	0.71

NTB2012-196	0	0	63.47	0.49	0.11	12.06	7.74	0.25	0.04	0.73	5.74	3.22	0.53	0.28	94.68	0.29	94.39	5.22	99.62
0	2	2,2	4.68	0.00	0.04	1.83	2.08	0.09	0.04	0.29	0.69	0.82	0.18	0.12	1.50	0.10	1.60	0.77	0.83
NTB2104-321	0	0	60.32	0.41	0.10	15.89	5.83	0.23	0.18	1.29	6.45	4.85	0.45	0.19	96.18	0.23	95.95	6.26	102.21
0	13	1,1	0.81	0.13	0.04	1.19	1.27	0.05	0.03	0.06	1.24	0.19	0.05	0.03	2.06	0.02	2.06	1.10	1.16
NTB2104-322	0	0	60.52	0.44	0.11	14.96	6.32	0.25	0.19	1.21	5.52	5.04	0.42	0.19	95.18	0.22	94.96	6.45	101.41
0	10	1,1	1.27	0.11	0.04	1.57	1.13	0.05	0.11	0.30	1.54	0.31	0.09	0.08	1.56	0.05	1.57	1.10	0.84
NTB2104-323	0	0	61.06	0.37	0.14	14.72	6.13	0.24	0.06	1.09	5.57	5.18	0.60	0.20	95.36	0.30	95.06	6.47	101.53
0	12	1,1	0.67	0.03	0.03	0.19	0.18	0.03	0.01	0.05	1.38	0.18	0.11	0.01	1.83	0.04	1.81	1.36	0.97
NTB2104-324	0	0	61.04	0.44	0.20	13.20	7.46	0.29	0.04	0.87	6.13	4.85	0.72	0.30	95.53	0.37	95.16	6.10	101.26
0	11	1,1	0.67	0.04	0.05	0.59	0.28	0.04	0.01	0.10	1.50	0.23	0.08	0.05	2.01	0.04	2.01	1.23	1.06
NTB2014-325	0	0	61.28	0.41	0.19	13.45	7.29	0.27	0.04	0.91	6.23	4.79	0.65	0.31	95.81	0.34	95.47	5.53	101.00
0	12	1,1	0.46	0.06	0.05	0.40	0.51	0.03	0.01	0.08	1.43	0.21	0.04	0.03	1.55	0.02	1.55	0.75	1.12
NTB2014-326	0	0	61.26	0.41	0.17	13.28	7.21	0.28	0.04	0.94	5.63	4.81	0.66	0.28	94.97	0.34	94.64	5.76	100.40
0	12	1,1	0.99	0.07	0.06	0.80	1.07	0.06	0.01	0.16	1.03	0.29	0.16	0.06	1.70	0.08	1.71	1.24	1.74
NTB2014-327	0	0	61.63	0.41	0.16	13.86	7.00	0.27	0.05	0.89	6.38	4.87	0.67	0.26	96.45	0.34	96.11	5.15	101.26
0	13	1,1	1.32	0.08	0.04	0.59	0.99	0.06	0.02	0.20	1.59	0.24	0.21	0.07	2.33	0.10	2.36	1.61	1.46
NTB2014-328	0	0	60.11	0.41	0.24	11.28	8.43	0.32	0.03	0.62	3.76	4.84	1.01	0.41	91.45	0.52	90.93	7.14	98.06
0	12	1,1	2.09	0.03	0.04	0.42	0.37	0.03	0.01	0.04	1.76	0.26	0.68	0.04	3.83	0.29	3.86	1.42	2.78
NTB2014-329	0	0	58.81	0.42	0.13	13.38	6.98	0.27	0.04	0.86	4.09	4.90	0.52	0.30	90.70	0.29	90.41	7.05	97.46
0	15	1,1	2.38	0.04	0.05	0.61	0.28	0.03	0.01	0.06	1.81	0.64	0.08	0.04	3.90	0.04	3.93	1.15	3.30
NTB2014-330	0	0	60.86	0.53	0.10	13.79	7.96	0.33	0.09	1.10	5.54	4.84	0.48	0.22	95.84	0.25	95.59	5.75	101.34
0	16	1,1	0.82	0.05	0.05	0.34	0.60	0.03	0.04	0.17	1.51	0.15	0.11	0.07	1.98	0.06	1.98	1.47	0.93
NTB2014-331	0	0	61.79	0.46	0.16	13.33	7.65	0.31	0.05	0.82	6.35	4.69	0.51	0.29	96.42	0.28	96.14	5.14	101.28
0	12	1,1	0.47	0.03	0.04	0.27	0.09	0.02	0.01	0.03	1.69	0.27	0.04	0.02	2.08	0.02	2.08	1.06	1.29
NTB2014-333	0	0	62.15	0.48	0.17	12.80	8.20	0.32	0.06	0.77	5.44	4.62	0.64	0.33	95.98	0.34	95.64	5.04	100.68
0	11	1,1	1.36	0.06	0.04	0.76	0.91	0.05	0.01	0.12	2.02	0.46	0.12	0.05	2.80	0.06	2.82	2.28	1.01
NTB2014-334	0	0	63.08	0.48	0.20	12.27	8.24	0.32	0.04	0.68	7.51	4.43	0.63	0.37	98.12	0.35	97.77	3.87	101.64
0	20	1,1	0.78	0.02	0.06	0.18	0.15	0.03	0.01	0.02	0.42	0.05	0.04	0.02	1.19	0.02	1.20	0.62	0.78
NTB2014-335	0	0	63.19	0.49	0.20	12.67	8.62	0.33	0.05	0.78	7.38	4.57	0.62	0.31	99.21	0.33	98.88	2.81	101.68
0	5	1,1	1.43	0.04	0.06	0.70	0.29	0.03	0.02	0.16	0.87	0.23	0.07	0.06	2.89	0.04	2.91	2.49	0.67
NTB2014-355	0	0	60.97	0.49	0.16	13.15	7.77	0.29	0.07	0.80	4.91	4.24	0.52	0.29	93.67	0.28	93.39	5.12	98.51

0	4	2,2	3.64	0.03	0.06	0.75	0.41	0.08	0.02	0.12	2.69	0.70	0.04	0.05	8.31	0.00	8.31	3.26	5.59
<b>K4 Trendlind</b>																			
<b>Trachytes</b>	<b>No.</b>	<b>M,N</b>	<b>SiO<sub>2</sub></b>	<b>TiO<sub>2</sub></b>	<b>ZrO<sub>2</sub></b>	<b>Al<sub>2</sub>O<sub>3</sub></b>	<b>FeO</b>	<b>MnO</b>	<b>MgO</b>	<b>CaO</b>	<b>Na<sub>2</sub>O</b>	<b>K<sub>2</sub>O</b>	<b>F</b>	<b>Cl</b>	<b>Sum</b>	<b>less O</b>	<b>Sum</b>	<b>H<sub>2</sub>O</b>	<b>Total</b>
CAT97-70	0.00	0.00	60.04	0.72	0.05	15.24	5.94	0.18	0.53	2.04	5.19	3.91	0.36	0.13	94.33	0.18	94.14	7.95	102.09
0	3.00	2,2	0.83	0.11	0.04	0.11	0.33	0.01	0.06	0.21	0.71	0.08	0.02	0.03	1.12	0.01	1.12	1.43	0.55
CAT97-74	0.00	0.00	61.38	0.53	0.04	15.19	5.22	0.18	0.39	1.65	5.58	4.30	0.37	0.15	94.97	0.19	94.78	7.10	101.88
0	32	1,1	1.94	0.18	0.04	0.28	0.95	0.03	0.20	0.53	0.46	0.47	0.04	0.04	0.80	0.02	0.80	0.62	0.51
CAT02-27	0.00	0.00	62.50	0.36	0.08	15.73	3.78	0.12	0.29	1.14	4.89	5.11	0.27	0.17	94.45	0.15	94.29	6.22	100.51
0	17	1,1	0.88	0.06	0.05	0.43	0.19	0.02	0.06	0.11	0.58	0.23	0.04	0.05	1.46	0.02	1.47	1.16	1.44
McB97-01	0	0	61.82	0.32	0.06	15.33	4.25	0.15	0.09	1.08	4.94	5.03	0.25	0.14	93.48	0.14	93.34	5.47	98.81
0	30	1,1	0.75	0.06	0.05	0.50	0.61	0.04	0.02	0.10	1.17	0.17	0.07	0.03	0.95	0.03	0.97	1.02	0.82
MB97-02	0	0.00	61.90	0.39	0.07	14.82	4.35	0.14	0.21	1.14	5.03	4.41	0.34	0.17	92.97	0.18	92.79	7.42	100.21
0	27	1,1	1.70	0.18	0.04	0.41	1.07	0.04	0.17	0.40	0.56	0.41	0.06	0.04	1.29	0.03	1.29	0.82	0.96
McB2010-1	0	0.00	56.98	0.88	0.02	15.98	6.97	0.21	1.00	3.14	5.91	3.53	0.28	0.13	95.04	0.15	94.89	4.52	99.41
0	17	1,1	2.05	0.19	0.03	0.38	0.76	0.03	0.35	0.75	0.49	0.64	0.15	0.02	2.33	0.06	2.31	1.24	1.48
McB2010-3	0	0.00	59.92	0.44	0.08	15.16	5.17	0.19	0.26	1.43	6.09	4.77	0.35	0.17	94.04	0.19	93.85	6.28	100.13
0	18	1,1	2.72	0.24	0.06	0.92	1.41	0.05	0.29	0.89	0.39	0.73	0.09	0.07	2.70	0.05	2.69	1.71	1.56
McB2010-4	0	0.00	60.89	0.38	0.06	15.05	4.39	0.16	0.20	1.25	5.99	4.90	0.25	0.18	93.71	0.15	93.56	5.65	99.22
0	17	1,1	3.73	0.24	0.05	1.07	1.56	0.05	0.23	0.72	0.68	0.72	0.09	0.08	2.01	0.04	2.02	1.40	1.47
McB2011-2	0	0.00	62.56	0.28	0.06	15.01	3.97	0.14	0.09	0.87	6.03	5.21	0.34	0.19	94.75	0.18	94.57	4.83	99.40
0	21	1,1	1.03	0.04	0.05	0.26	0.18	0.02	0.01	0.04	0.22	0.11	0.05	0.02	1.48	0.02	1.47	0.54	1.07
NTB2010-1	0	0.00	57.03	0.95	0.04	16.19	7.28	0.21	1.06	3.24	5.15	3.20	0.18	0.12	94.65	0.10	94.55	3.86	98.41
0	16	1,1	1.37	0.15	0.05	0.51	0.65	0.03	0.13	0.29	0.83	0.12	0.04	0.01	1.84	0.02	1.85	1.37	0.74
NTB2010-2	0	0.00	61.24	0.30	0.10	14.66	4.03	0.14	0.10	0.88	5.58	5.19	0.14	0.21	92.59	0.11	92.48	6.23	98.71
0	15	1,1	1.60	0.04	0.05	0.50	0.25	0.03	0.02	0.06	0.19	0.18	0.12	0.03	2.06	0.05	2.07	1.20	1.49
NTB2011-1	0	0.00	60.37	0.81	0.03	15.39	6.30	0.19	0.83	2.45	5.52	4.04	0.20	0.14	96.28	0.12	96.16	2.87	99.03
0	31	1,1	2.65	0.43	0.05	0.56	1.89	0.05	0.65	1.29	0.31	0.82	0.04	0.05	1.68	0.02	1.69	1.90	0.52
NTB2011-24	0	0.00	61.40	0.41	0.08	15.24	4.78	0.17	0.18	1.21	5.93	4.93	0.34	0.18	94.83	0.18	94.64	4.73	99.37
0	22	1,1	2.04	0.18	0.07	0.58	1.09	0.04	0.21	0.67	0.32	0.57	0.05	0.06	2.23	0.03	2.23	1.16	1.44
NTB2011-44	0	0.00	65.33	0.21	0.08	14.57	2.95	0.09	0.08	0.74	5.20	5.18	0.24	0.25	94.91	0.16	94.76	5.05	99.81
0	16	1,2	0.45	0.03	0.05	0.11	0.10	0.02	0.01	0.02	0.14	0.09	0.04	0.01	0.66	0.02	0.66	0.26	0.65

NTB2011-45	0	0.00	57.57	0.91	0.01	16.24	7.15	0.21	1.05	3.25	5.57	3.40	0.32	0.13	95.81	0.17	95.65	3.18	98.83
0	4	1,3	2.05	0.08	0.01	0.86	0.50	0.01	0.03	0.16	0.40	0.30	0.08	0.02	4.23	0.03	4.20	1.63	2.57
NTB2011-46	0	0.00	60.27	0.52	0.05	15.41	5.52	0.20	0.33	1.67	5.91	4.55	0.34	0.15	94.92	0.18	94.74	3.88	98.62
0	20	1,1	2.21	0.24	0.05	0.75	1.57	0.05	0.28	0.88	0.77	0.71	0.07	0.04	2.45	0.03	2.45	1.90	1.17
NTB2011-48	0	0.00	56.88	0.90	0.03	16.02	7.05	0.22	0.95	3.08	5.54	3.37	0.28	0.13	94.46	0.15	94.31	4.55	98.86
0	14	1,1	1.69	0.09	0.04	0.44	0.19	0.02	0.13	0.29	0.47	0.21	0.12	0.02	2.65	0.05	2.64	1.61	1.50
NTB2013-222	0	0.00	63.80	0.54	0.11	15.67	5.24	0.17	0.42	1.86	5.71	4.36	0.15	0.13	98.15	0.09	98.06	4.58	102.64
0	8	2,2	2.07	0.26	0.04	0.68	1.62	0.06	0.32	0.74	0.35	0.55	0.25	0.03	1.47	0.10	1.48	0.96	1.32
NTB2014-340	0	0.00	63.03	0.47	0.08	15.17	4.85	0.17	0.34	1.44	5.38	4.36	0.34	0.18	95.79	0.18	95.61	4.89	100.50
0	28	1,1	2.20	0.22	0.04	0.48	1.18	0.05	0.26	0.65	0.54	0.55	0.06	0.04	1.50	0.03	1.51	0.64	1.41
NTB2014-342	0	0.00	63.24	0.44	0.09	15.39	4.58	0.15	0.29	1.36	5.29	4.37	0.32	0.16	95.67	0.17	95.50	4.51	100.01
0	20	1,1	2.60	0.21	0.04	0.52	1.32	0.05	0.23	0.56	0.58	0.55	0.05	0.04	1.31	0.02	1.33	0.76	1.08
NTB2014-357	0	0.00	64.16	0.31	0.07	16.27	3.84	0.13	0.18	1.03	6.02	4.93	0.32	0.15	97.41	0.17	97.25	4.10	101.35
0	13	1,1	2.90	0.18	0.04	1.22	1.64	0.07	0.19	0.60	0.87	0.60	0.11	0.06	2.80	0.06	2.83	1.67	1.94
NTB2014-358	0	0.00	61.93	0.53	0.08	15.96	5.16	0.16	0.45	1.79	5.40	4.41	0.35	0.15	96.38	0.18	96.19	4.09	100.29
0	20	1,1	3.62	0.38	0.04	0.88	1.69	0.07	0.55	1.38	0.64	0.85	0.07	0.06	4.18	0.04	4.20	1.60	3.40
NTB2014-359	0	0.00	62.09	0.52	0.08	15.69	5.33	0.20	0.48	1.75	5.61	4.46	0.36	0.16	96.72	0.19	96.53	4.41	100.95
0	6	1,1	2.96	0.29	0.02	0.35	1.47	0.04	0.53	1.23	0.57	0.96	0.05	0.03	1.36	0.02	1.37	0.84	0.97
NTB2014-360	0	0.00	62.40	0.63	0.11	16.34	5.65	0.18	0.58	2.05	5.90	4.37	0.36	0.14	98.71	0.18	98.53	3.19	101.72
0	5	1,1	3.72	0.29	0.04	0.33	1.56	0.05	0.45	1.14	0.34	0.96	0.04	0.03	1.69	0.02	1.67	1.58	0.56
NTB2014-361	0	0.00	61.44	0.62	0.05	16.21	5.97	0.20	0.55	2.08	5.82	4.21	0.38	0.14	97.66	0.19	97.47	3.86	101.34
0	14	1,1	2.52	0.29	0.04	0.56	1.54	0.04	0.45	1.13	0.47	0.93	0.09	0.03	1.46	0.03	1.46	1.55	2.10
<b>K4 Distal</b>																			
<b>Tephra #1</b>	<b>No.</b>	<b>M,N</b>	<b>SiO<sub>2</sub></b>	<b>TiO<sub>2</sub></b>	<b>ZrO<sub>2</sub></b>	<b>Al<sub>2</sub>O<sub>3</sub></b>	<b>FeO</b>	<b>MnO</b>	<b>MgO</b>	<b>CaO</b>	<b>Na<sub>2</sub>O</b>	<b>K<sub>2</sub>O</b>	<b>F</b>	<b>Cl</b>	<b>Sum</b>	<b>less O</b>	<b>Sum</b>	<b>H<sub>2</sub>O</b>	<b>Total</b>
NTB2014-339	0	0	61.30	0.26	0.08	15.97	5.39	0.23	0.09	1.22	5.52	4.95	0.44	0.26	95.71	0.24	95.47	5.30	100.77
0	13	1,1	0.70	0.02	0.05	0.21	0.27	0.04	0.03	0.05	1.20	0.36	0.06	0.02	2.12	0.03	2.11	1.32	1.19
<b>K4 Distal</b>																			
<b>Tephra #2</b>	<b>No.</b>	<b>M,N</b>	<b>SiO<sub>2</sub></b>	<b>TiO<sub>2</sub></b>	<b>ZrO<sub>2</sub></b>	<b>Al<sub>2</sub>O<sub>3</sub></b>	<b>FeO</b>	<b>MnO</b>	<b>MgO</b>	<b>CaO</b>	<b>Na<sub>2</sub>O</b>	<b>K<sub>2</sub>O</b>	<b>F</b>	<b>Cl</b>	<b>Sum</b>	<b>less O</b>	<b>Sum</b>	<b>H<sub>2</sub>O</b>	<b>Total</b>
CAT02-21	0	0	59.18	0.48	0.11	14.19	7.71	0.28	0.07	1.11	5.69	4.53	0.60	0.17	94.13	0.29	93.84	6.44	100.28
0	25	1,1	0.50	0.05	0.04	0.18	0.12	0.02	0.01	0.09	1.48	0.28	0.05	0.02	1.46	0.03	1.47	1.13	0.63
CAT02-25	0	0	59.43	0.49	0.13	14.20	7.56	0.28	0.07	1.06	5.76	4.52	0.60	0.18	94.27	0.30	93.98	7.50	101.48

0	23	1,1	0.81	0.04	0.04	0.32	0.40	0.04	0.02	0.12	1.63	0.43	0.10	0.04	2.15	0.05	2.16	1.48	1.21
CAT97-70	0	0	59.03	0.49	0.14	13.96	7.66	0.28	0.07	0.99	4.66	4.37	0.69	0.21	92.55	0.34	92.21	9.30	101.51
0	7	1,2	0.90	0.06	0.05	0.40	0.10	0.02	0.04	0.11	2.33	0.46	0.09	0.03	3.78	0.05	3.79	2.13	1.98
NTB2012-205	0	0	58.99	0.47	0.11	14.63	7.94	0.30	0.08	1.14	6.94	2.67	0.54	0.20	94.02	0.27	93.75	4.62	98.37
0	9	1,1	0.93	0.07	0.06	0.48	0.13	0.03	0.02	0.15	0.59	0.73	0.11	0.04	1.41	0.05	1.44	0.85	0.75
<b>K4 Distal Tephra #3</b>																			
	<b>No.</b>	<b>M,N</b>	<b>SiO<sub>2</sub></b>	<b>TiO<sub>2</sub></b>	<b>ZrO<sub>2</sub></b>	<b>Al<sub>2</sub>O<sub>3</sub></b>	<b>FeO</b>	<b>MnO</b>	<b>MgO</b>	<b>CaO</b>	<b>Na<sub>2</sub>O</b>	<b>K<sub>2</sub>O</b>	<b>F</b>	<b>Cl</b>	<b>Sum</b>	<b>less O</b>	<b>Sum</b>	<b>H<sub>2</sub>O</b>	<b>Total</b>
NTB2014-341	0	0	58.45	0.26	0.04	16.29	7.10	0.34	0.12	1.88	6.03	5.26	0.35	0.17	96.31	0.19	96.12	5.15	101.27
0	12	1,1	0.42	0.02	0.04	0.17	0.35	0.07	0.02	0.16	1.00	0.30	0.04	0.01	2.16	0.02	2.15	0.92	1.45
NTB2013-223	0	0	59.86	0.29	0.03	16.55	7.21	0.28	0.13	2.11	6.13	5.41	0.43	0.15	98.57	0.22	98.36	5.20	103.56
0	7	1,1	1.43	0.06	0.03	0.29	0.85	0.04	0.02	0.09	1.09	0.32	0.08	0.02	1.68	0.04	1.66	0.75	1.66
CAT02-22	0	0	56.35	0.29	0.04	16.26	6.73	0.30	0.15	1.87	5.11	5.01	0.08	0.16	92.37	0.07	92.30	7.52	99.82
0	19	1,1	1.58	0.03	0.05	0.56	0.22	0.04	0.02	0.09	0.74	0.25	0.05	0.01	2.70	0.02	2.69	1.28	2.38
<b>K4 Distal Tephra #4</b>																			
	<b>No.</b>	<b>M,N</b>	<b>SiO<sub>2</sub></b>	<b>TiO<sub>2</sub></b>	<b>ZrO<sub>2</sub></b>	<b>Al<sub>2</sub>O<sub>3</sub></b>	<b>FeO</b>	<b>MnO</b>	<b>MgO</b>	<b>CaO</b>	<b>Na<sub>2</sub>O</b>	<b>K<sub>2</sub>O</b>	<b>F</b>	<b>Cl</b>	<b>Sum</b>	<b>less O</b>	<b>Sum</b>	<b>H<sub>2</sub>O</b>	<b>Total</b>
CAT02-23	0	0	56.66	0.27	0.07	16.12	5.90	0.25	0.09	1.54	3.63	4.48	0.00	0.20	89.21	0.05	89.16	5.36	94.52
0	15	1,1	0.96	0.04	0.05	0.44	0.33	0.04	0.03	0.15	1.39	0.58	0.07	0.02	2.38	0.03	2.38	2.06	1.67
<b>Koimolot Tuff</b>																			
	<b>No.</b>	<b>M,N</b>	<b>SiO<sub>2</sub></b>	<b>TiO<sub>2</sub></b>	<b>ZrO<sub>2</sub></b>	<b>Al<sub>2</sub>O<sub>3</sub></b>	<b>FeO</b>	<b>MnO</b>	<b>MgO</b>	<b>CaO</b>	<b>Na<sub>2</sub>O</b>	<b>K<sub>2</sub>O</b>	<b>F</b>	<b>Cl</b>	<b>Sum</b>	<b>less O</b>	<b>Sum</b>	<b>H<sub>2</sub>O</b>	<b>Total</b>
CAT01-67	0	0	59.36	0.55	0.23	11.86	9.28	0.37	0.13	0.81	5.11	4.00	0.89	0.40	92.98	0.47	92.51	7.42	99.93
0	21	1,1	0.99	0.04	0.06	0.22	0.46	0.05	0.02	0.05	2.73	0.61	0.12	0.06	4.20	0.06	4.19	3.14	1.34
CAT02-20	0	0	59.16	0.53	0.24	11.92	8.79	0.34	0.12	0.84	5.87	4.18	0.69	0.35	93.01	0.37	92.65	5.52	98.16
0	22	1,1	1.38	0.11	0.07	0.95	1.33	0.09	0.03	0.16	1.53	0.44	0.22	0.10	2.19	0.11	2.21	2.14	0.85
<b>Wakondo Tuff</b>																			
	<b>No.</b>	<b>M,N</b>	<b>SiO<sub>2</sub></b>	<b>TiO<sub>2</sub></b>	<b>ZrO<sub>2</sub></b>	<b>Al<sub>2</sub>O<sub>3</sub></b>	<b>FeO</b>	<b>MnO</b>	<b>MgO</b>	<b>CaO</b>	<b>Na<sub>2</sub>O</b>	<b>K<sub>2</sub>O</b>	<b>F</b>	<b>Cl</b>	<b>Sum</b>	<b>less O</b>	<b>Sum</b>	<b>H<sub>2</sub>O</b>	<b>Total</b>
NB10-07	0	0	57.96	0.52	0.09	14.80	7.71	0.33	0.28	0.98	8.19	4.81	0.56	0.30	96.53	0.30	96.23	5.23	101.46
0	28	1,1	1.34	0.04	0.05	0.38	0.25	0.03	0.04	0.03	0.84	0.23	0.05	0.04	2.59	0.02	2.57	1.88	1.28
NTB2012-146	0	0	58.85	0.52	0.13	15.95	7.98	0.34	0.33	1.03	6.83	2.03	0.39	0.31	94.70	0.24	94.46	3.11	97.57
0	19	1,1	0.95	0.09	0.04	0.20	0.22	0.03	0.01	0.03	1.04	1.10	0.17	0.02	2.64	0.07	2.65	1.11	1.81

found ~10-25 km south of Korosi in the Kapthurin Formation west of Lake Baringo, glass of the KAP is preserved as 20-100  $\mu\text{m}$  with angular to subround margins indicating that more highly fragmented glass has traveled further from the source.

#### Chemical Composition of the Korosi Airfall Pumices:

The Korosi Airfall Pumices represent a chemically variable suite of trachytic tephras (Table 4; Fig 8). This chemical variability is the product of a single pumiceous magmatic eruption (Dunkley et al., 1993). All major chemical variants of the KAP exhibit the same fresh, large, angular pumiceous lithology and these variants are stacked directly on top of one another in the same stratigraphic order with no apparent disconformity separating them in the four sections north of the town of Loruk (Figs. 1a, 2). Additionally, while the chemical variants of the KAP can look discrete when sampled individually, together the chemical variants of the KAP show continuous variation in bivariate plots (Fig. 7).

#### Chronometric dating of the Korosi Airfall Pumices:

Potassium feldspars of the KAP were directly dated to  $380 \pm 7$  ka by the  $^{40}\text{Ar}/^{39}\text{Ar}$  method at their most proximal and thickest exposure at the Tangul Bei Roadcut Section by Dr. Alan Deino



at Berkeley Geochronology Center (Dunkley et al., 1993; Table 5, Figs. 1a, 2).

#### Correlation of the Korosi Airfall Pumices:

Field stratigraphy and EMPA chemical characterization of glass phase indicates the KAP are a chemically variable magmatic eruption of pumiceous deposits (Fig. 7) that can be correlated throughout the north of Loruk and southwest to the Kapthurin Formation west of Lake Baringo (Figs. 1a, 2). The KAP are best represented at the Tangul Bei Roadcut Section, a ~20 m high section of proximal pumice deposits exposed at their source by blasting into the slopes of Korosi for the road over this volcano from Loruk to the town of Tangul Bei (Figs. 1a, 2) and also at the > 10m high Korosi West Section, the Kulbulwa section and the Chepilat section north of Lake Baringo (Figs. 1a, 2).

#### The K4 Trendline Trachytes:

Multiple 'pumiceous trachytic tuffs' (Tryon and McBrearty, 2006: 503) overlie the lower and upper basaltic units and the KAP in the Bedded Tuff Member (Tryon and McBrearty, 2002; Tryon and McBrearty, 2006). Like the basaltic units of the Bedded Tuff Member, the pumiceous trachytic tuffs fall along the same trendline defined by a compositional evolving magma chamber

from a single volcanic source (Fig. 6a; Tryon and McBrearty, 2002; Tryon and McBrearty, 2006).

The ‘pumiceous trachytic’ label has been used to refer to these tuff units specifically and distinguish them from more fine-grained distal trachytic deposits of the Bedded Tuff Member such as the Koimilot Tuff and the ‘Felsic Dust Tuffs’ (Tryon and McBrearty, 2006: 500-503). Several of these pumiceous trachytic tuffs have also been directly dated by the  $^{40}\text{Ar}/^{39}\text{Ar}$  method (see below and Deino and McBrearty, 2002). We modify the name of this group to K4 Trendline Trachytes.

The addition of ‘K4,’ (the abbreviation of the Bedded Tuff Member originally defined by (Fig. 1b; Tallon, 1976, 1978) distinguishes these tuffs from pumiceous units from underlying member of the Kapthurin Formation such as the Pumice Tuff which itself constitutes part of the Pumice Tuff Member (K2) (Deino and McBrearty, 2002; Tallon, 1976, 1978). The addition of ‘trendline’ to the name distinguishes this group from the many compositions of the pumiceous and trachytic Korosi Airfall Pumices (discussed above) which are stratigraphically lower, chronometrically older by ~100 kyr and do not conform to the compositional trendline of magmatic evolution defined for the basaltic tuffs and trachytic units found at JLC and NRS (Figs. 6a-f, 7; Tryon, 2003; Tryon and McBrearty, 2002; Tryon and McBrearty, 2006). Four K4 Trendline Trachytes are dated by the  $^{40}\text{Ar}/^{39}\text{Ar}$  method to distinct time intervals between ~200 –300 ka and thus represent a series of separate eruptions. We refer to these after the locality at which they were first recog-

nized and  $^{40}\text{Ar}/^{39}\text{Ar}$  dated.

Lithology of the K4 Trendline Trachyte tuffs:

Field and petrographic observations under 40-100x magnification show all exposures of the K4TT are coarse grained, round, subround or angular < 0.25-6 cm pumices, usually 0.5-2 cm, with intact round to elongated vesicles. K4TT tuffs were produced by the magmatic eruption associated with the long and continuous process of magma chamber evolution from a single source, the shield volcano Korosi (Tryon and McBrearty, 2002; Tryon and McBrearty, 2006). These units are most common north of the town of Kampi-ya-Samaki and south of the town of Loruk (Figs. 1a, 2) though units of the Middle Trendline Trachytic tuff are found as far south as the Ndau River (Figs. 1a, 2). The K4TT tuffs are not known from north of the town of Loruk (Figs 1a, 2). South of the town of Kampi-ya-Samaki they are only encountered at and around the Ndau River Section (Fig. 2).

Chemical Composition of the K4 Trendline Trachytes:

Glass from the pumices of the K4 Trendline Trachyte tuff is chemically variable (Figs 6f, 7).

However, all compositional variability in samples of this tuff group is arranged around the same

trendline shown in the basaltic and K4TT tuffs and best visualized in CaO versus MgO (Fig. 6f) as well as CaO and Al<sub>2</sub>O<sub>3</sub> versus FeO (Fig. 7) bivariate plots (Tryon and McBrearty, 2002; Tryon and McBrearty, 2006). This fact, as well as freshness of the coarse pumices show compositional variation in this group is the product of magmatic processes during eruption rather than post-depositional mechanical admixture of multiple discrete chemical compositions produced by different eruptions (Tryon, 2003: 126-127).

#### Chronometric dating of the K4 Trendline Trachytes:

Sample McB97-02 (Table 4), a 0.50 m coarse pumiceous tuff located above the lower and upper basaltic units at the top half of the ~20m section of the Bedded Tuff Member sediments at the Ndau River Section (NRS) produced the date of  $284 \pm 12$  ka (Deino and McBrearty, 2002; Tryon and McBrearty, 2002; Tryon and McBrearty, 2006). Sample McB97-01 taken at Johnny Leakey's Compound (JLC) locality and  $^{40}\text{Ar}/^{39}\text{Ar}$  to  $235 \pm 2$  ka (Table 5; Deino and McBrearty, 2002) is from a 0.75 m unit of fresh, crisp black 0.5 to 3.0 cm pumices. In the immediate vicinity of section JLC the unit from which the dated and geochemically characterized sample McB97-01 was taken trends from black to grey in color. The 235 ka  $^{40}\text{Ar}/^{39}\text{Ar}$  date agrees with K / Ar dates of 240 –250 ka taken from the same vicinity as JLC and reported by Tallon (1976, 1978)

and Cornelissen et al. (1990). The  $^{40}\text{Ar}/^{39}\text{Ar}$  dates, K /Ar dates and U-series dating of fault cracks interrupting the Bedded Tuff Member (Le Gall et al., 2000) agree in demonstrating a age of > 200 ka for all sediments, including tuffs such as the K4 TT of the Bedded Tuff Member. Additionally, potassium bearing feldspars separated from fresh pumices of the coarse pumiceous tuff capping the Sibilo School Road Site were amenable to dating by the  $^{40}\text{Ar}/^{39}\text{Ar}$  method and have produced dates of  $196 \pm 4$  ka (Deino pers comm). Glass separated from pumices found *in situ* during excavation of the Sibilo School Road Site and glass separated from the tuffaceous matrix of the excavation is chemically identical to glass from a coarse angular pumiceous unit ~5 km away on the Kampi-ya-Samaki Peninsula dated to  $226 \text{ ka} \pm 1.4 \text{ ka}$  by the  $^{40}\text{Ar}/^{39}\text{Ar}$  method (Figs. 1a, 2). These new  $^{40}\text{Ar}/^{39}\text{Ar}$  dates agree with all previous chronometric dates from the Bedded Tuff Member in showing the deposition of these sediments predates 200 ka. The minimum age of the archaeological material at the Sibilo School Road Site is  $196 \pm 4$  ka and the maximum age of the site produced by  $^{40}\text{Ar}/^{39}\text{Ar}$  dating and tephra correlation is  $226 \text{ ka} \pm 1.4 \text{ ka}$ .

#### Correlation of the K4 Trendline Trachytes:

Aside from the dated samples McB97-01 and McB97-02 K4 TT tuffs have been sampled in the immediate vicinity of section JLC and throughout the eastern portion of the Kampi-ya-Samaki

peninsula the K4 TT tuffs are commonly found as a ~1.5-.50 m pumiceous units stratigraphically bracketing an indurated, finely laminated unit of the Evolved Basaltic Tuff Group (sampled as McB2010-2) display bedding < 1-2 mm thick. This unit of the Evolved Basaltic Tuff, in turn overlies K4TT tuffs of less evolved composition (Figs. 1a, 2). K4 TT tuffs are also documented at Section.2014.B as NTB2014-340 and also at Section.2012.E as NTB2013-222 (Fig. 2). The K4TT tuffs are also exposed in shallow outcrops, generally exposed  $\leq 2$  m high in drainages in the north of the Kapthurin Formation (Fig. 2). At Section WPT 157 this tuff, (sample NTB2011-48) is exposed above a sample of the Upper Basaltic Tuff Group NTB2011-47. This tuff is exposed further north in the same drainage at Section WPT 158 as a discrete mode of glass, NTB2011-45 (Fig. 2), and also stratigraphically overlies *in situ* archaeological materials at the Sibilo School Road Site as sample NTB2011-1.

Distal tephras of the Bedded Tuff and Upper Silts and Gravels Members:

At least five trachytic tuffs of the Bedded Tuff Member and a single phonolitic tuff from above the Bedded Tuff Member in the Upper Silts and Gravels Member (K5) display fine-grained distal lithologies suggesting they do not necessarily derive from a proximal volcanic source in the Baringo Basin such as Korosi or Karau (Fig 1a). Tryon and McBrearty (2006) defined and named

one of these tuffs, the Koimilot Tuff, and grouped several others under the label, “Felsic Dust Tuffs.” In this study we recognize six distinct felsic tephras based on stratigraphic position and chemical composition (Fig. 8). In stratigraphic order from top to bottom these are: 1) “K4 Distal Tephra #1” a trachytic distal tuff found below the NRS Tuff, 2) “K4 Distal Tephra #2” a trachyte from above the NRS Tuff, 3) “K4 Distal Tephra #3” a trachyte from above “K4 Distal Tephra #2”, 4) “K4 Distal Tephra #4” a third trachyte from above “K4 Distal Tephra #3”, 5) The Koimilot Tuff and 6) The Wakondo Tuff, a phonolite, and correlated to dated context of ~100 ka in Late Pleistocene exposures of the eastern Lake Victoria Basin (Blegen et al., 2015; Tryon et al., 2010).

The source or sources of these distal K4 tephras is unknown but grain size and in the case of the Wakondo Tuff, the chemical composition of the tuff, suggests they derived from some source other than Korosi or any proximal source in the Baringo basin (Tryon and McBrearty, 2006).

Of the distal tephras in this study the long distance correlation of the tuff capping the site of Keraswanin to the Wakondo Tuff in western Kenya is the most significant. This chemical homogeneity of this tuff and the chemical similarity of samples attributed to it relative to other tephras can be visualized in bivariate in the four bivariate plots presented in figure 8. The Wakondo Tuff

is named after the Wakondo locality on Rusinga Island where it was first recognized (Table 4; Blegen et al., 2015; Tryon et al., 2010). In the Kapthurin Formation the Wakondo Tuff is preserved discontinuously over a restricted ~500 m<sup>2</sup> area ~100-200 m south of the south bank of the Ndaui River west of the split between the Ndaui and Barsemoi rivers and ~5 km west of where the Ndaui river intersects the main road (Figs 1a). This tuff also overlies the archaeological site of Keraswanin (GnJh-78) and is exposed around the immediate vicinity around this archaeological site (NTB2012-146) (Figs. 1a, 2).

The age of the Wakondo Tuff is constrained by several methods of chronometric dating in the eastern Lake Victoria Basin. On Rusinga Island OSL dates from the archaeological site of Wakondo at the Wakondo locality, collected from sediments above the Wakondo Tuff, provide a minimum age of ~68 ka (Blegen et al., 2015). U-series dates of  $94.0 \pm 3.3$  ka and  $111.4 \pm 4.2$  ka from tufa deposits at the base of the sequence in the Nyamita Valley, Rusinga (Beverly et al., 2015), provide a maximum age for the Wakondo Tuff, as well as for the entire Pleistocene sedimentary sequence of the eastern Lake Victoria Basin. Because the Wakondo Tuff is always found at the base of the late Pleistocene sedimentary sequence in the eastern Lake Victoria Basin the ~100 ka age is currently the most accurate age approximation. Further, the U / Th date of ~100



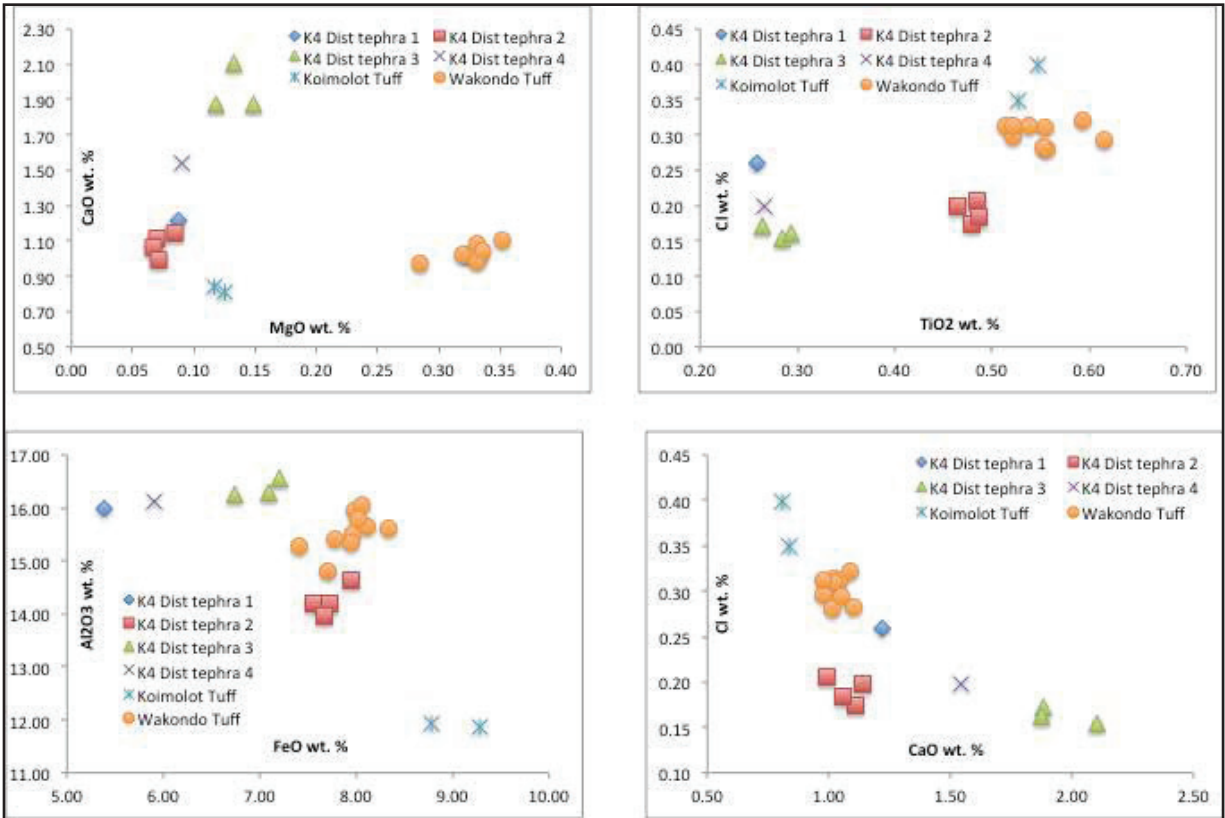


Figure. 8: Bivariate plots for the means of all the six distal tephra discussed in this study. A) CaO versus MgO, B) Cl versus TiO<sub>2</sub>, C) Al<sub>2</sub>O<sub>3</sub> versus FeO, D) Cl versus CaO. Eight samples of the Wakondo Tuff from the eastern Lake Victoria Basin (see Blegen et al., 2015 and Fig. 10) included showing chemically similarity and correlation of the Wakondo Tuff in the eastern Lake Victoria Basin to Keraswanin in the Kapthurin Formation.

ka conforms to maximum age estimates of the Wakondo Tuff based on compositional similarities of this tephra to explosive phonolitic volcanism from the rift volcano Suswa (Fig. 1b; Tryon et al., 2010) dated to  $100 \pm 10$  ka by the potassium-argon (K / Ar) method (Baker et al., 1988).

## Discussion:

Correlation of tuffs from the Bedded Tuff Member within the Baringo Basin and the long distance inter-basinal correlation of the tuff at the site of Keraswanin to the Wakondo Tuff in the

eastern Lake Victoria Basin produce two stratigraphically and chronologically significant results.

These are discussed first followed by the significant archaeological implications of these correlations.

1) Correlations of the basaltic tuffs found near the base of the Bedded Tuff Member in the Kapthurin Formation west of Lake Baringo to the slopes of the volcano Korosi northeast of the lake confirm Korosi as the source of these units (Tallon, 1978), and, by association, all of the more evolved basaltic through trachytic tuff units falling along the evolving magma chamber trendline (Fig. 6; Tryon and McBrearty, 2002; Tryon and McBrearty, 2006). Correlation has also been established for the Korosi Airfall Pumices, found as proximal pumiceous facies at four sections north of Loruk with more distal glass encountered as discrete chemical modes found alongside modes of upper/lower basaltic glass at in tuff units at Rorop Lingop, The Lake Baringo Trachyte Cliffs Section, The Ndau River Section, Section.2012.E, Section.2012.I (Figs. 1a, 2). The consistent relationship between the basaltic tuffs and Korosi Airfall Pumices dated to  $\geq 380 \pm 7$  ka confirms the temporally contemporaneous relationship between these compositionally distinct groups. These findings further confirm the long-held assertion that Korosi is the source of the majority of tuffs in the Bedded Tuff Member (Tallon, 1976, 1978; Tryon and McBrearty,

2002; Tryon and McBrearty, 2006) and demonstrates that deposition of the Bedded Tuff Member begins with volcanic activity related to the formation of Korosi dated to sometime shortly before  $380 \pm 7$  ka. These correlations provide a refined stratigraphic and chronological context for previously excavated and reported archaeological material. Archaeological sites situated beneath a tuff of the Upper or Lower Basaltic Tuff Groups such as Rorop Lingop and GnJh-63 (Tryon and McBrearty, 2002, 2006) date to  $\geq 380 \pm 7$  ka. Archaeological sites such as the four sites of the Leakey's "Living Site" area: the Leakey Handaxe Area (GnJh-02), the Leakey Handaxe Rectangle (LHR= GnJh-03), the Peter Nzube Gulley (PZG= GnJh-11), and the Leakey Handaxe Site (LHS=GnJh-12) as well as GnJh-17 and GnJh-15 situated in the Middle Silts and Gravels Member and below basaltic tuffs of the Bedded Tuff Member thus predate deposition of the Bedded Tuff Member and are older than  $380 \pm 7$  ka (Cornelissen, 1992; Cornelissen et al., 1990; Leakey et al., 1969; McBrearty, 1999; McBrearty et al., 1996; McBrearty and Tryon, 2006; Tryon, 2003; Tryon and McBrearty, 2002; Tryon and McBrearty, 2006; Van Noten, 1982; Van Noten et al., 1987).

2) Chemical characterization and comparison of the K4 trendline trachytes dated to 235 –284 ka with the coarse pumiceous tuff capping the Sibilo School Road Site establish a minimum age of

> 200 ka for MSA archaeological material at this site making it one of the oldest sites in Africa containing multiple aspects of MSA technology including Levallois points and diverse Levallois core preparation methods. The Sibilo School Road Site is thus contemporaneous with the two localities at the site of Koimilot, two sites from Member 1 in the Kibish Formation of the southern Ethiopian Rift and GDM7 in Gademotta Formation of the middle Ethiopian rift (Morgan and Renne, 2008; Sahle et al., 2014; Shea, 2008; Tryon, 2006).

The coarse pumiceous tuff (sample NTB2011-1) found ~1.0 m above *in situ* archaeological material at the SSRS falls along the same evolving trendline as both the JLC Tuff  $^{40}\text{Ar}/^{39}\text{Ar}$  dated to 235 ka and the NRS Tuff  $^{40}\text{Ar}/^{39}\text{Ar}$  dated to 284 ka from the Bedded Tuff Member of the Kapthurin Formation (Fig. 6f). This demonstrates the tuff capping the SSRS is from the same monogenic volcanic source, the volcano Korosi immediately north of Lake Baringo and belongs to the Bedded Tuff Member (Fig. 1; Tryon and McBrearty, 2002). As all chronometric age estimates suggest deposition of the Bedded Tuff Member, including the K4 TT tuffs, is > 200 ka archaeological materials at the Sibilo School Road Site must be older than this age. The > 200 ka age based on tephra composition is thus a conservative minimum age estimate of the SSRS archaeological and fossil materials. Preliminary  $^{40}\text{Ar}/^{39}\text{Ar}$  dating of tuffs at and around the SSRS

agrees with all previous age estimates on the Bedded Tuff Member and provide a more precise  $196 \pm 4$  ka minimum age for archaeological material at the SSRS and the maximum age of  $226 \text{ ka} \pm 1.4 \text{ ka}$  produced by  $^{40}\text{Ar}/^{39}\text{Ar}$  dating and tephra correlation.

3) Correlation of the distal tuff capping archaeological material at Keraswanin in the western Kapthurin Formation to the Wakondo Tuff in the eastern Lake Victoria Basin establish a minimum age of 100 ka Late Pleistocene age for the site of Keraswanin (Beverly et al., 2015; Blegen et al., 2015; Tryon et al., 2010).

Archaeological implications of revised Bedded Tuff Member Tephrostratigraphy:

The Levallois technology in the Kapthurin Formation is shown to be  $\geq 380$  ka,  $\sim 100$  ka older than previous estimated. Reanalysis of Levallois material from the excavated assemblages of the Leakey “Living Site” area (Leakey et al., 1969) shows this technology is more diverse than previously estimated at this early date as discussed below. Combined, the new date and lithic analysis demonstrates this important technological feature is present and well developed in association with typologically Acheulean material before 380 ka in East Africa,  $\sim 100$  ka years before Levallois prepared core technology is found associated with MSA material in East Africa at the SSRS

and Gademotta GDM7 (Sahle et al., 2014). The >380 ka age is closer to the earliest age estimates on Levallois technology reported from South Africa (Wilkins et al., 2012) and as early or earlier than Levallois technology reported outside Africa (Adler et al., 2014).

#### Levallois technology in the Kapthurin Formation:

Prompted by the revised tephrostratigraphy and new age estimate reported here, we review artifacts recovered from the surface and *in situ* from excavated assemblages of the Leakey “Living Site” area, including the Leakey Handaxe Rectangle (LHR= GnJh-03), the Peter Nzube Gulley (PZG= GnJh-11), and the Leakey Handaxe Site (LHS=GnJh-12) supplement previous reports on this material (Leakey et al., 1969; Tryon et al., 2005) and show diverse methods of Levallois core preparation and reduction, including recurrent methods, were well established in association with typologically Acheulean tools by at least 380 ka. The use of Levallois preferential method for the production of a single large flake often subsequently modified into a cleaver-flake, cleaver or biface is well established (Leakey et al., 1969; McBrearty, 1999; McBrearty et al., 1996; Tryon et al., 2005). In the original publication on material from the Leakey “Living Site” area at least two cores fitting the criteria of Levallois centripetal or recurrent bidirectional cores (Boëda, 1994) are illustrated (Leakey et al., 1969: 65 figure 11 B and C). At PZG one core from the surface (Fig. 9a

of this study and Leakey et al., 1969: 63 figure 9a) and one core from the PZG excavated material (Fig. 9b) approximate the Levallois centripetal approach by displaying a preferred upper debitage surface and an asymmetrically convex lower preparatory surface preserving cortex. A third small core from the PZG excavation is either a Levallois recurrent centripetal or a small discoid (Fig. 9c). At LHR two cores from the surface collection display the same characteristics of centripetal cores (Fig. 10a, b) and a third core (Fig. 10c) from surface is probably a high-backed radial core flaked all over with no cortex on the lower surface. Additionally, the excavated assemblage from LHR provides at least seven refitting sets attesting to technological production of flakes and blades at the site (Leakey et al., 1969: 62-64). Two of these refitting sets show clear evidence for Levallois bidirectional recurrent debitage for the production of blades. One refitting set consists of six pieces comprised of two flakes refitting to opposite lateral margins of the core's debitage surface, a proximal flake fragment and a large overshoot distal flake fragment conjoining to form a single large overshoot flake (Fig 11). The overshoot flake refits to the core fragment to form a Levallois core displaying evidence of at least five bidirectional flake or blade removals from the same prepared debitage surface (Fig. 11). It was the last removal, the overshoot knapping mistake, which spelled the demise of this recurrent bidirectional Levallois core. A second refitting set consists of 13 pieces. These refitting pieces comprised eight separate blade or

elongated flake removals (Fig. 12a). The first three removals are from a single prepared platform aligned in the same direction (Fig 12 b, c.). The core was then rotated 180 degrees and the next two removals on the same debitage surface are from a second, opposed prepared platform (Fig. 12d). Debitage then rotates again to the first platform direction for two more removals and finally reverses 180 degrees again to the first platform for the final removal (Fig. 12d). While the core itself is not part of this refitting set these removals definitely derived from the debitage surface of a Levallois core as all flake platforms are faceted or multifaceted and three of the flake removals are debordant flakes preserve cortical margin of the lower preparatory surface to shape the convexity of the upper debitage surface (Figs, 12a left, 12d left, 12e left). Additionally, a refitting set for the LHR excavation consisting of a large partially hinge terminated preferential Levallois flake refitting to an éclat debordant shows correction of knapping errors and reparation of Levallois debitage surfaces for multiple removals (Fig. 13).

The improved chronology of the twelve Kapthurin Formation archaeological sites show the process of technological change from Acheulean to MSA in the later Middle Pleistocene of East Africa was longer and more gradual than previously appreciated. Nine sites at or beneath the base of the Bedded Tuff Member, and dating to  $\geq 380$  ka, contain aspects of both Acheulean technology in the forms of large cutting tools such as bifacial handaxes, cleavers and large cleaver flakes



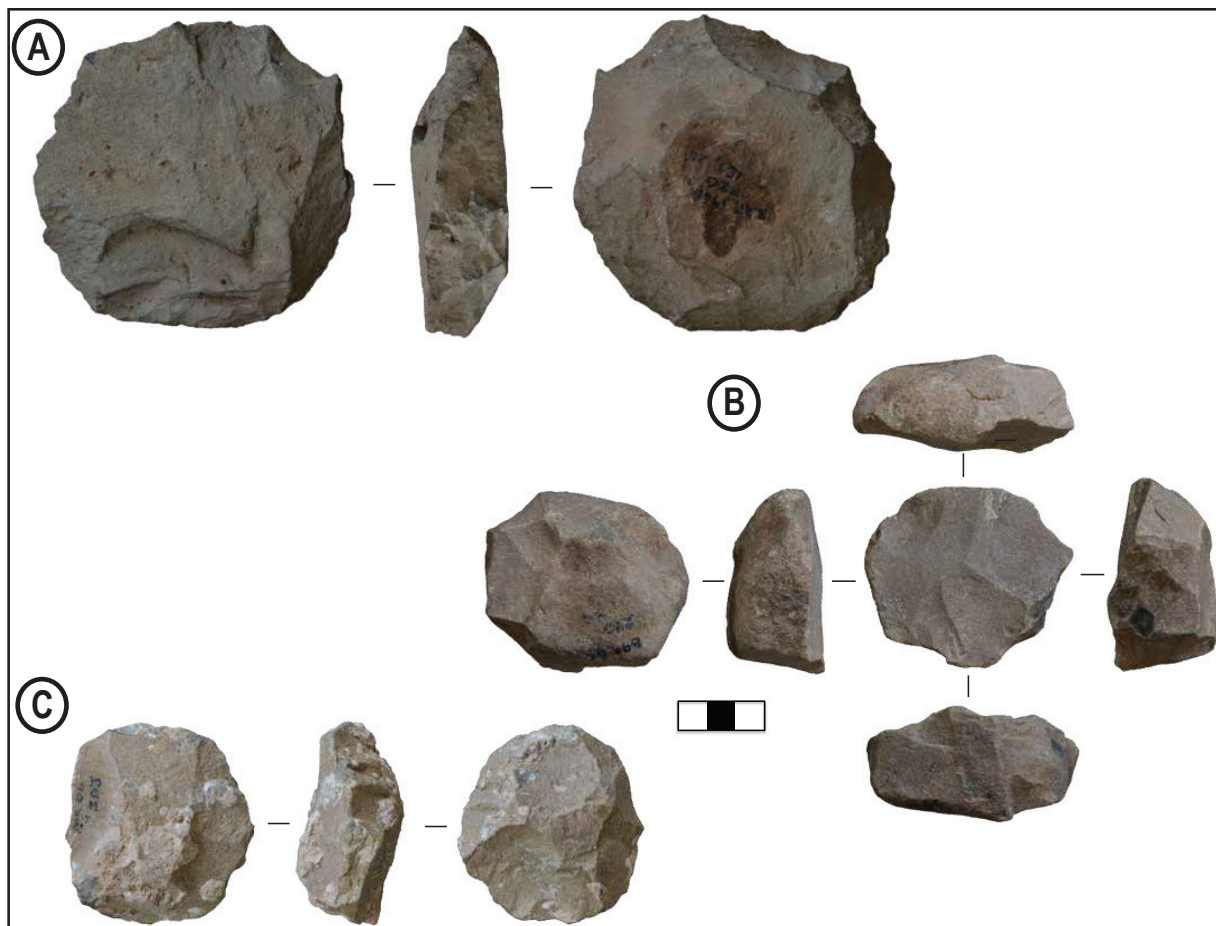


Figure. 9: Cores from the surface and excavation step trench of the Peter Nzube Gulley (PZG=GnJh-11) on the eastern margin of the Leakey “Living Site” area (Leakey et al., 1969). A) Levallois centripetally flaked core collected from the surface of the PZG also illustrated in figure 9a of Leakey et al., 1969. B) Levallois centripetally flaked core from the PZG excavation. C) Small discoïd core from the PZG excavation.

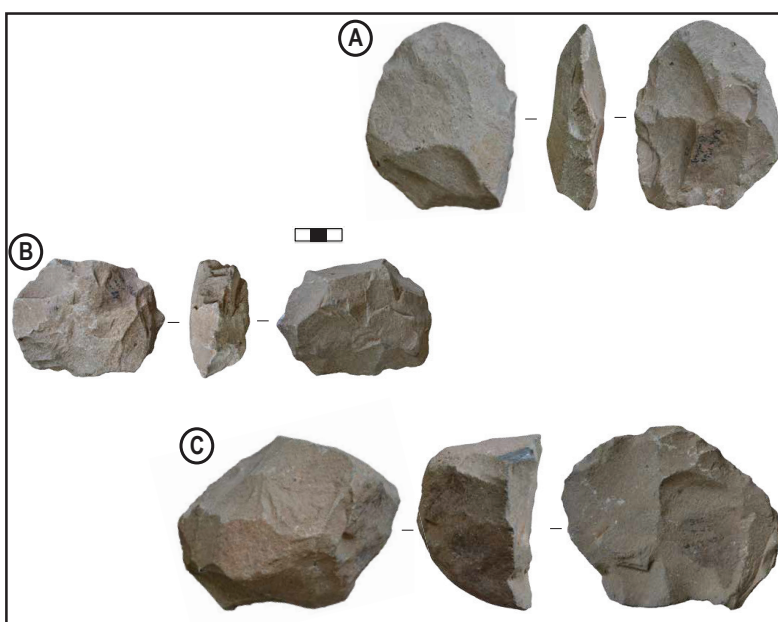


Figure. 10: Cores collected from the surface of the Leakey Handaxe Rectangle area in the central part of the Leakey “Living Site” area (Leakey et al., 1969). A) Levallois centripetally flaked core. B) Discoïd core flake all over on both faces; preserving no cortex. C) Levallois bidirectional core collected from surface.

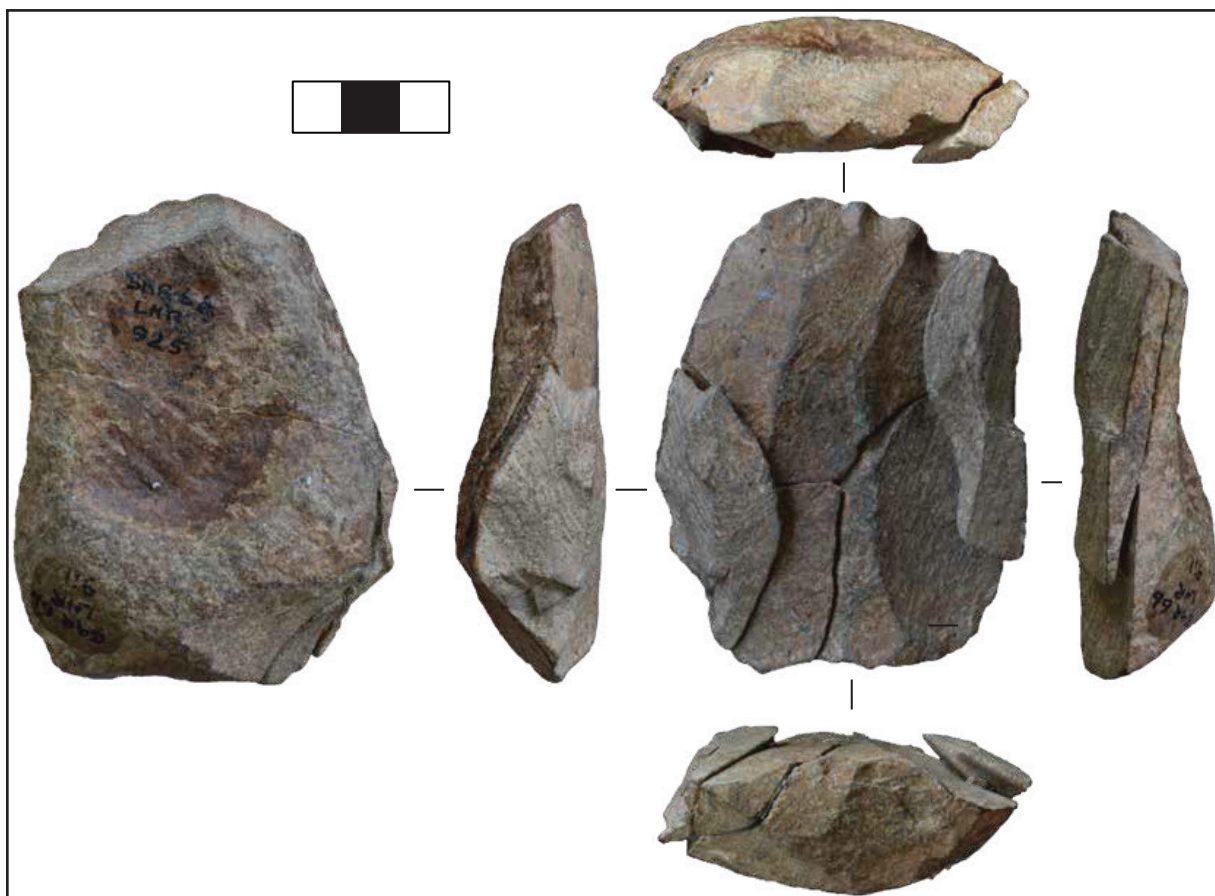


Figure. 11: Levallois recurrent bidirectional core reconstructed from refits of two flake fragments and a core fragment and displaying two refits from either lateral margin of the cores. All pieces from the LHR excavation (Leakey et al., 1969).

as well as aspects of Levallois prepared-core technology (Cornelissen, 1992; Cornelissen et al., 1990; Leakey et al., 1969; Tryon and McBrearty, 2002; Tryon and McBrearty, 2006; Tryon et al., 2005). Four archaeological localities from three sites including the Sibilo School Road Site, Keraswanin and two localities of Koimilot are shown to date between 100 – 250 ka and demonstrate multiple methods of core reduction including Levallois preferential flake removal, Levallois point production and Levallois recurrent centripetal core reduction.

Thus, the process of technological change from Acheulean to MSA in the later Middle Pleisto-

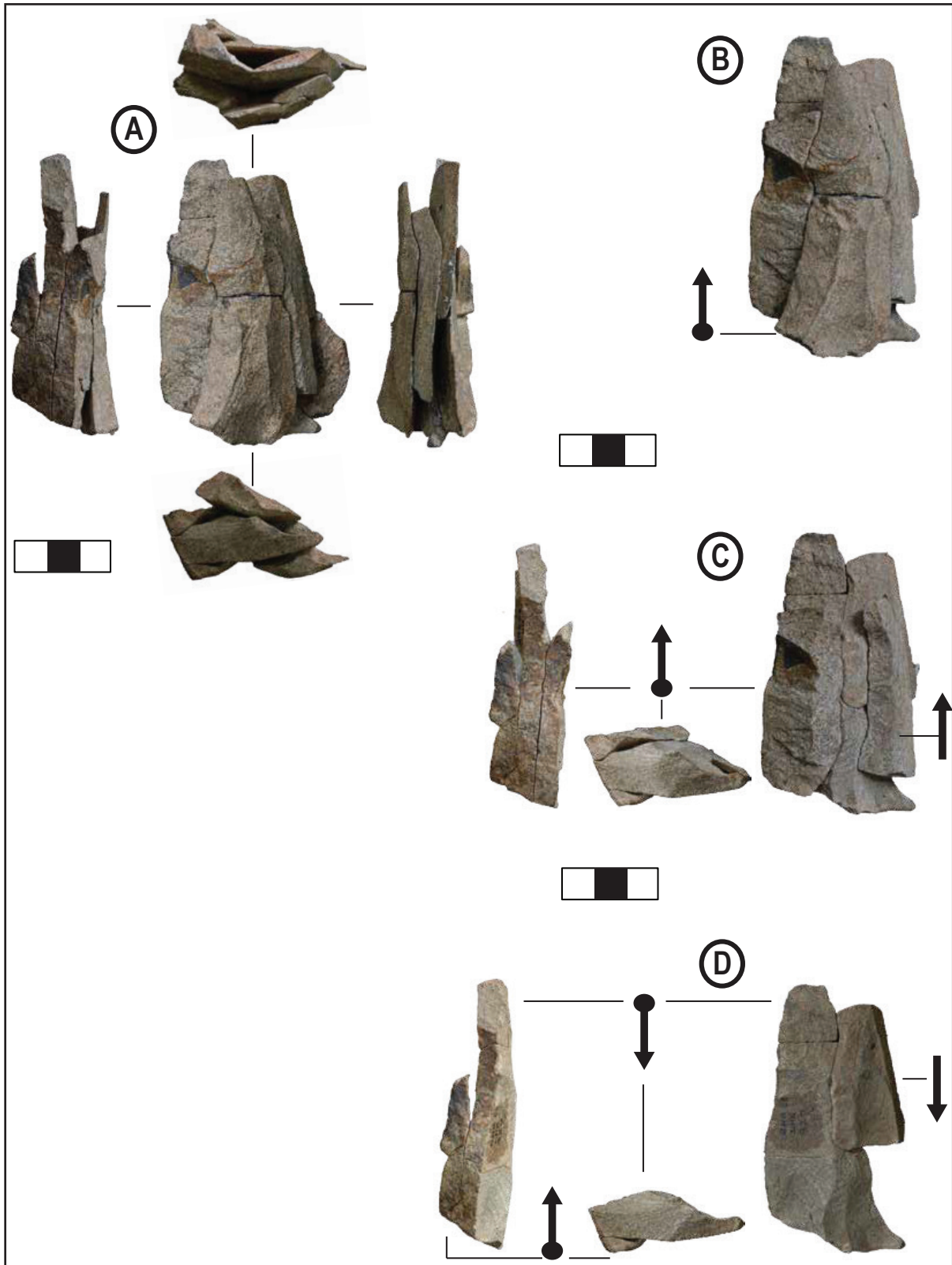


Figure. 12: Thirteen flakes and flake fragments refitting to form six elongated flakes and blades sequentially removed from the debitage surface of a recurrent bidirectional Levallois core. All pieces from LHR excavation (Leakey et al., 1969).

cene of East Africa was longer and more gradual than previously appreciated with aspects of technology such as diverse methods of Levallois core preparation, commonly associated with MSA technologies, occurred in association with Acheulean technologies occurring ~100 kyr before they are found in association with the MSA in the Baringo Basin.

The correlation of the Wakondo tuff from Keraswanin to the eastern Lake Victoria Basin > 200 km away also opens the possibility that more of the distal tephras of the Bedded Tuff Member characterized in Tryon and McBrearty's (2006) study and further refined here may correlate to Middle or Late Pleistocene deposits in other basins of the Kenyan Rift. In the Baringo Basin this correlation expands the upper age limit of MSA archaeological material in the Kapthurin Formation by ~130 kyr. It is possible that this tuff or other Late Pleistocene tuffs associated with archaeological material are exposed elsewhere in the Baringo Basin. The correlation of the Wakondo Tuff between Keraswanin in the Baringo Basin and several sites in the eastern Lake Victoria Basin confirms predictions that several widespread tephras in the African Pleistocene (Pyle, 1999) and particularly in the Middle and Late Pleistocene (Blegen et al., 2015; Brown et al., 2012) have yet to be found. Based on this work and recent related studies (Blegen et al., 2015) we predict more large-scale eruptions in the later Middle and Late Pleistocene of East Africa will





Figure. 13: Refitting Levallois preferential flake and éclat debordant from LHR excavation. The éclat debordant appears to have reprepared the debitage surface of the Levallois cores as well as removed a hinge fracture created by the removal of the preferential flake.

be found.

#### Conclusion:

Chemical characterization combined with field stratigraphy and robust tephrostratigraphic data sets from previous studies of the Bedded Tuff Member, Kapthurin Formation demonstrate the presence of at least 14 distinct tuffs or tuff groups. Of these, 13 are found in the Bedded Tuff Member of the Kapthurin Formation. A single tuff at the site of Keraswanin, attributed to the Upper Silts and Gravels Member of the Kapthurin Formation can be correlated ~200 km west to the Wakondo Tuff found at six localities in the late Pleistocene deposits of Rusinga Island and Karungu in the eastern Lake Victoria Basin. These correlations provide an expanded and refined

tephrostratigraphy for the upper two members of the Kapthurin Formation and provided new and refined ages for seven archaeological sites in the Kapthurin Formation. Tephra correlations of a basaltic tuff to the volcano Korosi as well as correlations of the Korosi Airfall Pumices directly  $^{40}\text{Ar}/^{39}\text{Ar}$  dated to  $380 \pm 7$  ka to the Bedded Tuff Member exposed west of Lake Baringo demonstrate deposition of the Bedded Tuff Member began at  $380 \pm 7$  ka. This provides new minimum age of  $> 380 \pm 7$  ka for nine sites in or immediately below the base of the Bedded Tuff Member. Tephra analysis as well as preliminary results of direct  $^{40}\text{Ar}/^{39}\text{Ar}$  dating of the coarse pumiceous tuff unit capping archaeological material at the Sibilo School Road Site provides a minimum age of 200 ka for archaeological material found *in situ* below this tuff unit. The correlation of the tuff unit capping *in situ* archaeological material at the site of Keraswanin to the Wakondo Tuff in the eastern Lake Victoria Basin provides an age of  $\sim 100$  ka for MSA artifacts at this site. The updated tephrostratigraphy of the Bedded Tuff Member and new correlations to a tuff in the Upper Silts and Gravels Members provide evidence for well developed Levallois technology  $> 380$  ka in East Africa, at least  $\sim 100$  kyr earlier than allowed by previous estimates (Deino and McBrearty, 2002). This updated archaeological sequence for the Kapthurin Formation demonstrates technological change in the later Middle Pleistocene and through the late Pleistocene of East Africa and indicates a more prolonged, gradual and dynamic technological

transition from Acheulean technology to MSA technology than previously realized. Finally, the tephrostratigraphy and refined chronology presented here allows us to better understand the process of technological change related to the development of modern human behavior.





Paper #3

Evidence of long-distance obsidian transport and early Middle Stone Age technology at the ~200 ka BP Sibilo School Road Site GnJh-79), Baringo, Kenya:

Nick Blegen

Department of Anthropology

University of Connecticut

Storrs, CT 06269, USA

E-mails: [nicholas.blegen@uconn.edu](mailto:nicholas.blegen@uconn.edu), [nick.blegen@gmail.com](mailto:nick.blegen@gmail.com)

(TO BE SUBMITTED TO The Journal of Human Evolution)

## Abstract:

This study presents the geology, archaeology and lithic artifact analysis from the 196 - 226 ka Sibilo School Road Site (SSRS= GnJh-79), an early Middle Stone Age (MSA) site from the Kapthurin Formation, Kenya. The later Middle Pleistocene of East Africa (130 –400 ka) spans significant behavioral and biological changes including the decline of the Acheulean and the beginning of the MSA as well as the first appearance of *Homo sapiens*. Recent tephrostratigraphic correlation and  $^{40}\text{Ar}/^{39}\text{Ar}$  dating, provide a minimum age of > 200 ka for the SSRS, making it one of the few early MSA sites in later Middle Pleistocene of East Africa. MSA technology including Levallois points and diverse methods of Levallois core preparation are present at the SSRS. Additionally, a significant portion (43%) of the SSRS lithic assemblage is composed of obsidian, a material not local to the Tugen Hills west of Lake Baringo. The early date of the SSRS MSA material and the preponderance of obsidian at the site provide two significant results related to early MSA technology and raw material transport distances: 1) Acquisition of obsidian from at least three geographically distinct sources ranging from 25 km to 166 km straight-line site to source distances show that early MSA hominins transported high quality raw materials farther than in Early Stone Age (ESA) contexts. 2) SSRS and contemporaneous East African early MSA sites show greater reduction intensity of non-local obsidian and that the production

of smaller flakes coincides with greater raw material transport distances. Together, these insights may be a significant factor in explaining the Acheulean to MSA transition in the later Middle Pleistocene of East Africa.

#### Introduction:

During the Middle Pleistocene in Africa (780-130 ka) large, hand-held stone tools of the Acheulean, such as handaxes and cleavers, are replaced by more diverse stone tool assemblages of the Middle Stone Age (MSA) characterized by diverse core preparation technology, smaller cores and flakes, pointed pieces and hafted tools (Clark, 1988; Tryon et al., 2005; Wilkins et al., 2012). The decline of typologically Acheulean tools in Africa after more than one million years of use, and the concomitant appearance of MSA technologies and the first appearance of our species, *Homo sapiens*, in the Middle Pleistocene of East Africa (McDougall et al., 2005; White et al., 2003) is conspicuous.

McBrearty and Brooks (2000) argue that since human evolution is characterized by the incremental acquisition of both behavioral and biological adaptations throughout the Pleistocene, these phenomenon are connected. Ultimately, they resulted in the emergence of biologically and behaviorally modern *Homo sapiens* in the Late Pleistocene and Holocene of Africa and their

spread throughout the world. McBrearty and Brooks' (2000) model posits that understanding the evolution of modern human behavior relies on understanding the timing and pattern in which behaviorally modern traits including new technologies and mobility patterns, subsistence strategies and ecological adaptations were acquired through the Middle and Late Pleistocene of sub-Saharan Africa.

This study seeks to contribute to this research goal by documenting MSA hominin behavior at the Sibilo School Road Site (SSRS). In particular it focuses on raw material acquisition and the intensity of lithic reduction to investigate raw material transport distance in the MSA of Middle Pleistocene East Africa. This study complements other recent work on the “early MSA,” or eMSA: the MSA of the Middle Pleistocene > 130 ka (Douze, 2014; McBrearty et al., 1996; McBrearty and Tryon, 2006; Morgan and Renne, 2008; Sahle et al., 2013; Sahle et al., 2014; Shea, 2008; Tryon, 2006; Tryon, 2003; Tryon et al., 2005). The SSRS is an open-air, single occupation archaeological site preserved in a well-dated context (196-226 ka) in the Kapthurin Formation, Kenya. The site's lithic assemblage evidences diverse methods of Levallois core preparation and reduction and the production of characteristically MSA artifacts such as Levallois points. Despite its rarity of obsidian in the Tugen Hills west of Lake Baringo (Chapman, 1971; Chapman and Brook, 1978), this raw material is common at the SRSS. Because obsidian is chemically distin-

guishable to source (Ambrose, 2012; Brown et al., 2013), its presence alongside eMSA technology enables a rare investigation into raw material transport and its impact on eMSA technologies in East Africa.

#### Background and previous research:

To appreciate the contribution of the SRSS to our understanding of later Middle Pleistocene hominin behavior it is necessary to situate it in its regional context. Available East African eMSA sites in well-dated contexts are reviewed followed by East African Middle and Late Pleistocene MSA sites for which obsidian sourcing has been undertaken.

#### Early MSA archaeology in East Africa:

Relatively few later Middle Pleistocene eMSA sites in East Africa preserve archaeological material in well-dated contexts. Members I of the Kibish Formation in southern Ethiopian Rift and the Upper Herto Member of the Bouri Formation in northern Ethiopian Rift yield MSA lithic technological markers such as points and multiple methods of Levallois preparation alongside aspects of Acheulean technology such as handaxes from the later Middle Pleistocene through the Late Pleistocene (Fig. 1; Clark et al., 2003; Shea, 2008). Two *in situ* archaeological occurrences in

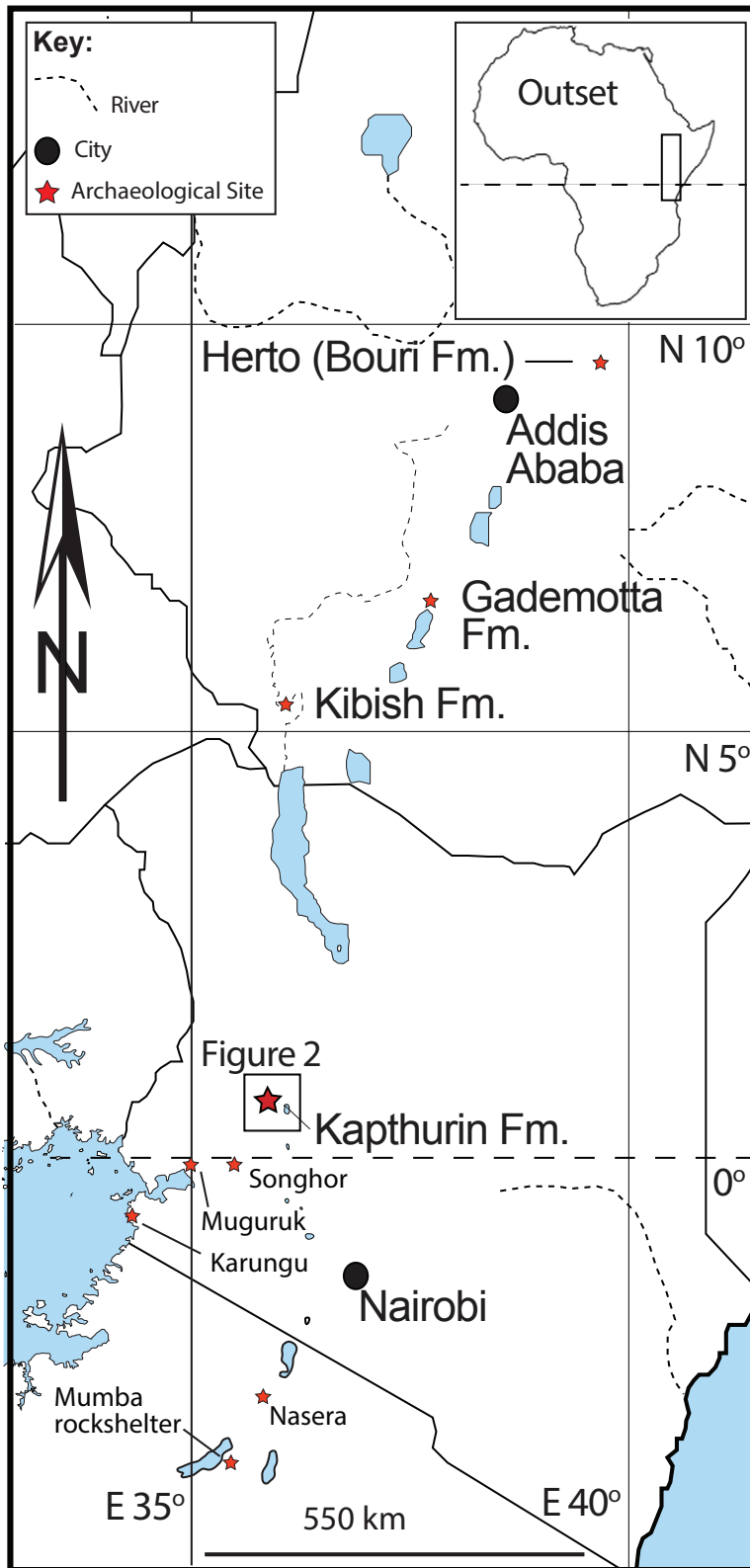


Figure 1: A) East African Rift showing Middle Pleistocene “Early Middle Stone Age (eMSA)” sites discussed in this study.

the Kibish—Kamoya’s Hominid Site (KHS) and Awoke’s Hominid Site (AHS) in Member I are dated to ~195 ka (McDougall et al., 2005, 2008; Shea, 2008). Similar MSA and Acheulean material is known from controlled surface collections at Herto (Clark et al., 2003). In the Kapthurin Formation two localities from the ~200–250 ka site of Koimilot shows characteristically MSA tools such as Levallois points and diverse methods of Levallois flake production on locally available raw materials (Figs. 1, 2; Tryon, 2006;

Tryon, 2010; Tryon, 2003; Tryon

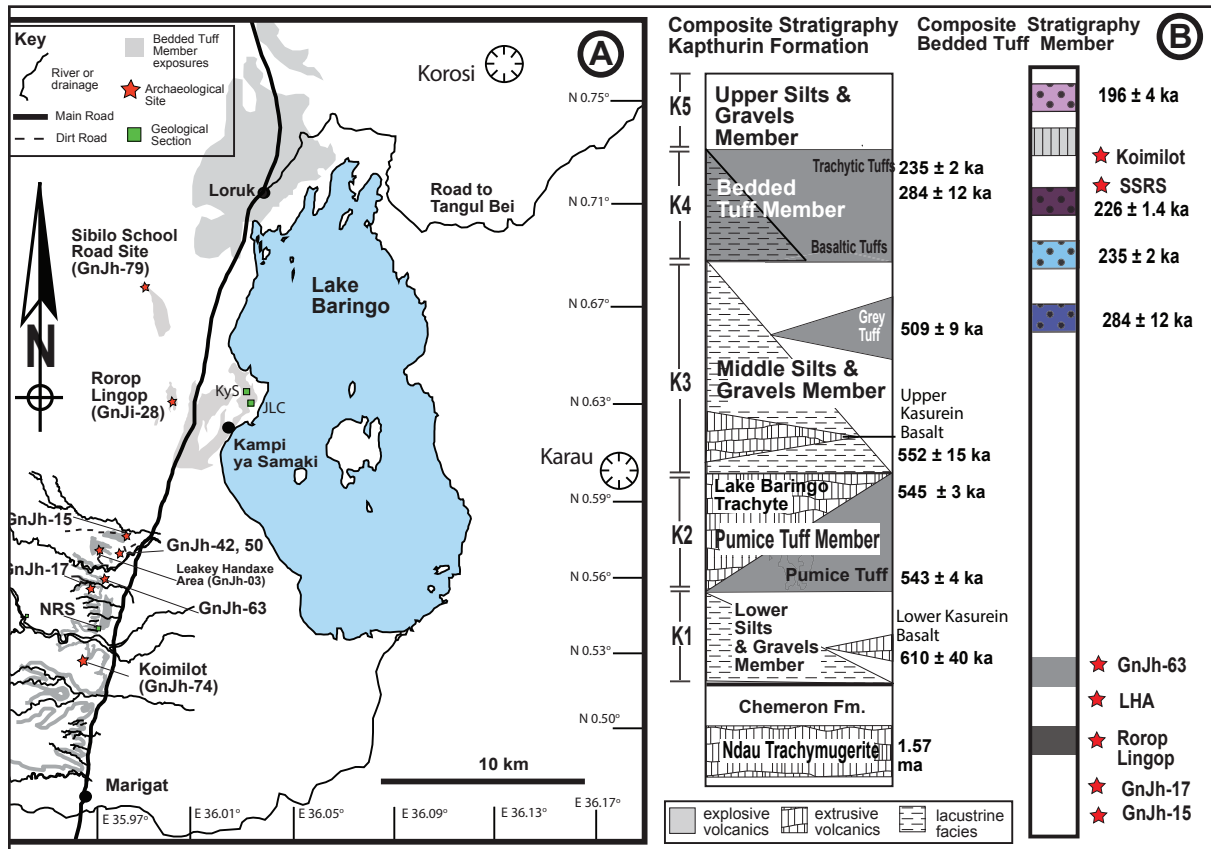


Figure 2: A) Plan Map of Baringo showing extent of Bedded Tuff Member exposures as well as location of archaeological sites in the Kapthurin Formation. B) Schematic stratigraphic section of the Kapthurin Formation with chronometric dates and expanded stratigraphy of the Bedded Tuff Member with chemically unique tuffs, chronometric dates and the stratigraphic position of archaeological sites in and beneath the Bedded Tuff Member set right.

and Faith, 2013; Tryon et al., 2005). The eMSA sites of the Gademotta Formation in the middle Ethiopian Rift (>183 –279 ka) show evidence of point production as well as diverse prepared cores made of locally available obsidian (Fig. 1; Douze, 2011, 2012, 2014; Morgan and Renne, 2008; Sahle et al., 2013; Sahle et al., 2014; Wendorf and Schild, 1974). No Levallois point cores are reported from the recently excavated site of Gademotta GDM7 (>279 ka), the best documented of the Gademotta sites (Douze, 2014; Sahle et al., 2013; Sahle et al., 2014). However, pseudo Levallois points and several unifacially trimmed pointed pieces produced on centripetally pre-

pared flakes or bifacially trimmed pieces made on flakes are present (Sahle et al., 2013; Sahle et al., 2014). Discoid cores and the Levallois recurrent method are reported in addition to casual, blade and discord cores. Levallois preferential cores are tentatively reported from Gademotta GDM7 (but see Sahle et al., 2014: 13 figure 6g).

#### East African Middle-Late Pleistocene obsidian sourcing:

Several studies of East African obsidian sources have been published (Ambrose, 2012; Brown et al., 2013; Merrick and Brown, 1984; Merrick et al., 1994; Negash and Shackley, 2006; Negash et al., 2006). Obsidian sources in East Africa are, with few exceptions, geographically restricted and well-defined points on the landscape characterized by chemically diagnostic fingerprints (Ambrose, 2012; Brown et al., 2013). Obsidian has thus proven useful for tracing hominin mobility and, mapping exchange networks, especially in later time periods such as the Holocene in East Africa (Ambrose, 2012; Merrick and Brown, 1984; Merrick et al., 1994). Material from MSA sites factor prominently into many obsidian-sourcing studies (Ambrose, 2012; Merrick and Brown, 1984; Merrick et al., 1994). Long distance (>150 km) raw material transport of obsidians shown in some MSA contexts are argued to evidence increased mobility, increases in intergroup interactions and expansion of social networks compared to ESA sites (Merrick et al., 1994). As



such, long distance transport of obsidians in the MSA factor prominently into arguments for the origins and evolution of modern human behavior (McBrearty and Brooks, 2000: 513-517).

Obsidian artifacts are only documented from a small number of Acheulean sites in the Middle Pleistocene of East Africa including Kariandusi and Kilombe in the central Kenyan Rift (Crompton and Gowlett, 1993; Gowlett and Crompton, 1994; Merrick et al., 1994). None of the obsidian from these sites was transported more than 15 km (Merrick and Brown, 1984; Merrick et al., 1994; Negash et al., 2006). The obsidian source was probably not much farther away than the source of other, coarser grained, raw materials such as lavas (Ambrose, 2012; Merrick and Brown, 1984; Negash et al., 2006). Obsidian is documented in Acheulean and MSA contexts at Melka Kunture and Garba III in the Ethiopian rift (Chavaillon, 1976; Mussi et al., 2014; Negash et al., 2006). Transport distances for Acheulean obsidian artifacts from the later Middle Pleistocene site of Melka Kunture are < 20 km from site to source (Negash et al., 2006). No ESA or well-dated Middle Pleistocene MSA sites containing obsidian in East Africa have site to source transport distances > 50 km (Merrick and Brown, 1984).

In MSA contexts evidence of obsidian transport between 185 and 190 km is shown for Song-

hor and Muguruk (McBrearty, 1981, 1986; Merrick and Brown, 1984; Merrick et al., 1994) and source to site transport distances of 250 km have recently been shown for obsidians associated with MSA technologies in the exposures of Karungu in western Kenya (Faith et al., 2015). The rockshelters of Nasera and Mumba in northern Tanzania demonstrate obsidian transport distances of 240 and 307 –325 km respectively (Mehlman, 1989; Merrick and Brown, 1984; Merrick et al., 1994). While these sites demonstrate long transport distances they constitute only a very small part (< 0.01 %) of the total lithic assemblages (Ambrose, 2012; Faith et al., 2015; McBrearty, 1981, 1986). At the MSA site of GvJm-16 at Lukenya Hill, Kenya, obsidians comprises 8.4% of the total lithic assemblage and over half of these (~58%) derive from the central rift 65 –135 km away (Ambrose, 2012; Merrick, 1975; Merrick et al., 1994).

All of the MSA sites reviewed above for which obsidians are transported significantly further than other raw materials, with the possible but undated exception of Muguruk, are from Late Pleistocene contexts and thus younger than the earliest MSA sites in East Africa by perhaps 70 –150 kyr (see Ambrose, 2012; Faith et al., 2015; Tryon and Faith, 2013). The lack of obsidian sourcing studies in eMSA contexts demonstrating long distance transport of obsidian in the eMSA leads to the valid critique that long distance raw material transport and the attendant im-

pacts of this practice on mobility and intergroup interactions and the economy of raw materials were not an important part of the eMSA hominins behavioral repertoire (Ambrose, 2012: 64).

The reviews of eMSA technology and obsidian sourcing presented above emphasize: 1) the relative rarity of well dated eMSA sites in East Africa documenting the character of MSA technology, and 2) even rarer opportunities to document raw material transport distances in later Middle Pleistocene eMSA contexts. New geological and archaeological work in the Kapthurin Formation of Baringo, Kenya, presents the opportunity to address these gaps in the later Middle Pleistocene archaeological record.

#### Geology and Chronology of the Kapthurin Formation:

The Kapthurin Formation is a series of sedimentary and volcanic units 125-150 m thick and exposed over an area of ~150 km<sup>2</sup> west of Lake Baringo in the Central Rift Valley of Kenya (Fig. 2). The formation is divided into five members labeled K1—K5 from lowest to highest stratigraphically (Fig. 1c). All Kapthurin Formation sediments are normally magnetized (Dagley et al., 1978), and thus postdate the Matuyama– Brunhes boundary, currently estimated at  $778.0 \pm 1.7$  (Love and Mazaud, 1997). The Pumice Tuff Member (K2) separating K1 and K3 is comprised

of a voluminous pumiceous eruption, the Pumice Tuff, coincident with a large effusive lava flow, the Lake Baringo Trachyte. These are  $^{40}\text{Ar}/^{39}\text{Ar}$  dated to  $545 \pm 3$  ka and  $543 \pm 4$  ka respectively and provide the earliest radiometric dates for the formation (Fig. 2b; Deino and McBrearty, 2002; Tallon, 1976). A single tuff unit, the Grey Tuff, from the Middle Silts and Gravels Member (K3), is directly dated to  $509 \pm 9$  ka by the  $^{40}\text{Ar}/^{39}\text{Ar}$  method (Deino and McBrearty, 2002). The Bedded Tuff Member (K4), is composed of a series of over a dozen alternating sedimentary and volcaniclastic units measuring a maximum thickness of 30-35 m (Tryon, 2003). To date The Bedded Tuff Member has produced two  $^{40}\text{Ar}/^{39}\text{Ar}$  dates of  $284 \pm 12$  ka and  $235 \pm 2$  ka (Fig. 2b; Deino and McBrearty, 2002; Tryon and McBrearty, 2002; Tryon and McBrearty, 2006). Large scale faulting followed the deposition of the Bedded Tuff Member. The age of these faulting events are estimated between 198 and 345 ka by Uranium-series (U-series) method on hydrothermal silica in-filling faulted cracks (Le Gall et al., 2000; Tallon, 1976). No exposures of the Bedded Tuff Member of the Kapthurin Formation are known to date  $< 200$  ka. In places, the Kapthurin Formation is unconformably overlain by deposits of the Holocene age, the Lobo Silts (Bishop et al., 1971; Renault and Owen, 1980).

Archaeology of the Kapthurin Formation:

Sediments in the Kapthurin Formation contain dozens of archaeological and paleontological localities, including several hominid sites, in well-dated contexts (Cornelissen, 1992; Cornelissen et al., 1990; Deino and McBrearty, 2002; Johnson and McBrearty, 2010; Leakey et al., 1969; Tryon and McBrearty, 2002; Tryon and McBrearty, 2006; Van Noten, 1982; Van Noten et al., 1987; Wood and Van Noten, 1986). Johnson and McBrearty (2010) describe two archaeological localities with evidence of blade technology dating to > 500 ka from the Middle Silts and Gravels Member (K3) of the Kapthurin Formation (Fig. 2b). The Bedded Tuff Member (K4) also contains both Acheulean and MSA sites (Deino and McBrearty, 2002; McBrearty, 1999, 2001b; McBrearty et al., 1996; McBrearty and Brooks, 2000; McBrearty and Tryon, 2006; Tryon and McBrearty, 2002; Tryon and McBrearty, 2006; Tryon et al., 2005). A tephrostratigraphic program of relative dating for the archeological sites of the Bedded Tuff Member established by Tryon and McBrearty (2006) shows that most archaeological sites situated in or beneath the Bedded Tuff Member containing Acheulean and MSA technologies are considerably older than 284 ka (Fig. 2). The single exception is the archaeological site of Koimilot (GnJh-74) estimated to date between 200 and 250 ka (Tryon, 2006; Tryon, 2003; Tryon and McBrearty, 2006; Tryon et al., 2005). This younger site contains pointed pieces alongside cores produced using diverse methods of Levallois technology and demonstrating that technological changes in the production of MSA

tools coincided with typological differences in the intended products (Tryon, 2006; Tryon, 2003; Tryon and McBrearty, 2006; Tryon et al., 2005).

Previous research in the Kapthurin Formation demonstrates important differences in the age, typology, technology and size of intended products between Acheulean and MSA assemblages within the same geological formation (McBrearty and Tryon, 2006). However, these studies still leave a large archaeological gap between the MSA site of Koimilot at ~200 ka and the Acheulean/ MSA assemblages at the base of the Bedded Tuff Member that are significantly older than 284 ka. In the 200-300 ka time interval during the later Middle Pleistocene, aspects of Middle Stone Age/ Middle Paleolithic technologies and behaviors are now known to occur in other regions of Africa and Eurasia (Adler et al., 2014; Wilkins et al., 2012), as well as in the East African Rift (Sahle et al., 2014). Geological and archaeological investigation at the 196- 226 ka eMSA SSRS presented here helps fill this archaeological gap and adds an important data point to the study of human behavior in East Africa in the later Middle Pleistocene.

The goals of the work presented here are:

1) To document the geological work, archaeological excavations, and artifact analysis completed at the SSRS to establish its later Middle Pleistocene age, taphonomic integrity and MSA character.

2) To use the large proportion of obsidian MSA artifacts at the SSRS to investigate raw material transport distances by:

1. Obsidian chemical characterization using electron microprobe of a representative sample (n=29) of SSRS obsidian artifacts. These artifact compositions will be correlated with source obsidians (Blegen et al., 2015; Brown et al., 2013) to determine straight-line site to source transport distances.

2. Quantifying reduction intensity for locally available lava raw materials and nonlocal obsidians at the SSRS. Comparisons between SSRS raw material categories and contemporaneous and technologically comparable East African eMSA sites from the Kapthurin, Kibish and Gademotta Formations of East Africa will be made to investigate the differential treatment of locally available versus exotic raw materials.

## Materials and Methods:

### The Sibilo School Road Site:

The Sibilo School Road Site (SSRS) is located in the north of the Kapthurin Formation ~5 km southeast of the town of Loruk (Fig. 2) at the intersection of a small dirt track and a dry seasonal drainage (Fig. 3). Andrew Hill and John Kimengich discovered the site on February 1, 1988. The artifact and fossil-bearing exposure at the SSRS measures approximately ~50m long, ~20m wide and ~4.5m thick. Controlled excavations were not carried out prior to this study because the isolated location of the site and the ambiguous lithology of the coarse pumiceous tuff capping local exposures (Fig. 3b) obscured its stratigraphic position and age.

### Archaeological excavation methods:

From 2011-2015 Blegen took geological samples for chemical characterization of the tephras. In June of 2013 Blegen and Deino took pumice samples for  $^{40}\text{Ar}/^{39}\text{Ar}$  dating by Deino. Excavations at the SSRS were carried out over four weeks in the winter of 2013-2014 and two additional weeks in June of 2014. Spatial data was collected in three dimensions using a 6" Leica total station connected to a PC laptop (Fig. 3b) operating EDM for windows excavation software





Figure 3: A) Photo of SSRS under excavation standing at intersection of road and drainage looking east. B) Picture of the coarse pumiceous tuff (SSRS Unit #3) capping the local stratigraphic section of the site and  $^{40}\text{Ar}/^{39}\text{Ar}$  dated to  $196 \pm 4$  ka. C) Photograph of one of many dense concentrations of artifacts found in SSRS Unit #1 tuffaceous silt soil during excavation. D) Local SSRS schematic stratigraphic section. E) The main trench (east of the ~N-S dirt road visible in the top right of the photograph) under excavation in January 2014 as viewed looking south from the vantage point of the total station during excavation.

(McPherron and Dibble, 2011). Prior to excavation, artifacts and fossils on the surface or exposed *in situ* at the surface were recorded and collected. A 1 x 1 m alphanumeric grid was laid out over the intended area of excavation. Excavations were carried out in arbitrary 10 cm horizontal levels because of the absence of any visible natural stratigraphy within the artifact and fossil-bearing matrix. All *in situ* lithic and fossil faunal material with a maximum dimension >2 cm was piece-plotted. All material with a discernable long axis was plotted with two points one at each end. All excavated sediment was screened through 1/8" mesh and sieved material was collected in bags specific to date, square and level.

#### Artifact Analysis:

No single, standardized framework for lithic analysis exists in MSA archaeology. To standardize data collection as much as possible, lithic analysis procedures and terminology follows that of recent studies of MSA and prepared core technologies in the Kapthurin Formation (Tryon, 2006; Tryon, 2003; Tryon et al., 2005). Artifact data reporting follows recent studies of Middle Pleistocene MSA material in East Africa (Sahle et al., 2014; Shea, 2008).

#### Tephra and obsidian analysis:

The geochemical analysis of tephra and obsidians focuses on electron microprobe characterization of eleven major element oxide proportions in volcanic glass from tuffaceous deposits, sediments and obsidian artifacts. Preparation protocols for tephra analysis and microprobe analysis for tephra and obsidian follow University of Utah Microprobe facilities equipment and methodologies outlined in Blegen et al. (2015) for tephra analysis and Brown et al. (2013) for obsidian analysis. Electron microprobe analysis of major element oxides on volcanic glass is the favored method of obsidian sourcing because this methodology has been tested and proven valid for obsidians from stone-age assemblages in East Africa (Brown et al., 2013; Merrick and Brown,

1984; Merrick et al., 1994). A large comparative dataset of geological obsidian sources characterized by electron microprobe analysis is available (Brown et al., 2013).

#### Obsidian sampling strategy:

Each obsidian specimen from the SSRS was macroscopically characterized based on the texture of its cortex and patina at the National Museum of Kenya, Nairobi. Twenty-nine pieces of obsidian recovered *in situ* at the SSRS were then sampled for chemical characterization by microprobe analysis. The goals of this sampling strategy were: 1) to chemically identify the source or sources of the obsidian and 2) to characterize the cores and flaked materials to determine the diversity of sources represented in the flaked waste and abandoned core assemblages from the site. To fulfill these objectives, small chips (0.5-1mm size; n=26) were sampled from the flake, flake fragment and angular waste of the three dense concentrations in the main trench of the SSRS (shown in Fig. 3e) and from 16 separate 1x1 m<sup>2</sup> units from the main trench where obsidian was less densely concentrated. Three obsidian samples were taken directly from each of the three obsidian cores.

#### Correlation of SSRS artifactual obsidians to sources:

Correlation of the chemical compositions of SSRS obsidian artifacts and discrete chemical and

geographic sources required the overlap of the oxide values of all measured major element  $\pm 1$  standard deviation, visual inspection of the data in bivariate plots and an empirically informed similarity coefficient methodology for correlating volcanic glass of discrete modal compositions based on Borchardt (1972) and outlined in Blegen et al. (2015). The only departure from the methodology defined in Blegen et al. (2015: 100) is the addition of three elements, Si, Na and K, because they could be accurately measured in the obsidians studied here. Mg was excluded from this study because its proportional representation was too low ( $\leq 0.02$  wt. %) for consistently accurate measurement of this element in the majority of obsidians considered here. Correlation of glass from the SSRS tuffaceous artifact matrix to a unit directly dated by the  $^{40}\text{Ar}/^{39}\text{Ar}$  method follows the same procedure but uses ten available element oxides as these could all be measured accurately.

#### Reduction Intensity quantification:

The reduction intensity of raw materials found at the SSRS and the comparative eMSA sites was systematically quantified as a ratio of flaked products (flakes and flake fragments or “debitage” and angular waste or “debris”) divided by flaked remnants (cores and core fragments) as indicated by the following equations:

1)

Debitage (pieces)\* Debitage (weight) + Debris (pieces)\* Debris (weight)

Cores (pieces)\* Cores (weight) + Core fragments (pieces)\*Core fragments (weight)

and as the simplified equation excluding measured weights:

2)

Debitage (pieces) + Debris (pieces)

cores (pieces) + core fragments (pieces)

These equations assume that as lithic raw materials are more intensively reduced, the number of flaked products and their total weight increase, while the number of flaked remnants remain constant while their total weight decreases. Thus, higher values obtained from either of the above equations, indicate more intense reduction. The first equation includes weights and is thus a more sensitive measure of reduction intensity since the specific density (density = mass / volume) of different raw materials may vary, but can be controlled when weight is included as a variable. All of the volcanic raw materials at the SSRS have the same relative density as measured by water

displacement. These raw materials also have the same chemical and atomic composition (phonolites/trachytes) since their non-vesicular, fine-grained texture was produced by the same effusive style of eruption. Experiments have shown that raw materials commonly selected for knapping as compositionally disparate as chert and obsidian have the same macroscopic density as measured by water displacement (Dibble et al., 2005). However, the second equation, excluding weights, is more generally applicable as weights of lithic artifacts are not always reported in publications (see Sahle et al., 2014; Shea, 2008). These equations were applied to SSRS obsidian and other local raw material assemblages at the site. They were also calculated for all identified raw materials from comparative eMSA sites that preserved both knapped products (debitage + debris) and remnants (cores + core fragments) in taphomically undisturbed primary contexts.

## Results:

### 1a) Geological context and age of the SSRS:

Establishing the age of the archaeological material from the SSRS requires direct dating as well as linkage between the site's local stratigraphy and the larger known tephrostratigraphic and chronostratigraphic framework of the Bedded Tuff Member (Deino and McBrearty, 2002; McBrearty et al., 1996; Tryon, 2003; Tryon and McBrearty, 2002; Tryon and McBrearty, 2006). The

local stratigraphy of the SSRS consists of three lithologically distinct units (from stratigraphically lowest to highest): Unit 1) a light brown, massive tuffaceous silty-soil over 1.5 m thick and exposed at the base of the dry seasonal drainage. This unit contains all *in situ* archaeological material at the SSRS (Fig. 3a, c, d, e). The SSRS Unit #1 tuffaceous soil is capped by Unit 2) a non-tuffaceous silty-clay soil, ~1m thick and displaying vertic structures and slickenslide features. This silty-clay soil is eroded at the top and disconformably overlain by Unit 3) a fresh, vitric, coarse pumice tuff composed of fresh, angular to subround pumices, 1-5 cm in diameter (Fig. 3b, d). Potassium bearing feldspars separated from fresh pumices of SSRS Unit #3 coarse pumiceous tuff were amenable to dating by the  $^{40}\text{Ar}/^{39}\text{Ar}$  method and have produced dates of  $196 \pm 4$  ka (Deino pers comm). Analysis of glass and pumices found *in situ* in the tuffaceous silt matrix of SSRS Unit #1 during excavation yields glass of a trachytic chemical composition (see Table 1; Figs. 4, 5). Glass separated from pumices found *in situ* during excavation of the SSRS and glass separated from the tuffaceous matrix of SSRS Unit #1 is chemically identical to glass from a coarse angular pumiceous unit ~5 km away on the Kampi-ya-Samaki Peninsula dated to  $226 \text{ ka} \pm 1.4 \text{ ka}$  by the  $^{40}\text{Ar}/^{39}\text{Ar}$  method (Figs. 4, 5 and caption). Thus, the minimum age of the archaeological material at the SSRS is  $196 \pm 4$  ka and the maximum age of the site produced by  $^{40}\text{Ar}/^{39}\text{Ar}$  dating and tephra correlation is  $226 \text{ ka} \pm 1.4 \text{ ka}$ .

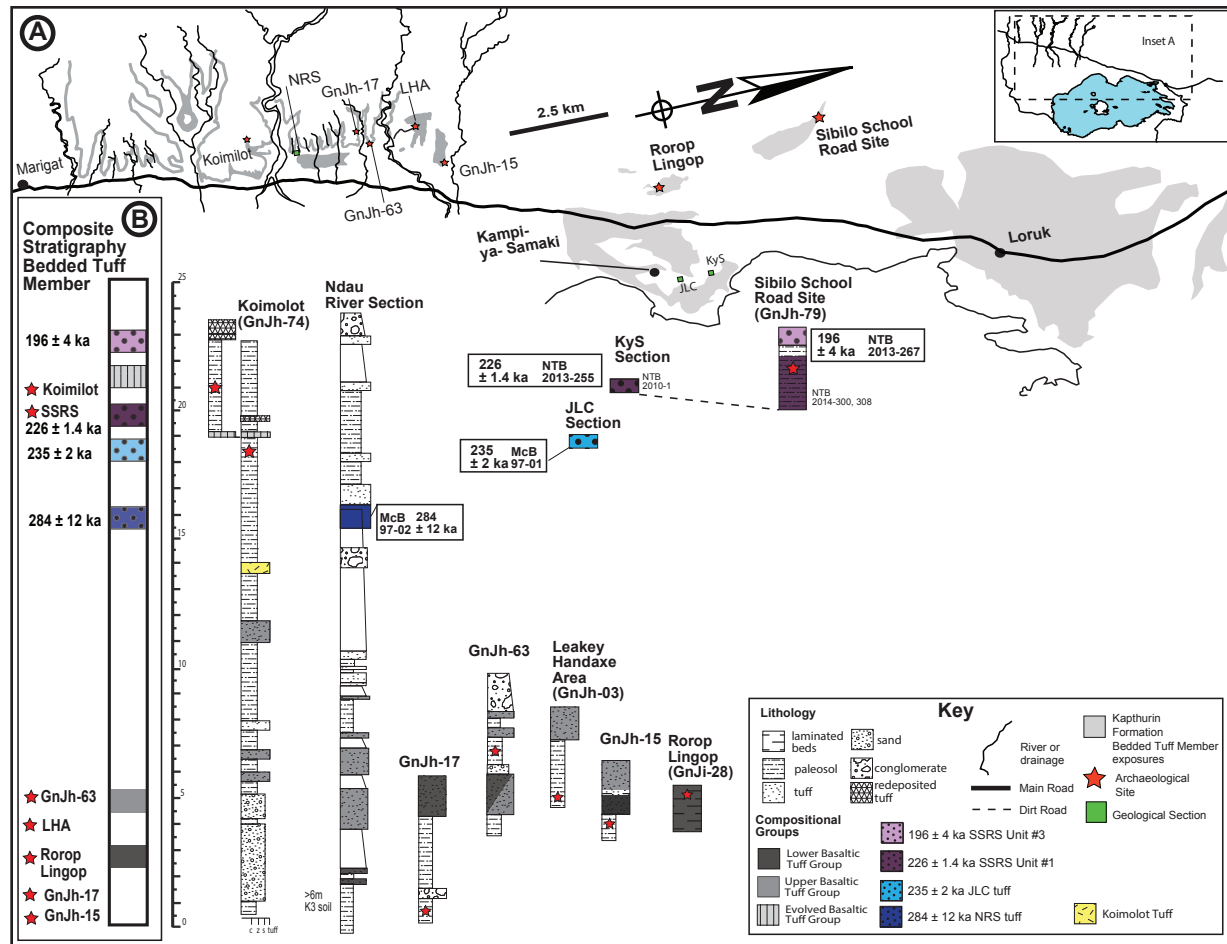


Figure 4: A) Schematic stratigraphic sections for relevant archaeological sites and  $^{40}\text{Ar}/^{39}\text{Ar}$  dated units from the Bedded Tuff Member of the Kapthurin Formation. Tuffs of unique colors corresponding to chemically defined tephras or groups of tephras (after Tryon, 2003; Tryon and McBrearty, 2002, 2006). Dotted lines represent tephra correlations based on glass chemistry. White area represents non-volcaniclastic sediments not used for correlation. B) Expanded schematic stratigraphy of the Bedded Tuff Member showing distinct tephras or tuff groups and  $^{40}\text{Ar}/^{39}\text{Ar}$  dates for the Bedded Tuff Member of the Kapthurin Formation.

#### 1b) Excavation of the SSRS:

Excavations in the tuffaceous silt SSRS unit #1 cover a total area of 80 m<sup>2</sup> in two separate

trenches east and west of the road (Fig. 6a). A single contiguous excavation could not connect

these trenches due to the presence of the dirt road intersecting the drainage. A total of 2506 lithic



Table 1: Mean major and minor element oxides by weight percent. Sample listed on left (No . number of analyses). One standard deviation from the mean listed below each element oxide mean.

Samples	n	SiO	TiO	ZrO	Al	FeO	MnO	MgO	CaO	Na	K	F	Cl	Sum	less O	Sum	H	Total
JLC Pumices 235 ± 2 ka																		
McB97-01		61.82	0.32	0.06	15.33	4.25	0.15	0.09	1.08	4.94	5.03	0.25	0.14	93.48	0.14	93.34	5.47	98.81
	30	0.75	0.06	0.05	0.50	0.61	0.04	0.02	0.10	1.17	0.17	0.07	0.03	0.95	0.03	0.97	1.02	0.82
KyS Pumices 226 ± 1.4 ka																		
		57.03	0.95	0.04	16.19	7.28	0.21	1.06	3.24	5.15	3.20	0.18	0.12	94.65	0.10	94.55	3.86	98.41
NTB2010-1	16	1.37	0.15	0.05	0.51	0.65	0.03	0.13	0.29	0.83	0.12	0.04	0.01	1.84	0.02	1.85	1.37	0.74
		56.39	0.94	0.02	16.03	7.19	0.22	1.12	3.40	5.79	3.31	0.27	0.13	94.82	0.14	94.67	4.56	99.23
NtB2010-1.1	15	1.27	0.05	0.03	0.38	0.23	0.03	0.06	0.14	0.31	0.12	0.14	0.02	2.25	0.06	2.24	1.17	1.47
SSRS Unit #1 Tuff																		
		52.68	1.18	-0.02	13.21	8.57	0.29	1.12	3.24	5.91	3.42	0.27	0.11	89.98	0.14	89.85	8.19	98.04
NTB2014-300	2	7.51	0.26	0.10	4.46	1.02	0.01	0.21	0.15	0.50	0.21	0.02	0.01	4.78	0.00	4.77	1.39	3.39
		58.64	0.91	0.10	15.80	7.41	0.21	1.06	3.19	4.73	3.19	0.27	0.11	95.63	0.14	95.49	5.28	100.77
NTB2014-308	8	0.50	0.14	0.08	2.23	1.06	0.03	0.14	0.41	0.77	0.49	0.12	0.02	3.00	0.05	2.99	1.48	1.76

artifacts were recovered *in situ* from SSRS Unit #1 including 1479 individually piece plotted lithic artifacts. Tables 2 and 3 list all general assemblage attribute data for excavated lithic material. The faunal sample consisted of 319 bone or tooth specimens recovered *in situ* and piece plotted. Vertical distribution of all piece-plotted material is close to two meters (1.84 m; 1.15 - 2.99 m below datum) over the entire site, although artifacts depths gradually increased relative to the datum, toward the western edge of the site (Fig. 6b). The main trench east of the road covered 66 m<sup>2</sup>, and was excavated to an average depth of ~70 cm below surface and preserves abundant lithic and faunal materials (Fig. 6). Artifacts and fossils with a long axis were piece- plotted with two points and show no preferred orientation (Fig. 6c and caption). The small trench west of the

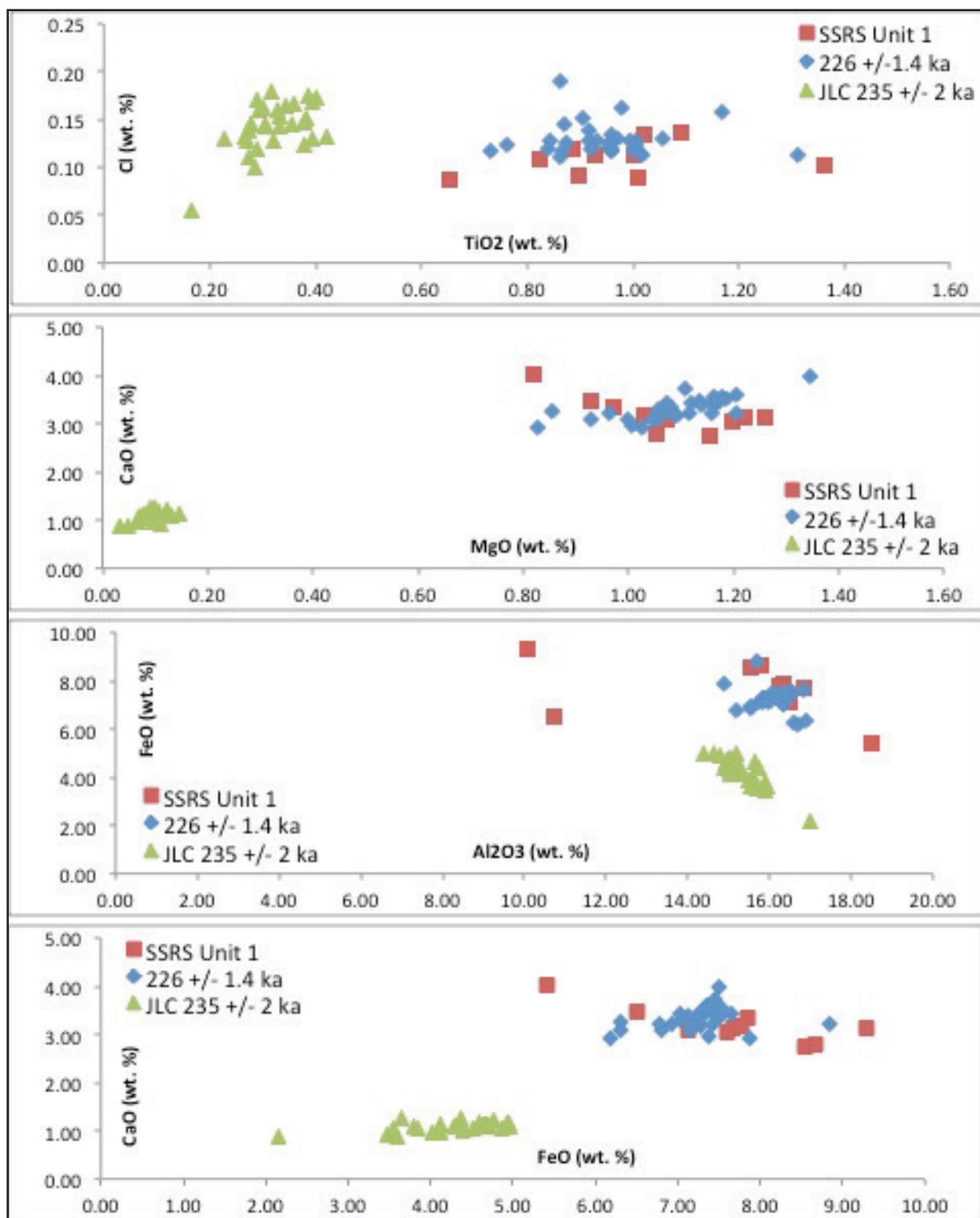


Figure 5: Bivariate plots of element oxides for glass showing correlation of Sibilo School Road Site Unit #1 glass (SSRS Unit #1= red squares) with pumiceous trachytic tuffs at section KyS (blue diamonds) directly  $^{40}\text{Ar}/^{39}\text{Ar}$  dated to  $226 \pm 1.4$  ka. A lithologically similar coarse pumiceous tuff  $^{40}\text{Ar}/^{39}\text{Ar}$  dated to  $235 \pm 2$  ka at the nearby locality of JLC (green triangles) shown as an 'outgroup' for comparison.

Table 2: Summary of assemblage composition for SSRS lithic artifacts.

Core		n	% w/ out debris	light lava	dark lava	yellow welded tuff	obsidian
	Casual	7.00	0.82	1	4	1	1
	Multiplatform	1.00	0.12	1			
	Levallois preferential	3.00	0.35		1	1	1
	Levallois point	1.00	0.12		1		
	Levallois recurrent	3.00	0.35	2			1
	Blade	1.00	0.12	1			
	Core on flake	1.00	0.12	1			
	Core fragment	2.00	0.23		2		
	Core subtotal	19.00	2.23	6	8	2	3
Debitage							
	Initial cortical flake	1.00	0.12				1
	Residual cortical flake	67.00	7.85	22	33	2	10
	Levallois flake	0.00	0.00				
	Levallois point	12.00	1.41	7	3	2	
	non- cortical flake	296.00	34.70	118	119	8	51
	Flake fragment proximal	171.00	20.05	51	74	5	41
	Flake fragment other	281.00	32.94	60	123	7	91
	Flake subtotal	828.00	97.07	258	352	24	194
Debris							
	Debris and subtotal	0.00					
Tool							
	side scraper	3.00	0.35	2	1		
	end scraper	1.00	0.12		1		
	chopper	1.00	0.12	1			
	biface	1.00	0.12		1		
	Tool subtotal	6.00	0.70				
TOTAL		853	100				
	n, % w/out debris	853	100				

Table 3: Summary statistics of dimensions (mm) of whole flakes from SSRS sorted by macroscopically identified raw material.

	Whole flakes	Mean flake length (mm)	Mean flake width (mm)	Mean flake thickness (mm)	Mean flake platform width (mm)	Mean flake platform thickness (mm)	Flake frags + AW	Total number of pieces	Total weight debitage & debris (g)	Total weight (g)
Light lava	157	32.62	27.47	8.77	17.80	6.80	360	517	1810.74	2223.53
± 1 SD		18.33	14.84	5.67	12.04	4.40				
Dark lava	156	35.65	32.41	10.51	22.49	9.16	677	833	3521.92	4590.32
± 1 SD		21.75	18.18	6.11	13.17	110.93				
Yellow welded tuff	13	52.10	37.98	15.26	28.76	12.31	29	42	820.50	864.60
± 1 SD		21.23	14.16	6.14	10.92	5.08				
Obsidian	64	15.88	15.85	4.84	11.63	3.98	996	1060	351.32	471.39
± 1 SD		7.01	7.73	2.67	7.02	2.34				
TOTAL	390							2452		8149.84

road preserves mostly bones in a small ~0.50 m wide by > 6 m long channel feature. Most pieces plotted with two points were aligned parallel to flow through the channel or perpendicular to it (Fig. 6d and caption).

Taphonomic context of SSRS lithic archaeological material:

The fine-grained tuffaceous silty matrix in which *in situ* artifacts and bones are preserved at the SSRS indicates a low-energy depositional environment. Stone artifacts occur in discrete patches at the site with large and small cores and flakes of the same raw material found in discrete clusters (Figs. 3c, 6a). The west and the main trenches separated by the road, sample the same land surface gently sloping toward a linear depression or small channel feature occupying a

topographic low in the western trench (Figs. 6a, b). This is supported by the lower average depth below datum of piece-plotted artifacts and fossils in the west trench versus the main trench (Fig. 6b) as well as the weak alignment of bones and lithic artifacts with the channel's original flow (Fig. 6d and caption). In the SSRS main trench, east of the road, artifacts occur at slightly higher elevations relative to the datum (Fig. 6b) and have no preferred orientation (Fig. 6c and caption). Size class analysis of all flaked stone artifacts shows that 72.4 % of all artifacts are  $\leq 2$  cm in maximum dimension. This pattern holds for each of the four identified categories of raw material (see below; Table 4, Fig. 7). When compared to experimental evidence, these numbers suggest on-site knapping preserved in primary context (Schick, 1986). The excavation of the SSRS likely documents deposition of stone artifacts and fossils on a single land surface over a short period of time, perhaps on the order of hours or minutes in the case of the lithic artifacts. No tooth marks or cutmarks were observed on the surfaces of the bones.

#### 1c) Raw material categories at the SSRS:

Four different macroscopically distinguishable general categories of raw material are present:

- 1) a light colored lava consisting of a fine-grained light brown groundmass with a banded appearance that is macroscopically indistinguishable from Tryon's (2003) raw material type 3

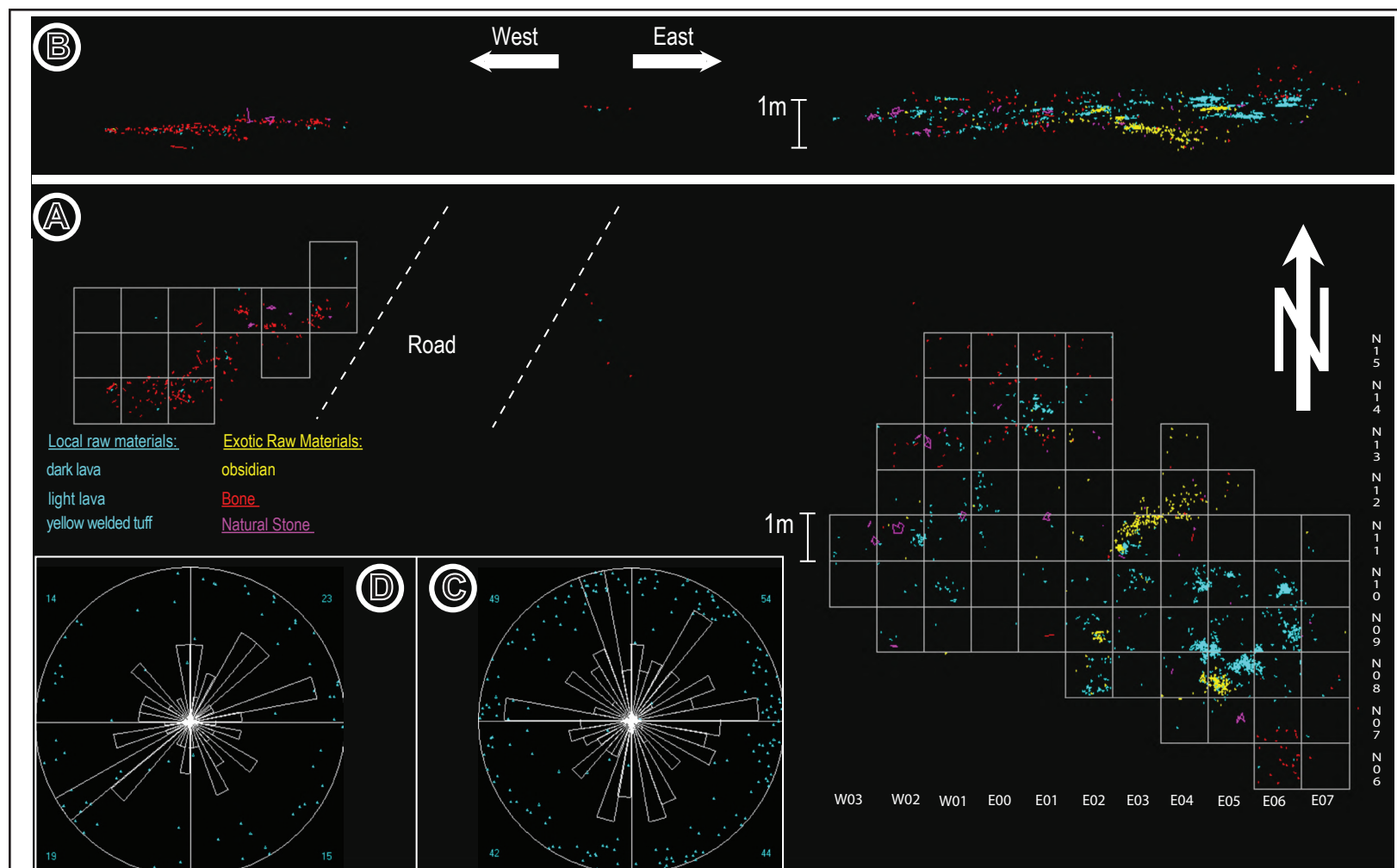


Figure 6: A) Plan map of SSRS excavation with piece-plotted lithic artifacts of local raw materials, obsidians, fossil bones/teeth, and natural rock color-coded by category. B) Cross sectional view (looking north) of the SSRS excavations with piece-plotted materials (as above) color coded (as above). C) Rose diagram of fossils and artifacts from the SSRS main trench, east of the road, with a long axis showing no preferred directional orientation of these pieces (Rayleigh's  $R = 0.08371$ ,  $\chi^2 = 52.99$ ,  $p = 0.02616$ , Rao's  $U = 136$ ,  $p = 0.2957$ , Watson's  $U_2 = 0.02701$ ,  $p > 0.5$ ). D) Rose diagram of fossils and artifacts from SSRS west trench showing pieces showing minor preferred directional orientation of these pieces aligned with or perpendicular to northeast-southwest flow of this small channel feature (Rayleigh's  $R = 0.05$ ,  $p = 0.85$ ,  $\chi^2 = 5.901$ ,  $p = 0.1165$ ; Rao's  $U = 144.4$ ,  $p = 0.1444$ ; Watson's  $U_2 = 0.06756$ ,  $p = 0.025 < p < 0.05$ ).

Table 4: SSRS lithic artifacts size classes listed by macroscopically identified raw material.

	SC1	%	SC2	%	SC3	%	SC4	%	SC5	%	SC6	%	SC7	%	SC8	%	SC9	%	SC10+	%
All	811	0.32	1010	0.40	310	0.12	159	0.06	92	0.04	49	0.02	23	0.01	21	0.01	6	0.00	11	0.00
Light basalt	65	0.12	237	0.45	95	0.18	66	0.13	36	0.07	12	0.02	5	0.01	6	0.01	1	0.00	3	0.01
dark basalt	116	0.14	381	0.45	154	0.18	75	0.09	51	0.06	32	0.04	16	0.02	12	0.01	4	0.00	7	0.01
obsidian	624	0.59	369	0.35	54	0.05	13	0.01		0.00	2	0.00		0.00		0.00		0.00		0.00
ylw welded tuff	3	0.07	16	0.36	6	0.14	4	0.09	5	0.11	3	0.07	2	0.05	3	0.07	1	0.02	1	0.02

phonolite, 2) a dark lava resembling the Lake Baringo Trachyte in hand sample (Type 6 in Tryon,

2003), 3) a yellow welded tuff and 4) obsidian (see Figs. 9-13). These four categories of raw

material include both locally available and exotic raw materials. The light and dark lavas can be

found as variously-sized cobbles in the conglomerates of the Kapthurin Formation and modern

riverbeds west of Lake Baringo (Fig. 2; Tryon, 2003). The yellow welded tuff is a common and

abundant raw material in the north of the Kapthurin Formation from Rorop Lingop to at least

~15 km north of Loruk (Fig. 2, Blegen pers obs.) These three materials derive from older extru-

sive volcanic flows of the Tugen Hills (Chapman, 1971; Chapman and Brook, 1978) and consti-

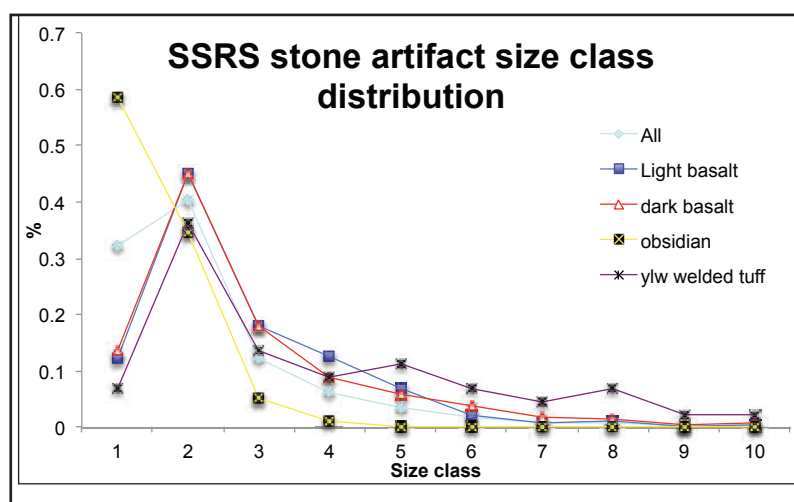


Figure 7: Size class distributions of artifacts by raw material category.

tute the locally available (< 5  
km distance from source to site)  
tool stones used at the SSRS  
(56.57% by individual pieces,  
94% by weight= 7678.45 g;

Fig. 8). The obsidian forms a

significant portion (43.43% individual pieces and 6 % by weight= 471.39 g; Fig. 8) of the SSRS assemblage and is represented by materials with at least three distinct chemical compositions not local to the Tugen Hills west of modern Lake Baringo (see below). These four macroscopically distinguishable raw material categories: the light lava, the dark lava, the yellow welded tuff, and the obsidian are found in discrete patches of knapped stones (Fig. 6a) and have produced refitting sets with flake fragments conjoining, multiple flakes refitting to one another and/or to a single core or multiple core fragments refitting to one another.

#### 1d) Lithic Technology of the SSRS:

Twenty-two triangular pointed pieces including 13 Levallois points representing all three locally

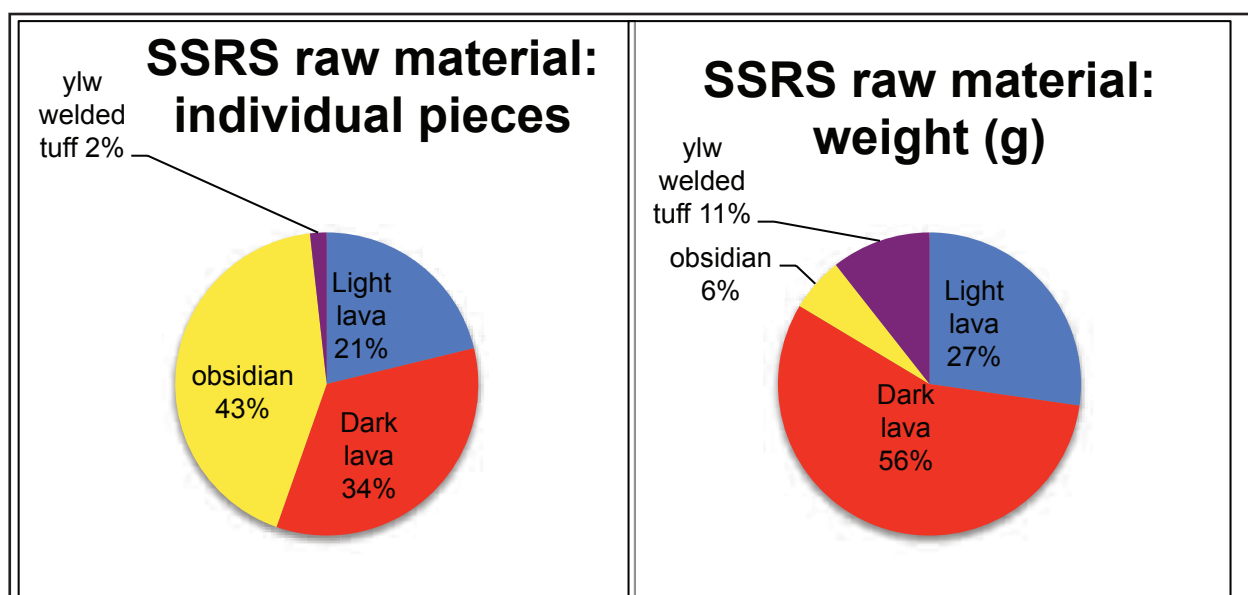


Figure 8: Raw material categories by A) individual pieces as percentages of total individual piece count and B) weight (g) as a percentages of total



Table 5: SSRS Levallois point metrics (mm) listed by macroscopically identified raw material.

SSRS Levallois Points	n	Mean Length (mm)	Mean Breadth (mm)	Mean Thickness (mm)	Mean Platform Width (mm)	Platform Thickness (mm)
Light lava	8	57.54	44.40	12.86	41.23	12.38
± 1 SD		13.19	10.36	3.61	9.50	3.69
Dark lava	2	46.81	41.32	14.05	35.42	13.04
± 1 SD		13.44	13.01	3.73	5.72	3.78
Yellow welded tuff	2	55.10	39.17	11.48	35.45	11.31
± 1 SD		7.55	11.80	1.30	9.97	1.56
All	12	59.34	44.07	13.47	40.11	12.55
± 1 SD		21.77	10.59	3.46	9.80	3.15

available raw materials were recovered from the excavations (Table 5; Fig. 9). Nineteen cores and three core fragments were also recovered *in situ*. Three additional cores were recovered from the surface. Eleven of the cores are made on the dark lava, three cores are made on the light lava, five cores are made on the yellow welded tuff and three cores are made on obsidian (Table 6; Fig. 10-12). The three core fragments are made on dark lava. Six of the cores are technologically Levallois cores of various types including four preferential flake cores and two recurrent centripetal Levallois cores (Fig. 10-12). One of these obsidian cores is a preferential Levallois core and another a discoid core, rectangular in plan view (Figs. 11c, 12c). The Levallois preferential flake method of flake production is applied to all of the four major categories of raw material used on the site.

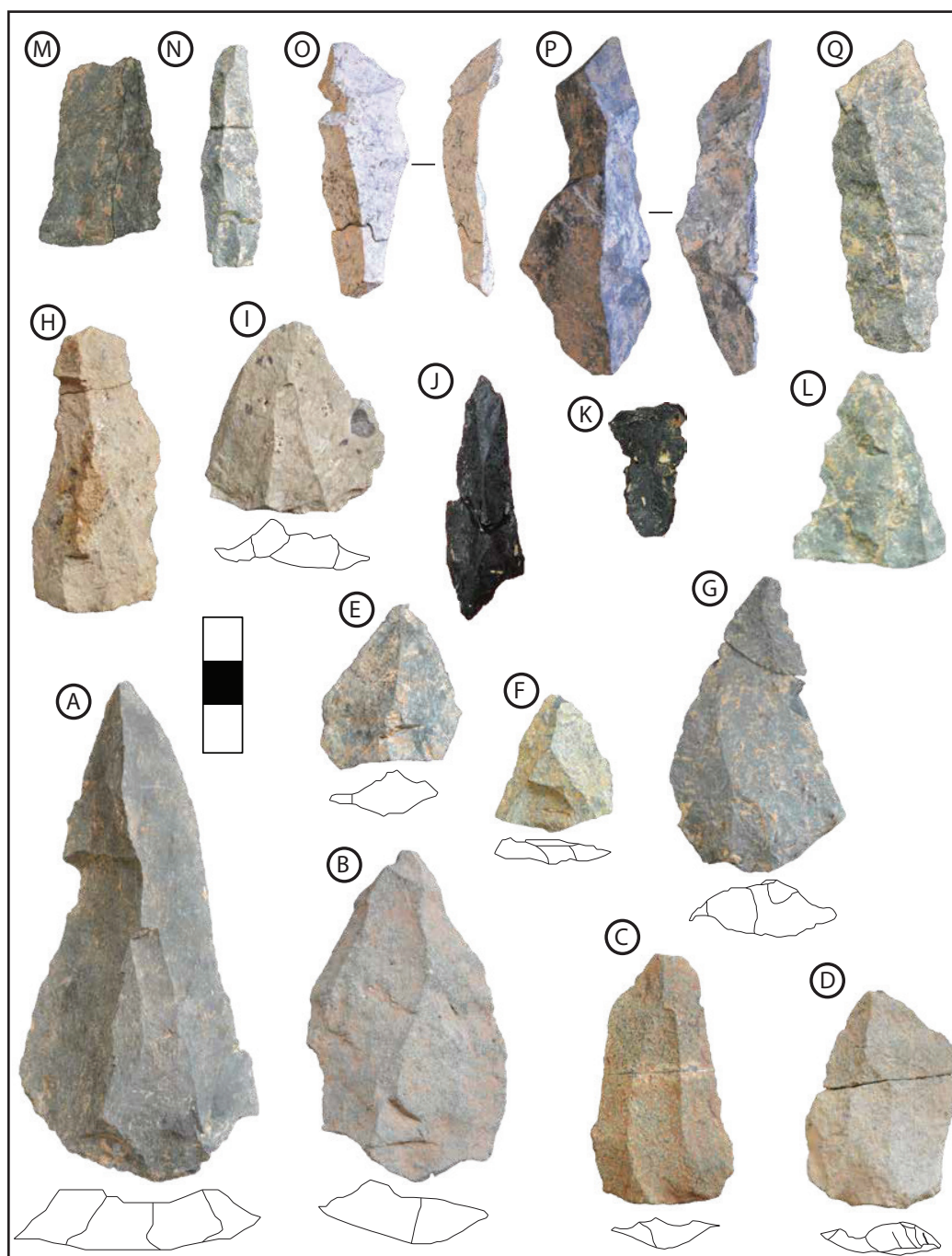


Figure 9: Levallois points and pointed pieces recovered *in situ* from the excavations of the main trench. A-D ) Levallois points made of the light lava raw material similar to Tryon #3 phonolite (Tryon, 2003). E-G) Levallois points made on dark lava raw material similar to the Lake Baringo Trachyte. H-I) Levallois points made on yellow welded tuff. J) Pointed blade made of obsidian (same lithic artifact concentration as sourced pieces of trachytic SSRS obsidian type #3). K) Obsidian blade made. L) Distal point fragment, dark lava. M) Two blades made on dark lava with technological refit. N) Blade on dark lava with distal tip broken. O) Curved blade (overshot?) on light lava. P) Curved blade (overshot?) on dark lava. Q) Blade on dark lava. All points (A-J and L) except 'J' exhibit tip damage. Four points (D,G,H,K) exhibit proximal-distal breaks. Conjoins of these were found during analysis ('C' is a fresh break during excavation).

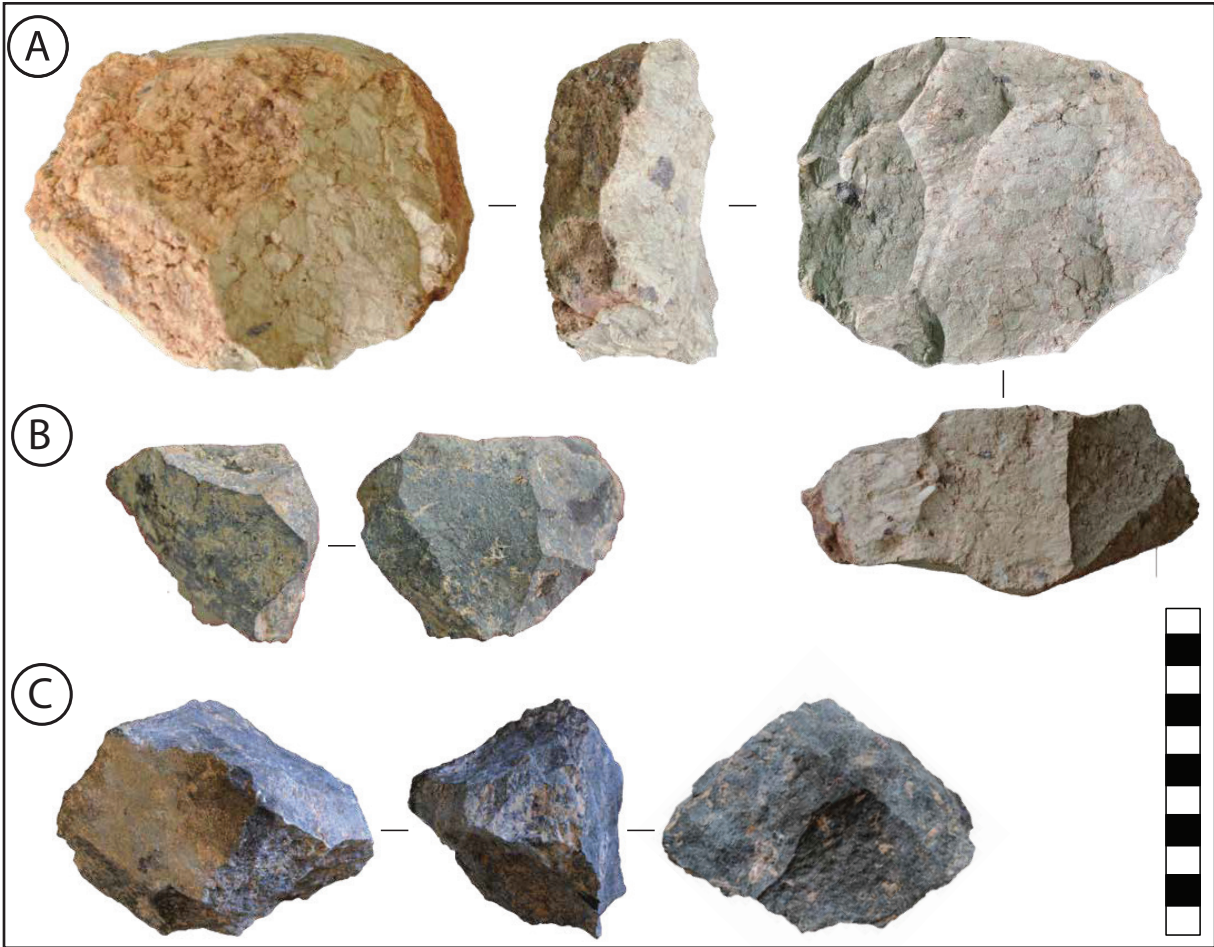


Figure 10: A) A Levallois cores (preferential) made on yellow welded tuff recovered from the surface near western edge of main trench. B) Levallois core (preferential and overshoot) found *in situ*. C) Levallois point core made on dark lava (found *in situ*).

#### Refitting:

Two recurrent centripetal cores made on light lava have refitting flakes (Fig. 12). One of these shows five refitting centripetal removals from a single debitage surface (Fig. 12a). The single obsidian Levallois preferential-flake core at the site could be refit with three successive preparation flakes on the right edge of the core's debitage surface (Fig. 12c). Additionally, seven pieces of yellow welded tuff from adjacent squares refit together. This large refitting set as well as the



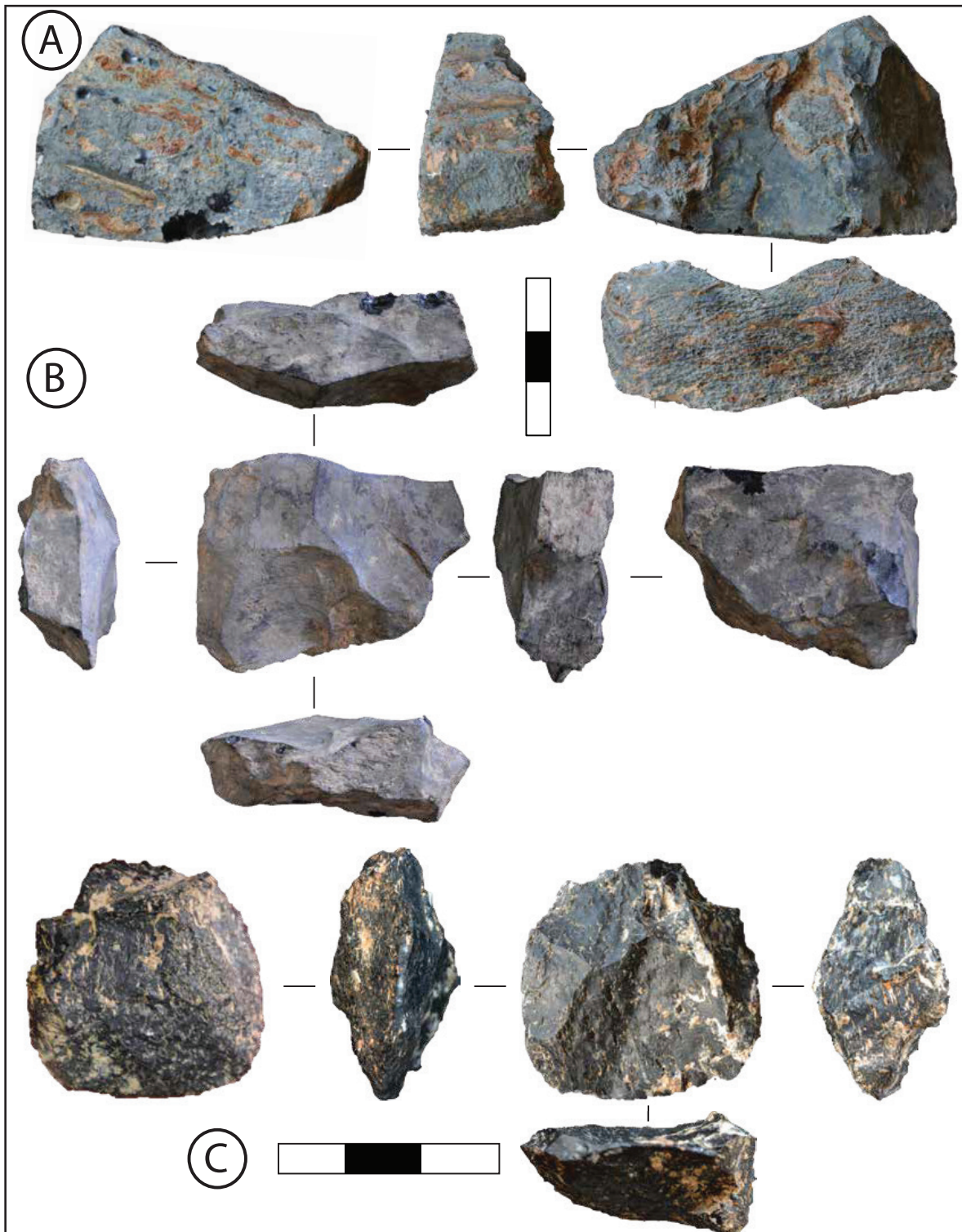


Figure 11: SSRS cores made on obsidian. A) single platform core with two unidirectional removals presumably abandoned because of large pearlite inclusion. Made on SSRS obsidian type #1 phonolitic composition from Karau. B) Discoid core flaked all over on both surfaces. Covered in matte patina. Made on SSRS obsidian type #1 phonolite. C) Levallois preferential flake core with cortex on lower surface. Made on SSRS obsidian type #3 trachytic composition.

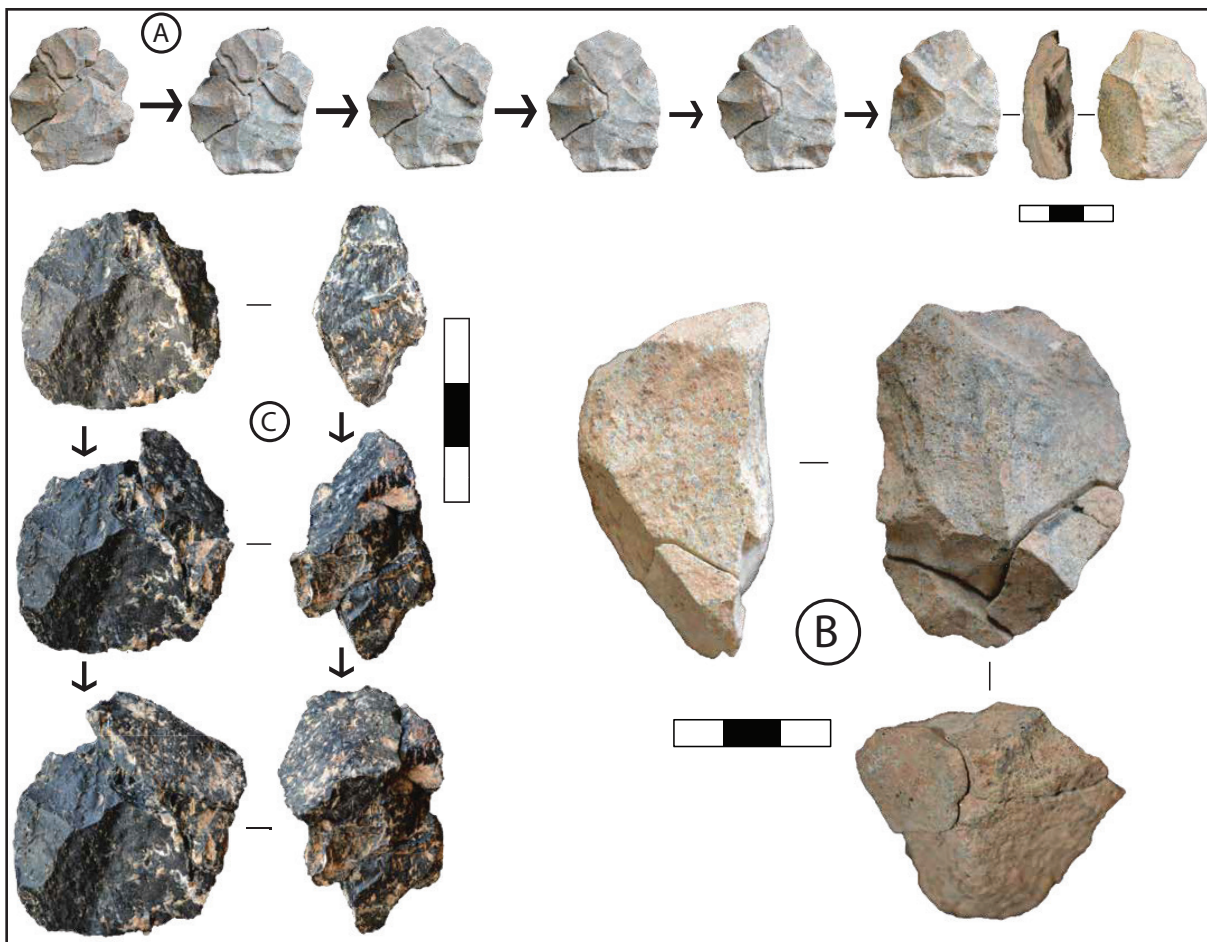


Figure 12: SSRS core exhibiting refits. A) A recurrent centripetal core (N08E02-4) on light lava with sequential pictures of five refitting flake removals from the same recurrent centripetal debitage surface. B) Recurrent centripetal Levallois core (N08E02-12) on light lava with two refitting preparation flakes. C) A preferential Levallois flake core (N09E02-20) on obsidian type #3 (trachytic composition) with three refitting pieces constituting two preparatory flakes from right margin of debitage surface (also pictured Fig. 11c).

relatively small number of total pieces of yellow welded tuff recovered on-site (13 whole flakes, 42 total pieces Table 2) suggests much of this material derives from the same large cobble. Multiple refitting sets of artifacts (Fig. 12) from the main trench on the east side of the site (Fig. 6a) confirm this and add support the argument that lithic artifacts at the SSRS represent the preserved product of a single occupation.



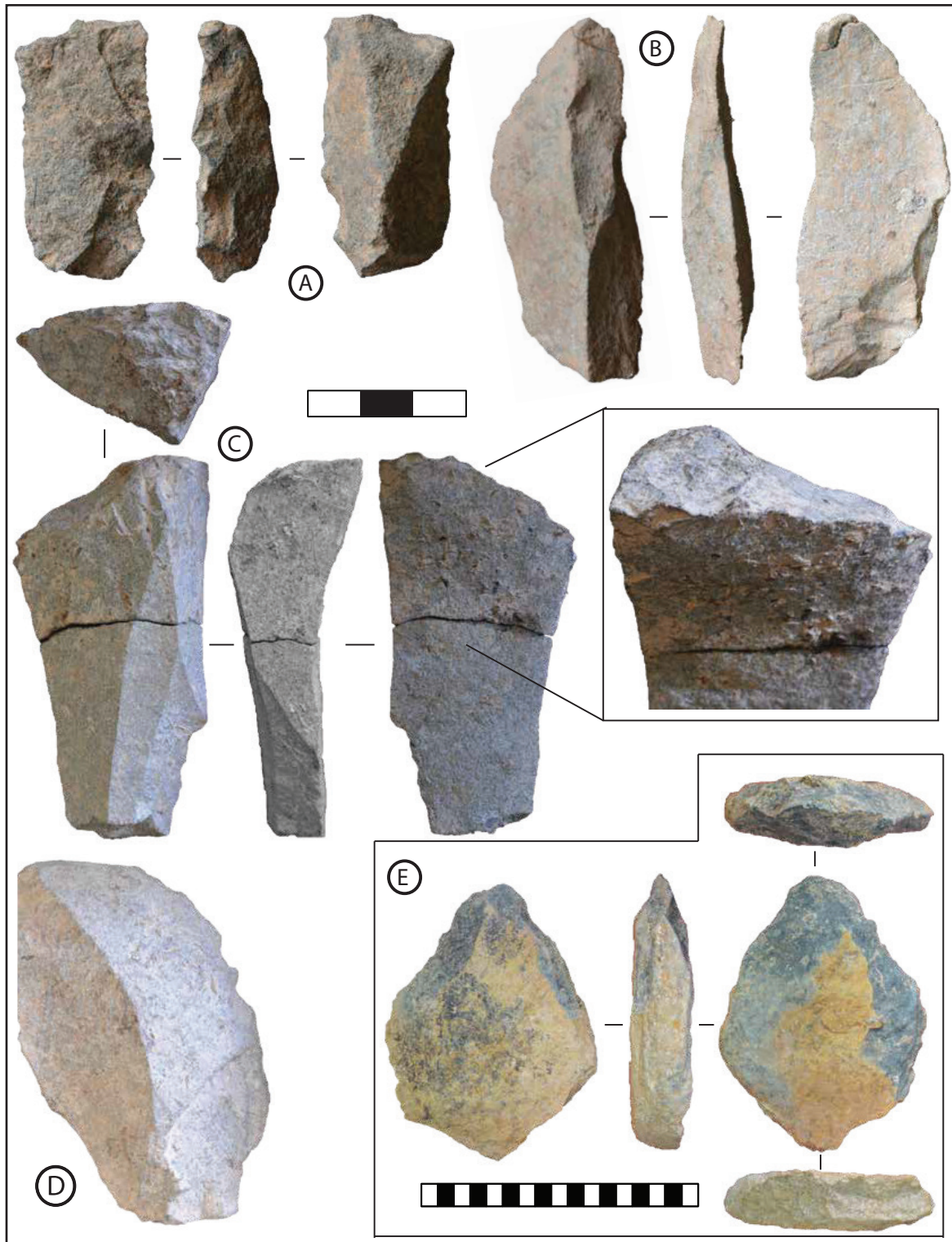


Figure 13: Selected SSRS retouched pieces and tools: A) A side scraper made on a light lava blade. B) End scraper made on cortical light lava blade. C) An end scraper made on a light lava blade. D) A side scraper made on a light lava flake. E) A biface found *in situ* exposed at the surface ~28 m east of eastern edge of main trench.

Table 6: SSRS core metrics (mm) listed by macroscopically identified raw material.

Cores	n	Mean length (mm), $\pm 1$ SD	Mean width (mm), $\pm 1$ SD	Mean thickness (mm), $\pm 1$ SD	Total weight (g)
Light lava	6	47.68	38.53	31.50	412.79
$\pm 1$ SD		7.14	6.51	14.79	
Dark lava	8	62.74	57.10	38.02	1068.40
$\pm 1$ SD		29.38	14.73	11.95	
yellow welded tuff	5	72.14	91.66	44.10	514.52
$\pm 1$ SD		22.43	33.01	2.69	
obsidian	3	43.58	40.47	20.24	120.07
$\pm 1$ SD		15.04	11.58	4.90	
Total	22				6362.56

Tools:

The percentage of retouched pieces categorized as formal tools from the SSRS is low for all raw material categories (Table 2), as is typical of most East African MSA sites (McBrearty, 2001a; retouched tools and selection of blades pictured in Fig. 13). Two piece-plotted artifacts were found *in situ* on the surface of the tuffaceous silty soil (SSRS Unit #1) ~28 m east of the eastern edge of the main trench at a slightly higher elevation relative to datum (~0.50 m). Both these artifacts were made of the dark lava. One is a flake and the second is a crude pointed biface, preserving cortex on both faces (Fig. 13e).

## 2) Obsidian sourcing:

Three compositionally distinct obsidians from three different sources were identified by the

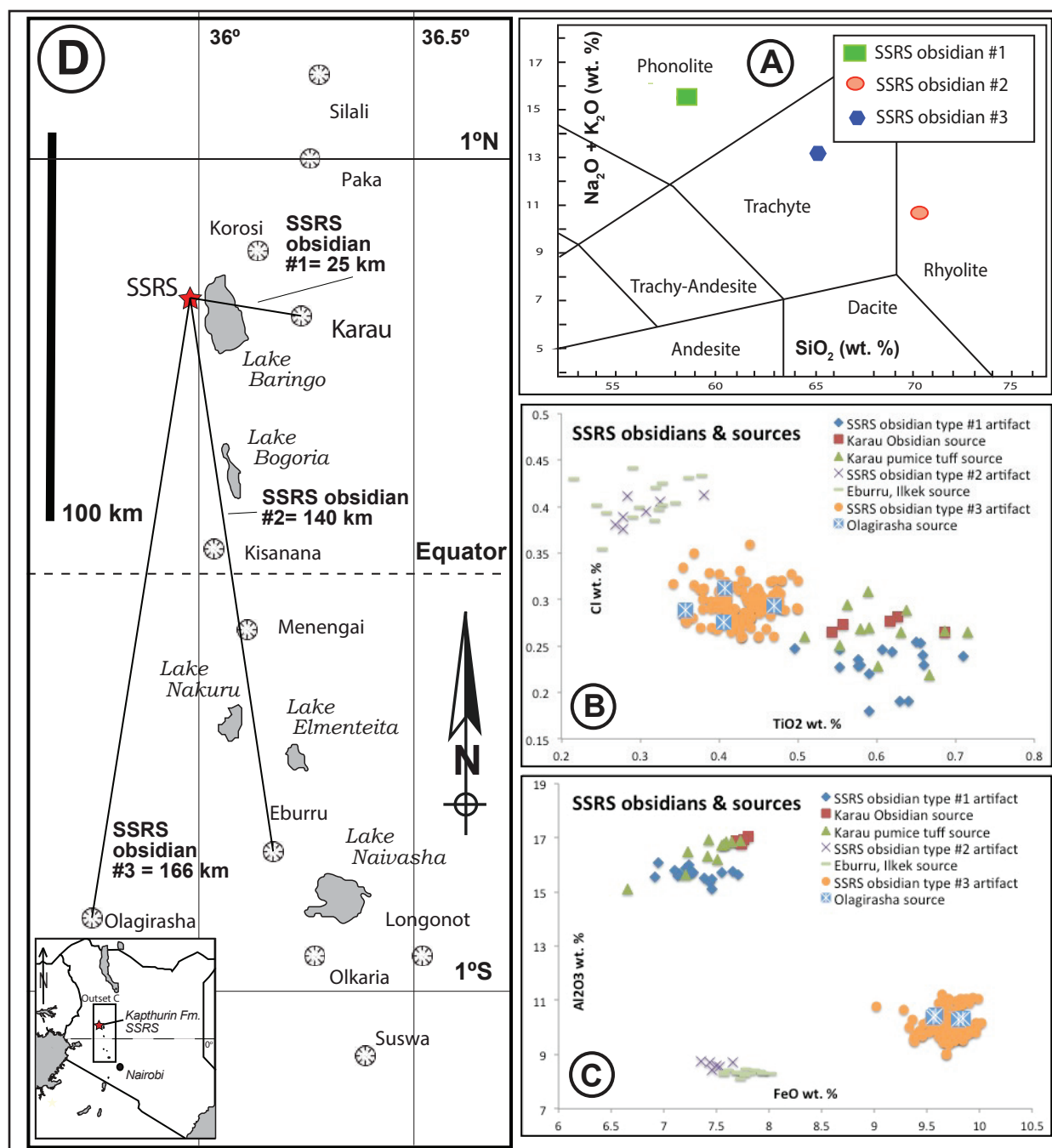


Figure 14: A) Total Alkali Silica graph (after Le Bas et al., 1986) showing categorically distinct compositional nature of three SSRS obsidians. B) Cl versus  $\text{TiO}_2$  bivariate plot showing difference between SSRS obsidian compositions and similarities between SSRS obsidians #1, #2 and #3 with their geological sources at Karau and Eburru, Ilkek and Olagirasha respectively (Eburru, Ilkek and Olagirasha source means published Brown et al., 2013, individual analyses donated by F.H. Brown). C)  $\text{Al}_2\text{O}_3$  versus FeO bivariate plot showing difference between SSRS obsidian compositions and similarities between SSRS obsidians #1, #2 and #3 with their geological sources at Karau and Eburru, Ilkek and Olagirasha respectively (For figure 13 B and C Eburru, Ilkek and Olagirasha source means published Brown et al., 2013 and supplementary information, individual analyses donated by F.H. Brown). D) Map of central and south Kenyan rift showing some prominent volcanoes and obsidian sources (after Brown et al., 2013) as well as the SSRS and distances from this site to correlated sources of chemically characterized obsidian artifacts on the site.



electron microprobe analyses (147 analyses on 29 samples) at the SSRS (Table 7, Fig. 14). These samples have a categorically different normalized total-alkali silica chemical composition (Fig. 14a; Le Bas et al., 1986). SSRS obsidian type #1 has a phonolitic composition, SSRS obsidian type #2 has a rhyolitic composition and SSRS obsidian type #3 has a trachytic composition (Fig. 14a). These obsidians can be differentiated to source by the composition of their major element oxides and their correlation with published source data (Brown et al., 2013; Merrick and Brown, 1984; Merrick et al., 1994). SSRS obsidian type #1 phonolite is from the closest obsidian source to the SSRS, the volcano Karau on the East side of Lake Baringo. This source is a ~25 km straight-line distance from SRSS as (Table 8; Fig. 14), but the distance would have been further if the lake was present. At the SSRS this obsidian is macroscopically distinct from others. Surfaces of SSRS obsidian type #1 phonolitic material flaked in antiquity exhibit a matte black patina (Figs. 11a, b). The unflaked, cortical surfaces have a rough weathered and oxidized texture (Fig. 11a). This material is represented by two cores (samples NTB2015-380, 381; Fig. 11a, b) and a single size class 4 flake (sample NTB2015-583) from unit N08E02 (Fig. 6a). Of the chemically analyzed obsidian samples, only pieces exhibiting the matte patina on their flaked surfaces have a phonolitic composition, and all of these matches the phonolitic chemical composition are correlated to Karau.

Table 7: Individual obsidian artifacts analyzed for sourcing. Mean major and minor element oxides by weight percent. Sample listed on left (No. number of analyses). One standard deviation from the mean listed below each element oxide mean.

SSRS Obsidian Artifact Samples		No.	SiO <sub>2</sub>	TiO <sub>2</sub>	ZrO <sub>2</sub>	Al <sub>2</sub> O <sub>3</sub>	FeO	MnO	MgO	CaO	Na <sub>2</sub> O	K <sub>2</sub> O	F	Cl	Sum
SSRS type #1															
NTB2014-348tuff	source		58.70	0.61	0.12	16.46	7.42	0.38	0.36	1.11	7.33	5.40	0.50	0.24	98.63
Karau	15		0.82	0.06	0.03	0.57	0.29	0.04	0.02	0.04	3.38	0.55	0.06	0.02	4.46
NTB2014-351tuff	source		57.31	0.55	0.10	15.80	7.06	0.34	0.35	1.05	1.89	5.38	0.44	0.24	90.50
Karau	12		2.44	0.06	0.04	0.65	0.26	0.04	0.01	0.12	3.15	0.67	0.06	0.06	5.64
NTB2014-354	source		59.66	0.57	0.11	15.57	7.77	0.31	0.30	1.17	7.14	4.68	0.45	0.24	97.98
Karau	19		0.75	0.12	0.03	0.28	0.54	0.03	0.03	0.07	1.42	0.16	0.04	0.02	2.50
NTB2014-348obs	source		59.99	0.61	0.11	16.91	7.74	0.40	0.38	1.10	9.39	5.14	0.52	0.23	102.52
Karau	5		0.17	0.06	0.04	0.10	0.04	0.03	0.02	0.04	0.23	0.07	0.01	0.02	0.36
NTB2014-380	artifact		57.11	0.60	0.12	15.66	7.23	0.38	0.34	1.09	9.71	5.26	0.56	0.24	98.31
N09E07-1 core	6		0.24	0.08	0.04	0.07	0.24	0.02	0.01	0.03	0.34	0.10	0.02	0.01	0.49
NTB2014-381	artifact		57.57	0.61	0.11	15.87	7.22	0.36	0.34	1.09	9.09	5.31	0.60	0.24	98.42
N12E01-1 core	6		0.30	0.04	0.02	0.15	0.20	0.02	0.01	0.04	0.46	0.08	0.03	0.01	0.64
NTB2015-583	artifact		58.08	0.62	0.13	15.41	7.49	0.38	0.65	1.07	9.67	5.43	0.36	0.20	101.79
N08E02	5		0.93	0.03	0.02	0.20	0.12	0.01	0.04	0.02	0.20	0.04	0.05	0.02	0.78
SSRS type #2															
MER 70	source		71.24	0.34	0.41	8.33	7.93	0.23	0.01	0.30	6.42	4.62	0.76	0.42	101.00
Eburru, Ilkek	5		0.19	0.03	0.05	0.03	0.07	0.03	0.01	0.02	0.12	0.07	0.02	0.02	0.28
K80-403	source		70.69	0.27	0.49	8.25	7.70	0.23	0.01	0.25	6.68	4.57	0.76	0.41	100.30
Eburru, Ilkek	5		0.13	0.05	0.03	0.09	0.08	0.04	0.01	0.01	0.20	0.07	0.04	0.02	0.36
MER 71	source		71.26	0.30	0.45	8.39	7.70	0.21	0.01	0.30	6.27	4.60	0.78	0.40	100.66
Eburru, Ilkek	5		0.23	0.03	0.06	0.07	0.12	0.02	0.01	0.01	0.05	0.07	0.03	0.03	0.32
NTB2014-313	artifact		72.64	0.30	0.38	8.20	7.49	0.25	0.03	0.26	6.44	4.67	0.94	0.40	102.00
N14W19	7		0.35	0.04	0.02	1.13	0.09	0.03	0.03	0.02	0.14	0.09	0.13	0.01	1.22
SSRS type #3															
MER 59	source		63.97	0.41	0.16	10.36	9.70	0.36	0.02	0.73	8.57	4.53	0.45	0.29	100.63
Olagirasha	4		0.40	0.05	0.03	0.08	0.16	0.05	0.01	0.02	0.11	0.07	0.03	0.02	0.69
NTB2013-314	artifact		66.24	0.43	0.20	10.33	9.82	0.38	0.05	0.74	8.23	4.40	0.66	0.29	101.77
N08E05	7		0.56	0.06	0.09	1.48	0.10	0.03	0.01	0.02	1.66	0.15	0.11	0.01	2.42
NTB2013-315	artifact		66.58	0.43	0.19	10.95	9.78	0.38	0.05	0.74	8.47	4.39	0.63	0.27	102.87
N08E05	8		0.13	0.06	0.04	0.06	0.10	0.04	0.01	0.02	0.33	0.08	0.10	0.01	0.43
NTB2013-316	artifact		66.62	0.40	0.16	10.78	9.78	0.37	0.05	0.71	8.89	4.37	0.62	0.27	103.03
N11E03	7		0.24	0.05	0.06	0.79	0.10	0.02	0.01	0.03	0.44	0.09	0.08	0.01	0.78
NTB2014-379	artifact		63.88	0.44	0.16	10.30	9.46	0.36	0.04	0.76	8.59	4.42	0.63	0.33	99.37
N15W16	5		0.11	0.04	0.03	0.29	0.26	0.02	0.01	0.02	0.29	0.05	0.06	0.02	0.48
NTB2014-382	artifact		63.08	0.39	0.17	10.00	9.58	0.40	0.04	0.76	8.69	4.39	0.64	0.33	98.47
N09E02-20 core	6		0.87	0.05	0.04	0.19	0.15	0.02	0.02	0.05	0.52	0.09	0.05	0.01	0.96
NTB2015-565	artifact		63.44	0.42	0.19	9.74	10.54	0.41	0.05	0.73	8.72	4.58	0.56	0.31	99.70
N11W02	5		0.11	0.04	0.03	0.17	0.25	0.02	0.01	0.02	0.26	0.11	0.06	0.00	0.34
NTB2015-566	artifact		63.96	0.43	0.21	10.15	10.89	0.40	0.04	0.74	8.78	4.62	0.45	0.28	100.94

N13E00	3	0.18	0.03	0.07	0.10	0.07	0.01	0.01	0.01	0.01	0.21	0.03	0.04	0.02	0.30
NTB2015-567	artifact	63.50	0.45	0.17	9.93	10.84	0.38	0.03	0.73	8.62	4.58	0.62	0.29	100.14	
N13E01	5	0.42	0.02	0.03	0.18	0.06	0.02	0.01	0.03	0.29	0.05	0.03	0.02	0.31	
NTB2015-568	artifact	65.99	0.45	0.18	10.17	11.04	0.36	0.03	0.74	8.71	4.56	0.50	0.30	103.03	
N13E01	4	0.60	0.03	0.07	0.10	0.08	0.03	0.01	0.02	0.23	0.08	0.03	0.00	0.48	
NTB2015-569	artifact	63.88	0.45	0.19	9.87	10.80	0.39	0.01	0.71	8.71	4.51	0.50	0.30	100.32	
N13E01	3	0.70	0.03	0.06	0.03	0.06	0.02	0.01	0.02	0.12	0.09	0.04	0.02	0.80	
NTB2015-570	artifact	64.75	0.44	0.18	10.00	10.93	0.37	0.01	0.74	8.61	4.50	0.50	0.30	101.34	
N14E02	3	1.00	0.03	0.06	0.12	0.11	0.02	0.02	0.02	0.18	0.05	0.02	0.01	1.23	
NTB2015-571	artifact	64.98	0.41	0.17	10.16	10.93	0.38	0.01	0.73	8.12	4.52	0.41	0.30	101.13	
N13E01	4	0.66	0.02	0.04	0.28	0.11	0.02	0.01	0.01	0.38	0.11	0.04	0.01	0.64	
NTB2015-572	artifact	62.68	0.44	0.18	9.84	10.80	0.37	0.01	0.75	8.72	4.53	0.51	0.28	99.10	
N13E01	5	0.91	0.02	0.04	0.12	0.12	0.02	0.01	0.03	0.21	0.03	0.06	0.01	1.08	
NTB2015-573	artifact	63.93	0.42	0.18	9.81	10.79	0.36	0.01	0.73	8.79	4.56	0.52	0.31	100.41	
N13E02	5	0.32	0.03	0.05	0.20	0.07	0.03	0.01	0.02	0.14	0.03	0.03	0.02	0.46	
NTB2015-574	artifact	64.38	0.47	0.18	9.70	10.90	0.38	-0.00	0.73	8.70	4.56	0.49	0.30	100.78	
N13E02	3	0.71	0.03	0.02	0.31	0.11	0.02	0.02	0.02	0.14	0.02	0.08	0.01	1.22	
NTB2015-575	artifact	64.70	0.45	0.20	10.39	10.70	0.36	0.03	0.72	8.58	4.47	0.48	0.27	101.36	
N13E02	5	2.05	0.03	0.02	0.19	0.09	0.02	0.01	0.02	0.13	0.03	0.04	0.02	1.13	
NTB2015-576	artifact	65.20	0.44	0.19	10.25	10.66	0.39	0.04	0.71	8.58	4.45	0.49	0.30	101.00	
N12E00	5	0.90	0.03	0.03	0.25	0.21	0.02	0.01	0.02	0.19	0.10	0.05	0.02	0.61	
NTB2015-577	artifact	63.82	0.44	0.24	9.84	10.75	0.38	0.06	0.74	8.59	4.38	0.47	0.30	100.55	
N11W02	5	1.76	0.04	0.04	0.23	0.21	0.02	0.01	0.02	0.20	0.09	0.03	0.02	1.24	
NTB2015-578	artifact	62.70	0.43	0.19	9.45	10.80	0.38	0.07	0.70	8.80	4.42	0.57	0.29	100.03	
N12E02	5	1.74	0.04	0.05	0.25	0.06	0.03	0.01	0.02	0.16	0.03	0.08	0.02	1.32	
NTB2015-579	artifact	63.82	0.42	0.16	9.74	10.78	0.39	0.09	0.72	8.72	4.48	0.51	0.29	100.66	
N12W01	5	0.66	0.03	0.04	0.16	0.15	0.01	0.01	0.03	0.15	0.12	0.04	0.01	0.56	
NTB2015-580	artifact	65.05	0.41	0.18	9.76	10.73	0.36	0.12	0.72	8.72	4.45	0.51	0.30	101.30	
N12W02	5	0.73	0.05	0.05	0.31	0.21	0.02	0.02	0.03	0.18	0.13	0.06	0.02	0.48	
NTB2015-581	artifact	64.80	0.42	0.17	9.59	9.64	0.36	0.19	0.72	8.71	4.50	0.50	0.29	101.12	
N13E01	5	0.46	0.02	0.03	0.17	0.13	0.04	0.03	0.01	0.13	0.02	0.03	0.02	0.24	
NTB2015-582	artifact	64.57	0.42	0.19	9.96	9.39	0.36	0.29	0.70	8.75	4.44	0.40	0.27	101.21	
N10W01	5	0.69	0.06	0.05	0.75	0.73	0.05	0.03	0.06	0.09	0.15	0.12	0.04	0.67	
NTB2015-585	artifact	63.87	0.44	0.21	9.81	9.76	0.40	0.32	0.74	8.71	4.52	0.51	0.29	101.33	
N09E06	5	0.93	0.02	0.01	0.47	0.05	0.04	0.16	0.02	0.13	0.05	0.03	0.02	0.61	

The SSRS obsidian type #2 rhyolite matches several samples from Eburru, Ilkek (Brown et al., 2013), a source located ~140 km south of the SSRS in the region just north of Lake Naivasha (Table 8; Figs. 14b, c, d). Only a single flake fragment recovered from the west trench of the SSRS in square N14W19 (Fig. 6a) matched this rhyolitic composition. None of the SSRS obsidian cores match the chemistry of this distant source.

The SSRS obsidian type #3 trachyte matches the composition of a source sampled from the area of Olagirasha on the western Mau escarpment of the Kenyan rift (Table 8; Fig. 14b, c, d; Brown et al., 2013; Merrick and Brown, 1984; Merrick et al., 1994). Most obsidian material sampled from the SSRS (118 analyses from 24 samples) match this source including multiple samples from each of the three obsidian patches in the main trench of the SSRS and all of the sampled debitage dispersed throughout the main trench of the site (Fig. 6 a, b). One single preferential flake Levallois core (Fig. 11c) and two preparation flake refits from its debitage surface (Fig. 12c) are of SSRS type #3 indicating that this obsidian was partially decortified, prepared, flaked and discarded on the site.

3) Reduction intensity:

	NTB2014-348t (0.86)	MER 70 (0.89)	MER 59 (0.93)
NTB2014-348t		0.67	0.79
NTB2014-351t	0.88	0.62	0.73
NTB2014-354	0.93	0.71	0.81
NTB2014-348o	0.95	0.65	0.80
NTB2014-380	0.95	0.65	0.80
NTB2014-381	0.96	0.65	0.81
NTB2015-583	0.94	0.64	0.78
MER 70	0.67		0.76
K80-403	0.66	0.94	0.74
MER 71	0.66	0.96	0.74
NTB2014-313	0.67	0.95	0.74
MER 59	0.79	0.76	
NTB2013-314	0.80	0.75	0.97
NTB2013-315	0.80	0.74	0.96
NTB2013-316	0.79	0.75	0.97
NTB2014-379	0.79	0.76	0.97
NTB2014-382	0.78	0.76	0.96
NTB2015-565	0.77	0.75	0.96
NTB2015-566	0.79	0.74	0.96
NTB2015-567	0.79	0.74	0.96
NTB2015-568	0.78	0.75	0.96
NTB2015-569	0.78	0.74	0.96
NTB2015-570	0.78	0.75	0.96
NTB2015-571	0.79	0.76	0.97
NTB2015-572	0.79	0.74	0.96
NTB2015-573	0.77	0.76	0.97
NTB2015-574	0.79	0.74	0.96
NTB2015-575	0.79	0.74	0.97
NTB2015-576	0.78	0.75	0.97
NTB2015-577	0.78	0.74	0.96
NTB2015-578	0.78	0.75	0.96
NTB2015-579	0.78	0.75	0.96
NTB2015-580	0.77	0.76	0.97
NTB2015-581	0.78	0.77	0.98
NTB2015-582	0.79	0.76	0.97
NTB2015-585	0.79	0.75	0.97

Table 8: Similarity coefficients for three obsidian compositional groups based on nine-element list (after Blegen et al., 2015:100). Samples listed vertically (left); compared with type sample (from source) of every chemically unique composition listed horizontally (top). Lower 95% confidence limit for each type sample in parentheses. Shaded squares are samples or modes with similarity coefficient  $\geq$  the 95% lower confidence limit determined by randomization when compared to the type sample and overlap at two standard deviations for the seven element oxides used for correlation when compared to the type sample. Black squares are the type sample compared to itself.

Both measures of reduction intensity show that obsidian was flaked more intensively than locally available raw materials at the SSRS (Table 9; Figure 15). In fact, according to both metrics, the SSRS obsidian is more intensively reduced than all raw material categories represented in comparable eMSA lithic assemblages in East Africa (Table 9, Fig. 14; Sahle et al., 2014; Shea, 2008; Tryon, 2003). The SSRS differs from all other East African eMSA sites in its use of non-local obsidian and the intensity of its reduction compared to locally available raw materials at other eMSA sites. Intensive reduction of obsidian at the SRSS is confirmed by significantly

smaller mean dimensions (lengths, widths and thicknesses) of SSRS obsidian flakes versus flakes made on locally available raw materials (Table 9; Fig. 15). More intensive reduction of different raw materials at different sites correlate with significantly smaller flakes that are shorter in length, narrower in width, thinner in thickness, narrower in platform width and thinner in platform thickness (Table 9; Fig. 16).

#### Discussion:

##### 1) SSRS obsidian artifact chemistry and sourcing:

Long distances obsidian transport as well as the significant quantity of obsidian at the SSRS shows that eMSA transport distances are different from those in ESA contexts. Further, the long raw material transport distances and large quantity of nonlocal obsidian raw material at the SSRS is only comparable to very Late Pleistocene (<50 ka) MSA assemblages in East Africa (Ambrose, 2012; Merrick et al., 1994). In general, raw material transport distances in the eMSA are similar to earlier ESA contexts. However, transport distances up to 166 km for SSRS obsidians are significantly farther than for obsidian artifacts in contemporary ESA or earlier Middle Pleistocene Acheulean contexts in East Africa (Ambrose, 2012; Merrick and Brown, 1984; Merrick et al., 1994; Negash and Shackley, 2006; Negash et al., 2006). The significant proportion of obsidi-

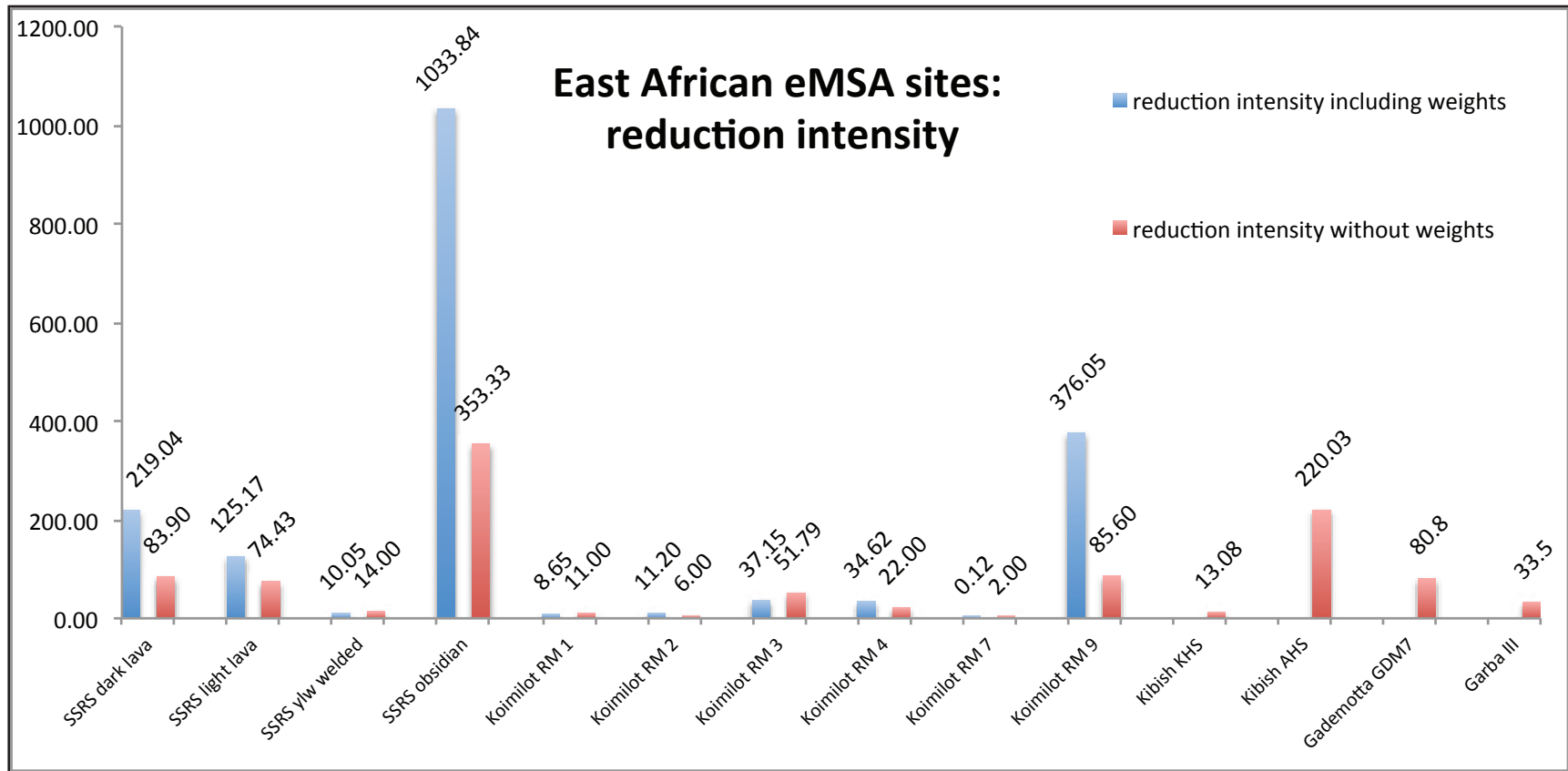


Figure 15: Reduction intensity of East African eMSA sites calculated with measured weights (in blue) for all possible raw material categories from the SSRS and Koimilot Locus 1 in the Kapthurin Formation and without measured weights (in red) for the above as well as sites not reporting this metric. Data from Koimilot (Tryon, 2003); Kibish Formation (Shea, 2008); Gademotta Formation GDM7 (Sahle et al., 2014) and Garba III (Mussi et al., 2013).

Table 9: Data for reduction intensity of East African eMSA sites calculated with measured weights for all possible raw material categories from the SSRS and Koimilot Locus 1 in the Kapthurin Formation and without measured weights for the above as well as eMSA Kibish Formation sites and Gademotta Formation sites not reporting this metric. Mean flake metrics for all the above raw materials and sites. Data from: Koimilot (Tryon, 2003); Kibish Formation (Shea, 2008); Gademotta Formation (Sahle et al., 2014); Garba III (Mussi et al., 2014).

	SSRS dark lava	SSRS light lava	SSRS ylw welded tuff	SSRS obsidian	KLT RM 1	KLT RM 2	KLT RM 3	KLT RM 4	KLT RM 7	KLT RM 9	Kibish KHS	Kibish AHS	GDM7	Garba III	flake metrics vs. reduction intensity (Fig. 16) pearson r value	flake metric vs reduction intensity (Fig. 16) p value
core+ core frags (n)	10	7	3	3	1	1	14	1	2	5	24	35	4848	4		
core+ core frags (wt in g)	3260.4	3673.19	895.52	120.07	84.76	19.8	5725.76	61.39	1825	607.74						
debris+ deb- itage (n)	839	521	42	1060	11	4	477.94	15.87	4	251	314	7701	60	134		
debris+ deb- itage (wt in g)	8512.09	6177.62	643.003	351.32	66.64	36.96	2690.4	47.45	125.57	1723.72						
reduction intensity (w/ out wt)	83.90	74.43	14.00	353.33	11.00	4.00	34.14	15.87	2.00	50.20	13.08	220.03	80.8	33.50		
reduction in- tensity (w/ wt)	219.04	125.17	10.05	1033.84	8.65	7.47	16.04	12.27	0.14	142.38						
mean flake length (mm)	35.65	32.62	52.10	15.88			39.00			40.20	42.00	30.00	44.86	64.60	-0.89	0.008
mean flake width (mm)	32.41	27.47	37.98	15.85			29.00			30.80	31.00	25.00	29.15	57.70	-0.90	0.049
mean flake thick (mm)	10.51	8.77	15.26	4.84			8.90			7.90	10.00	5.00	8.83		-0.75	0.019
mean plat width	22.49	17.80	28.76	11.63			19.30			20.50	22.00	18.00	19.12		-0.78	0.012
mean plat thick	9.16	6.80	12.31	3.98			6.50			6.20	7.00	4.00	7.81		-0.67	0.047



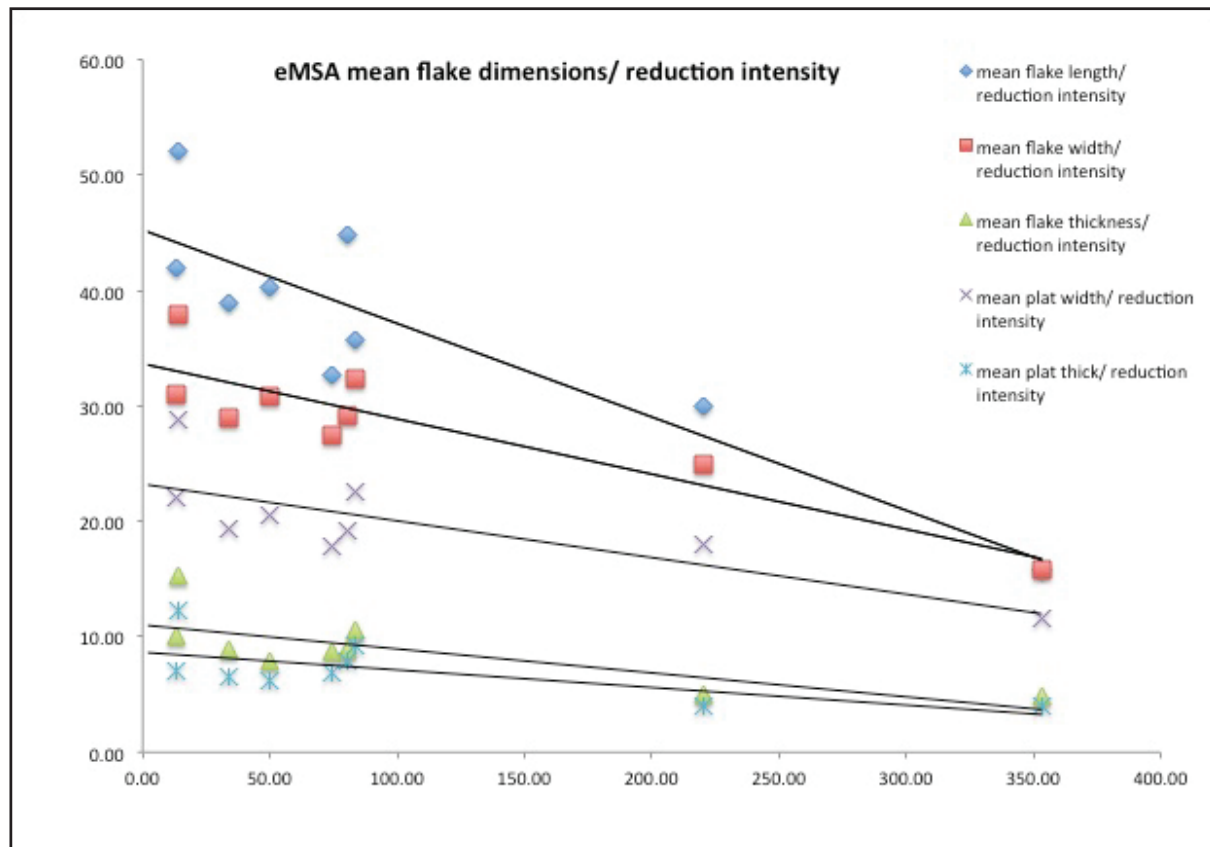


Figure 16: Scatter plot of flake dimension (length, width and thickness) measured in millimeters) over reduction intensity (see Table 9; Figure 14) for nine raw material groups from five East African eMSA sites discussed in this study for which appropriate data was available. Data from Kibish Formation sites KHS and AHS (Shea, 2008), Gademotta GD7A (Sahle et al., 2014) and Koimilot Locus 1 RM 3 and RM 9 (Tryon, 2003).

an lithic material at the SSRS demonstrates long distance obsidian transport in the eMSA of East Africa (Ambrose, 2012). At the SSRS 43% of the lithic assemblage by individual pieces and 6% by weight is obsidian (Fig. 8). Of the 29 obsidian pieces sampled from the site, the composition of the vast majority, 25 samples, match the source near Olagirasha (Table 7). The only sampled obsidian pieces that did not come from Olagirasha are a single ~1 cm piece of angular waste from the western trench that is chemically similar to the source from Eburru, Ilkek and three samples (2 cores and a flake) from the main trench that were chemically sourced to Karau. The

obsidian from Karau is macroscopically distinguishable by a matte black patina on old flaked surfaces. The other 25 obsidian samples from 16 separate 1x1 m<sup>2</sup> units of the main trench where obsidian was found were compositionally matched to Olagirasha. Because of the macroscopically distinguishing characteristics of the Karau obsidian as well as the preponderance of pieces chemically sourced to Olagirasha, the vast majority of obsidian at the SSRS, including a specifically sourced small Levallois core (sample= NTB2014-382) derives from Olagirasha. Subtracting the four individual pieces at the SSRS shown to be from sources other than Olagirasha (2 cores + 2 flakes= 356.96g) the SSRS total lithic assemblage is constituted of 43% Olagirasha obsidian by individual pieces and 4.4% Olagirasha obsidian by weight. The obsidian component of the SSRS lithic assemblage is thus composed of 99.5% Olagirasha obsidian by individual pieces and 75.7% Olagirasha obsidian by weight.

The large proportion of obsidian at the SSRS differs markedly from the rare appearance of obsidian Muguruk, Songhor, Karungu, Mumba and Nasera (Faith et al., 2015; McBrearty, 1986; Mehlman, 1977; Merrick and Brown, 1984; Merrick et al., 1994). Instead, SSRS Olagirasha obsidian is represented in similar proportions and transported similar distances as the obsidian from the MSA assemblages from Lukenya Hill. This includes GvJm-16 where 8.4% of the assemblage by individual pieces is obsidian and 58% percent of this obsidian (~5% of the total lithic

assemblage) originated from a variety of central rift sources located 65 –130 km from the site (Ambrose, 2012; Merrick et al., 1994). While undated, the MSA sites of Lukenya Hill including GvJm-16 are certainly Late Pleistocene and probably < 50 ka (Tryon et al., 2015) more than 150 kyr younger than the SSRS.

## 2) SSRS and East African eMSA whole assemblage comparisons:

Assemblage comparisons between the SSRS and other relevant East African eMSA sites from the Kapthurin, Kibish and Gademotta Formations show that greater intensity of reduction is correlated with reduced flake size. Further, the greatest reduction intensity and smallest corresponding flake dimensions in the eMSA data set present here is the SSRS obsidian, the raw material demonstrating the highest obsidian raw material transport distances in the eMSA of East Africa. Thus, data from the SSRS suggest long distance raw material transport in the East African eMSA had a substantial effect on raw material economy and the dimensions of stone tools produced.

The difference in reduction intensity and corresponding flake sizes of knapping products identified in eMSA assemblages including the SSRS are best explained as a function of raw material transport distances. This phenomenon cannot be explained as a function of raw material compo-

sition as multiple eMSA sites in the Kibish Formation (KHS and AHS) employ the same suite of cherts and basalts yet produce significantly different values of reduction intensity (Shea, 2008; Table 9; Fig. 15). The site of KHS in the Kibish Formation and MSA sites in the Kapthurin Formation show very similar levels of reduction intensity despite compositional differences in raw material (Fig. 15). Additionally, comparisons between obsidians at the SSRS and Gademotta GDM7 control for lithological variation in raw material and show that differences in reduction intensity and the size of intended knapping products at the SSRS and contemporaneous eMSA sites are a product of greater obsidian transport distance at the SSRS. Raw material transport distances differ significantly between the SSRS and GDM7, Gademotta. While SSRS obsidians are nonlocal (see above), the Worja obsidian used as raw material at GDM7, Gademotta (94.1% of the total assemblage) derives from < 5km away (Negash and Shackley, 2006; Negash et al., 2006; Sahle et al., 2014). Non-local obsidians at the SSRS are more intensely reduced (Table 9; Fig. 15) resulting in obsidian flakes that are almost one-third of the length (SSRS mean obsidian flake length= 15.88) of GDM7 obsidian flakes (GDM7 mean flake length= 44.86, t-value=17.7168;  $p < 0.001$ ) on average. Gademotta GDM7 flakes are also significantly larger in all other measured dimensions (see Table 10). Chi-squared tests on the reduction intensity ratios for locally available GDM7 obsidian compared to locally available lava raw materials at the SSRS

Table 10: Chi-squared test of reduction intensity values for SSRS locally available lavas, nonlocal obsidian, Koimilot locally available lavas and Gademotta GDM7 local obsidian.

		Koimilot Locus 1	GDM7 obsidian	SSRS local lavas	SSRS obsidian
	reduction intensitty	116.56	91.46	96.43	353.33
Koimilot Locus 1	116.56		0.08	0.17	<0.001
GDM7 obsidian	91.46	0.08		0.72	<0.001
SSRS local lavas	96.43	0.17	0.72		<0.001
SSRS obsidian	353.33	<0.001	<0.001	<0.001	

and Koimilot Locus 1 are statistically indistinguishable whereas the difference in reduction intensity of nonlocal SSRS obsidian and all other compared categories is highly significant ( $p < 0.001$ ; Table 9).

While obsidian is the only raw material that can be geochemically identified to source in East Africa, it is almost certainly not the only raw material that was transported distances greater than the 40 km defined as the radius for the average human foraging home range (Ambrose, 2012; Gamble, 1993; Kelly, 1995). Other fine-grained, high quality raw materials in East Africa such as chert may have been transported significant distances and reduced more intensely to produce correspondingly smaller flakes. This may be the case at Awoke's Hominid Site (AHS) in Member

I of the Kibish Formation where chert comprises a significant portion of the raw material. The presence of intensively reduced chert cores and smaller chert flakes also fit the pattern identified here (Table 9; Figs. 15, 16; Shea, 2008).

Raw material transport distance clearly has importance for explaining aspects of technological variation through the later Middle and Early Late Pleistocene MSA. The comparative obsidian source data available from the Middle Pleistocene ESA and eMSA through the Late Pleistocene MSA suggests that maximum transport distance increases through time (Merrick and Brown, 1984; Merrick et al., 1994). The size of flake products is a salient difference between Acheulean and MSA technologies (Tryon et al., 2005). Statistical correlation between raw material transport distance and flake dimensions cannot be demonstrated here the eMSA because only two data points (Gademotta and the SSRS) exist. However, if the trend of increasing transport distances, greater reduction intensity and diminished flake dimensions identified here holds true for a larger number of sites over a longer time period in the East African Middle and Late Pleistocene, it may be a significant factor explaining the disappearance of large flakes and tools characteristic of the Acheulean as well as the gradual process in which these tools are replaced by smaller and more diverse tools and technologies of the MSA (Tryon, 2003; Tryon and McBrearty, 2002; Tryon and

McBrearty, 2006).

#### Conclusion:

Excavations and artifact analyses at the SSRS, Kapthurin Formation, Baringo provides new evidence of early MSA lithic technology in a well-dated later Middle Pleistocene context between 196 and 226 ka. MSA material at the SSRS includes Levallois points and cores showing diverse methods of Levallois core preparation. Geochemical characterization of obsidian artifacts at the site shows three distinct compositions. Correlation of SSRS obsidian compositions to sources shows straight-line site to source obsidian raw material transport distances of 166 km for the majority of the obsidian at the SSRS. Comparison with eMSA assemblages throughout East Africa including the SSRS suggest that eMSA hominins economized long distance raw material transportation by increasing reduction intensity, which, in turn, significantly reduced flake dimensions. Thus, despite the limited availability of later Middle Pleistocene archaeological sites of the East African eMSA, it appears that long distance transport of high quality raw materials was a feature of eMSA hominin behavior in East Africa ~200 ka, the same time *Homo sapiens* first appears in the region. Furthermore, the effect of long distance raw material transport on reduction may suggest long distance raw material transport, whether because of increase mobil-

ity, trade desire for high quality raw material or some combination of the above, is a significant factor explaining the decline of the large-flake Acheulean and emergence of MSA technologies surrounding the emergence of *Homo sapiens*.



Paper #4

The East African Middle Stone Age at <50,000 years ago: Evidence from Nyamita Main (GrJa-3), Rusinga Island, western Kenya.

Nick Blegen\*

Department of Anthropology

University of Connecticut

Storrs, CT 06269, USA

E-mail: [nicholas.blegen@uconn.edu](mailto:nicholas.blegen@uconn.edu); [nick.blegen@gmail.com](mailto:nick.blegen@gmail.com)

J. Tyler Faith

School of Social Science

University of Queensland

Brisbane, QLD 4072, Australia

E-mail: [j.faith@uq.edu.au](mailto:j.faith@uq.edu.au)

Daniel J. Peppe

Terrestrial Paleoclimatology Research Group

Department of Geology

Baylor University

Waco, TX 76706, USA

E-mail: [daniel\\_peppe@baylor.edu](mailto:daniel_peppe@baylor.edu)

Christian A. Tryon

Department of Anthropology

Harvard University

Cambridge, MA 02138, USA

E-mail: [christiantryon@fas.harvard.edu](mailto:christiantryon@fas.harvard.edu)

## Abstract:

The Late Pleistocene of equatorial East Africa is important for understanding the evolution and dispersal of *Homo sapiens*. A conspicuous behavioral aspect of this period is the disappearance of Middle Stone Age (MSA) technology, after persisting for > 250 kyr throughout Africa, and its replacement by stone tools characteristic of the Later Stone Age (LSA). In recent years, the Late Pleistocene exposures of the eastern margin of the Lake Victoria basin have provided abundant data with which to investigate this transition. We add to this by reporting on excavations from the Late Pleistocene site of Nyamita Main from the upper Wasiriya beds (>33-49 ka) of the Nyamita Valley, Rusinga Island in the eastern Lake Victoria Basin of western Kenya. This as well as previous archaeological and chronological work on the Late Pleistocene of the eastern Lake Victoria Basin provides definitive evidence of MSA technology in equatorial East Africa chronologically younger than the appearance of LSA technology elsewhere in East Africa. The late persistence of the MSA at Nyamita Main and the eastern Lake Victoria basin suggests geographic variation in the nature and timing of the MSA-LSA transition comparable to that seen in southern Africa. We evaluate two hypotheses related to the temporal and spatial variability in the MSA/LSA transition across equatorial East Africa: 1) MSA and LSA technologies cannot represent different geographically and culturally isolated groups and 2) MSA and LSA technologies represent different

activities of the same hominin group or groups.

#### Introduction:

The behavioral context of hominin evolution in the East African Late Pleistocene is essential to understand the unique evolutionary trajectory of *Homo sapiens*. Fossil evidence shows that *Homo sapiens* was present in East Africa by the end of the Middle Pleistocene. The earliest specimens of our species date to 195 ka in the Kibish Formation of southern Ethiopia and between 154 –160 ka in the upper Herto Member of the Bouri Formation in central Ethiopia (Clark et al., 2003; McDougall et al., 2005; White et al., 2003). East Africa was also likely significant for subsequent human dispersals across and out of Africa in the Late Pleistocene between 50 – 130 ka (Rose et al., 2011; Soares et al., 2011). One particularly conspicuous aspect of hominin behavior in the Late Pleistocene of Africa is the disappearance of Middle Stone Age (MSA) technology, characterized by points and prepared core technologies after existing in Africa for > 250 kyr and its replacement by Later Stone Age (LSA) materials characterized by microliths and bipolar reduction sometime between ~30 – 60 ka (Ambrose, 1998; Deino and McBrearty, 2002; Morgan and Renne, 2008; Sahle et al., 2013; Sahle et al., 2014; Wadley, 2001, 2015). Further, the first appearances of several behavioral innovations considered “modern” are associated with

MSA technology within this time period in Africa (Henshilwood et al., 2002; Marean et al., 2007; McBrearty and Brooks, 2000). The proliferation, longevity and adaptability of the MSA technology make the explanations for its replacement by LSA technology a matter of interest and debate. The behavioral and biological explanations for this event are undoubtedly complex and the chronological, archaeological, paleontological and paleoenvironmental records are imperfect. To link the MSA/ LSA transition to any of the above records as an explanation it is essential to understand the timing of the MSA/ LSA transition in the African Late Pleistocene with as much confidence and precision as possible.

Here we report excavations from the Late Pleistocene site of Nyamita Main from the upper Wasiriya beds (>33-49 ka) of the Nyamita Valley, Rusinga Island in the eastern Lake Victoria Basin of western Kenya. These excavations provide the largest excavated sample of in situ artifacts from the Late Pleistocene of the eastern Lake Victoria Basin. Together with previous archaeological and chronological work in the eastern Lake Victoria Basin this excavation provides definitive evidence of MSA technology in equatorial East Africa chronologically younger than the early appearance of LSA technology elsewhere in the region. The late persistence of the MSA at Nyamita Main and the eastern Lake Victoria basin suggests geographic variation in the nature

and timing of the MSA-LSA transition comparable to that seen in southern Africa.

Chronology of the latest MSA and earliest LSA in East Africa:

The latest occurrences of the MSA and earliest occurrences of the LSA are staggered throughout Africa. In southern Africa, MSA technology is known to persist as late as 28 ka at Rose Cottage Cave (Wadley, 2001). At Border Cave the MSA/ LSA transition has been placed at ~38 ka, based on  $^{14}\text{C}$  and amino acid racemization (AAR) dates on ostrich eggshell (Beaumont, 1978). ESR dates suggest that it was occupied as late as 28 – 31 ka with no apparent occupational hiatus.

However, more recent reports place the Border Cave MSA/LSA transition between 45 – 49 ka (Villa et al., 2012). In Equatorial East Africa the latest MSA and earliest LSA industries are conventionally placed somewhat earlier. Evidence from both northern Tanzania and the central Kenyan rift indicates that LSA and transitional MSA/LSA technologies are present by ~45–60 ka.

In northern Tanzania the MSA Kisele industry from Bed VI of Mumba rockshelter, the stratigraphically highest and chronologically youngest definitively MSA assemblage in the sequence, is dated to >65 ka based on U-series dates from the overlying Bed V and  $63.4 \pm 5.7 - 73.6 \pm 3.8$  ka based on quartz and feldspar OSL dates from Bed VI-A (Glisanic et al., 2012; Mehlman, 1989). Overlying the Kisele industry, the Mumba industry from Bed V of Mumba rockshelter

is variably characterized as “transitional” between MSA and LSA technologies, because of the presence of backed geometric microliths, bifacial and unifacial points and prepared cores (Mehlman, 1989), or an LSA industry (Diez-Martín et al., 2009; Eren et al., 2013). MSA elements were incorporated into the assemblage due to the excavation of vertically thick, arbitrary excavation spits (Diez-Martín et al., 2009; Prendergast et al., 2007). Bed V and the Mumba industry are dated to between 45-65 ka based on amino acid racemization of ostrich eggshell fragments (Kokis, 1988) and  $49.1 \pm 4.3 - 56.9 \pm 4.8$  ka based on quartz grain OSL dates (Gliganic et al., 2012). A similar industrial succession is found at Nasera rockshelter northern Tanzania, although the strata containing the Kisele and Mumba industries are undated there (Mehlman, 1977, 1989).

The Naisiusiu beds of Olduvai Gorge have produced LSA archaeological materials (Leakey et al., 1972). Initial dates suggested very late to terminal Pleistocene ages between  $10.4 \pm 0.6 - 17.5 \pm 1.0$  ka based on radiocarbon dates on bone (Hay, 1976; Leakey et al., 1972). Later AAR dates on bone of  $>42$  ka on the Naisuisui Beds are considerably older (Manega, 1995; Manega, 1993).

The most recent estimation of their age is  $62 \pm 5$  ka based on electron spin resonance (ESR) techniques performed on equid teeth found in an archaeological excavation, though ESR on another tooth from a different location within the Naisiusiu beds produced an age of  $39 \pm 5$  ka

(Skinner et al., 2003).

At Enkapune-ya-Muto (“Twilight Cave”) in the central Kenyan rift, calibrated radiocarbon ages (using CalPal) as old as  $44.51 \pm 0.9$  ka calBC are reported from the Endingi industry containing faceted platform triangular points and discoid cores characteristic of MSA assemblages as well as backed microliths characteristic of the LSA. Radiocarbon ages of the overlying Sakutiek industry, an early LSA industry based on the presence of backed crescent microliths has radiocarbon dates ranging from  $19.72 \pm 1.1$  –  $41.93 \pm 1.2$  ka calBC (Ambrose, 1998). Based on a combination of radiocarbon, obsidian hydration and sedimentation rates, the LSA of Enkapune-ya-Muto in the Naivasha region of the central Kenyan Rift is considered to have begun ~50 ka (Ambrose, 1998: 385).

Western Kenya and the eastern Lake Victoria Basin:

Archaeological work on Pleistocene sediments in the Nyanza Province of western Kenya extends back to the beginning of the twentieth century, with early study of MSA materials by the Archdeacon W.E. Owen (Owen, 1939; Owen, 1937, 1938), at times in collaboration with L.S.B. Leakey (Leakey and Owen, 1945). Creighton Gabel (1969) excavated a series of rockshelters

along the Winam Gulf, one of which, Randhore, sampled undated strata attributed to the MSA.

McBrearty conducted modern excavations of Sangoan and MSA materials at Muguruk (Mc-

Brearty, 1986) and MSA material in the Pleistocene sediments of Songhor (McBrearty, 1981).

Recent work in the eastern Lake Victoria Basin including the Nyamita Main excavation presented here expands on these pioneering excavations (e.g. Faith et al., 2015).

The site of Nyamita Main in the Nyamita Valley is part of the Wasiriya beds of Rusinga Island.

The Wasiriya beds are part of a series of Late Pleistocene sediments that crop out on Rusinga

Island, Mfangano Island and at several localities near Karungu on the Kenyan mainland, which

we informally refer to as the eastern margin of Lake Victoria Basin (eLVB) (Fig. 1; Beverly et

al., 2015a; Beverly et al., 2015b; Blegen et al., 2015; Faith et al., 2015; MacInnes, 1956; Tryon

et al., 2010; Tryon et al., 2014; Tryon et al., 2012; Van Plantinga, 2011). We review the related

geological, paleontological and archaeological work of the eLVB, the Wasiriya beds and the site

of Nyamita Main in order of increasing specificity below.

Geology and chronology:



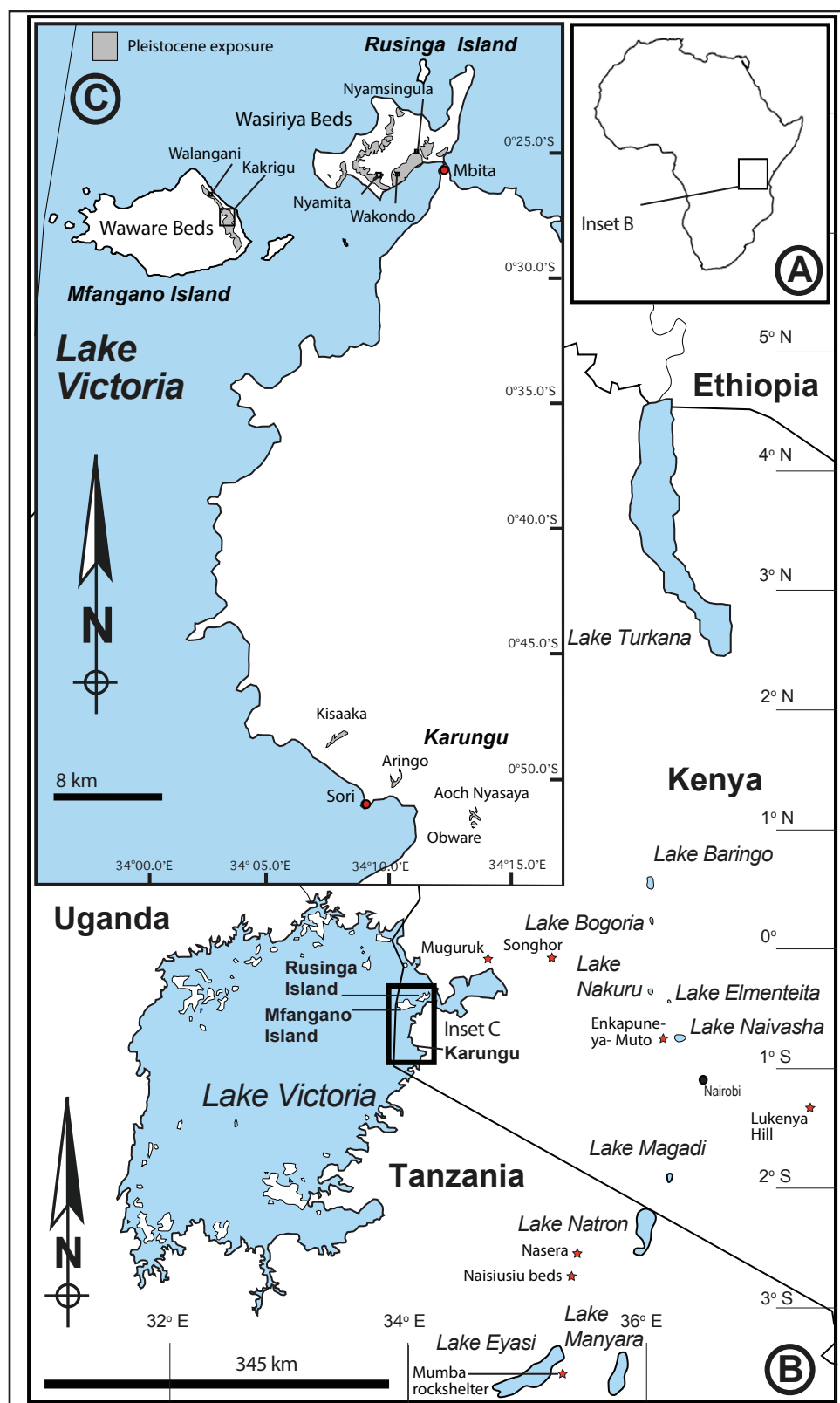


Figure 1: A. Map of East African focused Lake Victoria and eastern (Kenyan) rift region. C. Map of approximate area of the eastern Lake Victoria Basin (eLVB) referenced in this study. This includes Rusinga Island, Mfangano Island, and Karungu with localities with Late Pleistocene exposure labeled by name and marked in grey.

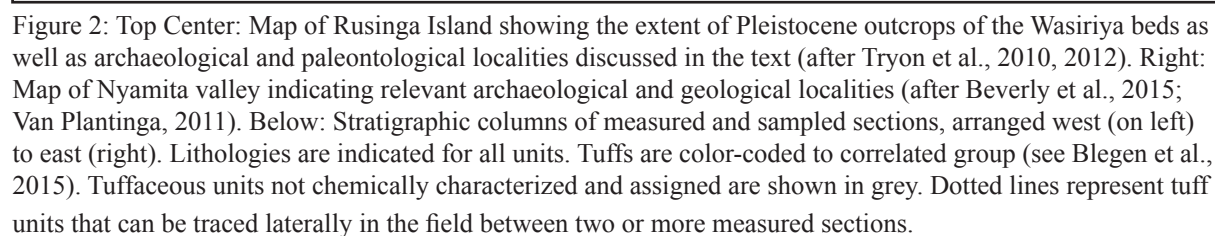
The eastern Lake Victoria Basin:

The eLVB constitutes the northeastern margin of the Lake Victoria Basin in equatorial East Africa (Fig. 1). This basin formed in the depression between the eastern and western branches of the East African Rift System (EARS), probably within the last few million years (see Danley et al., 2012 and refs therein). During the Late Pleistocene, the eLVB formed a repository for sediments, including volcanoclastic deposits from eruptions originating from sources outside of the basin in the eastern branch of the EARS. Late Pleistocene tephras are correlated over a ~60 km north-south transect between Rusinga Island, Mfangano Island and Karungu on the Kenyan mainland (Blegen et al., 2015) and this tephrostratigraphy as well as lithostratigraphic and chemical characterization of the paleosols between the tephras (Beverly et al., 2015a; Beverly et al., 2015b) indicate that in the eLVB, the same stratigraphic sequence is discontinuously preserved over hundreds of square kilometers. The Late Pleistocene exposures of the basin currently include the Wasiriya beds of Rusinga Island, the Waware beds of Mfangano Island, and the Pleistocene exposures of Karungu on the Kenyan mainland (Fig. 1c). Preliminary surveys have also found the same stratigraphic sequence of eLVB deposits at several other locations around the Winam Gulf. The Late Pleistocene of the eLVB thus constitutes a laterally extensive stratigraphic sequence of Late Pleistocene exposures encompassing >120 km<sup>2</sup>, and as detailed below, preserves different

depositional environments along the eastern shore of modern Lake Victoria.

The Wasiriya beds of Rusinga Island:

The Wasiriya beds are exposed over an area of approximately 10 km<sup>2</sup> on the hill slopes around Rusinga Island (Fig. 2; Tryon et al., 2010). These sediments were informally named by Pickford (1984) based on previous mapping and descriptions (Kent, 1942; Van Couvering, 1972). The first measured sections and sedimentary lithological descriptions of the Wasiriya beds were reported by Tryon et al. (2010, 2012) and expanded in recent related studies (Beverly et al., 2015b; Blegen et al., 2015; Garrett et al., 2015; Van Plantinga, 2011). The Wasiriya beds are exposed in sections that are up to ~18 m at their thickest points, and are primarily comprised of four distinct lithologies: 1) poorly sorted coarse sand and gravel channels cemented by carbonate representing episodic channel erosion and deposition, 2) fine grained mudstone, siltstone, and silty sandstone preserving evidence of incipient soil development indicating a more stable landscape, 3) tephra preserved as both primary fall-out deposits and tuffs that have undergone varying amounts of reworking and incipient pedogenesis, and 4) tufa deposits made primarily of calcium carbonate indicating the presence of springs and small ponded areas on the landscape (Beverly et al., 2015b; Tryon et al., 2010).



The site of Nyamita Main is located in the Nyamita Valley, Rusinga Island where Late Pleistocene exposures reach up to ~18m, attaining their maximum thickness on the island and disconformably overlying and draping well-consolidated early Miocene sediments (Fig. 3d; Van





Figure 3: A) Late Pleistocene barrage tufa at base of Nyamita Valley (Beverly et al., 2015b). B) Modern spring in Nyamita Valley. C) Close-up of spring showing presence of perennial fresh water. D) Photograph (looking ~southwest) at 2009 excavations at Nyamita Main. Note the Late Pleistocene fluvial sediments unconformably overlying more consolidated, variegated and tilted early Miocene sediments.

Plantinga, 2011). The fairly continuous Late Pleistocene exposures of this valley can be stratigraphically correlated to one another and to the larger stratigraphic and chronological framework of the eLVB with a high degree of accuracy and confidence through a continuing program of tepthrostratigraphy (Blegen et al., 2015; Tryon et al., 2010; Van Plantinga, 2011). The Nyamita Valley also preserves multiple exposures of tufa at the base of the sequence documenting the presence of one or more spring features (Beverly et al., 2015b) which persist today (Fig. 3). Tufa deriving from this spring ceased forming in the Late Pleistocene, but this spring exists today and has likely existed fairly continuously from the Late Pleistocene through the present providing a source of fresh water. The name “Nyamita” refers to a place with ever-present fresh water in the local Suba dialect of Luo people on Rusinga Island.

In the Nyamita Valley the base of the Wasiriya beds exposure is ~100 ka (Fig. 2; Beverly et al., 2015b). The phonolitic Wakondo Tuff, which was hypothesized by Tryon et al. (2010) to derive from the eruption of Longonot or Suswa dated to  $100 \pm 10$  ka (Baker et al., 1988), is near the base of the Nyamita Valley stratigraphic sequence and has been used to correlate these exposures to other deposits of the Wasiriya beds across Rusinga (Blegen et al., 2015; Tryon et al., 2010; Van Plantinga, 2011). Dates of 94 –111 ka on a tufa underlying the Wakondo Tuff at Nyamita

provide additional support for this age estimate. The most common stratigraphic marker in the Nyamita Valley is the Nyamita Tuff, which is exposed and chemically correlated throughout the valley, and also to the majority of Late Pleistocene exposures examined in eLVB (Blegen et al., 2015; Tryon et al., 2010; Van Plantinga, 2011). At section Nyamita 2 in the Nyamita Valley optically stimulated luminescence (OSL) dates bracketing the Nyamita Tuff provide ages of  $46 \pm 4$  ka and  $50 \pm 4$  ka above and below the tuff respectively, indicating the tephra was deposited  $\sim 49$  ka (Fig. 2; Blegen et al., 2015). The minimum age of the Wasiriya beds in the Nyamita Valley is  $>33$ - $45$  ka based on AMS  $^{14}\text{C}$  dates on gastropods that post-depositionally burrowed into the Nyamita Tuff and surrounding sediments at the Nyamita 2 and Nyamita 3 localities (Blegen et al., 2015; Tryon et al., 2010; Tryon et al., 2012). Based on our interpretation that the snails burrowed into the Wasiriya beds following deposition of the sediment, but prior to lithification, their dates provide a radiometric minimum age for the eLVB deposits. In the Nyamita Valley the absence of widespread tephras stratigraphically higher than the Nyamita Tuff is conspicuous (Blegen et al., 2015). At least two tuffs are widely encountered throughout the Late Pleistocene exposures of the eLVB stratigraphically above the Nyamita Tuff (Blegen et al., 2015). The complete absence of these tuffs in the Nyamita Valley may suggest the Late Pleistocene sediments preserved in this valley predate the tephras found stratigraphically above the Nyamita Tuff else-

where in the eLVB. Thus, the age of the Nyamita Valley exposures and the artifacts and fossils contained therein may be closer in age to the ~49 ka date of the Nyamita Tuff, consistent with the maximum age for one of the fossil gastropods (45 ka).

The artifact and fossil-bearing exposure at Nyamita Main measure approximately 30m long by 15m wide by 0.5- 2.0m thick (Fig. 4). These artifact and fossil bearing sediments are all ~ 4 –5 m above the ~49 ka Nyamita Tuff at section Nyamita 1 (Fig. 2).

#### Paleontology of the Wasiriya beds:

Fauna from the eLVB and most localities in the Wasiriya beds are abundant and collectively constitute one of the largest and most diverse Late Pleistocene faunal assemblages in East Africa (Faith, 2014; Faith et al., 2012; Faith et al., 2014; Faith et al., 2015; Garrett et al., 2015; Tryon et al., 2012). The eLVB and the Wasiriya beds in general include both extinct and extant taxa . The majority of specimens indicate open, semi-arid grasslands distinct from the evergreen bushlands, woodlands, and forests historically found in the region and otherwise common (Faith et al., 2011; Faith et al., 2012; Faith et al., 2014; Faith et al., 2015; Garrett et al., 2015; Tryon et al., 2010; Tryon et al., 2012). The Nyamita Valley follows the general open-arid pattern seen in the rest of the eLVB (Tryon et al., 2010). However the area of Nyamita Main is an exception in that this lo-



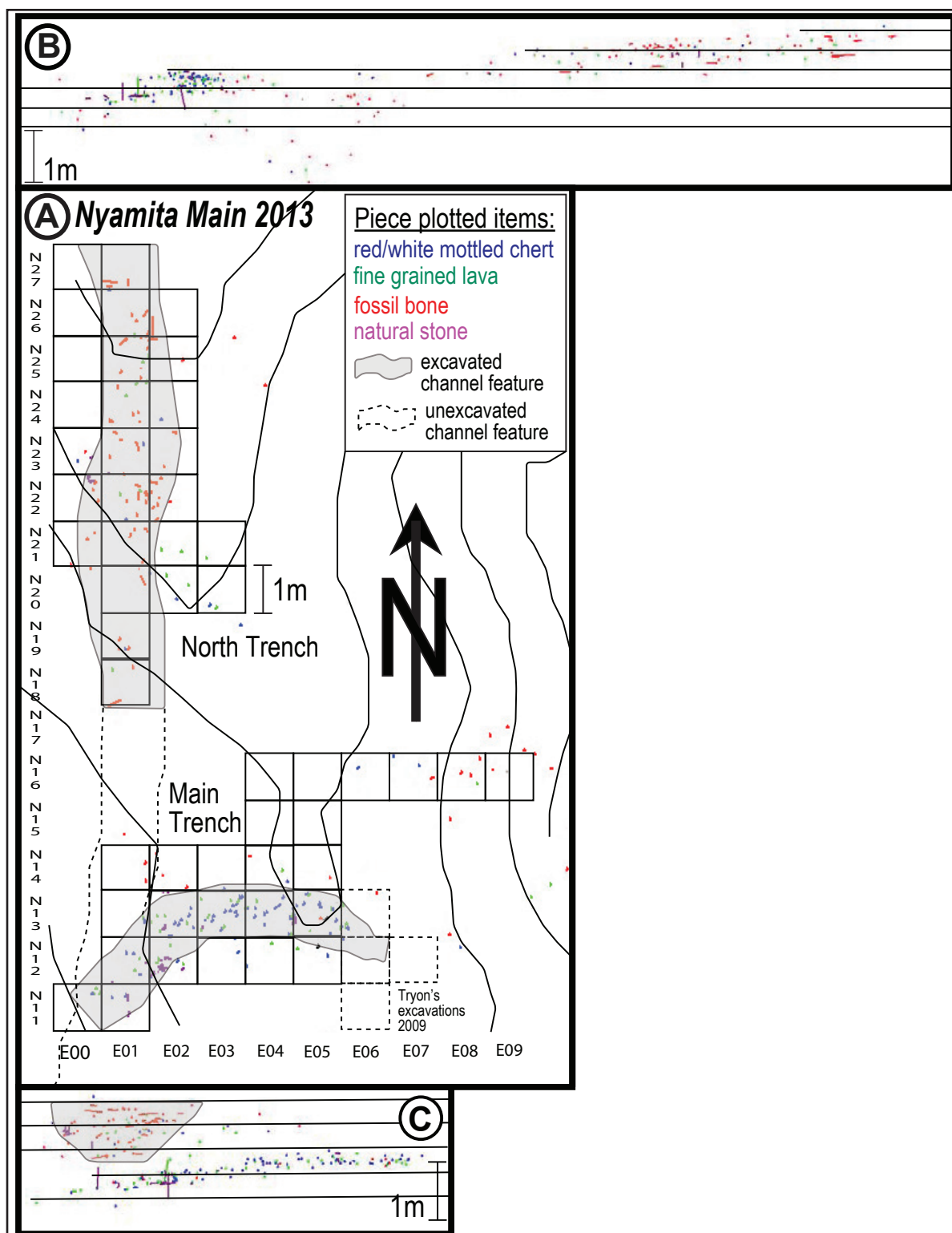


Figure 4: A) Plan map of Nyamita Main 2013 excavation with piece-plotted lithic artifacts sorted by raw materials, fossil bones/teeth, and natural rock color-coded by category. B) Side cross-section of Nyamita Main 2013 excavation (looking west) with piece-plotted lithic artifacts sorted as before. C) Front cross-section (looking north) of Nyamita Main 2013 excavation with piece-plotted lithic artifacts sorted as before.

cality exhibits greater species diversity. In addition to taxa with open-habitat preferences such as *Rusingoryx atopocranium*, *Damaliscus hypsodon* and zebra (*Equus grevyi*) found throughout the Nyamita landscape, Nyamita Main has produced reedbucks (*Redunca redunca*), duikers (*Sylvicapra grimmia*), bushbuck (*Tragelaphus scriptus*), impala (*Aepyceros* sp. nov.), and hippos (*Hippopotamus amphibius*), all fauna associated with leafy cover and trees. Water-dependent taxa such as hippopotamus indicate standing water in the vicinity and it may be that the spring served as a magnet for faunas in the area by providing fresh water and also supporting vegetation cover that favor taxa rarely found in other parts of Nyamita Valley or the eLVB. Isotopic reconstructions of Wasiriya beds paleosols also suggested the Nyamita Valley may have been characterized by ~46–82 % leafy cover, more than other parts of the Wasiriya and Waware beds (Garrett et al., 2015).

#### Archaeology of the eastern Lake Victoria Basin:

Stone artifacts reported from the eLVB are typologically and technologically characteristic of the Late Pleistocene MSA in East Africa (Faith et al., 2015; Tryon et al., in press; Tryon et al., 2010; Tryon et al., 2012). Levallois cores of both the recurrent and preferential methods and Levallois points as well as bifacial and unifacial, trimmed points are found in the Wasiriya beds of Rusinga

Island Tryon et al. (2010; 2012, 2014). Artifact collections from the surface of the Waware beds on Mfangano Island lack Levallois core technology in this small sample ( $n=12$ ), but contain bifacial points and can be also attributed to the MSA (Blegen et al., 2015; Tryon et al., 2012). The archaeology of Karungu is indistinguishable from that of the Wasiriya beds of Rusinga Island, including Levallois technology, as well as bifacial and unifacial points (Faith et al., 2015).

Four excavations have previously been conducted at three localities in the eLVB. One of these, Aringo 3, is a small 1 x 3m test excavation at the locality of Aringo, Karungu that recovered artifacts from a gravel channel near a tufa-cemented conglomerate indicative of the presence of a paleo-spring, found at the base of a large ~2-m-thick paleosol that is below the Nyamita Tuff and thus  $> 49$  ka (Faith et al., 2015). The excavated sample includes Levallois points as well as preferential and recurrent Levallois cores. It also includes a 2.0 cm flake of obsidian chemically sourced to the Olkaria volcanic complex south of Lake Naivasha and 250 km east of Aringo 3. This obsidian, along with obsidian pieces from Nasera and Mumba rockshelters in northern Tanzania, currently constitutes the farthest site to source transport distances for any raw material in the MSA of East Africa (Ambrose, 2012; Brown et al., 2013; Faith et al., 2015; Merrick and Brown, 1984; Merrick et al., 1994).

Three localities in the Wasiriya beds of Rusinga Island have previously been excavated: two at Wakondo (including one at the Bovid Hill locality) and a single site, Nyamita Main, at Nyamita. All other excavations followed arbitrary 10cm levels. Excavations of Bovid Hill used 5mm and 2mm mesh. Excavations at Aringo 3 and Nyamita were sieved with 1/8" or finer wire mesh and piece-plotted all surface and excavated artifacts and fossils relative to a site datum. A single 4m<sup>2</sup> trench dug to an average depth of 0.7 m at Wakondo recovered nine artifacts in situ. Bovid Hill, the larger of the two excavations at Wakondo, is a series of excavations totaling 19 m<sup>2</sup> with an average depth of 0.50 m into small and shallow braided stream channels cutting into a paleosol occurring above the Wakondo Tuff. (Blegen et al., 2015; Jenkins et al., 2012; Tryon et al., 2010; Tryon et al., 2014). The sand from this braided stream system has been OSL dated to 68 ka (Blegen et al., 2015). Stone artifacts from Bovid Hill excavation are few (n= 78 with 9 *in situ*), but these lithic artifacts are laminar, include those produced by Levallois methods, and are consistent with an MSA attribution (Jenkins et al., 2012; Tryon et al., 2010; Tryon et al., 2014). Cut-marked bone at Bovid Hill indicates that stone tools were used at the site and not solely transported in by the stream system (Jenkins et al., 2012; Tryon et al., 2010).

Tryon carried out controlled 4m<sup>2</sup> excavations on Nyamita Main in the winter of 2009 with the goal of establishing the source of the artifacts found on the surface (Fig. 5; Tryon et al., 2010).

This excavation recovered 93 pieces from the surface of the Nyamita Main area and 26 *in situ*

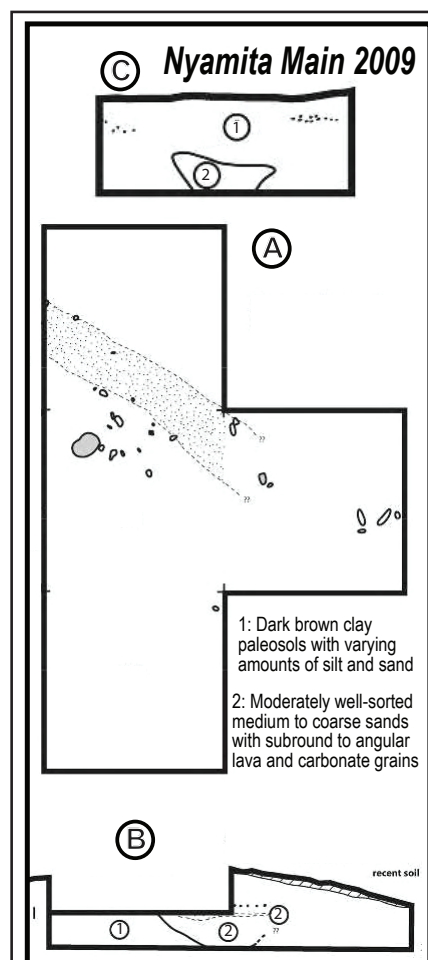


Figure 5: A) Plan map drawing of Tryon's 2009 Nyamita Main excavation (area outline in dotted lines in figure 4a showing approximate extent of channel feature from which lithic artifacts derive in the Main Trench of Nyamita Main excavations. B) Profile (looking west) of unit N12E07 west wall showing cross section of channel feature in Main Trench of Nyamita Main excavations (drawing by Tryon). C) Profile (looking west) of unit N13E06 showing cross section of channel feature in Main Trench of Nyamita Main excavations (drawing by Tryon).

from the excavation (Tryon et al., 2014). Raw material types and technology suggest that the surface and *in situ* material sample the same assemblage.

The review of recent research demonstrates that paleontological and archaeological collections conducted to date on the Late Pleistocene exposures of the eLVB have produced modest-to-large samples of archaeological and faunal material. However, relatively little of this material derives from an excavated context (Tryon et al., 2014).

The lack of excavated materials partially obscures the stratigraphic position, age and the relationship of paleontological and archaeological materials to one another. To this end the enlarged excavations at Nyamita Main reported in this study

were conducted to recover a larger and more representative sample of in situ archaeological and paleontological materials, as well as to investigate the relationship of these materials to one another.

#### Methods:

Excavations at Nyamita Main were carried out over three weeks in the summer of 2013. Spatial data was collected in three dimensions using a 6'' total station connected to a PC laptop operating EDM for windows excavation software (McPherron and Dibble, 2011). Prior to excavation the topography of the locality was mapped in 0.40 m intervals. Artifacts and fossils on the surface or exposed *in situ* at the surface were recorded and collected. A 1 x 1 m alphanumeric grid was laid out over the intended area of excavation.

Excavations were aligned north-south along the western edge of Tryon's 2009 trench and carried out with arbitrary 10 cm levels because of the absence of any natural stratigraphy within the artifact and fossil-bearing matrix. All stone material that could be found in situ and all fossil faunal material with a maximum dimension >2 cm found *in situ* was piece-plotted. All material with a discernable long axis (length/ width approximately  $\geq 1.5$ ) was piece-plotted with a point at either end. All excavated sediment was screened through 1/8'' mesh and sieved material collected in

bags specific to date, square and level. All excavated material is housed in the collections of the Archaeology Department of the National Museums of Kenya, Nairobi.

#### Analysis:

##### Lithic artifacts:

No single, standardized framework of lithic analysis exists in the study of MSA archaeology in Africa. To standardize data collection as much as possible we follow the lithic analysis procedures, terminology and data reporting protocols of Shea (2008), Tryon et al. (2010), and Sahle et al. (2014).

##### Fauna:

Following our previous collections in the eLVB (Faith et al., 2015; Tryon et al., 2010; Tryon et al., 2012), identifications and analysis of fauna recovered from the surface and excavations focused on taxonomically informative specimens, which in this context were restricted to cranial and dental remains.

#### Results:

Table 1: Summary of assemblage composition for Nyamita Main lithic artifacts 2009 and 2013 excavations as well as 2008 - 2013 surface collections combined.

Core		n (subtotal %)	% w/ out debris	Red/ White Chert	Fine lava	Coarse lava	Quartz	Quartzite	Black chert	Green chert	other
	Casual	5	1.852	1	2	1		1			
	Multiplatform	1	0.370		1						
	Levallois preferential	2	0.741		2						
	Levallois point	0	0								
	Levallois recurrent	0	0								
	Blade	0	0								
	Core on flake	0	0								
	Core fragment	1	0.370	1							
	Core subtotal	9	3.333								
Debitage											
	Initial cortical flake	0	0								
	Residual cortical flake	0	0								
	Levallois flake	2	0.741		2						
	Levallois point	3	1.111		2				1		
	non- cortical flake	71	26.296	32	32			4	3		
	Flake fragment proximal	81	30	38	40		1	1	1		
	Flake fragment other	98	36.296	47	46		1	4			
	Flake subtotal	255	94.444								
Debris											
	Debris and subtotal	179		83	55	1	6	4	1		29
Tool											
	point	4	1.481	1	1		1			1	
	side scraper	1	0.370	1							
	end scraper	0	0								
	chopper	0	0								
	biface	1	0.370		1						
	Tool subtotal	6	2.222								
TOTAL		449		204	184	2	9	14	6	1	29
	n, % w/out debirs	270	100								



## 1) Excavations

In August 2013 new excavations covering a total area of 52m<sup>2</sup> were opened on the crest and eastern slope of a small hill forming the locality of Nyamita Main. The units uncovered channels filled with sand-to-gravel-sized clasts cross-cutting a silt-to-clay-rich paleosol unit (Figs. 4, 6).

Two new trenches added in situ piece-plotted lithic artifacts (n=133) and fossils (n=106) to material recovered by Tryon's 2009 excavations.

The main trench of the 2013 excavation was oriented approximately east-west and covered an area of 26m<sup>2</sup> to an average depth of 0.70 m below surface. It extended to Tryon's 2009 4m<sup>2</sup> trench to recover a larger sample of lithic artifact material in situ (Fig. 4). The north trench was oriented north-south along the crest of the hill and excavated an area of 26m<sup>2</sup> to an average depth of 0.85 m to recover faunal material in situ and establish its context.

Table 2: Summary statistics of dimensions (mm) of whole flakes of two most common raw materials types from Nyamita Main.

	Whole flakes	Mean flake length (mm)	Mean flake width (mm)	Mean flake thickness (mm)	Mean flake platform width (mm)	Mean flake platform thickness (mm)	Flake frags + AW	Total number of pieces	Total weight (g)
<b>Lava</b>	27	37.30	27.69	9.11	18.46	7.38	101	<b>128</b>	746.89
<b>± 1 SD</b>		22.33	12.36	4.95	9.48	4.99			
<b>Red/White Mottled Chert</b>	27	18.01	17.10	4.68	10.65	3.79	134	<b>161</b>	306.67
<b>± 1 SD</b>		9.98	8.50	3.96	5.44	2.17			



Figure 6: Photographs of Nyamita Main excavations in August of 2013. A) Wide-angle photograph (looking east) of excavations showing North trench on left and Main Trench to the right with total station set up to far right. B) Photograph of north wall profile of North trench showing the stream channel in cross section. C) Main trench under excavation viewed looking north.

Sediments encountered in the Nyamita Main excavations are variants of the first two general lithological categories found in the Wasiriya beds. These are: 1) dark brown clay paleosols with varying amounts of silt and sand and 2) moderately well-sorted medium to coarse sand with sub-round to angular lava and carbonate grains (Fig 3d-f).

## 2) Archaeology:

A total of 449 surface and in situ artifacts were recovered in 2009 and 2013 at Nyamita Main

(Table 1). Tryon's 2009 excavations recovered 26 of the *in situ* pieces and 95 of the surface collected pieces. The 2013 excavations recovered 295 artifacts in situ, (133 were piece-plotted and 162 were recovered from the sieve) and 33 from the surface, for a total of 321 *in situ* pieces and 126 from controlled surface collections.

#### Lithic Raw Materials:

Eight raw materials are recognized from the Nyamita Main excavations: 1) A red and white mottled chert, 2) a fine-grained (aphanitic) lava, 3) a coarse-grained lava, 4) quartz, 5) quartzite, 6) a green chert 7) a black chert and 8) 'other' small pieces of angular debris (n =29) that cannot be confidently attributed to any of the above categories (Table 1). The vast majority of all artifacts from the 2009 and 2013 excavations (n= 388) are made of the mottled chert (n= 204) or lava (n=184) and whole flake measurements by raw material group are provided in Table 2.

The mottled chert source is found on the eastern side of Rusinga Island and the aphanitic lava is derived from the Lunene Lavas, or similarly aged lavas from Kisingiri which are found in place at the top of the ridges on Rusinga Island and as cobbles in drainages off of the ridges (Tryon et al., 2014). The quartz and quartzite have been observed in Pleistocene gravels at Nyamita, and as

large clasts within granodiorite volcanic bombs in the early Miocene Kiahira Formation. All of these raw materials are local. The source of the green and black cherts has not been observed on Rusinga Island and these materials are likely non-local.

#### Taphonomic context of archeological materials:

Lithic artifacts excavated from the site represent the products of on site flint knapping in a minimally winnowed context. Both the mottled chert and the lava raw materials, the only raw materials represented by sufficiently large numbers to assess their taphonomic integrity, conform to experimental models for stone tools produced on-site and preserved in a primary context (Schick, 1986). Size class analysis of piece-plotted and sieve-recovered mottled chert artifacts shows that 80.0 % of all artifacts are  $\leq 2$  cm in maximum dimension (Fig. 7). This agrees with experimental evidence of on-site flint knapping preserved in primary context (Schick, 1986). The lava raw material is in a slightly winnowed context as lava pieces recovered from the excavation show slightly lower proportions of size class 1 flakes ( $< 1$  cm in maximum dimension). Accordingly, higher proportions of the flakes are from larger size classes 3 – 5, indicating some fluvial action sorted and removed smaller pieces. However the presence of both lava cores and flakes in the same part of the site, suggests the material was knapped onsite and has been subject to minimal

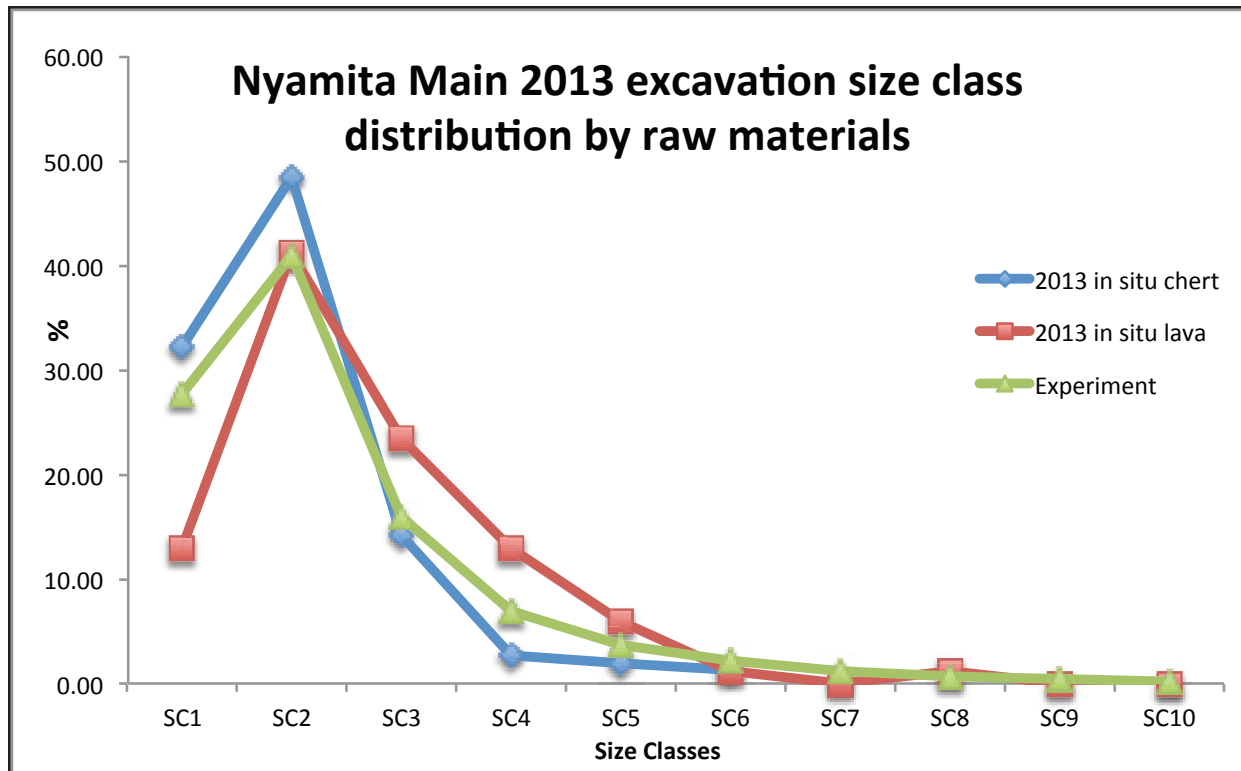


Figure 7: Size class distributions of artifacts by raw material category.

winnowing removing some of the smaller pieces.

Technology of archaeological materials:

Like all lithic artifacts known from the eLVB, lithic artifacts from Nyamita Main are typologically and technologically characteristic of the MSA (Fig. 8). Flaked pieces include bifacial and unifacial points collected from the surface in 2009-2010 (Tryon et al., 2010; Tryon et al., 2014), as well as Levallois points made in the red and white mottled chert and lava that dominate the lithic assemblage from the 2013 excavations (Fig. 8). Cores exhibit both the preferential and recurrent Levallois methods of flake production (Fig. 8).

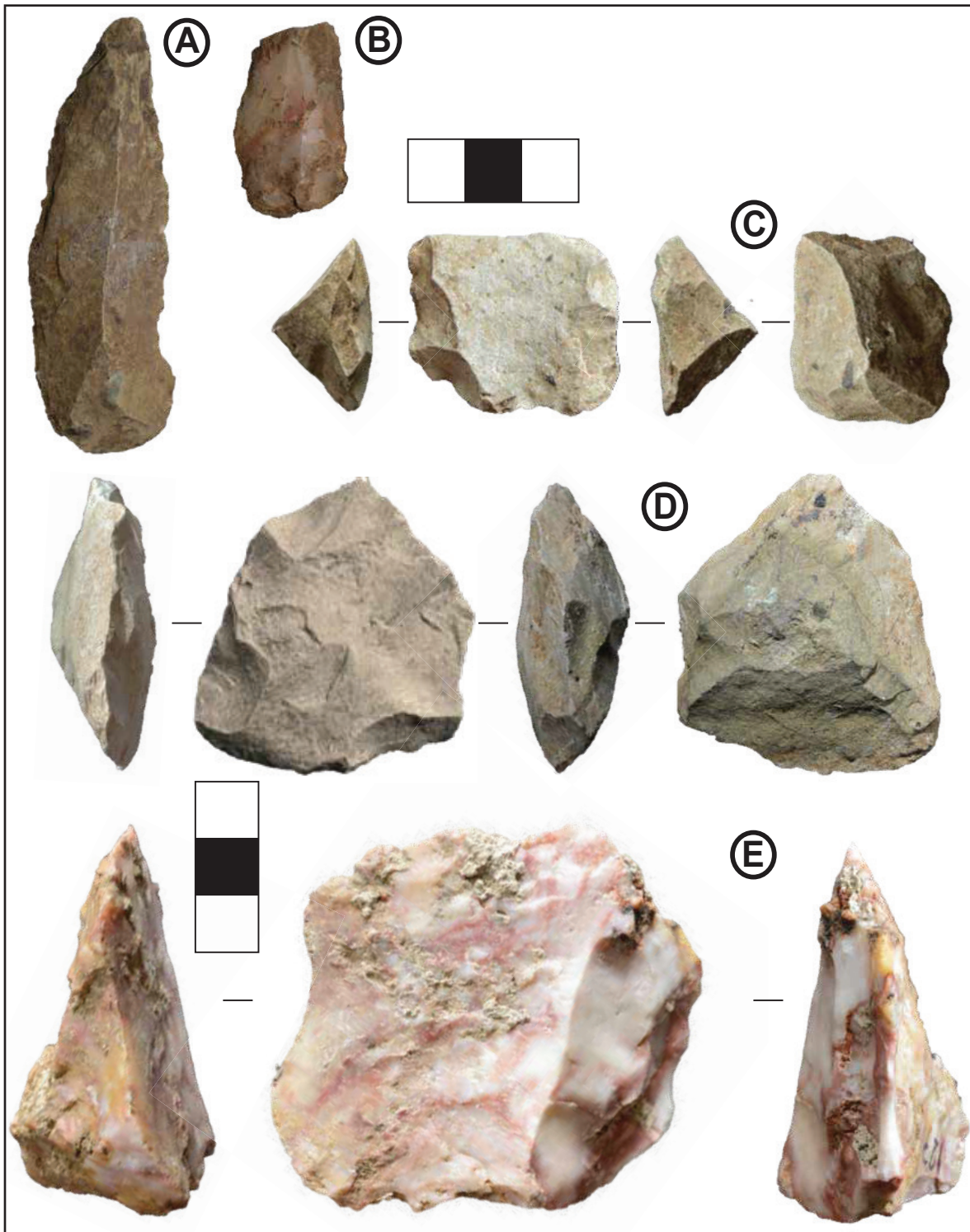


Figure 8: Artifacts A) Elongated Levallois point (lava) retouched on both dorsal margins. B) Proximal convergent flake or blade (Levallois point?) made on red/white mottled chert. C) Levallois core with overshot preferential flake made on lava (found on surface on main trench 2013. D) Recurrent Levallois or discoid core from Tryon's 2009 excavation (also see illustration in Tryon et al., 2010). E) Red/ white mottled chert Levallois core with recurrent unidirectional removals on debitage surface from Tryon's 2009 excavations on surface of main trench.



### 3) Paleontology:

Number and taphonomic context of bones recovered:

Fossil fauna at Nyamita Main derives from and immediately adjacent to a single ~2m wide by ~1m deep channel feature encountered along the north-south long axis of the north trench (Fig.

4). The general shape of this channel can be observed in the north facing cross-sectional profile of piece-plotted material in the north trench (red dots in Fig. 4c). The channels appear to drain south and west, similar to the trend of the modern Nyamita Valley. Faunal material comprised the majority of plotted material in this trench and was relatively complete with many specimens comprising entire elements such as hemi-mandibles. No cutmarks or percussion marks were observed. Very little faunal material was recovered in the Main Trench and what was recovered consisted mostly of isolated tooth or bone fragments.

### Faunal Identification:

All of the identifiable vertebrate remains from the Nyamita Main excavation are mammalian cranio-dental specimens. The taxonomically identifiable sample based on teeth consisted of 16 specimens identifiable to the level of tribe or lower (Table 3, NISP=16, MNI= 11). There are a minimum number of eleven individuals and all but one of these, a carnassial attributed to *Canis*,

Table 3: Nyamita Main faunal list including NISP and MNI counts.

<b>Taxon</b>	<b>NISP</b>	<b>MNI</b>
<i>Canis sp.</i>	1	1
<i>Tragelaphus scriptus</i>	1	1
<i>Redunca cf. redunca</i>	1	1
<i>Redunca cf. arundinum</i>	2	1
<i>Alcelaphus buselaphus</i>	2	2
<i>Damaliscus hypsodon</i>	1	1
<i>Rusingoryx atopocranion</i>	1	1
<i>Alcelaphini indet.</i>	6	2
<i>Ourebia ourebi</i>	1	1
<b>TOTAL</b>	<b>16</b>	<b>11</b>

are bovids (Table 3). The bovids represent at least

seven taxa from four tribes. Alcelaphine antelopes

dominate the assemblage (62.5% of all large mam-

mal specimens by NISP) and include the extinct

medium alcelaphine similar to a modern wilde-

beest (*Rusingoryx atopocranion*), the extinct small

alcelaphine similar to modern blesbok (*Damaliscus*

*hypsodon*), modern hartebeest (*Alcelaphus buselaphus*), and at least two alcelaphine individuals

that could not be diagnosed to a more specific taxonomic level.

Interpreting the record from Nyamita Main:

1) The Nyamita Main artifacts:

Lithic artifacts excavated from the site represent the products of onsite flint-knapping in a min-

imally winnowed context indicating that the Nyamita Main site was the location of tool man-

ufacture. Levallois technology is represented by Levallois points, a Levallois preferential core

and multiple cores exhibiting hierarchical core preparation and maintenance characteristic of

the recurrent method (Fig. 5; Boëda, 1994). The majority of flakes as well as some cores and



core-fragments are non-diagnostic. The lithic assemblage differs technologically from laminar lithic assemblage found at the site of Bovid Hill (Jenkins et al., 2012; Tryon et al., 2010; Tryon et al., 2014) dated to ~68 ka at the Wakondo locality on Rusinga Island (Blegen et al., 2015). Whether the differences between the lithic assemblages of Bovid Hill and Nyamita Main reflect change through time or different activities is unclear at present.

## 2) The Nyamita Main fauna:

The relative abundance of alcelaphine specimens among the bovids (66.7% of identified specimens) from the Nyamita excavation is similar to large samples of faunal material from the eLVB (Faith et al., 2015; Tryon et al., 2010, 2012, 2014), and is matched in contemporary arid to semi-arid grassland environments (Alemseged, 2003; Vrba, 1980). The extinct bovids at Nyamita Main, *R. atopocranion* and *D. hypsodon*, are characterized by exceptional hypsodonty (Faith et al., 2011; Faith et al., 2012). This adaptation is interpreted as suited to consuming grasses in dry and gritty environments (Damuth and Janis, 2011; Faith et al., 2012; Faith et al., 2015; Marean, 1992b). However the presence of bushbuck (*Tragelaphus scriptus*) and reedbuck (*Redunca redunca* and *Redunca cf. arundinum*) as well as hippopotamus fossils on the surface of the site (Tryon et al., 2010; Tryon et al., 2014; Tryon et al., 2012) suggest a component of closed habitats

and standing water respectively, agreeing with evidence from tufa and isotopic analyses of paleosol carbonates and organic material from the Nyamita Valley (Beverly et al., 2015a; Beverly et al., 2015b; Garrett et al., 2015).

The sand-to-gravel channel from which fossil fauna was recovered is variably cemented by carbonate and is more resistant to erosion than the surrounding silt-clay paleosols. The fact that all fauna derives from the same facies over a restricted area suggests the environmentally diverse faunal materials derive from the same relative time period and represent the inhabitants of a single ecologically diverse environment rather than a time averaged fauna from several temporally distinct environments. Fauna from the Nyamita Main excavation also proved to be in better and more complete condition than surface collected fossils from the eLVB that largely consist of mandible fragments, isolated teeth, and occasional horn cores. The Nyamita Main fauna, like faunal materials from the Wakondo, Bovid Hill excavations (Jenkins et al., 2012) consist of complete elements of mandible, cranium and postcrania. This collection makes a valuable contribution to paleontology in the eLVB. As many extinct species of bovid are only known from the Late Pleistocene exposures of the eLVB (Faith et al., 2011; Faith et al., 2012; Faith et al., 2014) more complete cranial and postcranial material is all the more valuable. Unfortunately, the fauna

cannot be directly related to the artifacts at Nyamita Main. The majority of artifacts occur in the main trench while almost all fauna was encountered in the small channel feature in the north trench (Fig. 4). Further, the fauna on the site cannot be confidently shown to be archaeological as no obvious cutmarks or percussion marks were observed.

Nyamita Main, the eLVB and the MSA/ LSA transition in East Africa:

New data from Nyamita Main presented here demonstrate that characteristically MSA technology is being produced in the eLVB of western Kenya after 49 ka and perhaps as late as 33 ka.

Archaeological work in the eLVB over the last seven years agrees with this conclusion. In seven continuous seasons of survey and excavation, not a single LSA microlith, backed piece, or microblade core has been encountered. In contrast, hundreds of characteristically MSA tools such as uni- and bifacial trimmed foliate points, Levallois points, Levallois preferential and recurrent cores have been recovered on the surface and in situ from all chronostratigraphically defined intervals between ~100 and >33 ka. The late persistence of the MSA through this time period contrasts markedly with the LSA or MSA/LSA transitional character of well-documented archaeological sequences at Mumba and Nasera rock shelters and the Naisiusiu beds of northern Tanzania as well as Enkapune-ya-Muto in the central Kenyan rift (Ambrose, 1998; Leakey et al., 1972;

Mehlman, 1979; Mehlman, 1977, 1989). This agrees with late MSA data from South Africa in showing the MSA/ LSA transition is not the product of a single event or cause, but is rather a temporally and geographically heterogeneous process occurring at different times in different places throughout the African continent, as well as within the region of equatorial East Africa.

Given this, we evaluate two hypotheses that might explain the temporal and spatial variability in the MSA/ LSA transition across equatorial East Africa: 1) MSA and LSA technologies represent different geographically and culturally isolated groups of the same species; and 2) MSA and LSA technologies represent different activities of the same hominin group or groups.

1) The late survival of the MSA in the eLVB between ~30-60 ka cannot be viewed as a product of geographic or cultural isolation in light of obsidian sourcing evidence from the Late Pleistocene of East Africa. Hominins in the eLVB sites of northern Tanzania and Enkapune-ya-Muto all shared access to similar resources and exploited at least one common area, the central Kenyan Rift. Obsidian sourcing studies from Mumba and Nasera show hominins at these sites had continued contact with the south Naivasha obsidian sources 240-320 km straight-line distances away from MSA times through the Holocene (Ambrose, 2012; Merrick and Brown, 1984; Merrick et

al., 1994). Obsidian artifacts of the Naisiusiu beds derive ~250 km north of Olduvai Gorge at the Sonanchi and Mundui sources immediately west of Lake Naivasha (Merrick and Brown, 1984). At Lukenya Hill proportions of obsidian appear to increase from MSA to LSA layers at GvJm-16 and GvJm-22 but appear to be deriving from similar Naivasha sources (Ambrose, 2012; Merrick and Brown, 1984; Tryon et al., 2015). Obsidians in MSA archaeological contexts from western Kenyan sites of Muguruk, Songhor and Karungu in the eLVB derive from Naivasha sources around the Ol Karia volcanic complex ~250 km directly east of where these obsidians were found (Faith et al., 2015; Merrick and Brown, 1984; Merrick et al., 1994). Enkapune-ya-Muto is in the Naivasha basin of the central Kenyan Rift (Ambrose, 1998, 2012). Whether the movement of these high quality obsidian raw materials was the product of trade or mobility is beside the point because in either case the humans making MSA or LSA assemblages from geographically disparate parts of the equatorial East Africa would likely have had knowledge of or contact with one another because they were using raw materials from the same source.

2) If the hominins of equatorial East Africa producing these MSA and LSA technologies in the same time period were all cognitively and culturally able, the overlap of ~10–30 kyr could possibly be the product of some other factor such as an locally-specific environmental adaptations.

The paleoenvironmental evidence from terrestrial faunas and other proxies found alongside late MSA and early LSA technologies present an opportunity to test environmental explanations for the geographic and temporal variability in the equatorial East African MSA/LSA transition. Isotopic, faunal and bulk soil geochemical evidence from the eLVB all suggest an open, semi-arid grassland environment with a desiccated, or at least a dramatically reduced, Lake Victoria throughout the sequence with patches of more closed environment spatially restricted near spring deposits (Beverly et al., 2015a; Beverly et al., 2015b; Faith et al., 2015; Garrett et al., 2015; Tryon et al., 2010). Available paleoenvironmental evidence from Enkapune-ya-Muto and Mumba, places with a very early LSA or transitional MSA/LSA assemblages, have more diverse environmental signatures indicating the presence of nearby lakes and potentially providing access to more diverse resources (Ambrose, 1998; Marean, 1992a, 1997; Mehlman, 1989). It is tempting to attribute technological variability seen at early LSA sites in equatorial East Africa to environmental variability and the homogeneity of the late surviving MSA in the eLVB to the environmental homogeneity of this open grassland environment through time. However, considering the long raw material transport distances discussed above, and the mobility these imply, all hominins in equatorial East Africa between ~30–60 ka almost certainly encountered a variety of environments. It is possible that the same highly mobile hominin population could have made LSA or

transitional materials in the variable environments of the Central Kenyan Rift or Northern Tanzania and classic MSA stone tools in the consistently open grasslands of the eLVB. However, if behavioral differences in different environments was the driver of the differential MSA-LSA transition, it would suggest that MSA technologies were better adapted to a homogenous environment and LSA technologies to more variable ones. This seems unlikely given that MSA technologies spanned a range of environments over the > 250 kyr of their existence across the entire African continent.

While the excavations at Nyamita Main and the archaeology of the eLVB do not resolve the MSA/LSA transition in equatorial East Africa, the refined chronological and geographic resolution imparted by this data allows us to winnow the field of hypotheses for the driver of the transition. The late persistence of classic MSA technology in the eLVB combined with known archaeological evidence from the Central Kenyan Rift and northern Tanzania confirms a staggered and geographically variable timing to the MSA/LSA transition.

Re-excavation and reanalysis of large multicomponent sites can produce new and valuable information (Diez-Martín et al., 2009; Gliganic et al., 2012; Mehlman, 1979; Prendergast et al., 2007),

but equally, the excavations presented here demonstrate that small, low-density, single-component sites like Nyamita Main, combined with a well-resolved chronostratigraphic framework, can reveal new and useful information about the MSA/LSA transition. Tephrostratigraphy combined with a robust chronostratigraphic framework for small open-air sites has been used to investigate the Acheulean to MSA transition in the Middle Pleistocene of equatorial East Africa (Deino and McBrearty, 2002; Tryon and McBrearty, 2002) but similar programs either within or between depositional basins have yet to be instituted for the MSA/LSA transition in the late Pleistocene of the same region. The work presented here along with recent geo-chronological work in the eLVB demonstrates that this kind of future research could produce new and valuable information.

#### Conclusion:

Excavations at the site of Nyamita Main provide new archaeological and paleontological evidence of on-site production of characteristically MSA technologies from an excavated context dated between >33–49 ka in the eLVB of western Kenya. This assemblage coupled with archaeological evidence from the eLVB demonstrates persistence of characteristically MSA technologies and absence of technologies of an LSA or transitional character < 49 ka and perhaps as late as >33ka in western Kenya at the same time that transitional and LSA industries are being



developed in the Central Kenyan Rift at Enkapune-ya-Muto and Nasera and Mumba rockshelters and the Naisiusiu beds of northern Tanzania. The late persistence of the MSA demonstrates geographic variation in the timing of the MSA/ LSA transition in equatorial East Africa corroborating data from sites in the southern part of the continent. The prolonged, temporally and geographically variable nature of the MSA/ LSA transition in equatorial East Africa and throughout the continent suggests that this phenomenon was complex. The combination of excavations from an open-air, low-density site situated in a well-resolved tephro and chronostratigraphic framework presented here suggests a methodology to further improve our understanding of this transition.

## Summary and Conclusion:

The concluding sections of this dissertation: 1) Summarize the key results on the chronology and character of MSA technology at both early and late MSA sites from each of the four papers. 2) Synthesize these results and their relevance to larger theoretical framework. 3) Present prospects for future work in tephrostratigraphy and archaeology related to the MSA of East Africa.

### 1) Summary:

The tephrostratigraphy studies constituting the first and second papers of this dissertation provide the stratigraphic control necessary for ongoing paleoenvironmental and human behavioral reconstructions based on fossils, soils and artifacts from the Middle – Late Pleistocene exposures in the eastern Lake Victoria Basin and Kapthurin Formation. The results of these papers show:

1) The same Late Pleistocene stratigraphic sequence bracketed by distal tephras and dating from 33-111 ka is found >150m<sup>2</sup> in the eastern Lake Victoria Basin of western Kenya. This tephrostratigraphic and be linked to the rift via correlation of the ~100 ka Wakondo Tuff to the Baringo Basin.

2) The base of the Bedded Tuff Member and nine archaeological sites found at or beneath this member are shown to be > 380 ka. Levallois prepared core techniques, important aspects of MSA technology, are shown to be >380 ka in the Kapthurin Formation, ~100 kyr older than previously estimated in East Africa.

The archaeological component constituting the third and fourth papers provide new MSA archaeological material in well-dated context and show:

3) Long distance transport (>166 km) of high quality obsidian for stone tool manufacture was a feature of hominin behavior associated with Middle Pleistocene MSA technology ~200 ka ago.

4) MSA technology persisted in East Africa later than 49 ka and perhaps later than 33 ka, after Later Stone Age technologies, often considered categorically superior, are documented in the region.

2) Synthesis:

By demonstrating both the early and late presence of various aspects of MSA technology and associated hominin behavior this work shows that tephrostratigraphy and the excavation of new archaeological material in East Africa are productive means of producing new and important data on the MSA and the evolution of human behavior.

The work presented here can further contribute to our understanding of the evolution of human behavior and biology as a coeval process in which behavior affects biology as much as the reverse (*sensu* McBrearty and Brooks, 2000).

### 3) Prospects for future work:

#### Tephrostratigraphy:

The long-distance correlation of the Wakondo Tuff between the Baringo and eastern Lake Victoria basins demonstrates that distal tephras can be an extremely useful tool in refining the stratigraphic and chronological resolution of fossil and artifact bearing Middle-Late Pleistocene sediments of East African depositional basins (Pyle, 1999). The work presented here predicts that the Late Pleistocene distal tephras of eLVB as well as the Middle-Late Pleistocene distal tephras of the Kapthurin Formation will be found in Pleistocene sediments of other depositional basins in East Africa, substantially expanding the scale of the work presented here and providing new ages

for existing archaeological material as well as previously unrealized venues of exposure in which to look for new MSA material.

#### Archaeology:

The SSRS is one of seven early MSA sites known from East Africa and only one of two early MSA sites preserving obsidian that is geochemically sourced. Therefore, the discovery of long distance obsidian transport associated with early MSA technology at the SSRS >200 ka (paper #3) suggests this behavior was more common in the Middle Pleistocene than previously appreciated. Considering the small number of Middle Pleistocene sites of MSA or ESA character currently known to preserve obsidian, it is also unlikely that the SSRS is the oldest evidence of long distance raw material transport. I predict that future sourcing studies of Middle Pleistocene sites such as GnJh-15, GnJi-28, GnJh-63 in the Kapthurin Formation, shown in paper #2 to be  $\geq 380$  ka, as well as potential obsidian sourcing studies in Middle Pleistocene sites in other areas will provide evidence of raw material transport distance longer than previously appreciated. This may serve to help elucidate the relationship between raw material transport distances and technological change surrounding the Acheulean to MSA technological shift in the Middle Pleistocene of Africa.

## Work Cited:

- Adler, D., Wilkinson, K., Blockley, S., Mark, D., Pinhasi, R., Schmidt-Magee, B., Nahapetyan, S., Mallol, C., Berna, F., Glauberman, P., 2014. Early Levallois technology and the Lower to Middle Paleolithic transition in the Southern Caucasus. *Science* 345, 1609-1613.
- Alemseged, Z., 2003. An integrated approach to taphonomy and faunal change in the Shungura Formation (Ethiopia) and its implication for hominid evolution. *Journal of Human Evolution* 44, 451-478.
- Ambrose, S.H., 1998. Chronology of the Later Stone Age and food production in East Africa. *Journal of Archaeological Science* 25, 377-392.
- Ambrose, S.H., 2012. Obsidian Dating and Source Exploitation Studies in Africa. *Obsidian and Ancient Manufactured Glasses*.
- Anderson, G., Talbot, L., 1965. Soil factors affecting the distribution of the grassland types and their utilization by wild animals on the Serengeti plains, Tanganyika. *The Journal of Ecology*, 33-56.
- Ashley, G.M., Tactikos, J.C., Owen, R.B., 2009. Hominin use of springs and wetlands: Paleoclimate and archaeological records from Olduvai Gorge (~ 1.79–1.74 Ma). *Palaeogeography, Palaeoclimatology, Palaeoecology* 272, 1-16.
- Assefa, Z., Lam, Y., Mienis, H.K., 2008. Symbolic Use of Terrestrial Gastropod Opercula during the Middle Stone Age at Porc-Epic Cave, Ethiopia. *Current Anthropology* 49, 746-756.
- Avery, G., Cruz-Urbe, K., Goldberg, P., Grine, F.E., Klein, R.G., Lenardi, M.J., Marean, C.W., Rink, W.J., Schwarcz, H.P., Thackeray, A.I., 1997. The 1992–1993 excavations at the Die Kelders Middle and Later Stone Age cave site, South Africa. *Journal of field archaeology* 24, 263-291.
- Backwell, L., d'Errico, F., Wadley, L., 2008. Middle stone age bone tools from the Howiesons Poort layers, Sibudu Cave, South Africa. *Journal of Archaeological Science* 35, 1566-1580.
- Baker, B., Mitchell, J., Williams, L., 1988. Stratigraphy, geochronology and volcano-tectonic evolution of the Kedong–Naivasha–Kinangop region, Gregory Rift Valley, Kenya. *Journal of the Geological Society* 145, 107-116.
- Beaumont, P.B., 1978. *Border Cave*. University of Cape Town.
- Behrensmeier, A.K., Kidwell, S.M., Gastaldo, R.A., 2000. Taphonomy and paleobiology. *Paleobiology* 26, 103-147.
- Beverly, E.J., Driese, S.G., Peppe, D.J., Arellano, L.N., Blegen, N., Faith, J.T., Tryon, C.A., 2015a. Reconstruction of a semi-arid Late Pleistocene paleocatena from the Lake Victoria region, Kenya. *Quaternary Research*.

Beverly, E.J., Driese, S.G., Peppe, D.J., Johnson, C.R., Michel, L.A., Faith, J.T., Tryon, C.A., Sharp, W.D., 2015b. Recurrent spring-fed rivers in a Middle to Late Pleistocene semi-arid grassland: Implications for environments of early humans in the Lake Victoria Basin, Kenya. *Sedimentology*.

Bishop, W., Chapman, G., Hill, A., 1971. Succession of Cainozoic vertebrate assemblages from the northern Kenya Rift Valley. *Nature* 233, 389-394.

Blegen, N., Tryon, C.A., Faith, J.T., Peppe, D.J., Beverly, E.J., Li, B., Jacobs, Z., 2015. Distal tephras of the eastern Lake Victoria basin, equatorial East Africa: correlations, chronology and a context for early modern humans. *Quaternary Science Reviews* 122, 89-111.

Blome, M.W., Cohen, A.S., Tryon, C.A., Brooks, A.S., Russell, J., 2012. The environmental context for the origins of modern human diversity: a synthesis of regional variability in African climate 150,000–30,000 years ago. *Journal of human evolution* 62, 563-592.

Blumenschine, R.J., Masao, F.T., Stollhofen, H., Stanistreet, I.G., Bamford, M.K., Albert, R.M., Njau, J.K., Prassack, K.A., 2012. Landscape distribution of Oldowan stone artifact assemblages across the fault compartments of the eastern Olduvai Lake Basin during early lowermost Bed II times. *Journal of human evolution* 63, 384-394.

Boëda, E., 1994. Le concept Levallois: variabilité des méthodes. CNRS éd.

Bootsma, H.A., Hecky, R.E., 2003. A comparative introduction to the biology and limnology of the African Great Lakes. *Journal of Great Lakes Research* 29, 3-18.

Borchardt, G., Aruscavage, P., Millard Jr, H., 1972. Correlation of the Bishop Ash, a Pleistocene marker bed, using instrumental neutron activation analysis. *Journal of Sedimentary Research* 42.

Bower, J., Gogan-Porter, P., 1981. Prehistoric cultures of the Serengeti National Park: initial archaeological studies of an undisturbed African ecosystem. *Papers in Anthropology* 3.

Bower, J.R., Gifford, D., Livingstone, D., 1985. Excavations at the Loiyangalani Site, Serengeti National Park, Tanzania. *National Geographic Society Research Reports* 20, 41-56.

Bräuer, G., 2008. The origin of modern anatomy: by speciation or intraspecific evolution? *Evolutionary Anthropology: Issues, News, and Reviews* 17, 22-37.

Bräuer, G., Singer, R., 1996. The Klasies zygomatic bone: archaic or modern? *Journal of Human Evolution* 30, 161-165.

Brooks, A., Feathers, J., d'Errico, F., Yellen, J., 2004. Middle Stone Age barbed bone points from Katanda (DR Congo): new perspectives on age and association, Poster presented at Paleoanthropology Meeting, Montreal.

- Brooks, A.S., Helgren, D.M., Cramer, J.S., Franklin, A., Hornyak, W., Keating, J.M., Klein, R.G., Rink, W.J., Schwarcz, H., Smith, J., 1995. Dating and context of three Middle Stone Age sites with bone points in the Upper Semliki Valley, Zaire. *Science* 268, 548-553.
- Brooks, A.S., Nevell, L., Yellen, J.E., Hartman, G., 2006. Projectile technologies of the African MSA, Transitions before the transition. Springer, pp. 233-255.
- Brown, F., Nash, B., Fernandez, D., Merrick, H., Thomas, R., 2013. Geochemical composition of source obsidians from Kenya. *Journal of Archaeological Science* 40, 3233-3251.
- Brown, F.H., Fuller, C.R., 2008. Stratigraphy and tephra of the Kibish Formation, southwestern Ethiopia. *Journal of Human Evolution* 55, 366-403.
- Brown, F.H., Haileab, B., McDougall, I., 2006. Sequence of tuffs between the KBS Tuff and the Chari Tuff in the Turkana Basin, Kenya and Ethiopia. *Journal of the Geological Society* 163, 185-204.
- Brown, F.H., McDougall, I., 2011. Geochronology of the Turkana depression of northern Kenya and southern Ethiopia. *Evolutionary Anthropology: Issues, News, and Reviews* 20, 217-227.
- Brown, F.H., McDougall, I., Fleagle, J.G., 2012a. Correlation of the KHS Tuff of the Kibish Formation to volcanic ash layers at other sites, and the age of early *Homo sapiens* (Omo I and Omo II). *Journal of human evolution* 63, 577-585.
- Brown, F.H., Sarna-Wojcicki, A.M., Meyer, C.E., Haileab, B., 1992. Correlation of Pliocene and Pleistocene tephra layers between the Turkana Basin of East Africa and the Gulf of Aden. *Quaternary International* 13, 55-67.
- Brown, F.H.N., B., 2014. Correlation: Volcanic Ash, Obsidian. , In: *Treatise of Geochemistry* 2nd Edition: Archaeology and Anthropology., 2nd ed, pp. 63-80.
- Brown, K.S., Marean, C.W., Jacobs, Z., Schoville, B.J., Oestmo, S., Fisher, E.C., Bernatchez, J., Karkanas, P., Matthews, T., 2012b. An early and enduring advanced technology originating 71,000 years ago in South Africa. *Nature* 491, 590-593.
- Caudill, M.R., Driese, S.G., Mora, C.I., 1996. Preservation of a paleo-Vertisol and an estimate of Late Mississippian paleoprecipitation. *Journal of Sedimentary Research* 66.
- Cerling, T.E., Brown, F.H., Bowman, J.R., 1985. Low-temperature alteration of volcanic glass: hydration, Na, K, 18 O and Ar mobility. *Chemical Geology: Isotope Geoscience section* 52, 281-293.
- Chapman, G.R., 1971. The geological evolution of the northern Kamasia Hills, Baringo district, Kenya.



Chapman, G.R., Brook, M., 1978. Chronostratigraphy of the Baringo basin, Kenya. Geological Society, London, Special Publications 6, 207-223.

Chavaillon, J., 1976. Evidence for the technical practices of early Pleistocene hominids, Shungura Formation, lower Omo Valley, Ethiopia. Earliest man and environments in the Lake Rudolf Basin, 565-573.

Chavaillon, J., Berthelet, A., 2004. The archaeological sites of Melka Kunture. Studies on the Early Paleolithic site of Melka Kunture, Ethiopia. Origines, Firenze, 25-80.

Chazan, M., Ron, H., Matmon, A., Porat, N., Goldberg, P., Yates, R., Avery, M., Sumner, A., Horwitz, L.K., 2008. Radiometric dating of the Earlier Stone Age sequence in excavation I at Wonderwerk Cave, South Africa: preliminary results. *Journal of Human Evolution* 55, 1-11.  
Chorowicz, J., 2005. The East African rift system. *Journal of African Earth Sciences* 43, 379-410.

Clark, J.D., 1959. Further excavations at Broken Hill, Northern Rhodesia. *Journal of the Anthropological Institute of Great Britain and Ireland*, 201-232.

Clark, J.D., 1982. The cultures of the Middle Palaeolithic/Middle Stone Age. *The Cambridge History of Africa* 1, 248-341.

Clark, J.D., 1988. The Middle Stone Age of East Africa and the beginnings of regional identity. *Journal of World Prehistory* 2, 235-305.

Clark, J.D., Beyene, Y., WoldeGabriel, G., Hart, W.K., Renne, P.R., Gilbert, H., Defleur, A., Suwa, G., Katoh, S., Ludwig, K.R., 2003. Stratigraphic, chronological and behavioural contexts of Pleistocene *Homo sapiens* from Middle Awash, Ethiopia. *Nature* 423, 747-752.

Clark, J.D., Cormack, J., Chin, S., 2001. Kalambo Falls Prehistoric Site: Volume 3, the Earlier Cultures: Middle and Earlier Stone Age. Cambridge University Press.

Clark-Balzan, L.A., Candy, I., Schwenninger, J.-L., Bouzouggar, A., Blockley, S., Nathan, R., Barton, R.N.E., 2012. Coupled U-series and OSL dating of a Late Pleistocene cave sediment sequence, Morocco, North Africa: significance for constructing Palaeolithic chronologies. *Quaternary Geochronology* 12, 53-64.

Cole, G., 1967. The later Acheulian and Sangoan of southern Uganda. University of Chicago Press.

Cornelissen, E., 1992. Site GNJH-17 and its implications for the Archaeology of the Middle Kapthurin Formation, Baringo, Kenya. Koninklijk Museum voor Midden Afrika.

Cornelissen, E., Boven, A., Dabi, A., Hus, J., Yong, K.J., Keppens, E., Langohr, R., Moeyersons, J., Pasteels, P., Pieters, M., 1990. The Kapthurin formation revisited. *African Archaeological Review* 8, 23-75.

Crompton, R.H., Gowlett, J.A., 1993. Allometry and multidimensional form in Acheulean bifaces from Kilombe, Kenya. *Journal of Human Evolution* 25, 175-199.

d'Errico, F., Henshilwood, C., Vanhaeren, M., Van Niekerk, K., 2005. Nassarius kraussianus shell beads from Blombos Cave: evidence for symbolic behaviour in the Middle Stone Age. *Journal of human evolution* 48, 3-24.

Dagley, P., Mussett, A.E., Palmer, H., 1978. Preliminary observations on the palaeomagnetic stratigraphy of the area west of Lake Baringo, Kenya. Geological Society, London, Special Publications 6, 225-235.

Damuth, J., Janis, C.M., 2011. On the relationship between hypsodonty and feeding ecology in ungulate mammals, and its utility in palaeoecology. *Biological Reviews* 86, 733-758.

Danley, P.D., Husemann, M., Ding, B., DiPietro, L.M., Beverly, E.J., Peppe, D.J., 2012. The impact of the geologic history and paleoclimate on the diversification of East African cichlids. *International journal of evolutionary biology* 2012.

Dawson, J.B., 2008. The Gregory rift valley and Neogene-recent volcanoes of northern Tanzania. Geological Society of London.

Day, M.H., 1986. Guide to fossil man. University of Chicago Press.

Deacon, H.J., 1979. Excavations at Boomplaas cave- a sequence through the upper Pleistocene and Holocene in South Africa. *World Archaeology* 10, 241-257.

Deino, A.L., McBrearty, S., 2002.  $^{40}\text{Ar}/^{39}\text{Ar}$  dating of the Kapthurin Formation, Baringo, Kenya. *Journal of Human Evolution* 42, 185-210.

Dibble, H.L., Schurmans, U.A., Iovita, R.P., McLaughlin, M.V., 2005. The measurement and interpretation of cortex in lithic assemblages. *American Antiquity*, 545-560.

Diez-Martín, F., Domínguez-Rodrigo, M., Sánchez, P., Mabulla, A.Z., Tarriño, A., Barba, R., Prendergast, M.E., de Luque, L., 2009. The Middle to Later Stone Age technological transition in East Africa. New data from Mumba Rockshelter Bed V (Tanzania) and their implications for the origin of modern human behavior. *Journal of African Archaeology*, 147-173.

Douze, K., 2011. L'Afrique de l'Est dans la réflexion globale sur le Middle Stone Age, *Annales d'Éthiopie*, pp. 15-51.

Douze, K., 2012. Le Early Middle Stone Age d'Éthiopie et les changements techno-économiques à la période de l'émergence des premiers Homo sapiens. *Bordeaux* 1.

Douze, K., 2014. A new chrono-cultural marker for the early Middle Stone Age in Ethiopia: The tranche blow process on convergent tools from Gademotta and Kulkuletti sites. *Quaternary International* 343, 40-52.

Driese, S.G., Jacobs, J.R., Nordt, L.C., 2003. Comparison of modern and ancient Vertisols developed on limestone in terms of their geochemistry and parent material. *Sedimentary Geology* 157, 49-69.

Driese, S.G., Mora, C.I., Stiles, C.A., Joeckel, R., Nordt, L.C., 2000. Mass-balance reconstruction of a modern Vertisol: implications for interpreting the geochemistry and burial alteration of paleo-Vertisols. *Geoderma* 95, 179-204.

Dunkley, P., Smith, M., Allen, D., Darling, W., 1993. The geothermal activity and geology of the northern sector of the Kenya Rift Valley.

Eren, M.I., Diez-Martin, F., Dominguez-Rodrigo, M., 2013. An empirical test of the relative frequency of bipolar reduction in Beds VI, V, and III at Mumba Rockshelter, Tanzania: implications for the East African Middle to Late Stone Age transition. *Journal of Archaeological Science* 40, 248-256.

Faith, J.T., 2014. Late Pleistocene and Holocene mammal extinctions on continental Africa. *Earth-Science Reviews* 128, 105-121.

Faith, J.T., Choiniere, J.N., Tryon, C.A., Peppe, D.J., Fox, D.L., 2011. Taxonomic status and paleoecology of *Rusingoryx atopocranium* (Mammalia, Artiodactyla), an extinct Pleistocene bovid from Rusinga Island, Kenya. *Quaternary Research* 75, 697-707.

Faith, J.T., Potts, R., Plummer, T.W., Bishop, L.C., Marean, C.W., Tryon, C.A., 2012. New perspectives on middle Pleistocene change in the large mammal faunas of East Africa: *Damaliscus hypsodon* sp. nov. (Mammalia, Artiodactyla) from Lainyamok, Kenya. *Palaeogeography, Palaeoclimatology, Palaeoecology* 361, 84-93.

Faith, J.T., Tryon, C.A., Peppe, D.J., Beverly, E.J., Blegen, N., 2014. Biogeographic and Evolutionary Implications of an Extinct Late Pleistocene Impala from the Lake Victoria Basin, Kenya. *Journal of Mammalian Evolution* 21, 213-222.

Faith, J.T., Tryon, C.A., Peppe, D.J., Beverly, E.J., Blegen, N., Blumenthal, S., Chritz, K.L., Driese, S.G., Patterson, D., 2015. Paleoenvironmental context of the Middle Stone Age record from Karungu, Lake Victoria Basin, Kenya, and its implications for human and faunal dispersals in East Africa. *J Hum Evol* 83, 28-45.

Feibel, C.S., 1999. Tephrostratigraphy and geological context in paleoanthropology. *Evolutionary Anthropology: Issues, News, and Reviews* 8, 87-100.

- Feibel, C.S., 2011. A geological history of the Turkana Basin. *Evolutionary Anthropology: Issues, News, and Reviews* 20, 206-216.
- Feibel, C.S., Brown, F.H., McDougall, I., 1989. Stratigraphic context of fossil hominids from the Omo Group deposits: Northern Turkana Basin, Kenya and Ethiopia. *American Journal of Physical Anthropology* 78, 595-622.
- Fleagle, J.G., Assefa, Z., Brown, F.H., Shea, J.J., 2008. Paleoanthropology of the Kibish Formation, southern Ethiopia: introduction. *Journal of Human Evolution* 55, 360-365.
- Froggatt, P., 1992. Standardization of the chemical analysis of tephra deposits. Report of the ICCT working group. *Quaternary International* 13, 93-96.
- Gabel, C., 1969. Six rock shelters on the northern Kavirondo shore of Lake Victoria. *African Historical Studies*, 205-254.
- Gamble, C., 1993. Exchange, foraging and local hominid networks. Trade and exchange in pre-historic Europe 33, 35-44.
- Garcea, E.A., Barton, N., 2010. South-eastern Mediterranean peoples between 130,000 and 10,000 years ago. Oxbow books.
- Garrett, N.D., Fox, D.L., McNulty, K.P., Faith, J.T., Peppe, D.J., Van Plantinga, A., Tryon, C.A., 2015. Stable isotope paleoecology of Late Pleistocene Middle Stone Age humans from the Lake Victoria basin, Kenya. *Journal of human evolution* 82, 1-14.
- Gliganic, L.A., Jacobs, Z., Roberts, R.G., Domínguez-Rodrigo, M., Mabulla, A.Z., 2012. New ages for Middle and Later Stone Age deposits at Mumba rockshelter, Tanzania: Optically stimulated luminescence dating of quartz and feldspar grains. *Journal of Human Evolution* 62, 533-547.
- Gowlett, J., Crompton, R., 1994. Kariandusi: Acheulean morphology and the question of allometry. *African Archaeological Review* 12, 3-42.
- Grün, R., Brink, J.S., Spooner, N.A., Taylor, L., Stringer, C.B., Franciscus, R.G., Murray, A.S., 1996. Direct dating of Florisbad hominid. *Nature* 382, 500-501.
- Haile-Selassie, Y., Asfaw, B., White, T.D., 2004. Hominid cranial remains from upper Pleistocene deposits at Aduma, Middle Awash, Ethiopia. *American Journal of Physical Anthropology* 123, 1-10.
- Hay, R.L., 1976. *Geology of the Olduvai Gorge: A study of sedimentation in a semiarid basin*. Univ of California Press.
- Hayward, C., 2011. High spatial resolution electron probe microanalysis of tephtras and melt

inclusions without beam-induced chemical modification. The Holocene, 0959683611409777.

Heiken, G., Heiken, G., 1974. An atlas of volcanic ash. Smithsonian Institution Press Washington, DC.

Henshilwood, C., d'Errico, F., Vanhaeren, M., Van Niekerk, K., Jacobs, Z., 2004. Middle stone age shell beads from South Africa. *Science* 304, 404-404.

Henshilwood, C.S., 2005. Stratigraphic integrity of the middle stone age levels at Blombos cave. From Tools to Symbols. From Early Hominids to Modern Humans. Witwatersrand University Press, Johannesburg, 441-458.

Henshilwood, C.S., D'errico, F., Marean, C.W., Milo, R.G., Yates, R., 2001. An early bone tool industry from the Middle Stone Age at Blombos Cave, South Africa: implications for the origins of modern human behaviour, symbolism and language. *Journal of Human Evolution* 41, 631-678.

Henshilwood, C.S., d'Errico, F., Watts, I., 2009. Engraved ochres from the middle stone age levels at Blombos Cave, South Africa. *Journal of Human Evolution* 57, 27-47.

Henshilwood, C.S., d'Errico, F., Yates, R., Jacobs, Z., Tribolo, C., Duller, G.A., Mercier, N., Sealy, J.C., Valladas, H., Watts, I., 2002. Emergence of modern human behavior: Middle Stone Age engravings from South Africa. *Science* 295, 1278-1280.

Henshilwood, C.S., d'Errico, F., Van Niekerk, K.L., Coquinot, Y., Jacobs, Z., Lauritzen, S.-E., Menu, M., García-Moreno, R., 2011. A 100,000-year-old ochre-processing workshop at Blombos Cave, South Africa. *Science* 334, 219-222.

Herries, A.I., 2011. A chronological perspective on the Acheulian and its transition to the Middle Stone Age in southern Africa: the question of the Fauresmith. *International Journal of Evolutionary Biology* 2011.

Hill, A., Curtis, G., Drake, R., 1986. Sedimentary stratigraphy of the Tugen Hills, Baringo, Kenya. Geological Society, London, Special Publications 25, 285-295.

Humphreys, A., 1970. The role of raw material and the concept of the Fauresmith. *The South African Archaeological Bulletin*, 139-144.

Hunt, J.B., Hill, P.G., 2001. Tephrological implications of beam size—sample-size effects in electron microprobe analysis of glass shards. *Journal of Quaternary Science* 16, 105-117.

Huntley, D.J., Lamothe, M., 2001. Ubiquity of anomalous fading in K-feldspars and the measurement and correction for it in optical dating. *Canadian Journal of Earth Sciences* 38, 1093-1106.

Jacobs, Z., Duller, G.A., Wintle, A.G., Henshilwood, C.S., 2006. Extending the chronology of deposits at Blombos Cave, South Africa, back to 140ka using optical dating of single and multiple grains of quartz. *Journal of Human Evolution* 51, 255-273.

Jenkins, K., Faith, J.T., Tryon, C., Peppe, D., Nightingale, S., Ogondo, J., Johnson, C.R., Driese, S., 2012. New excavations of a Late Pleistocene bonebed and associated MSA artifacts from Rusinga Island, Kenya. *PaleoAnthropology* 2012, A17.

Johnson, C.R., McBrearty, S., 2010. 500,000 year old blades from the Kapthurin Formation, Kenya. *Journal of Human Evolution* 58, 193-200.

Kelly, R.L., 1995. *The foraging spectrum*. Washington, DC: Smithsonian Institution Press.

Kendall, R.L., 1969. An ecological history of the Lake Victoria basin. *Ecological Monographs*, 121-176.

Kent, P.E., 1942. The Pleistocene beds of Kanam and Kanjera, Kavirondo, Kenya. *Geological Magazine* 79, 117-132.

Kiberd, P., 2006. Bundu Farm: a report on archaeological and palaeoenvironmental assemblages from a pan site in Bushmanland, Northern Cape, South Africa. *The South African Archaeological Bulletin*, 189-201.

Klein, R.G., 2000. Archeology and the evolution of human behavior. *Evolutionary Anthropology Issues News and Reviews* 9, 17-36.

Klein, R.G., 2008. Out of Africa and the evolution of human behavior. *Evolutionary Anthropology: Issues, News, and Reviews* 17, 267-281.

Kokis, J., 1988. Protein Diagenesis Dating of *Struthio camelus* Eggshell: An Upper Pleistocene Dating Technique. Unpublished M. Sc. thesis, George Washington University, Washington.

Kuehn, S., Froese, D., Shane, P., Participants, I.I., 2011. The INTAV intercomparison of electron-beam microanalysis of glass by tephrochronology laboratories: results and recommendations. *Quaternary International* 246, 19-47.

Kuehn, S.C., Foit, F.F., 2006. Correlation of widespread Holocene and Pleistocene tephra layers from Newberry Volcano, Oregon, USA, using glass compositions and numerical analysis. *Quaternary International* 148, 113-137.

Le Bas, M.J., 1977. *Carbonatite-nephelinite volcanism: an African case history*. John Wiley & Sons.

Le Bas, M.J., Le Maitre, R., Streckeisen, A., Zanettin, B., 1986. A chemical classification of volcanic rocks based on the total alkali-silica diagram. *Journal of petrology* 27, 745-750.

- Le Gall, B., Tiercelin, J.-J., Richert, J.-P., Gente, P., Sturchio, N., Stead, D., Le Turdu, C., 2000. A morphotectonic study of an extensional fault zone in a magma-rich rift: the Baringo Trachyte Fault System, central Kenya Rift. *Tectonophysics* 320, 87-106.
- Leakey, L., Owen, W., 1945. A contribution to the study of the Tumbian culture in East Africa: Coryndon Mem. Mus. Occ. Paper.
- Leakey, M., Tobias, P.V., Martyn, J.E., Leakey, R.E., 1969. An Acheulean Industry with Prepared Core Technique and the Discovery of a Contemporary Hominid Mandible at Lake Baringo, Kenya. *Proceedings of the Prehistoric Society (New Series)* 35, 48-76.
- Leakey, M.D., Hay, R.L., Thurber, D., Protsch, R., Berger, R., 1972. Stratigraphy, archaeology, and age of the Ndotu and Naisiusiu beds, Olduvai Gorge, Tanzania. *World Archaeology* 3, 328-341.
- Li, B., Li, S.-H., 2012. Luminescence dating of Chinese loess beyond 130 ka using the non-fading signal from K-feldspar. *Quaternary Geochronology* 10, 24-31.
- Li, B., Roberts, R.G., Jacobs, Z., Li, S.-H., Guo, Y.-J., 2015. Construction of a 'global standardised growth curve' (gSGC) for infrared stimulated luminescence dating of K-feldspar. *Quaternary Geochronology* 27, 119-130.
- Love, J., Mazaud, A., 1997. A database for the Matuyama-Brunhes magnetic reversal. *Physics of the earth and planetary interiors* 103, 207-245.
- Lowe, D.J., 2011a. Tephrochronology and its application: a review. *Quaternary Geochronology* 6, 107-153.
- Lowe, D.J., 2011b. Tephrochronology: principles, functioning, application.
- Macdonald, R., Navarro, J., Upton, B., Davies, G., 1994. Strong compositional zonation in per-alkaline magma: Menengai, Kenya Rift Valley. *Journal of volcanology and geothermal research* 60, 301-325.
- MacInnes, D.G., 1956. Fossil Tubulidentata from East Africa. order of the Trustees of the British Museum.
- Manega, P., 1995. New geochronological results from the Ndotu, Naisiusiu and Ngaloba Beds at Olduvai and Laetoli in Northern Tanzania: Their significance for evolution of modern humans. Preservation and Use of Olduvai Gorge, Laetoli, Rock Art, and other Palaeoanthropological Resources in Tanzania.
- Manega, P.C., 1993. Geochronology, geochemistry and isotopic study of the Plio-Pleistocene hominid sites and the Ngorongoro volcanic highland in northern Tanzania.



- Marean, C.W., 1992a. Hunter to herder: Large mammal remains from the hunter-gatherer occupation at Enkapune ya Muto rock-shelter, Central Rift, Kenya. *African Archaeological Review* 10, 65-127.
- Marean, C.W., 1992b. Implications of late Quaternary mammalian fauna from Lukenya Hill (south-central Kenya) for paleoenvironmental change and faunal extinctions. *Quaternary Research* 37, 239-255.
- Marean, C.W., 1997. Hunter-gatherer foraging strategies in tropical grasslands: model building and testing in the East African Middle and Later Stone Age. *Journal of Anthropological Archaeology* 16, 189-225.
- Marean, C.W., 2010. Pinnacle Point Cave 13B (Western Cape Province, South Africa) in context: the Cape floral kingdom, shellfish, and modern human origins. *Journal of Human Evolution* 59, 425-443.
- Marean, C.W., Bar-Matthews, M., Bernatchez, J., Fisher, E., Goldberg, P., Herries, A.I., Jacobs, Z., Jerardino, A., Karkanas, P., Minichillo, T., 2007. Early human use of marine resources and pigment in South Africa during the Middle Pleistocene. *Nature* 449, 905-908.
- Marean, C.W., Goldberg, P., Avery, G., Grine, F.E., Klein, R.G., 2000. Middle Stone Age stratigraphy and excavations at Die Kelders Cave 1 (Western Cape Province, South Africa): the 1992, 1993, and 1995 field seasons. *Journal of Human Evolution* 38, 7-42.
- Martyn, J., 1969. Geological history of the country between Lake Baringo and the Kerio river, Baringo district, Kenya. Royal Holloway, University of London.
- McBrearty, S., 1981. Songhor: a Middle Stone Age site in western Kenya. *Quaternaria. Storia Naturale e Culturale del Quaternario Roma* 23, 171-190.
- McBrearty, S., 1986. The archaeology of the Muguruk Site, western Kenya. University Microfilms.
- McBrearty, S., 1988. The Sangoan - Lupemban and middle stone age sequence at the Muguruk site, western Kenya. *World Archaeology* 19, 388-420.
- McBrearty, S., 1991. Recent research in western Kenya and its implications for the status of the Sangoan industry. *Cultural beginnings: approaches to understanding early hominid lifeways in the African savanna*, 159-176.
- McBrearty, S., 1992. Sangoan technology and habitat at Simbi. *Nyame Akuma*, 34-40.
- McBrearty, S., 1999. Archaeology of the Kapthurin formation. *Late Cenozoic environments and hominid evolution: a tribute to Bill Bishop*, 143-156.



- McBrearty, S., 2001a. Human Roots. Africa and Asia in the Middle Pleistocene.
- McBrearty, S., 2001b. The Middle Pleistocene of East Africa. Human roots: Africa and Asia in the Middle Pleistocene, 81-92.
- McBrearty, S., 2007. Down with the revolution. Rethinking the human revolution. Cambridge: MacDonald Institute for Archaeological Research Monographs, 133-152.
- McBrearty, S., Bishop, L., Kingston, J., 1996. Variability in traces of Middle Pleistocene hominid behavior in the Kapthurin Formation, Baringo, Kenya. *Journal of Human Evolution* 30, 563-580.
- McBrearty, S., Brooks, A.S., 2000. The revolution that wasn't: a new interpretation of the origin of modern human behavior. *Journal of human evolution* 39, 453-563.
- McBrearty, S., Tryon, C., 2006. From Acheulean to Middle Stone Age in the Kapthurin Formation, Kenya, Transitions before the Transition. Springer, pp. 257-277.
- McCall, G., Baker, B., Walsh, J., 1967. Late tertiary and Quaternary sediments of the Kenya Rift Valley. Background to evolution in Africa, 191-220.
- McCall, G.J.H., 1967. Geology of the Nakuru-Thomson's Falls-Lake Hannington Area: Degree Sheet No. 35 SW Quarter and 43 NW Quarter (with Coloured Maps). Geological Survey of Kenya.
- McDermott, F., Stringer, C., Grün, R., Williams, C., Din, V., Hawkesworth, C., 1996. New Late-Pleistocene uranium–thorium and ESR dates for the Singa hominid (Sudan). *Journal of Human Evolution* 31, 507-516.
- McDougall, I., Brown, F.H., Fleagle, J.G., 2005. Stratigraphic placement and age of modern humans from Kibish, Ethiopia. *Nature* 433, 733-736.
- McDougall, I., Brown, F.H., Fleagle, J.G., 2008. Sapropels and the age of hominins Omo I and II, Kibish, Ethiopia. *Journal of Human Evolution* 55, 409-420.
- McHenry, L.J., 2012. A revised stratigraphic framework for Olduvai Gorge Bed I based on tuff geochemistry. *Journal of human evolution* 63, 284-299.
- McHenry, L.J., Mollel, G.F., Swisher, C.C., 2008. Compositional and textural correlations between Olduvai Gorge Bed I tephra and volcanic sources in the Ngorongoro Volcanic Highlands, Tanzania. *Quaternary International* 178, 306-319.
- McPherron, S.P., Dibble, H.L., 2011. Using computers in archaeology: A practical guide.
- Mehlman, M., 1979. Mumba-Höhle revisited: The relevance of a forgotten excavation to some current issues in east African prehistory. *World Archaeology* 11, 80-94.

- Mehlman, M.J., 1977. Excavations at Nasera Rock, Tanzania. *AZANIA: Journal of the British Institute in Eastern Africa* 12, 111-118.
- Mehlman, M.J., 1989. Later Quaternary archaeological sequences in northern Tanzania. University of Illinois at Urbana-Champaign.
- Merrick, H.V., 1975. Change in later Pleistocene lithic industries in Eastern Africa. *Dissertation abstracts international. A. The humanities and social sciences* 37, 417-418.
- Merrick, H.V., Brown, F.H., 1984. Obsidian sources and patterns of source utilization in Kenya and northern Tanzania: some initial findings. *African Archaeological Review* 2, 129-152.
- Merrick, H.V., Brown, F.H., Nash, W.P., 1994. Use and movement of obsidian in the Early and Middle Stone Ages of Kenya and northern Tanzania. *Society, culture, and technology in Africa* 11, 29-44.
- Mora, C., Driese, S., 1999. Palaeoenvironment, Palaeoclimate and Stable Carbon Isotopes of Palaeozoic Red-Bed Palaeosols, Appalachian Basin, USA and Canada. *Palaeoweathering, palaeosurfaces and related continental deposits*, 61-84.
- Morgan, G., VI, London D (1996) Optimizing the electron microprobe analysis of hydrous alkali aluminosilicate glasses. *American Mineralogist* 81, 1176-1185.
- Morgan, L.E., Renne, P.R., 2008. Diachronous dawn of Africa's Middle Stone Age: new  $^{40}\text{Ar}/^{39}\text{Ar}$  ages from the Ethiopian Rift. *Geology* 36, 967-970.
- Mussi, M., Altamura, F., Macchiarelli, R., Melis, R.T., Spinapolice, E.E., 2014. Garba III (Melka Kunture, Ethiopia): a MSA site with archaic *Homo sapiens* remains revisited. *Quaternary international* 343, 28-39.
- Nash, W., 1992. Analysis of oxygen with the electron microprobe: Applications to hydrated glass and minerals. *American Mineralogist* 77, 453-457.
- Negash, A., Shackley, M.S., 2006. Geochemical provenance of obsidian artefacts from the MSA site of Porc Epic, Ethiopia. *Archaeometry* 48, 1-12.
- Negash, A., Shackley, M.S., Alene, M., 2006. Source provenance of obsidian artifacts from the Early Stone Age (ESA) site of Melka Konture, Ethiopia. *Journal of Archaeological Science* 33, 1647-1650.
- Nelson, C.M., Posnansky, M., 1970. The stone tools from the re-excavation of Nsongezi Rock Shelter, Uganda. *AZANIA: Journal of the British Institute in Eastern Africa* 5, 119-172.
- Nicholson, S.E., 1998. Historical fluctuations of Lake Victoria and other lakes in the northern

Rift Valley of East Africa, Environmental change and response in East African lakes. Springer, pp. 7-35.

Nomenclature, S., 2005. North American stratigraphic code. AAPG Bulletin 89, 1547-1591.

Orton, G., 1996. Volcanic environments. Sedimentary environments: Processes, facies and stratigraphy, 485-567.

Owen, A.W., 1939. An amateur field collector in Kavirondo. African Affairs 38, 220-226.

Owen, W., 1937. Draft of tentative preliminary report on the July 1937 investigations at Ng'ira Karungu. Unpublished manuscript housed in the archives of the Natural History Museum, London.

Owen, W., 1938. 218. The Kombewa Culture, Kenya Colony. Man, 203-205.

Pearson, O.M., 2000. Postcranial remains and the origin of modern humans. Evolutionary Anthropology: Issues, News, and Reviews 9, 229-247.

Pearson, O.M., Royer, D.F., Grine, F.E., Fleagle, J.G., 2008. A description of the Omo I postcranial skeleton, including newly discovered fossils. Journal of human evolution 55, 421-437.

Peppe, D.J., McNulty, K.P., Cote, S.M., Harcourt-Smith, W.E., Dunsworth, H.M., Van Couvering, J.A., 2009. Stratigraphic interpretation of the Kulu Formation (Early Miocene, Rusinga Island, Kenya) and its implications for primate evolution. Journal of Human Evolution 56, 447-461.

Peters, C.R., Blumenschine, R.J., Hay, R.L., Livingstone, D.A., Marean, C.W., Harrison, T., Armour-Chelu, M., Andrews, P., Bernor, R.L., Bonnefille, R., 2008. Paleoecology of the Serengeti-Mara ecosystem. Serengeti III: Human impacts on ecosystem dynamics, 47-94.

Pickering, E., 1959. The Serengeti Plain. Rec. Geol. Surv. Tanganyika 7, 11-13.

Pickford, M., 1982. The tectonics, volcanics and sediments of the Nyanza Rift Valley, Kenya. Z. Geomorphol 42, 1-33.

Pickford, M., 1984. Kenya palaeontology gazetteer. National Museums of Kenya, Dept. of Sites and Monuments Documentation.

Pickford, M., 1986. Cainozoic paleontological sites of Western Kenya. F. Pfeil.

Pickford, M., Senut, B., Poupeau, G., Brown, F.H., Haileab, B., 1991. Correlation of tephra layers from the western Rift Valley (Uganda) to the Turkana Basin (Ethiopia/Kenya) and the Gulf of Aden. Stratigraphy 313, 223-229.

Pickford, M., Thomas, H., 1984. An aberrant new bovid (Mammalia) in subrecent deposits from Rusinga island, Kenya, *Proceedings of the Koninklijke Nederlandse Akademie van Wetenschappen. Series B. Palaeontology, geology, physics and chemistry. North-Holland*, pp. 441-452.

Porat, N., Chazan, M., Grün, R., Aubert, M., Eisenmann, V., Horwitz, L.K., 2010. New radiometric ages for the Fauresmith industry from Kathu Pan, southern Africa: Implications for the Earlier to Middle Stone Age transition. *Journal of Archaeological Science* 37, 269-283.

Posnansky, M., 1970. The Stone Tools from the Re-excavation of Nsongezi Rock Shelter, Uganda. *Azania*, 119.

Potts, R., Behrensmeyer, A.K., Ditchfield, P., 1999. Paleolandscape variation and Early Pleistocene hominid activities: members 1 and 7, Olorgesailie Formation, Kenya. *Journal of Human Evolution* 37, 747-788.

Pouchou, J.-L., Pichoir, F., 1991. Quantitative analysis of homogeneous or stratified microvolumes applying the model "PAP", *Electron probe quantitation*. Springer, pp. 31-75.

Prendergast, M.E., Luque, L., Domínguez-Rodrigo, M., Díez-Martín, F., Mabulla, A.Z., Barba, R., 2007. New excavations at Mumba rockshelter, Tanzania. *Journal of African Archaeology* 5, 217-244.

Pyle, D.M., 1999. Widely dispersed Quaternary tephra in Africa. *Global and Planetary Change* 21, 95-112.

Renaut, R., Owen, R., 1980. Late Quaternary fluvio-lacustrine sedimentation and lake levels in the Baringo basin, northern Kenya, Rift Valley. *Recherches géologiques en Afrique* 5, 130-133.

Riehle, J., Ager, T., Reger, R., Pinney, D., Kaufman, D., 2008. Stratigraphic and compositional complexities of the late Quaternary Lethe tephra in South-central Alaska. *Quaternary International* 178, 210-228.

Rightmire, G.P., 1998. Human evolution in the Middle Pleistocene: The role of *Homo heidelbergensis*. *Evolutionary Anthropology* 6, 218-227.

Rightmire, G.P., 2008. *Homo* in the Middle Pleistocene: hypodigms, variation, and species recognition. *Evolutionary Anthropology: Issues, News, and Reviews* 17, 8-21.

Rightmire, G.P., 2009. Middle and later Pleistocene hominins in Africa and Southwest Asia. *Proceedings of the National Academy of Sciences* 106, 16046-16050.

Rightmire, G.P., Deacon, H.J., 1991. Comparative studies of Late Pleistocene human remains from Klasies River Mouth, South Africa. *Journal of Human Evolution* 20, 131-156.

- Rightmire, P.G., 1996. The human cranium from Bodo, Ethiopia: evidence for speciation in the Middle Pleistocene? *Journal of Human Evolution* 31, 21-39.
- Rito, T., Richards, M.B., Fernandes, V., Alshamali, F., Cerny, V., Pereira, L., Soares, P., 2013. The first modern human dispersals across Africa.
- Rogers, M.J., Harris, J.W., Feibel, C.S., 1994. Changing patterns of land use by Plio-Pleistocene hominids in the Lake Turkana Basin. *Journal of Human Evolution* 27, 139-158.
- Rose, J.I., Usik, V.I., Marks, A.E., Hilbert, Y.H., Galletti, C.S., Parton, A., Geiling, J.M., Cerny, V., Morley, M.W., Roberts, R.G., 2011. The Nubian complex of Dhofar, Oman: an African middle stone age industry in southern Arabia. *PLoS One* 6, e28239.
- Sahle, Y., Hutchings, W.K., Braun, D.R., Sealy, J.C., Morgan, L.E., Negash, A., Atnafu, B., 2013. Earliest stone-tipped projectiles from the Ethiopian Rift date to > 279,000 years ago.
- Sahle, Y., Morgan, L.E., Braun, D.R., Atnafu, B., Hutchings, W.K., 2014. Chronological and behavioral contexts of the earliest middle stone age in the gademotta formation, main ethiopian rift. *Quaternary International* 331, 6-19.
- Scerri, E.M., 2013. The Aterian and its place in the North African middle stone age. *Quaternary International* 300, 111-130.
- Scerri, E.M., Blinkhorn, J., Groucutt, H.S., Niang, K., 2015. The Middle Stone Age archaeology of the Senegal River Valley. *Quaternary International*.
- Schick, K.D., 1986. Stone Age sites in the making: experiments in the formation and transformation of archaeological occurrences. *British Archaeological Reports Ltd.*
- Schmid, R., 1981. Descriptive nomenclature and classification of pyroclastic deposits and fragments: Recommendations of the IUGS Subcommittee on the Systematics of Igneous Rocks. *Geology* 9, 41-43.
- Shane, P., Nairn, I.A., Martin, S.B., Smith, V.C., 2008. Compositional heterogeneity in tephra deposits resulting from the eruption of multiple magma bodies: implications for tephrochronology. *Quaternary International* 178, 44-53.
- Shea, J.J., 2006. The origins of lithic projectile point technology: evidence from Africa, the Levant, and Europe. *Journal of Archaeological Science* 33, 823-846.
- Shea, J.J., 2008. The Middle Stone Age archaeology of the Lower Omo Valley Kibish Formation: Excavations, lithic assemblages, and inferred patterns of early *Homo sapiens* behavior. *Journal of Human Evolution* 55, 448-485.

- Sheppard, P.J., Kleindienst, M.R., 1996. Technological change in the earlier and middle stone Age of Kalambo Falls (Zambia). *African Archaeological Review* 13, 171-196.
- Simon, J.I., Renne, P.R., Mundil, R., 2008. Implications of pre-eruptive magmatic histories of zircons for U–Pb geochronology of silicic extrusions. *Earth and Planetary Science Letters* 266, 182-194.
- Singer, R., 1954. The Saldanha skull from Hopefield, South Africa. *American journal of physical anthropology* 12, 345-362.
- Singer, R., Wymer, J., 1968. Archaeological investigations at the Saldanha skull site in South Africa. *The South African Archaeological Bulletin*, 63-74.
- Singer, R., Wymer, J.J., 1982. *The Middle Stone Age at Klasies River Mouth in South Africa*. University of Chicago Press.
- Skinner, A., Hay, R., Masao, F., Blackwell, B., 2003. Dating the Naisiusiu Beds, Olduvai Gorge, by electron spin resonance. *Quaternary science reviews* 22, 1361-1366.
- Smith, T.M., Tafforeau, P., Reid, D.J., Grün, R., Eggins, S., Boutakiout, M., Hublin, J.-J., 2007. Earliest evidence of modern human life history in North African early *Homo sapiens*. *Proceedings of the National Academy of Sciences* 104, 6128-6133.
- Smith, V.C., Pearce, N.J., Matthews, N.E., Westgate, J.A., Petraglia, M.D., Haslam, M., Lane, C.S., Korisettar, R., Pal, J., 2011. Geochemical fingerprinting of the widespread Toba tephra using biotite compositions. *Quaternary International* 246, 97-104.
- Soares, P., Alshamali, F., Pereira, J.B., Fernandes, V., Silva, N.M., Afonso, C., Costa, M.D., Musilová, E., Macaulay, V., Richards, M.B., 2011. The expansion of mtDNA haplogroup L3 within and out of Africa. *Molecular biology and evolution*, msr245.
- Spooner, E.T.C., Buckland, P., & Bishop, W.W. , n.d. *The Kampi-ya-Samaki and Kokwob beds of the Baringo basin, Kenya*. East African Geological Research Unit working paper .
- Spoor, F., Stringer, C., Zonneveld, F., 1998. Rare temporal bone pathology of the Singa calvaria from Sudan. *American journal of physical anthropology* 107, 41-50.
- Stern, N., 1994. The implications of time-averaging for reconstructing the land-use patterns of early tool-using hominids. *Journal of Human Evolution* 27, 89-105.
- Szabo, B., Butzer, K., 1979. Uranium-series dating of lacustrine limestones from pan deposits with final Acheulian assemblage at Rooidam, Kimberley district, South Africa. *Quaternary Research* 11, 257-260.

Tallon, P.W., 1976. The Stratigraphy, Palaeoenvironments and Geomorphology of the Pleistocene Kapthurin Formation, Kenya. Queen Mary, University of London.

Tallon, P.W., 1978. Geological setting of the hominid fossils and Acheulian artifacts from the Kapthurin Formation, Baringo District, Kenya. Geological Society, London, Special Publications 6, 361-373.

Tappen, N., 1979. Studies on the condition and structure of bone of the Saldanha fossil cranium. American journal of physical anthropology 50, 591-603.

Texier, P.-J., Porraz, G., Parkington, J., Rigaud, J.-P., Poggenpoel, C., Miller, C., Tribolo, C., Cartwright, C., Coudenneau, A., Klein, R., 2010. A Howiesons Poort tradition of engraving ostrich eggshell containers dated to 60,000 years ago at Diepkloof Rock Shelter, South Africa. Proceedings of the National Academy of Sciences 107, 6180-6185.

Thompson, J.C., 2005. The impact of post-depositional processes on bone surface modification frequencies: a corrective strategy and its application to the Loiyangalani site, Serengeti Plain, Tanzania. Journal of Taphonomy 3, 67-89.

Thomsen, K.J., Murray, A., Jain, M., Bøtter-Jensen, L., 2008. Laboratory fading rates of various luminescence signals from feldspar-rich sediment extracts. Radiation Measurements 43, 1474-1486.

Tribolo, C., Rasse, M., Soriano, S., Huysecom, E., 2015. Defining a chronological framework for the middle stone age in West Africa: Comparison of methods and models for OSL ages at oun-jougou (Mali). Quaternary Geochronology.

Tryon, C., 2006. "Early" Middle Stone Age Lithic Technology of the Kapthurin Formation (Kenya). Current anthropology 47, 367-375.

Tryon, C., 2010. How the geological record affects our reconstructions of Middle Stone Age settlement patterns: the case of alluvial fans in Baringo, Kenya. Settlement Dynamics of the Middle Paleolithic & Middle Stone Age 3, 39-66.

Tryon, C.A., 2003. The Acheulian to Middle Stone Age transition: tephrostratigraphic context for archaeological change in the Kapthurin Formation, Kenya. PhD dissertation, University of Connecticut.

Tryon, C.A., Crevecoeur, I., Faith, J.T., Ekshtain, R., Nivens, J., Patterson, D., Mbua, E.N., Spoor, F., 2015. Late Pleistocene age and archaeological context for the hominin calvaria from GvJm-22 (Lukenya Hill, Kenya). Proceedings of the National Academy of Sciences 112, 2682-2687.

Tryon, C.A., Faith, J.T., 2013. Variability in the Middle Stone Age of Eastern Africa. Current Anthropology 54, S234-S254.



Tryon, C.A., Faith, J.T., Peppe, D.J., Beverly, E.J., Blegen, N., Blumenthal, S., Chritz, K.L., Driese, S., Patterson, D., Sharp, W.D., in press. The Pleistocene prehistory of the Lake Victoria basin. *Quaternary International*.

Tryon, C.A., Faith, J.T., Peppe, D.J., Fox, D.L., McNulty, K.P., Jenkins, K., Dunsworth, H., Harcourt-Smith, W., 2010. The Pleistocene archaeology and environments of the Wasiriya Beds, Rusinga Island, Kenya. *J Hum Evol* 59, 657-671.

Tryon, C.A., Faith, J.T., Peppe, D.J., Keegan, W.F., Keegan, K.N., Jenkins, K., Nightingale, S., Patterson, D., Van Plantinga, A., Driese, S.G., 2014. Sites on the landscape: Paleoenvironmental context of late Pleistocene archaeological sites from the Lake Victoria basin, equatorial East Africa. *Quaternary International* 331, 20-30.

Tryon, C.A., McBrearty, S., 2002. Tephrostratigraphy and the Acheulian to Middle Stone Age transition in the Kapthurin formation, Kenya. *Journal of Human Evolution* 42, 211-235.

Tryon, C.A., McBrearty, S., 2006. Tephrostratigraphy of the Bedded Tuff Member (Kapthurin Formation, Kenya) and the nature of archaeological change in the later Middle Pleistocene. *Quaternary Research* 65, 492-507.

Tryon, C.A., McBrearty, S., Texier, P.-J., 2005. Levallois lithic technology from the Kapthurin formation, Kenya: Acheulian origin and Middle Stone Age diversity. *African Archaeological Review* 22, 199-229.

Tryon, C.A., Peppe, D.J., Faith, J.T., Van Plantinga, A., Nightingale, S., Ogondo, J., Fox, D.L., 2012. Late Pleistocene artefacts and fauna from Rusinga and Mfangano islands, Lake Victoria, Kenya. *Azania: Archaeological Research in Africa* 47, 14-38.

Tryon, C.A., Roach, N.T., Logan, M.A.V., 2008. The Middle Stone Age of the northern Kenyan Rift: age and context of new archaeological sites from the Kapado Tuffs. *Journal of Human Evolution* 55, 652-664.

Van Couvering, J.A., 1972. Geology of Rusinga Island and Correlation of the Kenya mid-Tertiary fauna. University of Cambridge.

Van Noten, F., 1982. New Acheulean Sites and a New Hominid from Kapthurin, Lake Baringo, Kenya. *Nyame Akuma. A Newsletter of African Archaeology* Calgary, 11-12.

Van Noten, F., Cornelissen, E., Gysels, J., Moeyersons, J., Nijs, K., Uytterschaut, H., 1987. The Kapthurin project, Baringo: the 1984 season. *Nyame akuma*, 20-27.

Van Peer, P., Fullagar, R., Stokes, S., Bailey, R., Moeyersons, J., Steenhoudt, F., Geerts, A., Vanderbeken, T., De Dapper, M., Geus, F., 2003. The Early to Middle Stone Age transition and the emergence of modern human behaviour at site 8-B-11, Sai Island, Sudan. *Journal of Human*



Evolution 45, 187-193.

Van Plantinga, A.A., 2011. Geology of the Late Pleistocene artifact-bearing Wasiriya Beds at the Nyamita locality, Rusinga Island, Kenya.

Villa, P., Pollarolo, L., Degano, I., Birolo, L., Pasero, M., Biagioni, C., Douka, K., Vinciguerra, R., Lucejko, J.J., Wadley, L., 2015. A milk and ochre paint mixture used 49,000 years ago at Sibudu, South Africa. *PloS one* 10, e0131273.

Villa, P., Soressi, M., Henshilwood, C.S., Mourre, V., 2009. The Still Bay points of Blombos Cave (South Africa). *Journal of Archaeological Science* 36, 441-460.

Villa, P., Soriano, S., Tsanova, T., Degano, I., Higham, T.F., d'Errico, F., Backwell, L., Lucejko, J.J., Colombini, M.P., Beaumont, P.B., 2012. Border Cave and the beginning of the Later Stone Age in South Africa. *Proceedings of the National Academy of Sciences* 109, 13208-13213.

Vrba, E.S., 1980. 14. The significance of bovid remains as indicators of environment and predation patterns Fossils in the making: Vertebrate taphonomy and paleoecology, 247.

Wadley, L., 2001. What is cultural modernity? A general view and a South African perspective from Rose Cottage Cave. *Cambridge Archaeological Journal* 11, 201-221.

Wadley, L., 2015. Those marvellous millennia: the Middle Stone Age of Southern Africa. *Azania: Archaeological Research in Africa* 50, 155-226.

Wadley, L., Jacobs, Z., 2006. Sibudu Cave: background to the excavations, stratigraphy and dating. *Southern African Humanities* 18, 1-26.

Wadley, L., Williamson, B., Lombard, M., 2004. Ochre in hafting in Middle Stone Age southern Africa: a practical role. *Antiquity* 78, 661-675.

Wendorf, F., Schild, R., 1974. A Middle Stone Age Sequence from the Central Rift Valley, Ethiopia. *Zakład Narodowy im. Ossolińskich*.

White, T.D., Asfaw, B., DeGusta, D., Gilbert, H., Richards, G.D., Suwa, G., Howell, F.C., 2003. Pleistocene homo sapiens from middle awash, ethiopia. *Nature* 423, 742-747.

Whitworth, T., 1961. The geology of Mfwanganu island, western Kenya. HM Stationery Office.

Wilkins, J., Schoville, B.J., Brown, K.S., Chazan, M., 2012. Evidence for early hafted hunting technology. *Science* 338, 942-946.

Williams, L., 1991. Geology of the Mau Area. Republic of Kenya Ministry of Environment and Natural Resources, Mines and Geological Department, Nairobi. Report.

- Wintle, A.G., 1973. Anomalous fading of thermo-luminescence in mineral samples.
- WoldeGabriel, G., Endale, T., White, T.D., Thouveny, N., Hart, W.K., Renne, P.R., Asfaw, B., 2013. The role of Tephra studies in African paleoanthropology as exemplified by the Sidi Hako-ma Tuff. *Journal of African Earth Sciences* 77, 41-58.
- WoldeGabriel, G., Hart, W.K., Katoh, S., Beyene, Y., Suwa, G., 2005. Correlation of Plio–Pleistocene Tephra in Ethiopian and Kenyan rift basins: Temporal calibration of geological features and hominid fossil records. *Journal of Volcanology and Geothermal Research* 147, 81-108.
- Wood, B., Van Noten, F., 1986. Preliminary observations on the BK 8518 mandible from Barin-go, Kenya. *American Journal of Physical Anthropology* 69, 117-127.
- Woodward, S., 1931. On the Broken Hill Skull. *Illustrated London News* 159, 682-685.
- Wurz, S., 1999. The Howiesons Poort backed artefacts from Klasies River: an argument for symbolic behaviour. *The South African Archaeological Bulletin*, 38-50.
- Yellen, J., Brooks, A., Helgren, D., Tappen, M., Ambrose, S., Bonnefille, R., Feathers, J., Goodfriend, G., Ludwig, K., Renne, P., 2005. The archaeology of Aduma Middle Stone Age sites in the Awash Valley, Ethiopia. *PaleoAnthropology* 10.
- Yellen, J.E., Brooks, A.S., Cornelissen, E., Mehlman, M.J., Stewart, K., 1995. A middle stone age worked bone industry from Katanda, Upper Semliki Valley, Zaire. *Science* 268, 553-556.



















